ATTACHMENT 2 – DU TRANSPORT THROUGH FEHM SOIL COLUMN MODEL

THIS PAGE WAS INTENTIONALLY LEFT BLANK

DU Transport Through Soil Column

- 6.56 ft (2m) x 6.56 ft (2m) x 40 ft (12.192m) column
  - ~7.5 feet loess at top of column
  - 32.5 feet ft of overburden
    - Similar lithology, some interbedded sands at depth
    - Compacted/stiff ~10-12 ft based on blow counts
- Discretization
  - dx = dy = 1.64 ft (0.5m)
  - dz = 0.5 ft (0.152m)
- Examine results at three locations to simulate thin (A), average (B) and thick (C) overburden depths to water.
- Run model for 1,000 years varying properties of materials to generate bounds on contamination potential to groundwater

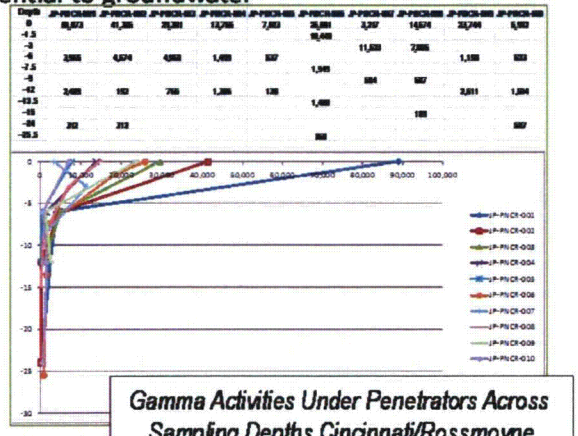

Gamma Activities Under Penetrators Across Sampling Depths Cincinnati/Rossmoyne

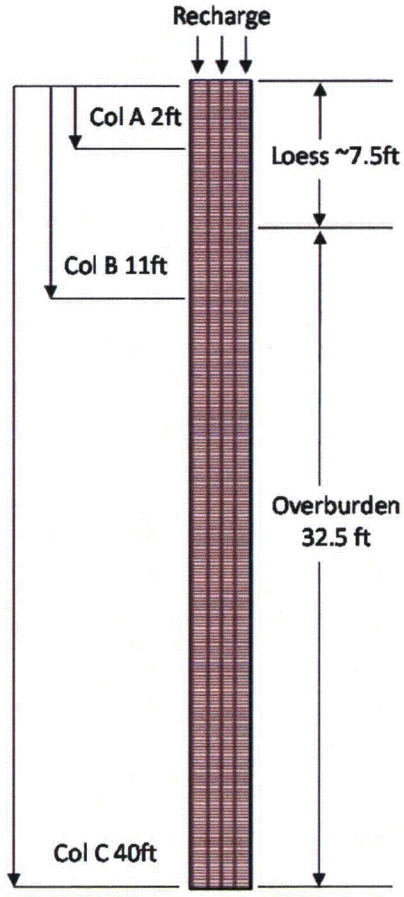

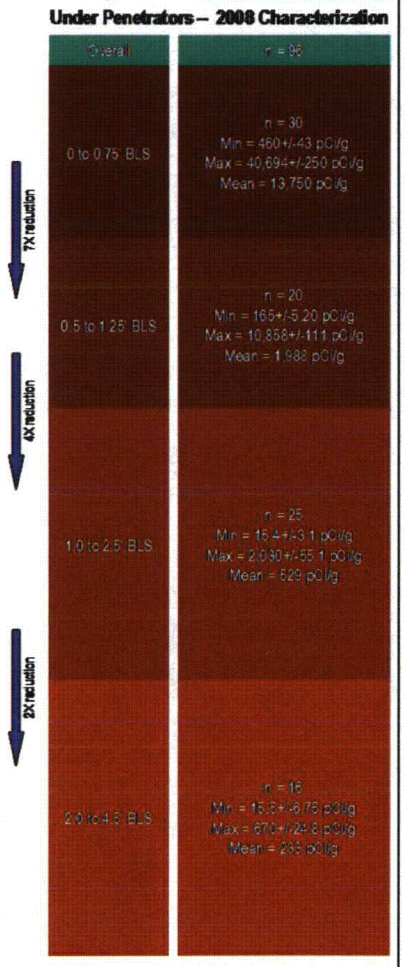

Major Input Parameters

(1) Van Genuchten parameters for unsaturated flow (Silty Clay Loam ( ))
Residual liquid saturation = 0.20%
Maximum liquid saturation = 100%
Inverse of air entry head = 1.0 per meter

(2) Total porosity = 0.45
(3) Density = 1460 Kg/m3
(4) Hydraulic conductivity
Kx = Ky = 1.250E-6 m/s (39.4 m/yr); Kz = 1.250E-7 m/s (3.94 m/yr)
(5) Recharge = 4 in/yr
(6) Sorption = 189 L/Kg

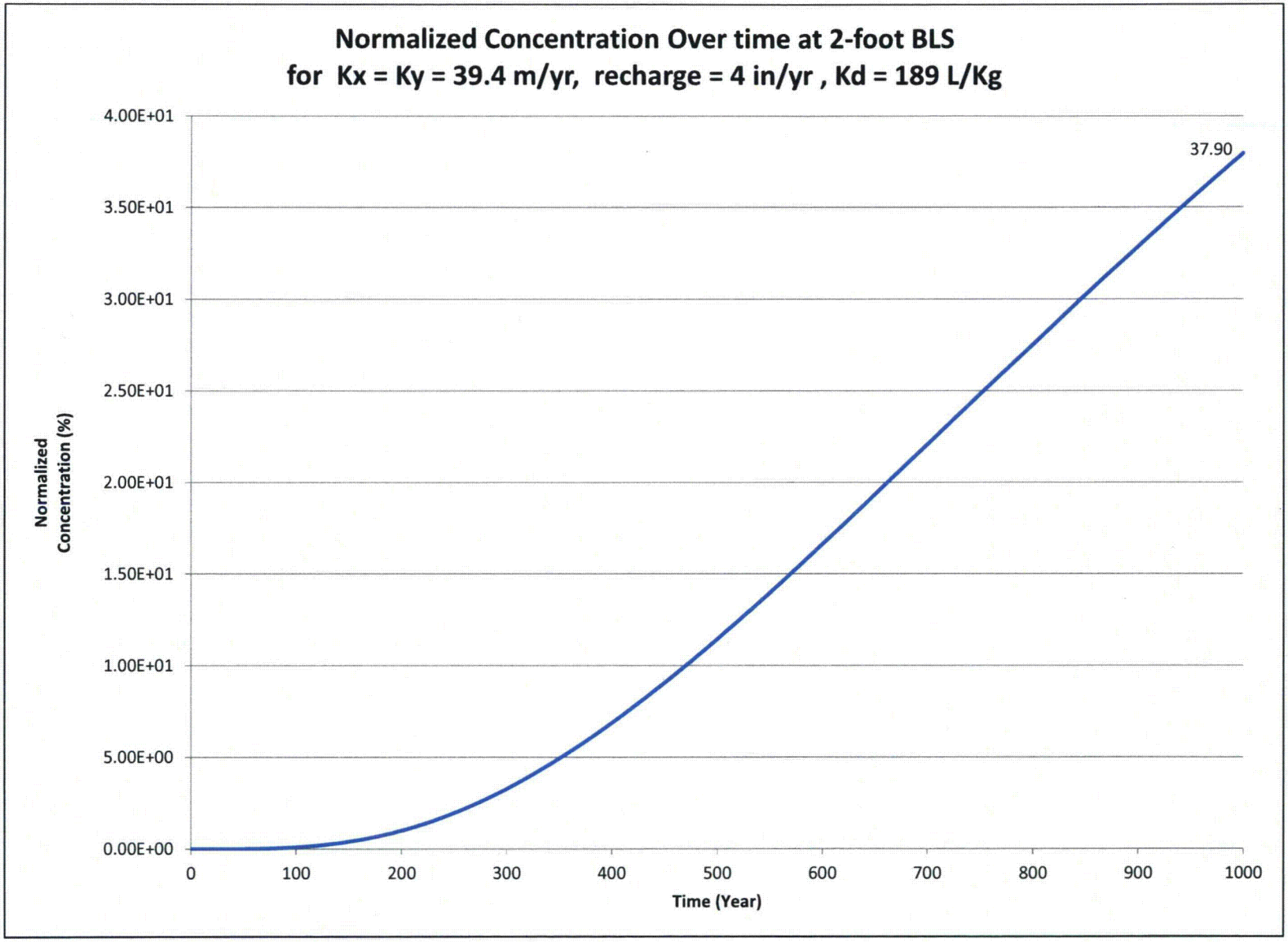
Normalized Concentration Over time at 2-foot BLS
for Kx = Ky = 39.4 m/yr, recharge = 4 in/yr , Kd = 189 L/Kg
Normalized Concentration (%)
4.00E+01
3.50E+01
3.00E+01
2.50E+01
2.00E+01
1.50E+01
1.00E+01
5.00E+00
0.00E+00
37.90
0
100
200
300
400
500
600
700
800
900
1000
Time (Year)

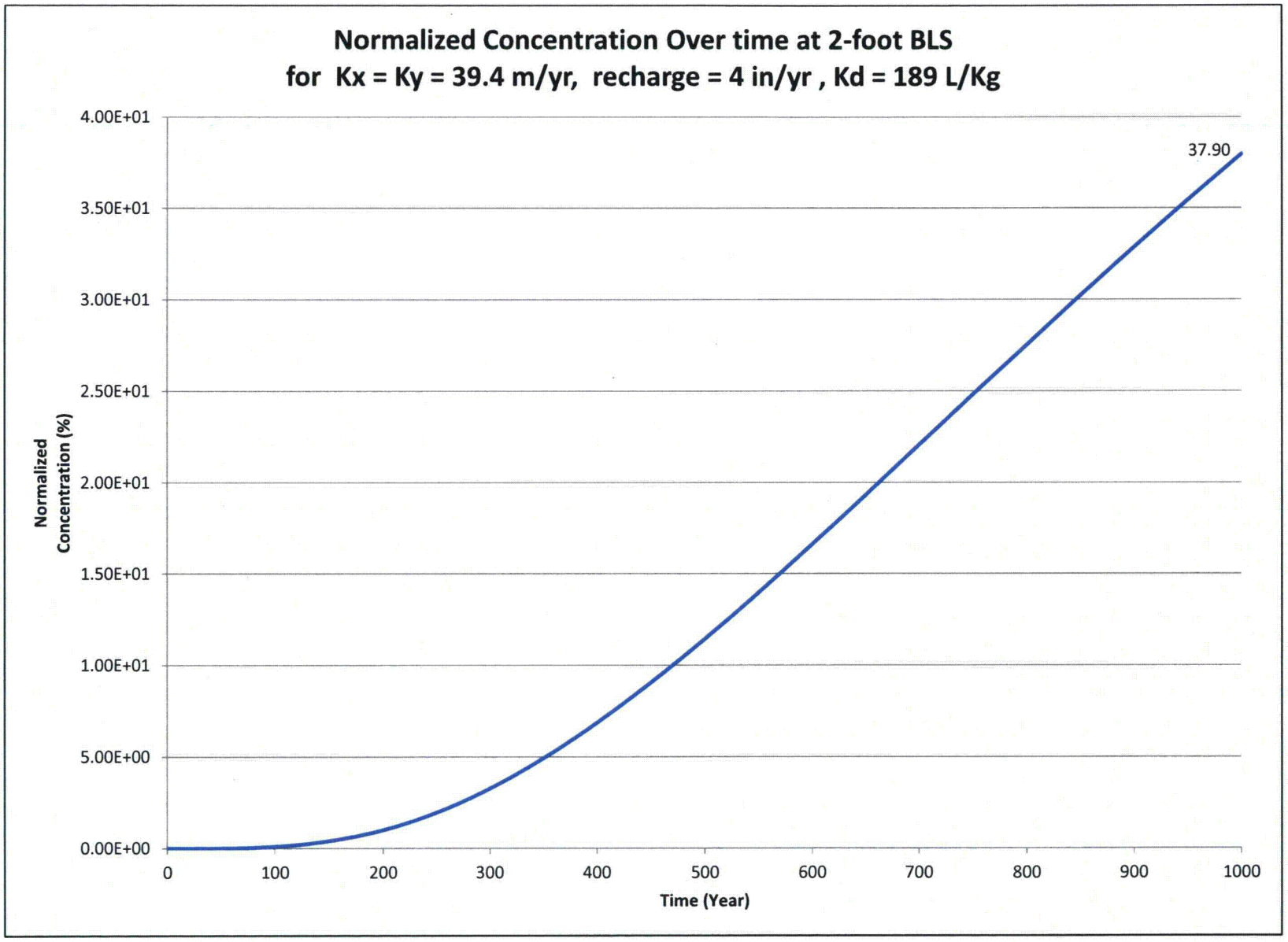
Normalized Concentration Over time at 2-foot BLS
for Kx = Ky = 39.4 m/yr, recharge = 4 in/yr , Kd = 189 L/Kg
Normalized Concentration (%)
4.00E+01
3.50E+01
3.00E+01
2.50E+01
2.00E+01
1.50E+01
1.00E+01
5.00E+00
0.00E+00
37.90
0
100
200
300
400
500
600
700
800
900
1000
Time (Year)

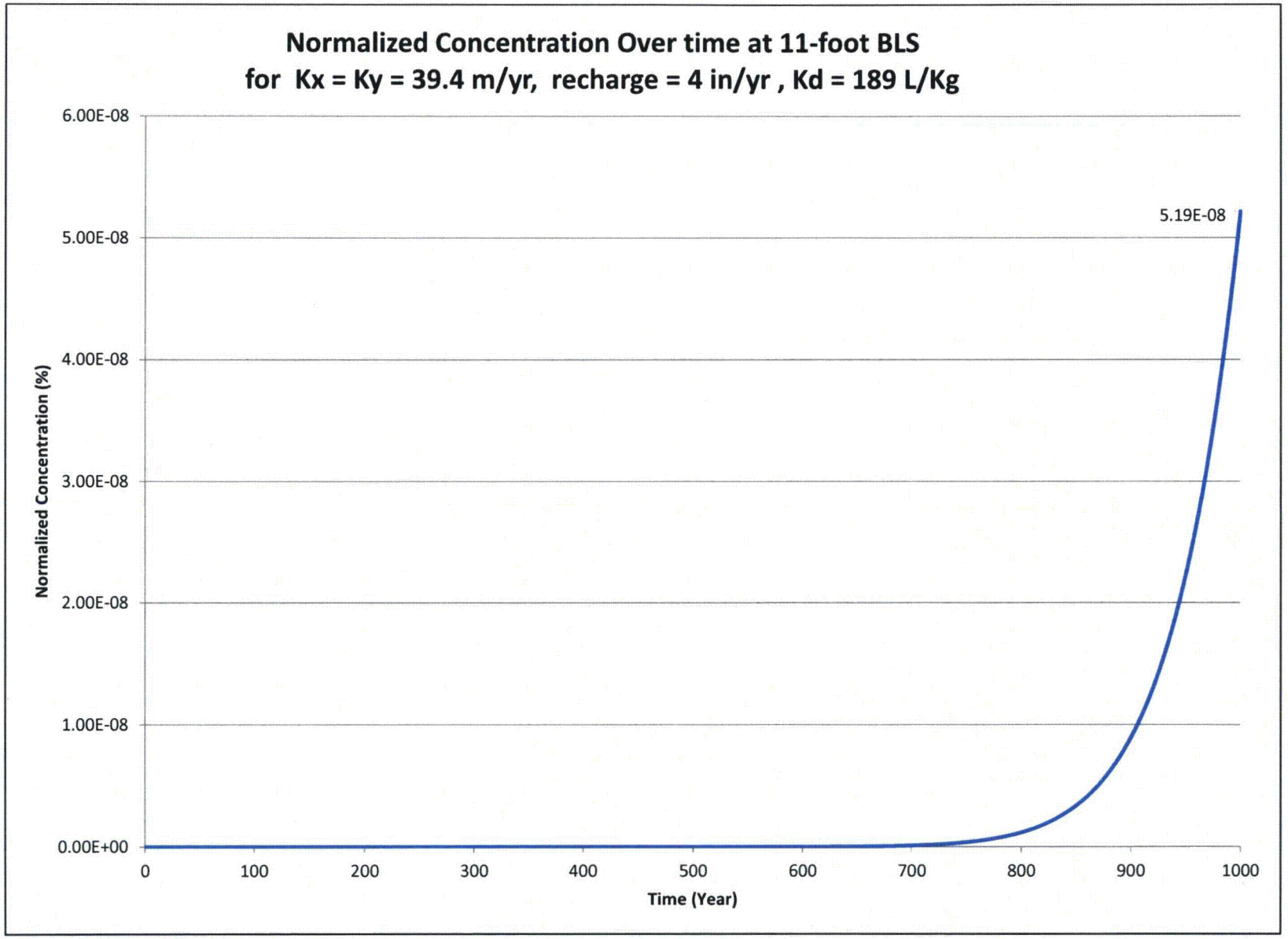
Normalized Concentration Over time at 11-foot BLS
for Kx = Ky = 39.4 m/yr, recharge = 4 in/yr , Kd = 189 L/Kg
6.00E-08
5.00E-08
4.00E-08
3.00E-08
2.00E-08
1.00E-08
0.00E+00
Normalized Concentration (%)
5.19E-08
0
100
200
300
400
500
600
700
800
900
1000
Time (Year)

Sensitivity Analysis 1		
Sensitivity Run	**Summary description**	**Purpose/objective**
1	Increase Hydraulic Conductivity (K) to 445 m/yr (upper end of published K for loess soil types, also greater than upper end of slug test results for over other properties remain same	Assess potential for leaching through soil column to groundwater at upper end of published hydraulic conductivity.

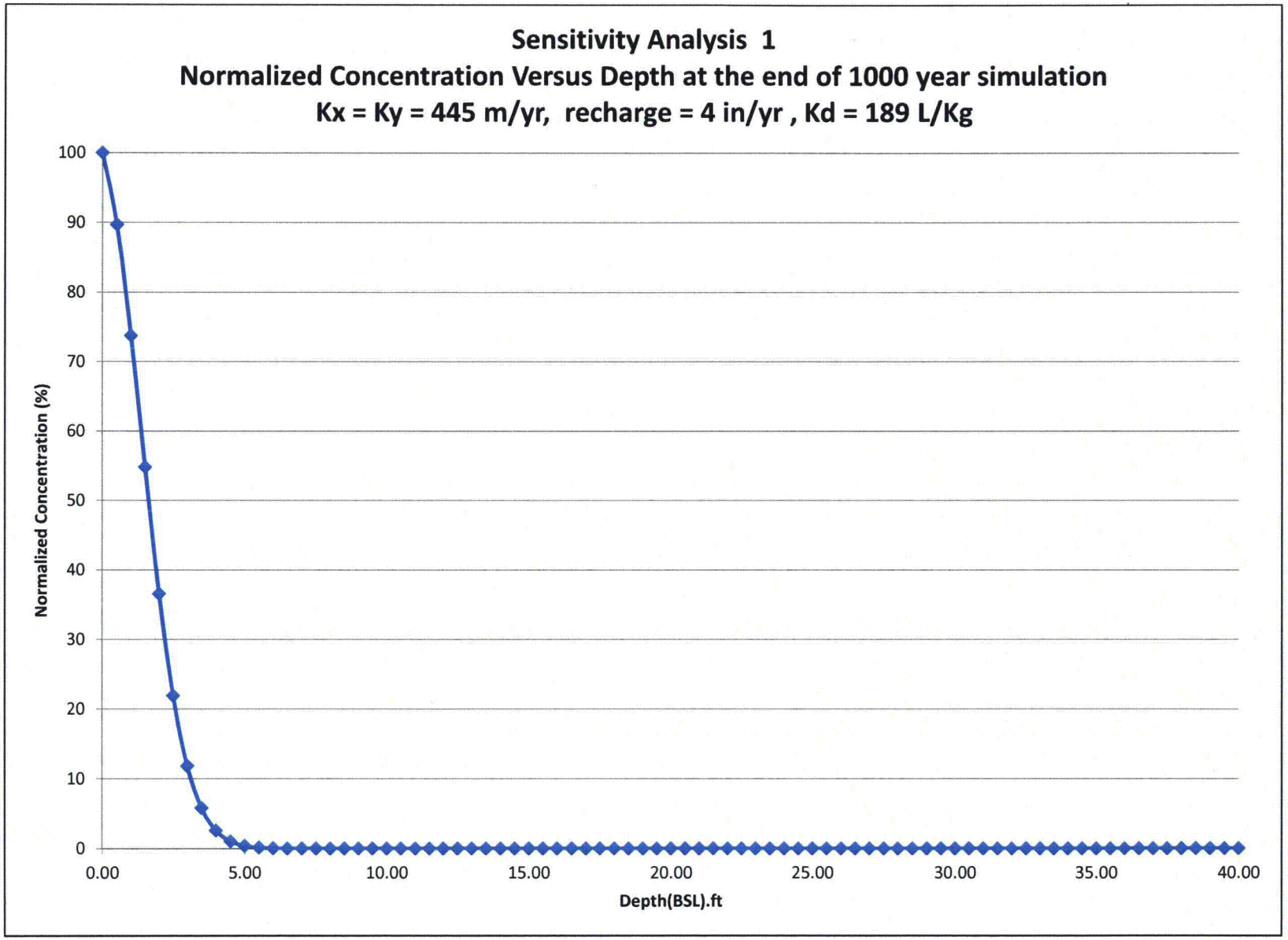
Sensitivity Analysis 1
Normalized Concentration Versus Depth at the end of 1000 year simulation
Kx = Ky = 445 m/yr, recharge = 4 in/yr , Kd = 189 L/Kg
Normalized Concentration (%)
100
90
80
70
60
50
40
30
20
10
0
0.00
5.00
10.00
15.00
20.00
25.00
30.00
35.00
40.00
Depth(BSL).ft

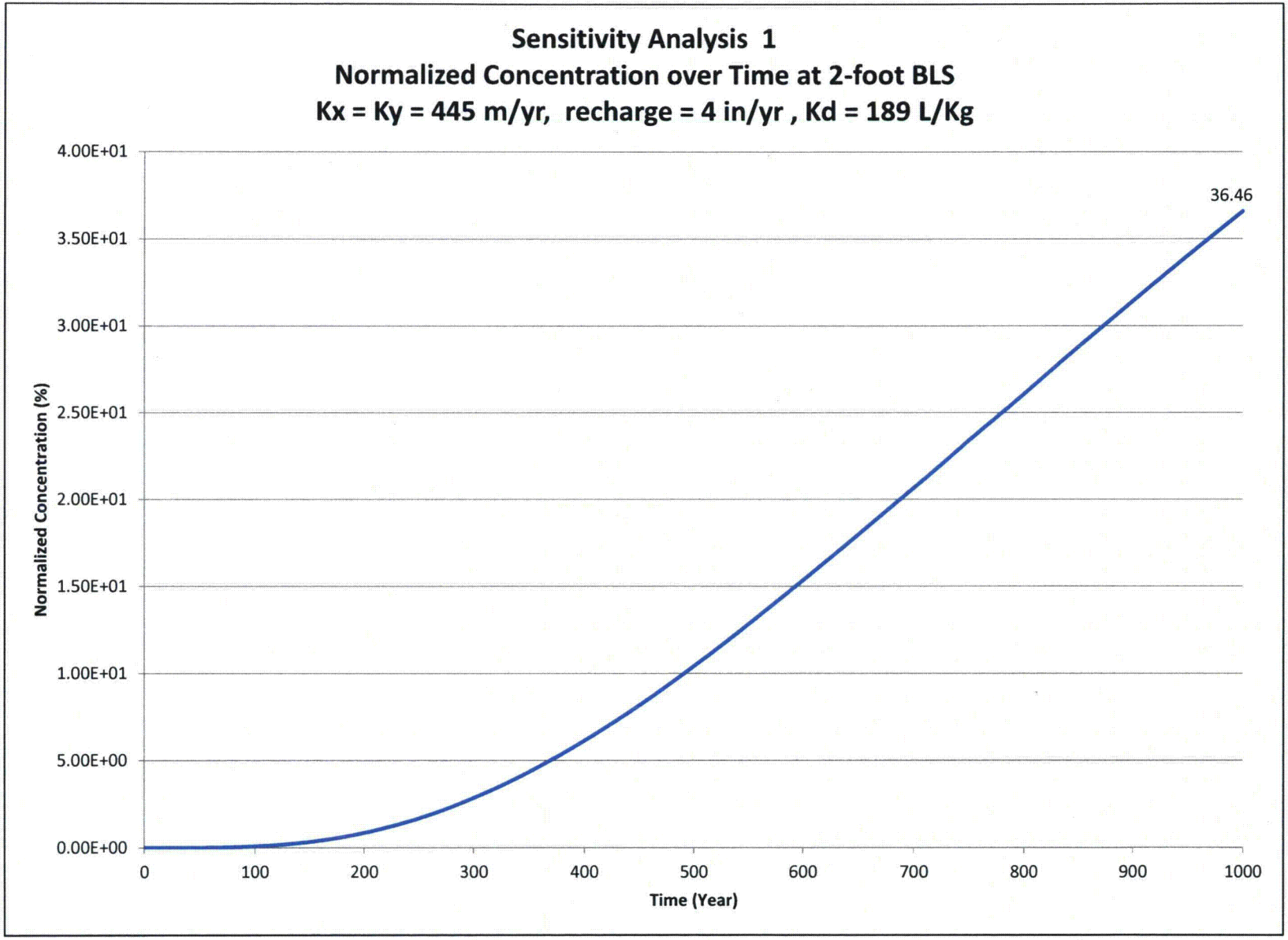
Sensitivity Analysis 1
Normalized Concentration over Time at 2-foot BLS
Kx = Ky = 445 m/yr, recharge = 4 in/yr , Kd = 189 L/Kg
Normalized Concentration (%)
4.00E+01
3.50E+01
3.00E+01
2.50E+01
2.00E+01
1.50E+01
1.00E+01
5.00E+00
0.00E+00
36.46
0
100
200
300
400
500
600
700
800
900
1000
Time (Year)

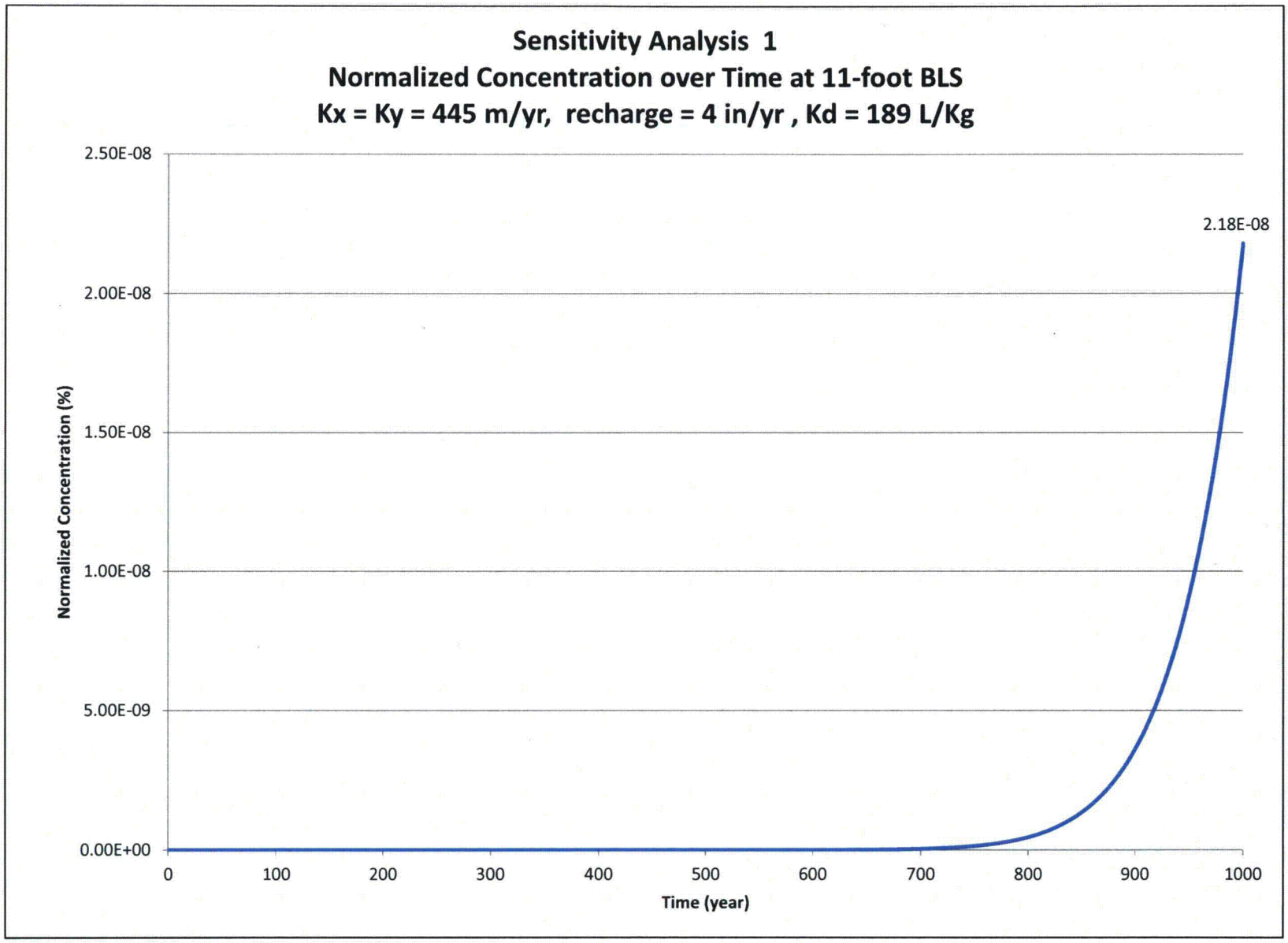
Sensitivity Analysis 1
Normalized Concentration over Time at 11-foot BLS
Kx = Ky = 445 m/yr, recharge = 4 in/yr , Kd = 189 L/Kg
Normalized Concentration (%)
2.50E-08
2.00E-08
1.50E-08
1.00E-08
5.00E-09
0.00E+00
2.18E-08
0
100
200
300
400
500
600
700
800
900
1000
Time (year)

Sensitivity Analysis 2		
Sensitivity Run	**Summary description**	**Purpose/objective**
2	Increase upper end K by 10 time	Assess sensitivity of hydraulic conductivity beyond upper range of published K

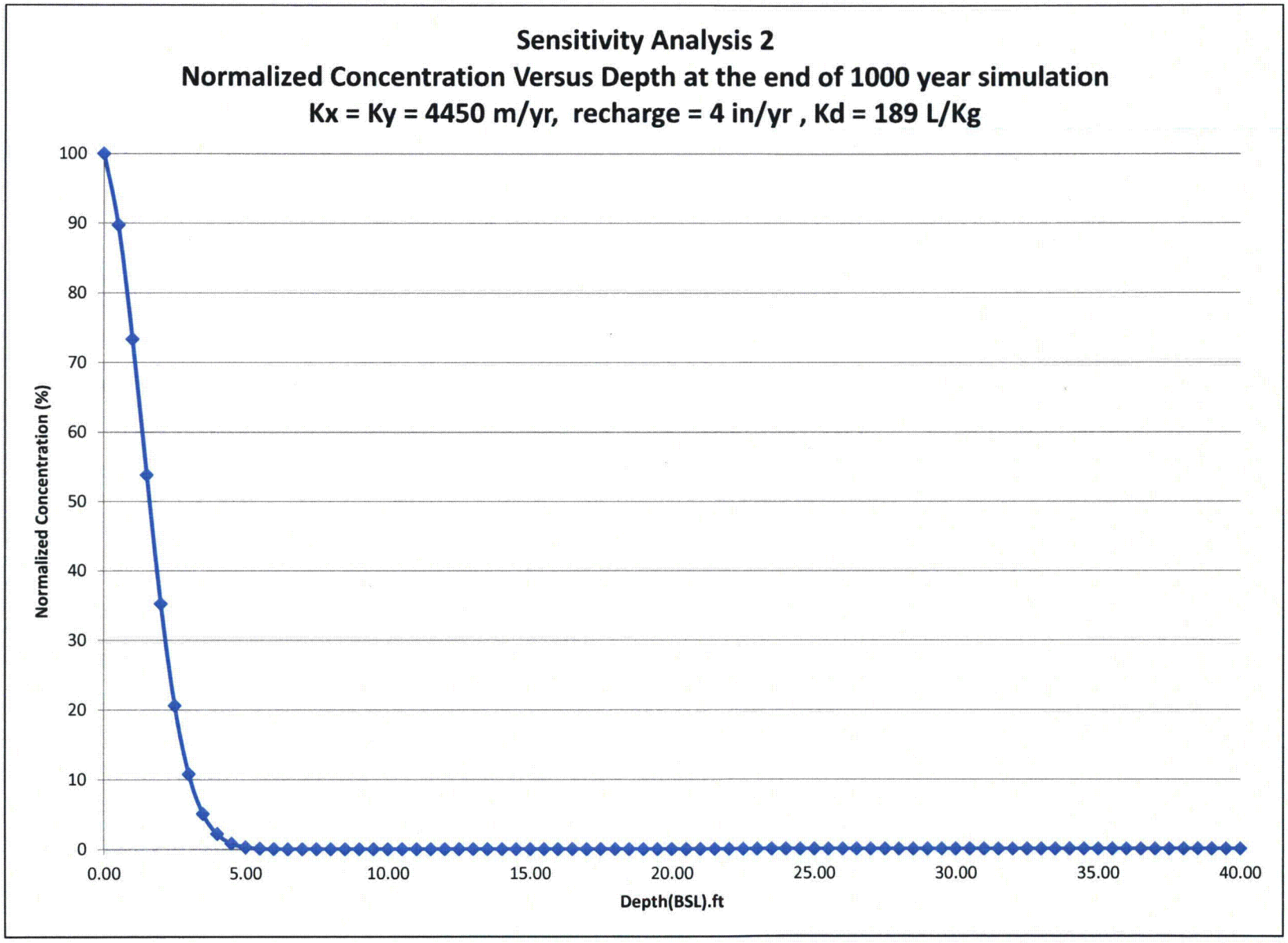
Sensitivity Analysis 2
Normalized Concentration Versus Depth at the end of 1000 year simulation
Kx = Ky = 4450 m/yr, recharge = 4 in/yr , Kd = 189 L/Kg
Normalized Concentration (%)
100
90
80
70
60
50
40
30
20
10
0
0.00
5.00
10.00
15.00
20.00
25.00
30.00
35.00
40.00
Depth(BSL).ft

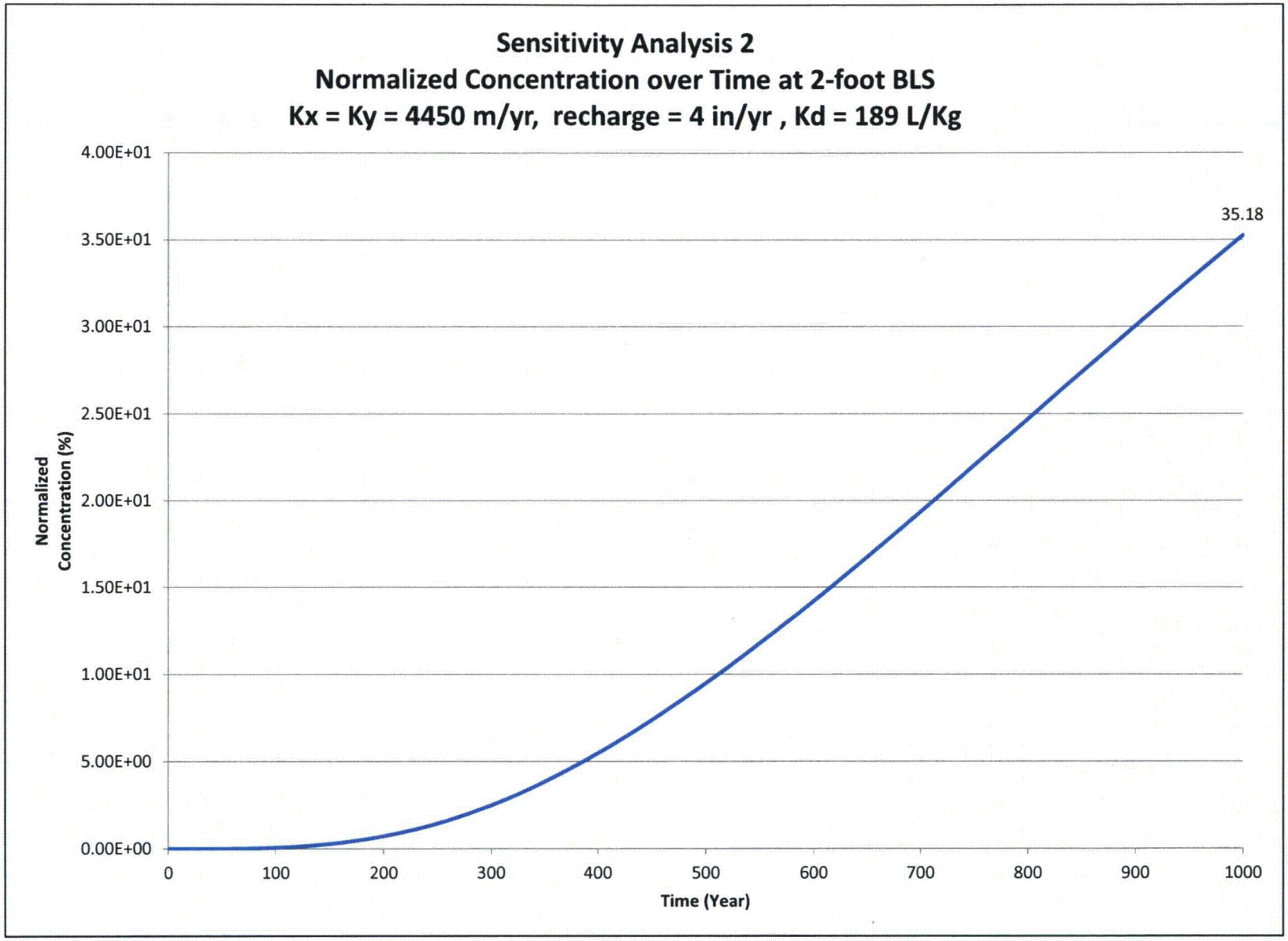
Sensitivity Analysis 2
Normalized Concentration over Time at 2-foot BLS
Kx = Ky = 4450 m/yr, recharge = 4 in/yr , Kd = 189 L/Kg
Normalized Concentration (%)
4.00E+01
3.50E+01
3.00E+01
2.50E+01
2.00E+01
1.50E+01
1.00E+01
5.00E+00
0.00E+00
35.18
0
100
200
300
400
500
600
700
800
900
1000
Time (Year)

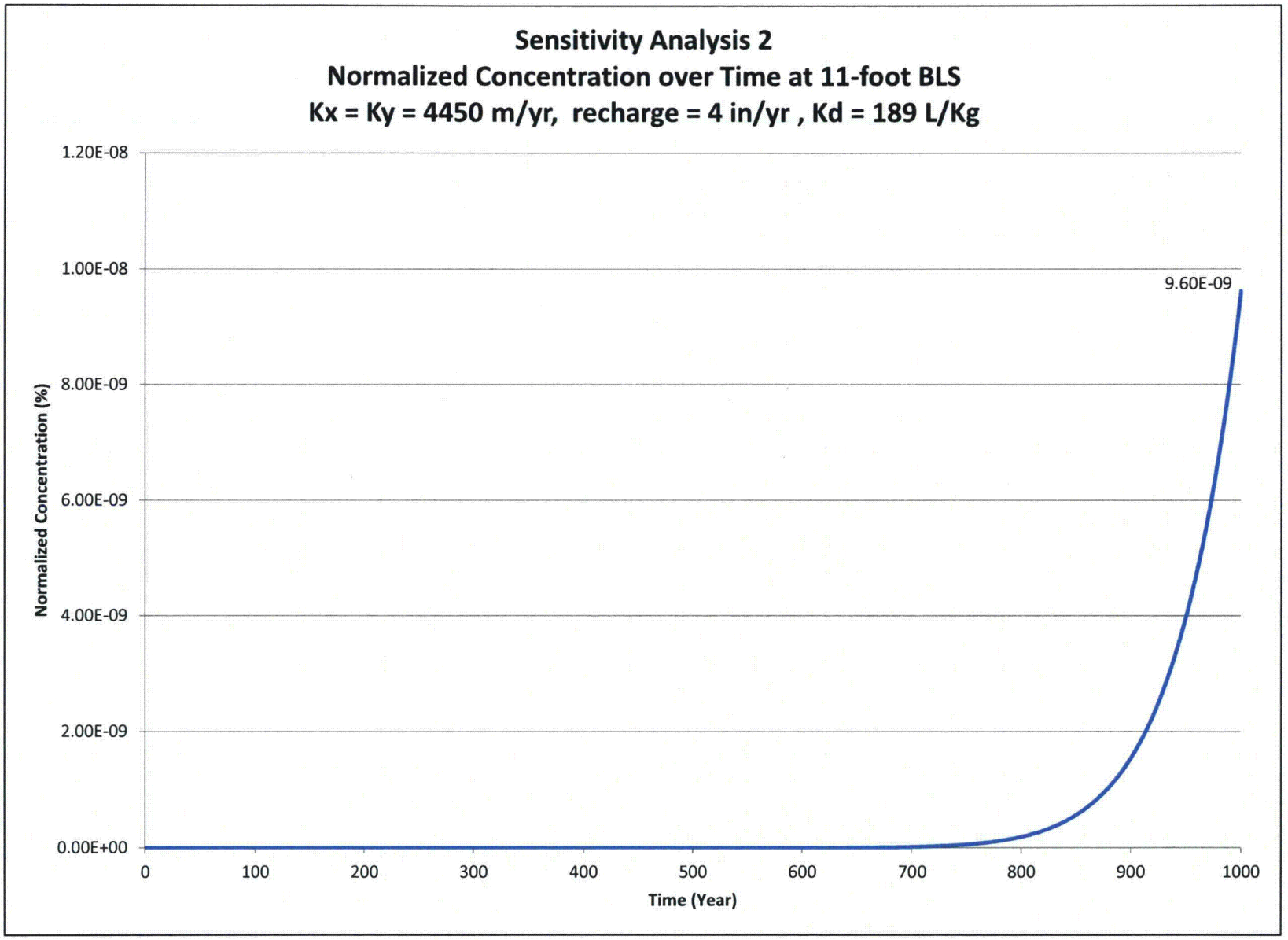
Sensitivity Analysis 2
Normalized Concentration over Time at 11-foot BLS
Kx = Ky = 4450 m/yr, recharge = 4 in/yr , Kd = 189 L/Kg
Normalized Concentration (%)
1.20E-08
1.00E-08
8.00E-09
6.00E-09
4.00E-09
2.00E-09
0.00E+00
9.60E-09
0
100
200
300
400
500
600
700
800
900
1000
Time (Year)

Sensitivity Analysis 3		
Sensitivity Run	**Summary description**	**Purpose/objective**
3	Baseline properties except for K; reduce K to lower end of published K for loess/soil types to 2.2 m/yr; note this is still above the low end range of 0.15 m/yr from slug testing where we were able to determine results (recall that several tested wells did not respond rapidly enough to allow K wells is therefore expected to be lower than 0.15 m/yr)	Assess potential for leaching through soil column at lower end of published range of hydraulic conductivity for soil types at JPG. This run is mainly to demonstrate extent of migration at the lower end of representative hydraulic conductivity values.

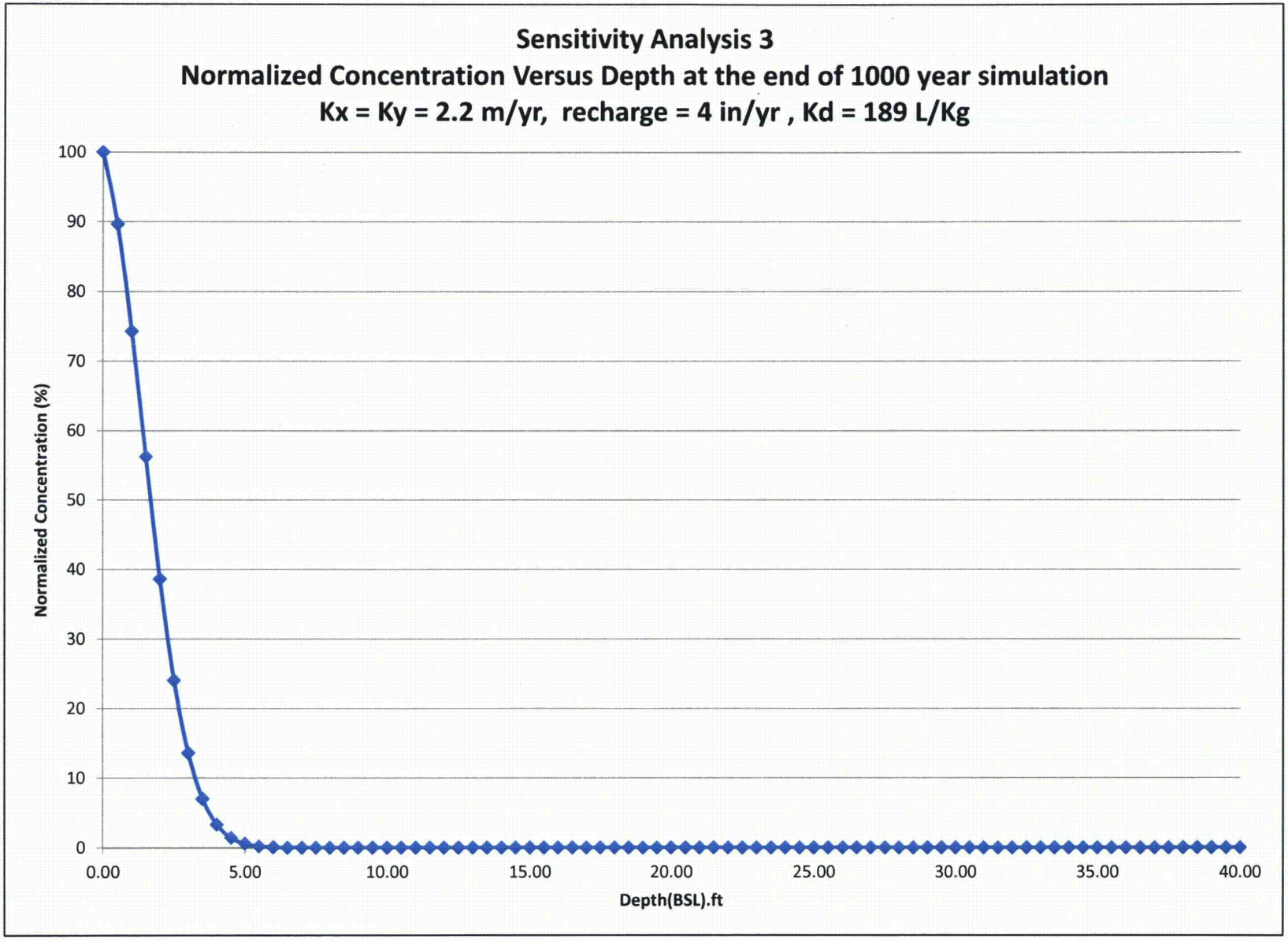
Sensitivity Analysis 3
Normalized Concentration Versus Depth at the end of 1000 year simulation
Kx = Ky = 2.2 m/yr, recharge = 4 in/yr , Kd = 189 L/Kg
Normalized Concentration (%)
100
90
80
70
60
50
40
30
20
10
0
0.00
5.00
10.00
15.00
20.00
25.00
30.00
35.00
40.00
Depth(BSL).ft

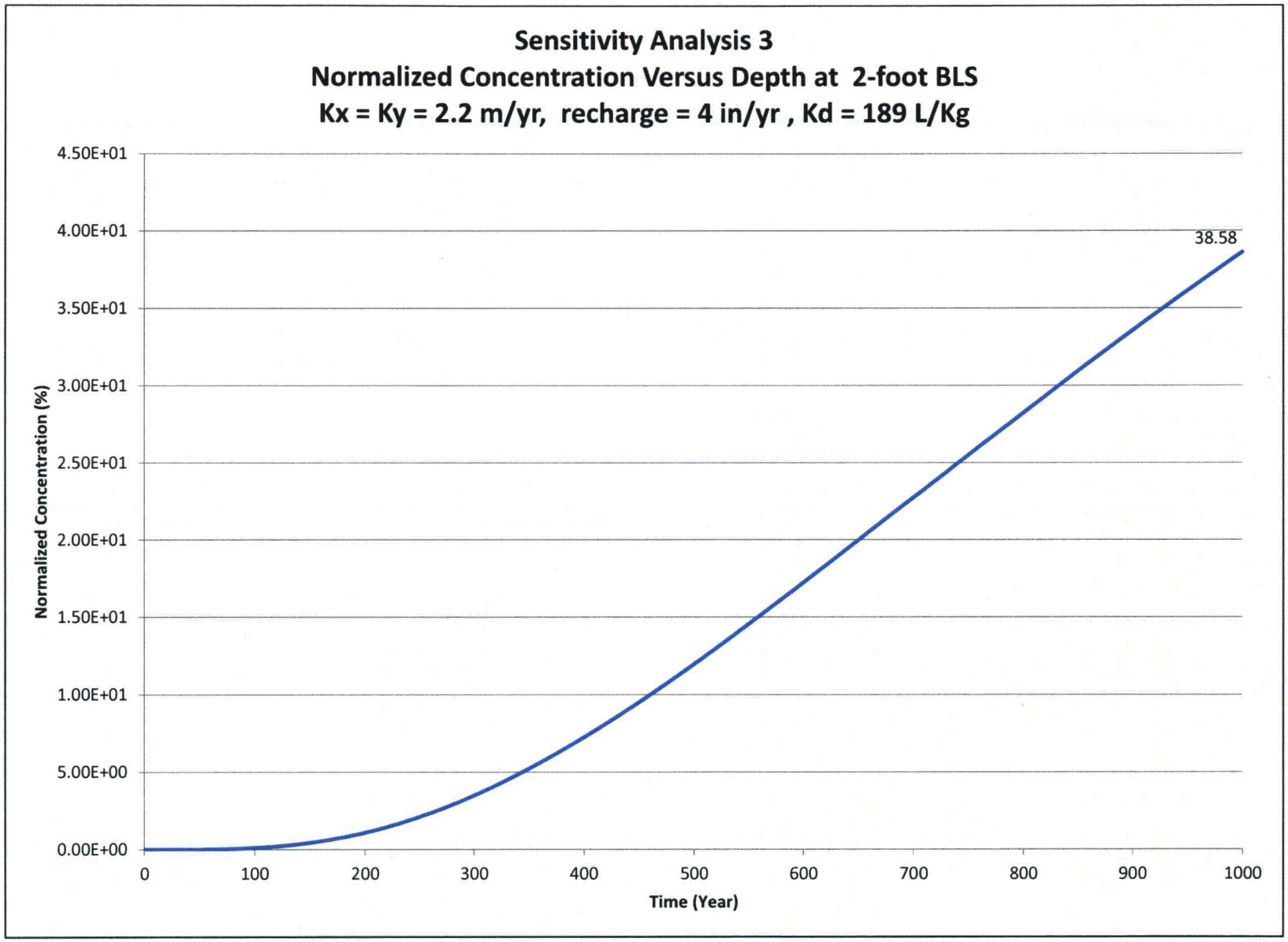
Sensitivity Analysis 3
Normalized Concentration Versus Depth at 2-foot BLS
Kx = Ky = 2.2 m/yr, recharge = 4 in/yr , Kd = 189 L/Kg
Normalized Concentration (%)
4.50E+01
4.00E+01
3.50E+01
3.00E+01
2.50E+01
2.00E+01
1.50E+01
1.00E+01
5.00E+00
0.00E+00
38.58
0
100
200
300
400
500
600
700
800
900
1000
Time (Year)

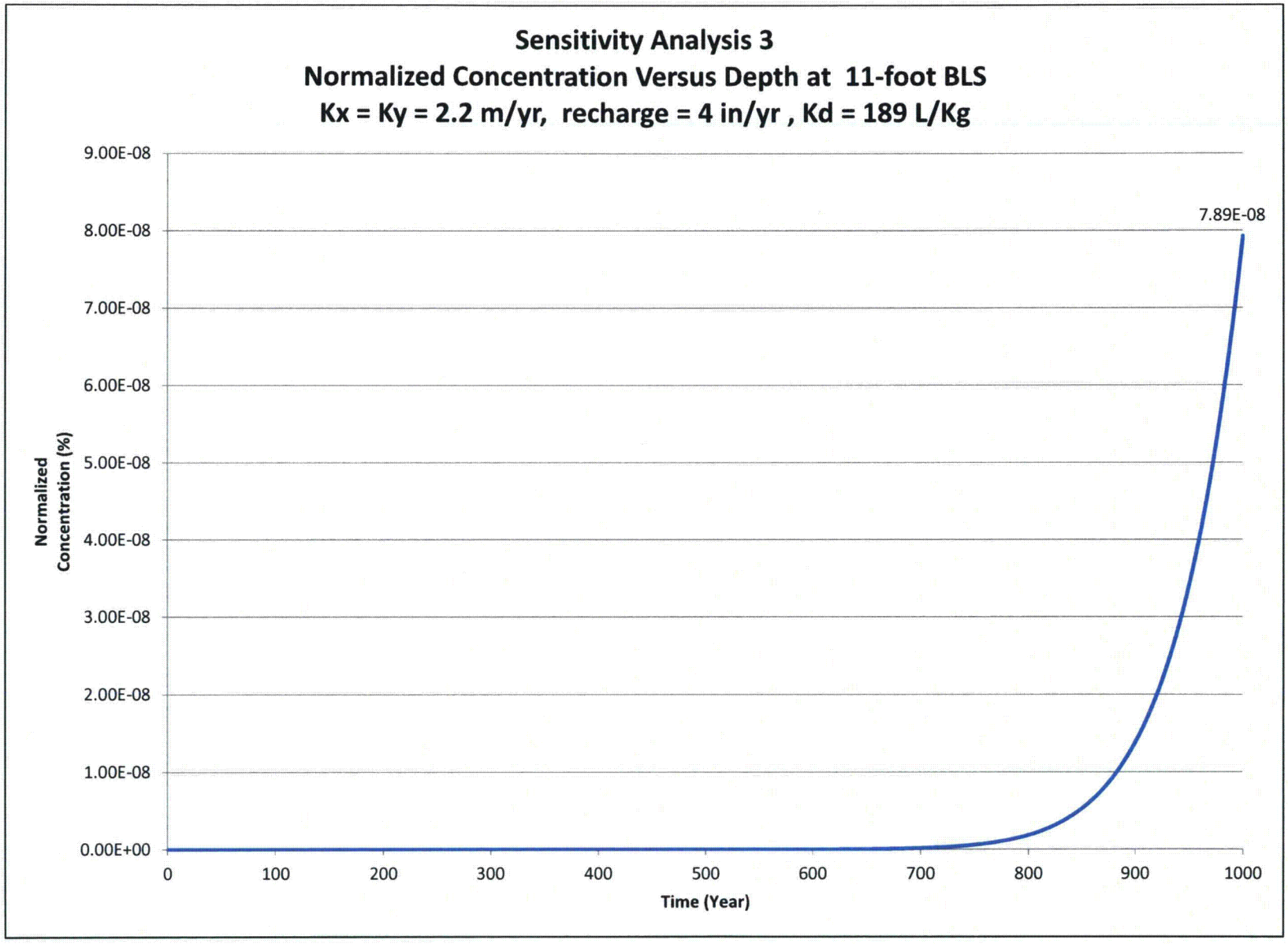
Sensitivity Analysis 3
Normalized Concentration Versus Depth at 11-foot BLS
Kx = Ky = 2.2 m/yr, recharge = 4 in/yr , Kd = 189 L/Kg
9.00E-08
8.00E-08
7.00E-08
6.00E-08
5.00E-08
4.00E-08
3.00E-08
2.00E-08
1.00E-08
0.00E+00
Normalized Concentration (%)
7.89E-08
0
100
200
300
400
500
600
700
800
900
1000
Time (Year)

Sensitivity Analysis 4		
Sensitivity Run	**Summary description**	**Purpose/objective**
4	Baseline properties except for recharge; increase recharge to 12 inches per year	Assess potential for leaching to groundwater under increased recharge conditions

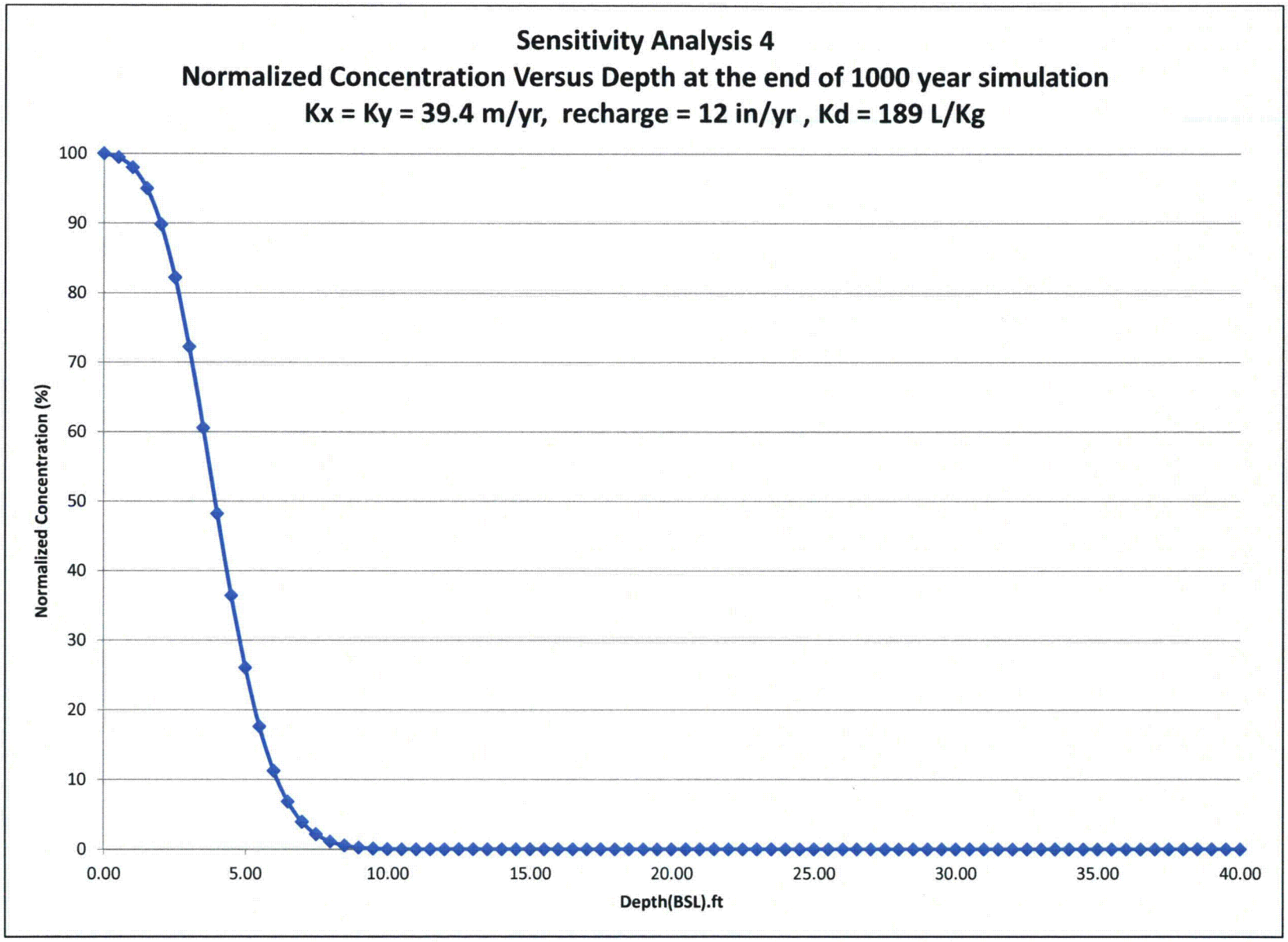
Sensitivity Analysis 4
Normalized Concentration Versus Depth at the end of 1000 year simulation
Kx = Ky = 39.4 m/yr, recharge = 12 in/yr , Kd = 189 L/Kg
Normalized Concentration (%)
100
90
80
70
60
50
40
30
20
10
0
0.00
5.00
10.00
15.00
20.00
25.00
30.00
35.00
40.00
Depth(BSL).ft

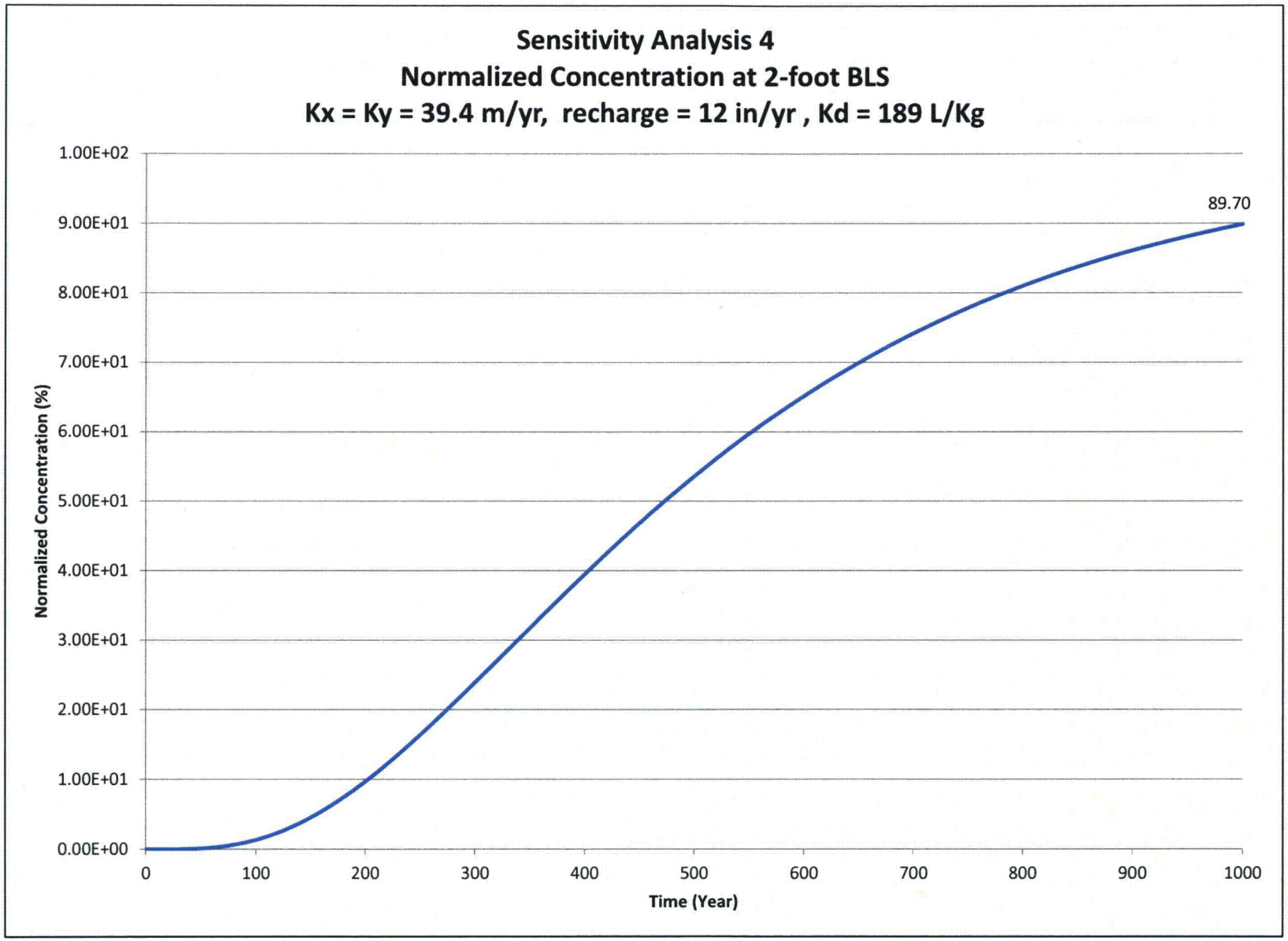
Sensitivity Analysis 4
Normalized Concentration at 2-foot BLS
Kx = Ky = 39.4 m/yr, recharge = 12 in/yr , Kd = 189 L/Kg
Normalized Concentration (%)
1.00E+02
9.00E+01
8.00E+01
7.00E+01
6.00E+01
5.00E+01
4.00E+01
3.00E+01
2.00E+01
1.00E+01
0.00E+00
89.70
0
100
200
300
400
500
600
700
800
900
1000
Time (Year)

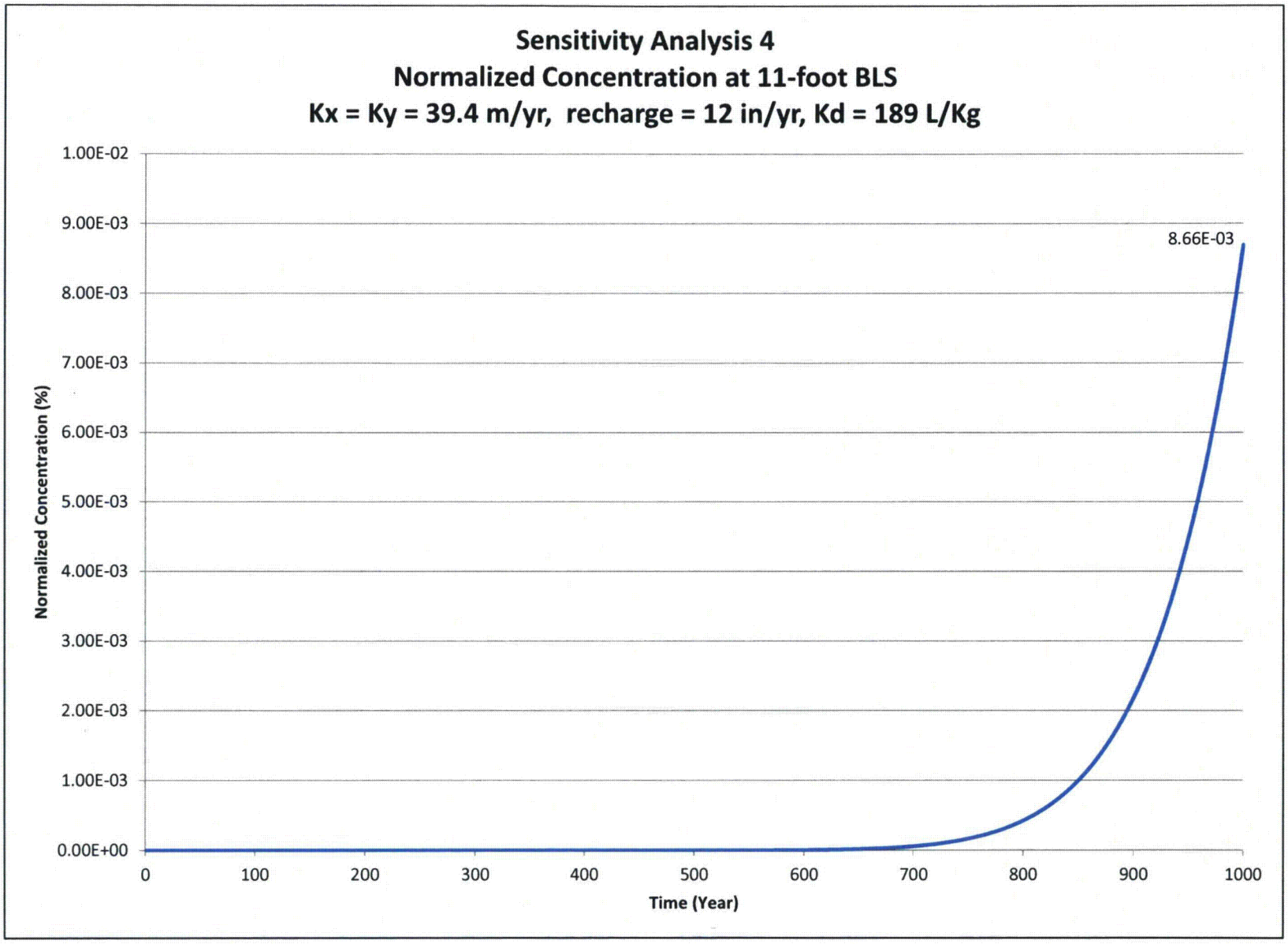
Sensitivity Analysis 4
Normalized Concentration at 11-foot BLS
Kx = Ky = 39.4 m/yr, recharge = 12 in/yr, Kd = 189 L/Kg
Normalized Concentration (%)
1.00E-02
9.00E-03
8.00E-03
7.00E-03
6.00E-03
5.00E-03
4.00E-03
3.00E-03
2.00E-03
1.00E-03
0.00E+00
8.66E-03
0
100
200
300
400
500
600
700
800
900
1000
Time (Year)

Sensitivity Analysis 5		
Sensitivity Run	**Summary description**	**Purpose/objective**
5	Baseline properties except use Kd of 591 L/Kg to represent Cincinnati-Rossmoyne for column	Assess the potential for leaching to groundwater in soils along drainages where Cincinnati-Rossmoyne soil types dominate. Since the soils are thinner here, we will want to look at predicted results in the upper few feet

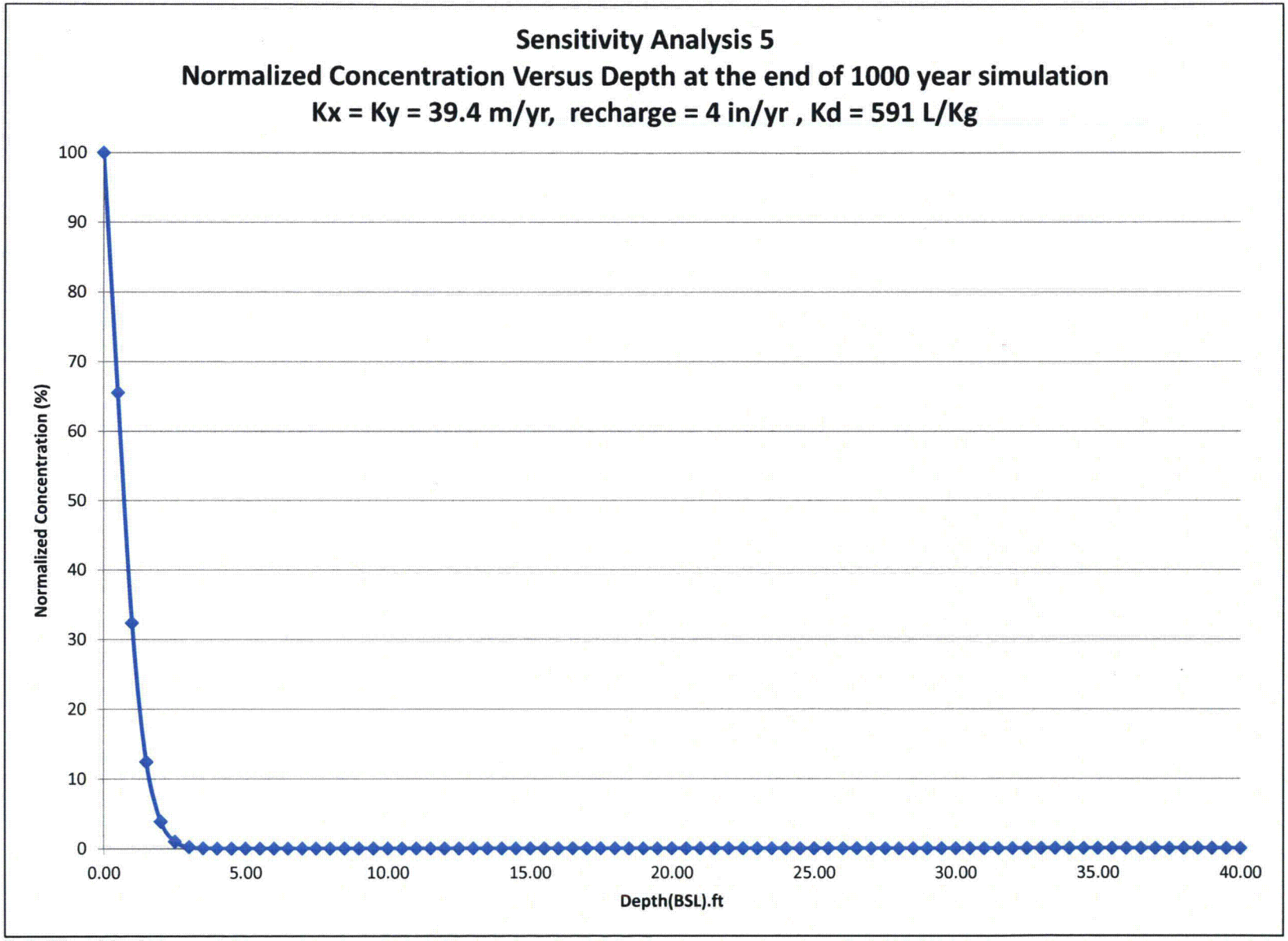
Sensitivity Analysis 5
Normalized Concentration Versus Depth at the end of 1000 year simulation
Kx = Ky = 39.4 m/yr, recharge = 4 in/yr , Kd = 591 L/Kg
Normalized Concentration (%)
100
90
80
70
60
50
40
30
20
10
0
0.00
5.00
10.00
15.00
20.00
25.00
30.00
35.00
40.00
Depth(BSL).ft

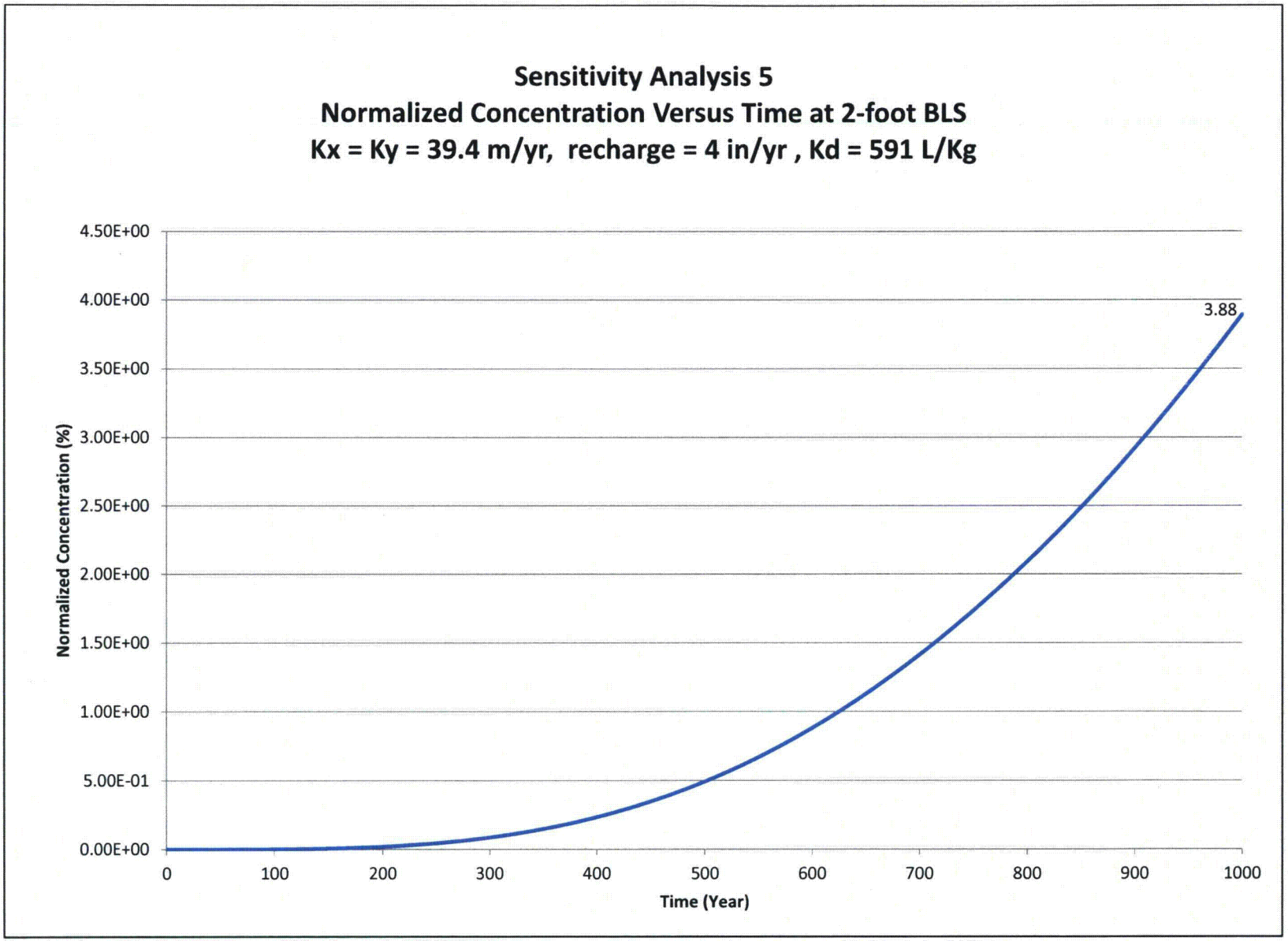
Sensitivity Analysis 5
Normalized Concentration Versus Time at 2-foot BLS
Kx = Ky = 39.4 m/yr, recharge = 4 in/yr , Kd = 591 L/Kg
Normalized Concentration (%)
4.50E+00
4.00E+00
3.50E+00
3.00E+00
2.50E+00
2.00E+00
1.50E+00
1.00E+00
5.00E-01
0.00E+00
3.88
0
100
200
300
400
500
600
700
800
900
1000
Time (Year)

Sensitivity Analysis 6		
Sensitivity Run	**Summary description**	**Purpose/objective**
6	Baseline properties for upper 7.5 feet, Kd 189, K = 39.4 m/yr etc; below 7.5 Kd = 1 L/Kg; K = 48.7 m/yr ; beneath Avonsburg-Cobbsfork soils.	Assess potential leaching groundwater with baseline parameters in upper 7.5 feet beneath Avonsburg-Cobbs Fork.

Major Input Parameters
Sensitivity Analysis 6

For upper 7.5-foot

(1) Van Genuchten parameters for unsaturated flow (Silty Clay Loam ( ))
- Residual liquid saturation = 0.20%
- Maximum liquid saturation = 100%
- Inverse of air entry head = 1.0 per meter

(2) Total porosity = 0.45
(3) Density = 1460 Kg/m3
(4) Hydraulic conductivity
- Kx = Ky = 1.250E-6 m/s (39.4 m/yr); Kz = 1.250E-7 m/s (3.94 m/yr)

(5) Recharge = 4 in/yr
(6) Sorption = 189 L/Kg

For lower 32.5-foot

(1) Van Genuchten parameters for unsaturated flow (Silty Clay ( ))
- Residual liquid saturation = 19%
- Maximum liquid saturation = 100%
- Inverse of air entry head = 0.5 per meter

(2) Total porosity = 0.15
(3) Density = 1920 Kg/m3
(4) Hydraulic conductivity
- Kx = Ky = 1.54E-6 m/s (48.7 m/yr); Kz = 1.54E-7 m/s (4.87 m/yr)

(5) Recharge = 4 in/yr
(6) Sorption = 1 L/Kg

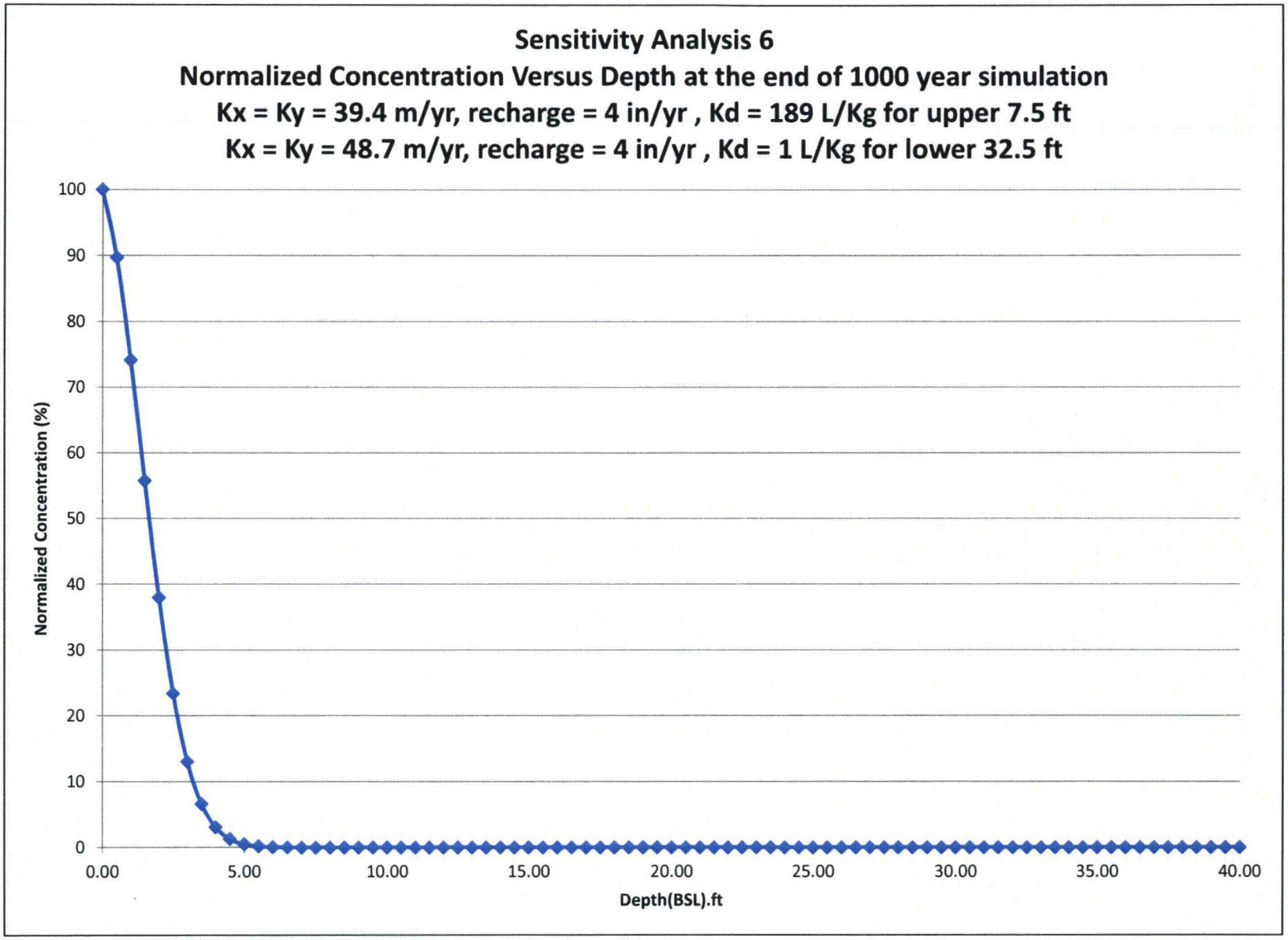
Sensitivity Analysis 6
Normalized Concentration Versus Depth at the end of 1000 year simulation
Kx = Ky = 39.4 m/yr, recharge = 4 in/yr , Kd = 189 L/Kg for upper 7.5 ft
Kx = Ky = 48.7 m/yr, recharge = 4 in/yr , Kd = 1 L/Kg for lower 32.5 ft
Normalized Concentration (%)
100
90
80
70
60
50
40
30
20
10
0
0.00
5.00
10.00
15.00
20.00
25.00
30.00
35.00
40.00
Depth(BSL).ft

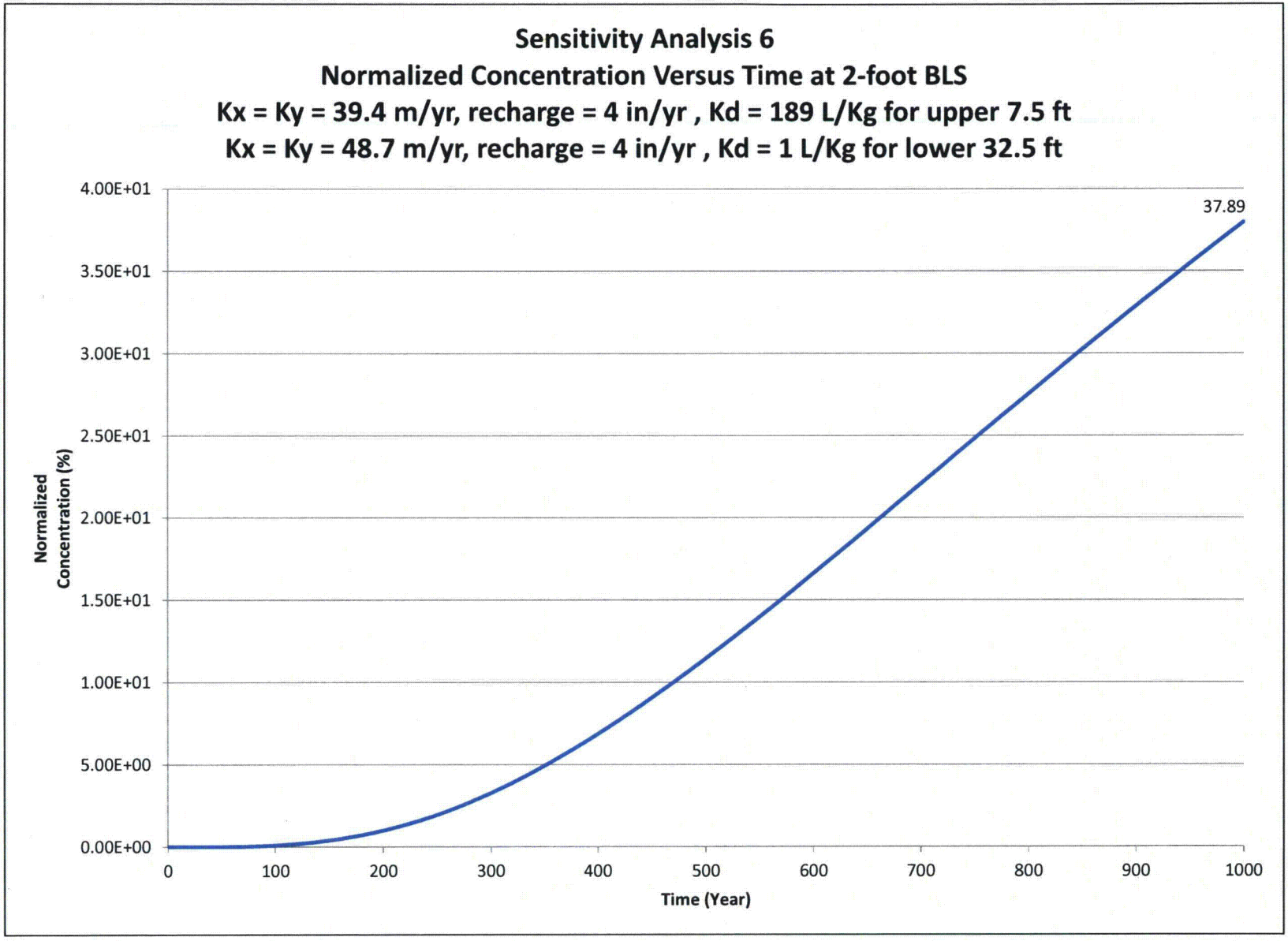
Sensitivity Analysis 6
Normalized Concentration Versus Time at 2-foot BLS
Kx = Ky = 39.4 m/yr, recharge = 4 in/yr , Kd = 189 L/Kg for upper 7.5 ft
Kx = Ky = 48.7 m/yr, recharge = 4 in/yr , Kd = 1 L/Kg for lower 32.5 ft
Normalized Concentration (%)
4.00E+01
3.50E+01
3.00E+01
2.50E+01
2.00E+01
1.50E+01
1.00E+01
5.00E+00
0.00E+00
37.89
0
100
200
300
400
500
600
700
800
900
1000
Time (Year)

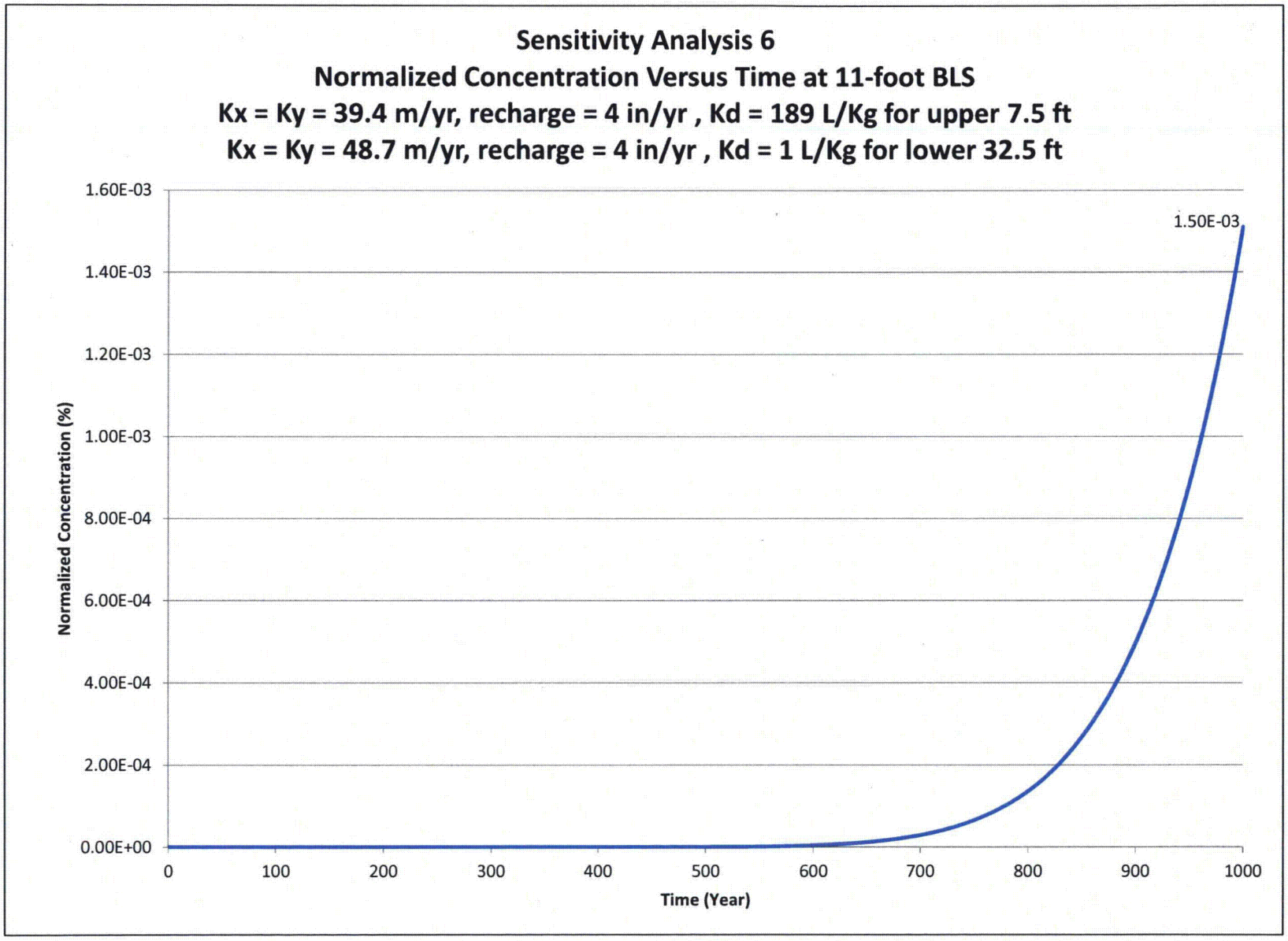
Sensitivity Analysis 6
Normalized Concentration Versus Time at 11-foot BLS
Kx = Ky = 39.4 m/yr, recharge = 4 in/yr , Kd = 189 L/Kg for upper 7.5 ft
Kx = Ky = 48.7 m/yr, recharge = 4 in/yr , Kd = 1 L/Kg for lower 32.5 ft
Normalized Concentration (%)
1.60E-03
1.40E-03
1.20E-03
1.00E-03
8.00E-04
6.00E-04
4.00E-04
2.00E-04
0.00E+00
1.50E-03
0
100
200
300
400
500
600
700
800
900
1000
Time (Year)

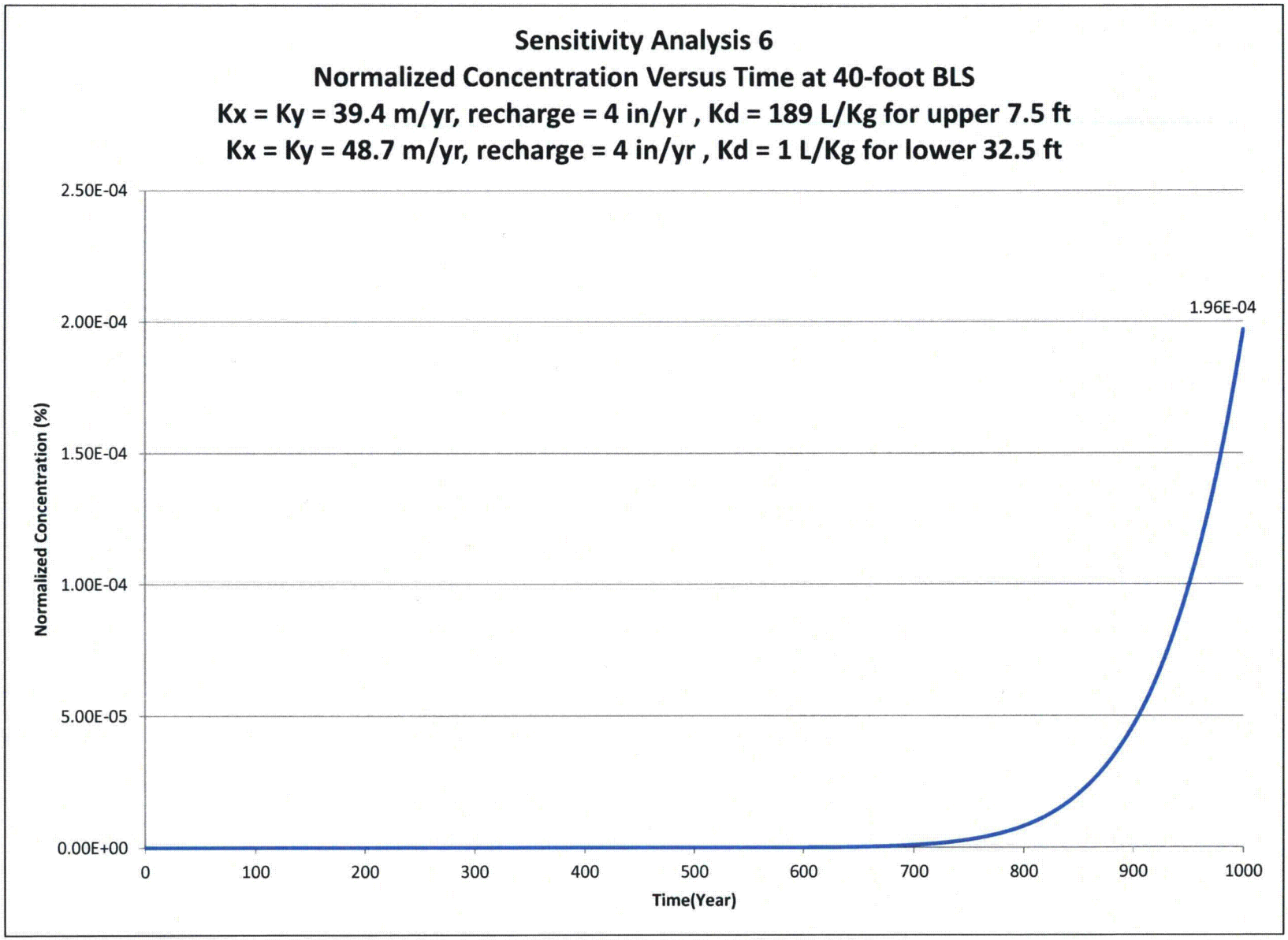
Sensitivity Analysis 6
Normalized Concentration Versus Time at 40-foot BLS
Kx = Ky = 39.4 m/yr, recharge = 4 in/yr , Kd = 189 L/Kg for upper 7.5 ft
Kx = Ky = 48.7 m/yr, recharge = 4 in/yr , Kd = 1 L/Kg for lower 32.5 ft
Normalized Concentration (%)
2.50E-04
2.00E-04
1.50E-04
1.00E-04
5.00E-05
0.00E+00
1.96E-04
0
100
200
300
400
500
600
700
800
900
1000
Time(Year)

ATTACHMENT 3 – GROUNDWATER MODEL SENSITIVITY ANALYSIS

THIS PAGE WAS INTENTIONALLY LEFT BLANK

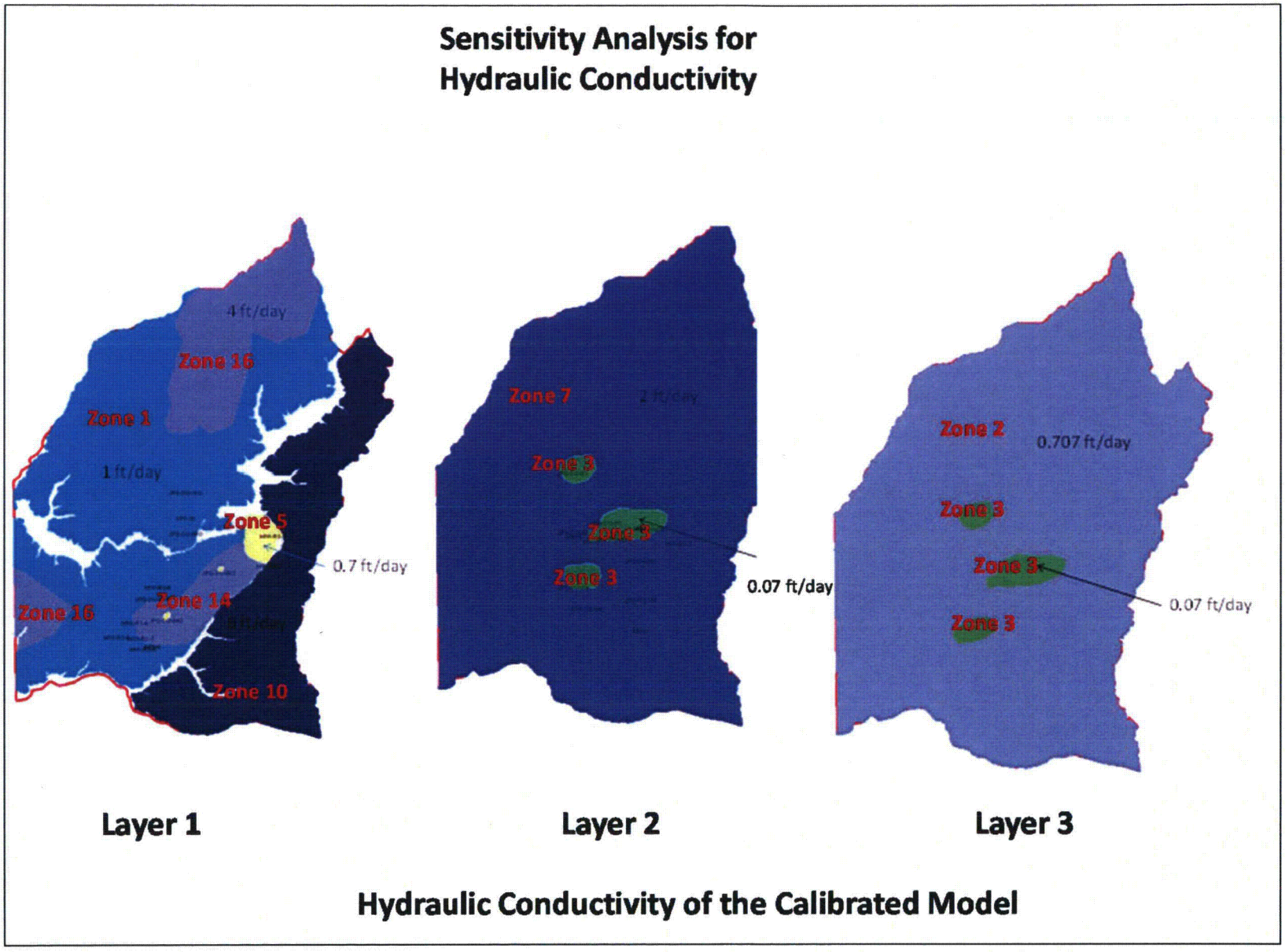
Sensitivity Analysis for
Hydraulic Conductivity
4 ft/day
Zone 16
Zone 1
1 ft/day
Zone 5
0.7 ft/day
Zone 16
Zone 14
Zone 10
Zone 7
Zone 3
Zone 3
Zone 3
0.07 ft/day
Zone 2
0.707 ft/day
Zone 3
Zone 3
0.07 ft/day
Zone 3
Layer 1
Layer 2
Layer 3
Hydraulic Conductivity of the Calibrated Model

Sensitivity Analysis for Horizontal Hydraulic Conductivity

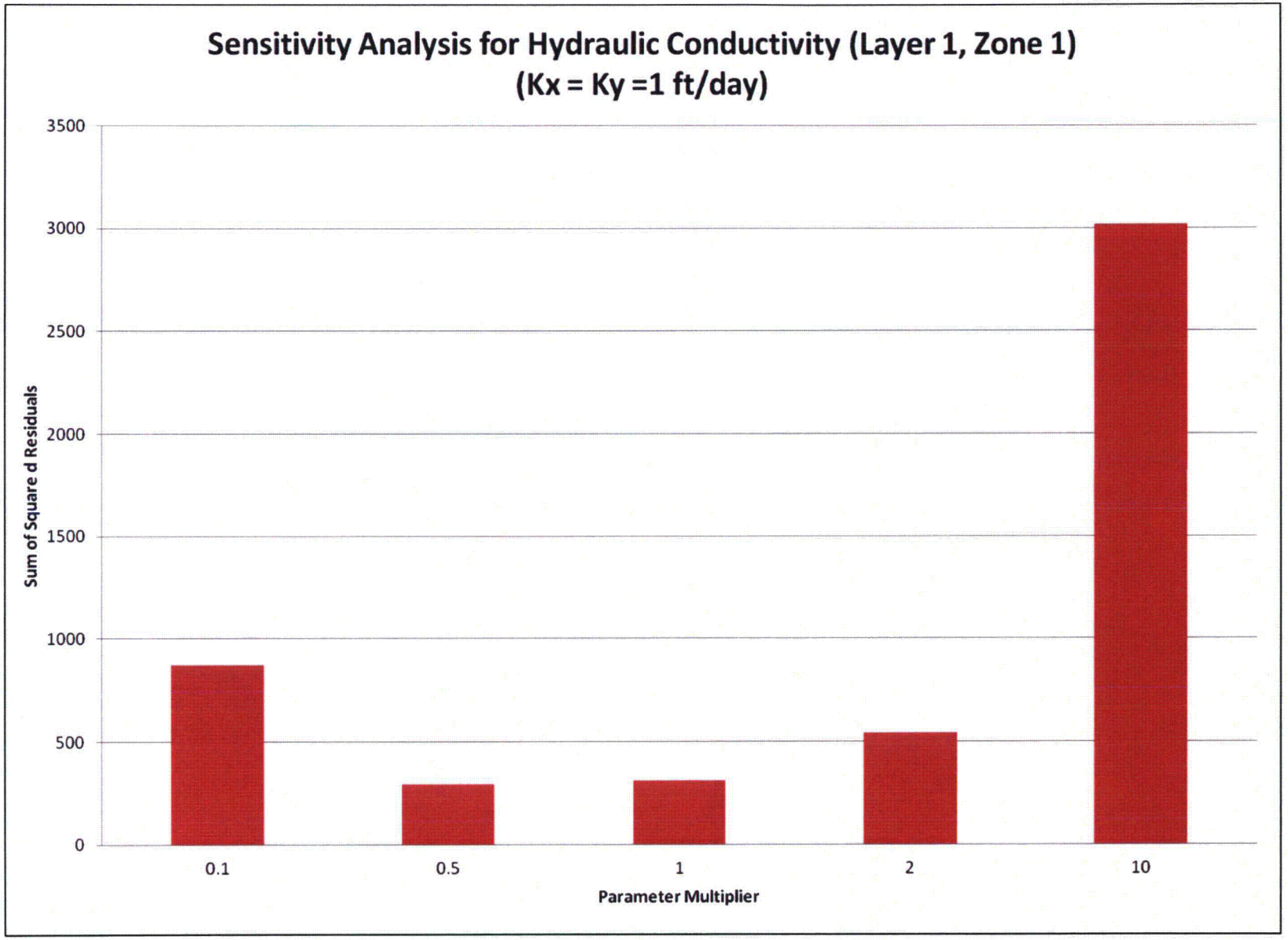
Sensitivity Analysis for Hydraulic Conductivity (Layer 1, Zone 1)
(Kx = Ky =1 ft/day)
Sum of Square d Residuals
3500
3000
2500
2000
1500
1000
500
0
0.1
0.5
1
2
10
Parameter Multiplier

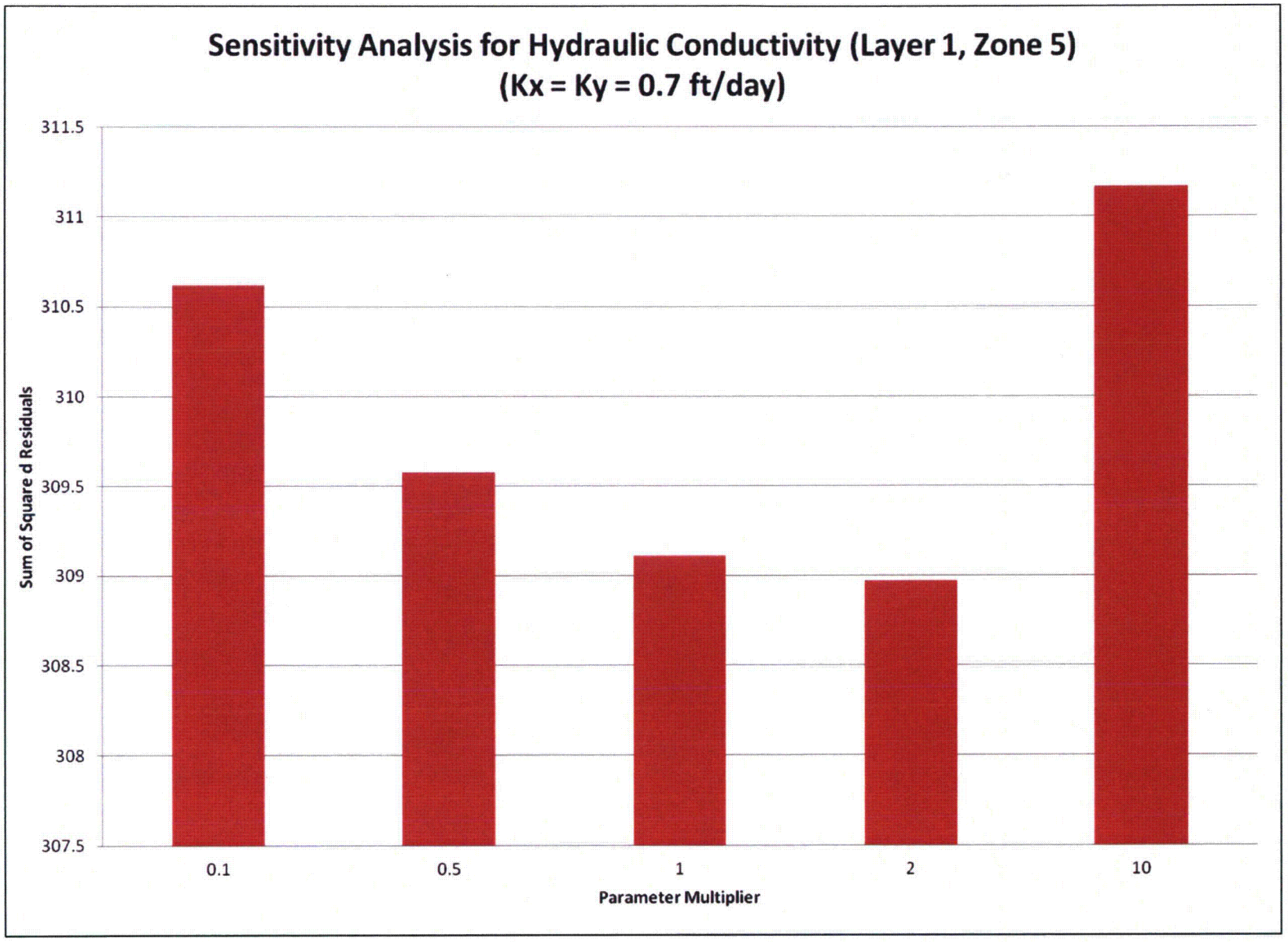
Sensitivity Analysis for Hydraulic Conductivity (Layer 1, Zone 5)
(Kx = Ky = 0.7 ft/day)
Sum of Square d Residuals
311.5
311
310.5
310
309.5
309
308.5
308
307.5
0.1
0.5
1
2
10
Parameter Multiplier

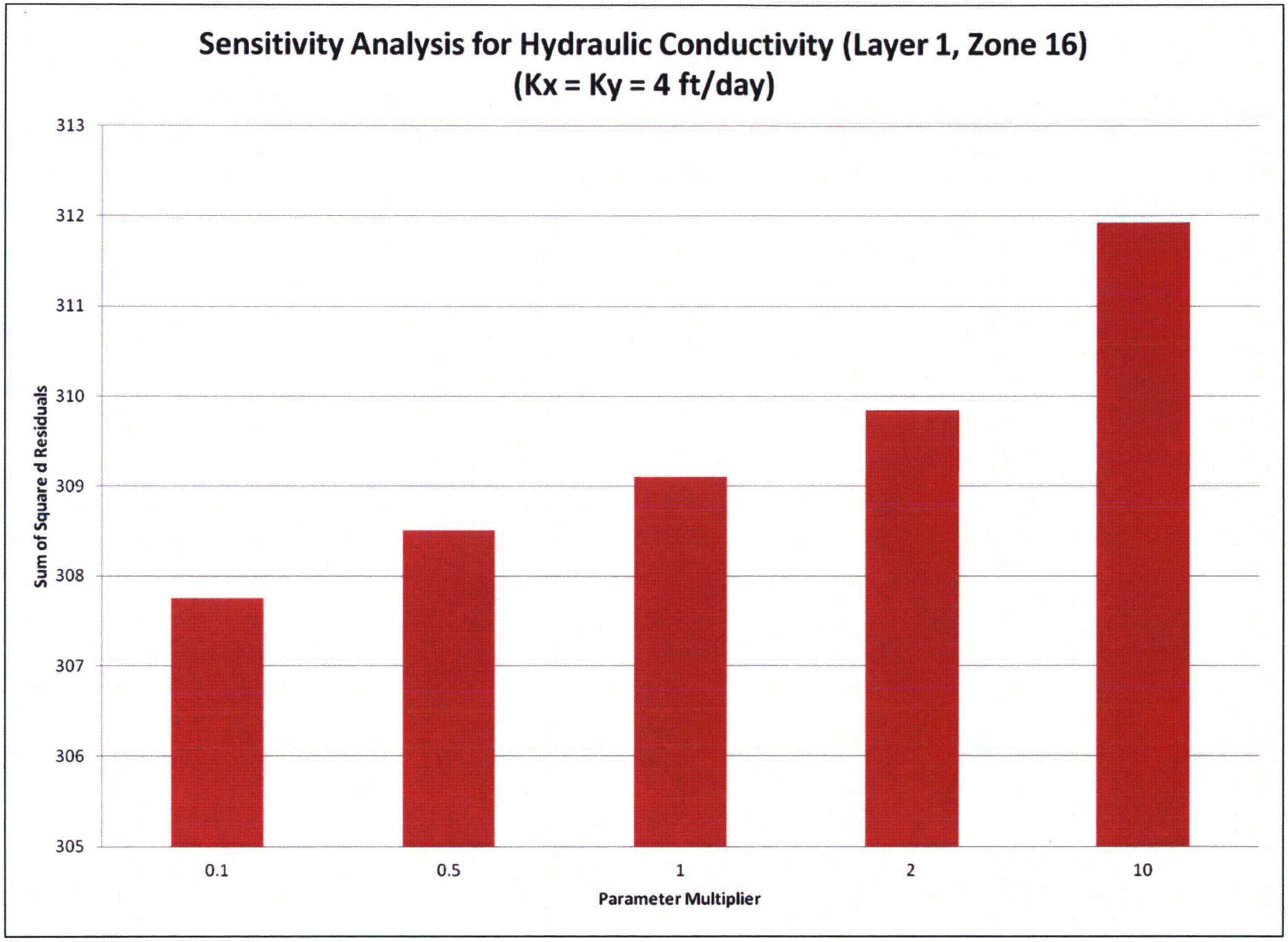
Sensitivity Analysis for Hydraulic Conductivity (Layer 1, Zone 16)
(Kx = Ky = 4 ft/day)
313
312
311
310
309
308
307
306
305
Sum of Square d Residuals
0.1
0.5
1
2
10
Parameter Multiplier

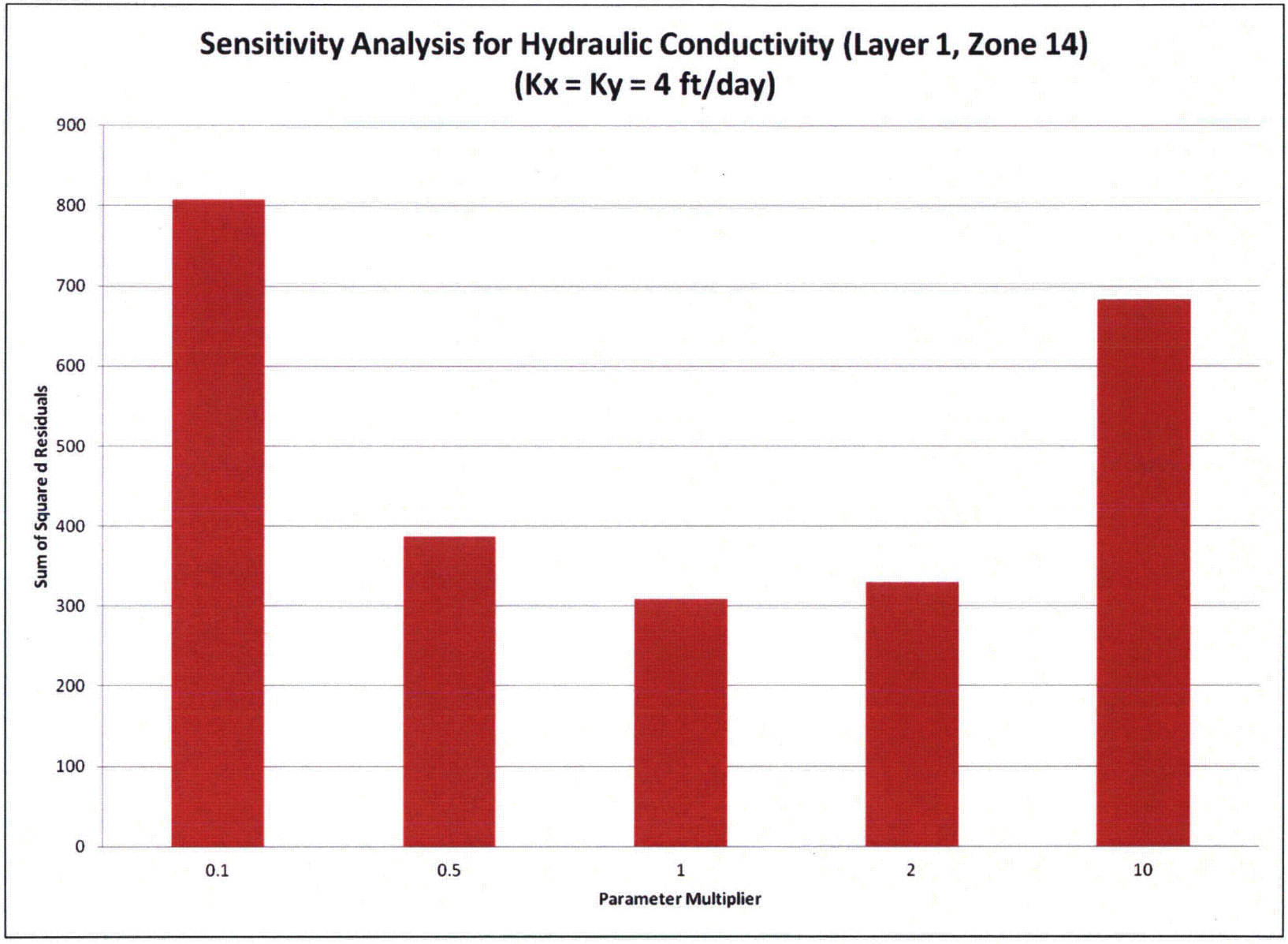
Sensitivity Analysis for Hydraulic Conductivity (Layer 1, Zone 14)
(Kx = Ky = 4 ft/day)
Sum of Square d Residuals
900
800
700
600
500
400
300
200
100
0
0.1
0.5
1
2
10
Parameter Multiplier

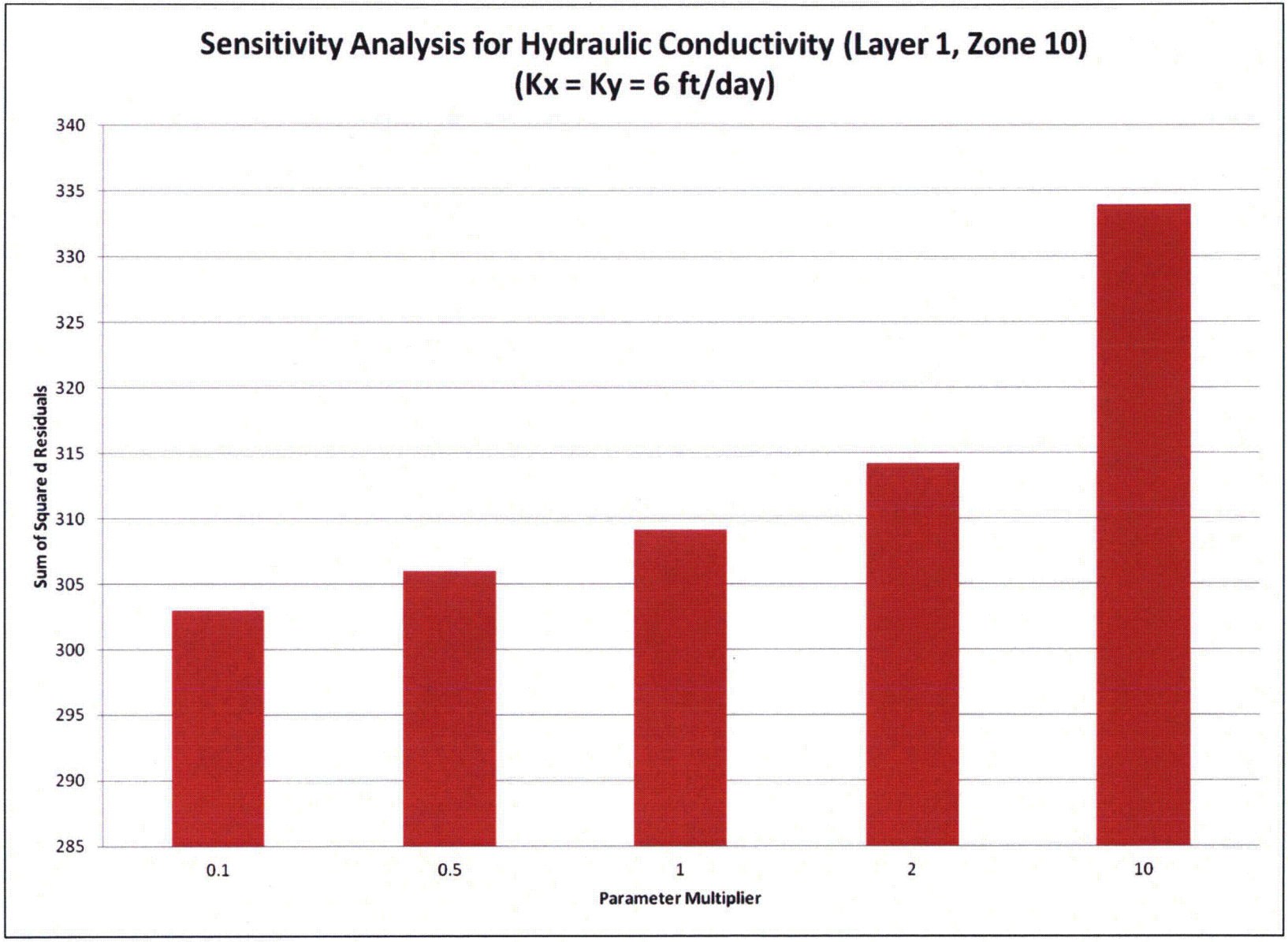
Sensitivity Analysis for Hydraulic Conductivity (Layer 1, Zone 10)
(Kx = Ky = 6 ft/day)
Sum of Square d Residuals
340
335
330
325
320
315
310
305
300
295
290
285
0.1
0.5
1
2
10
Parameter Multiplier

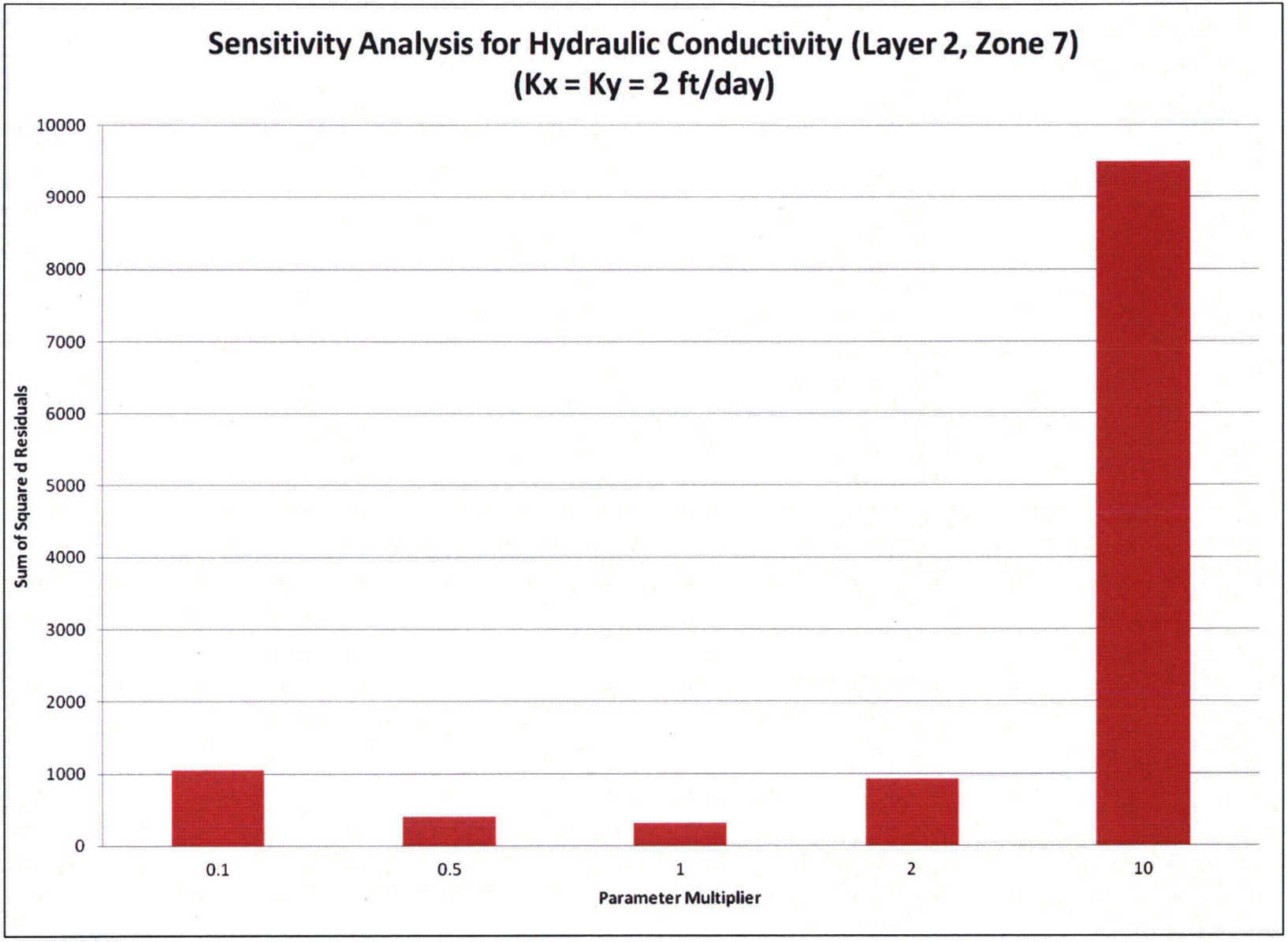
Sensitivity Analysis for Hydraulic Conductivity (Layer 2, Zone 7)
(Kx = Ky = 2 ft/day)
Sum of Square d Residuals
10000
9000
8000
7000
6000
5000
4000
3000
2000
1000
0
0.1
0.5
1
2
10
Parameter Multiplier

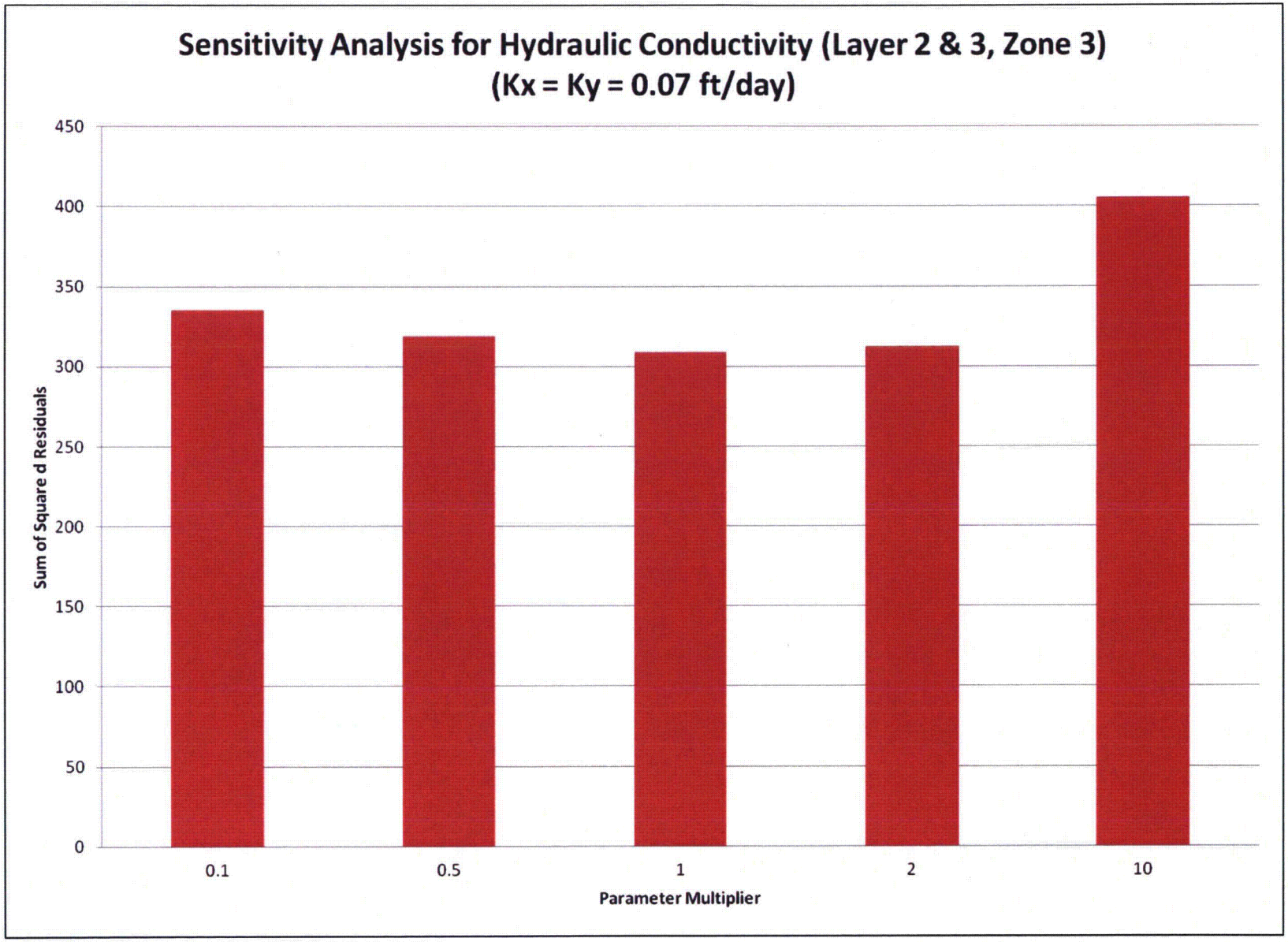
Sensitivity Analysis for Hydraulic Conductivity (Layer 2 & 3, Zone 3)
(Kx = Ky = 0.07 ft/day)
Sum of Square d Residuals
450
400
350
300
250
200
150
100
50
0
0.1
0.5
1
2
10
Parameter Multiplier

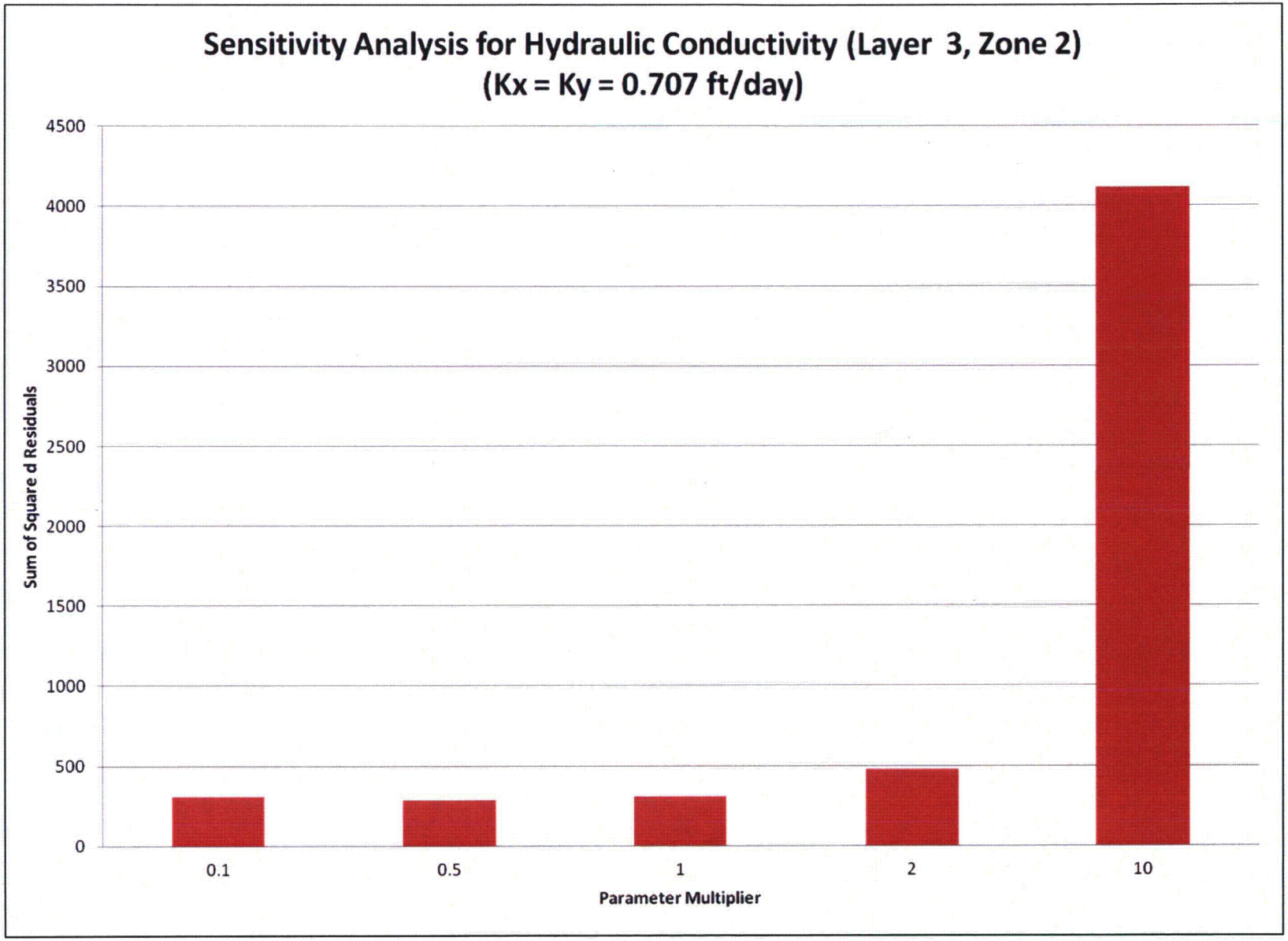
Sensitivity Analysis for Hydraulic Conductivity (Layer 3, Zone 2)
(Kx = Ky = 0.707 ft/day)
Sum of Square d Residuals
4500
4000
3500
3000
2500
2000
1500
1000
500
0
0.1
0.5
1
2
10
Parameter Multiplier

Sensitivity Analysis for Vertical Hydraulic Conductivity

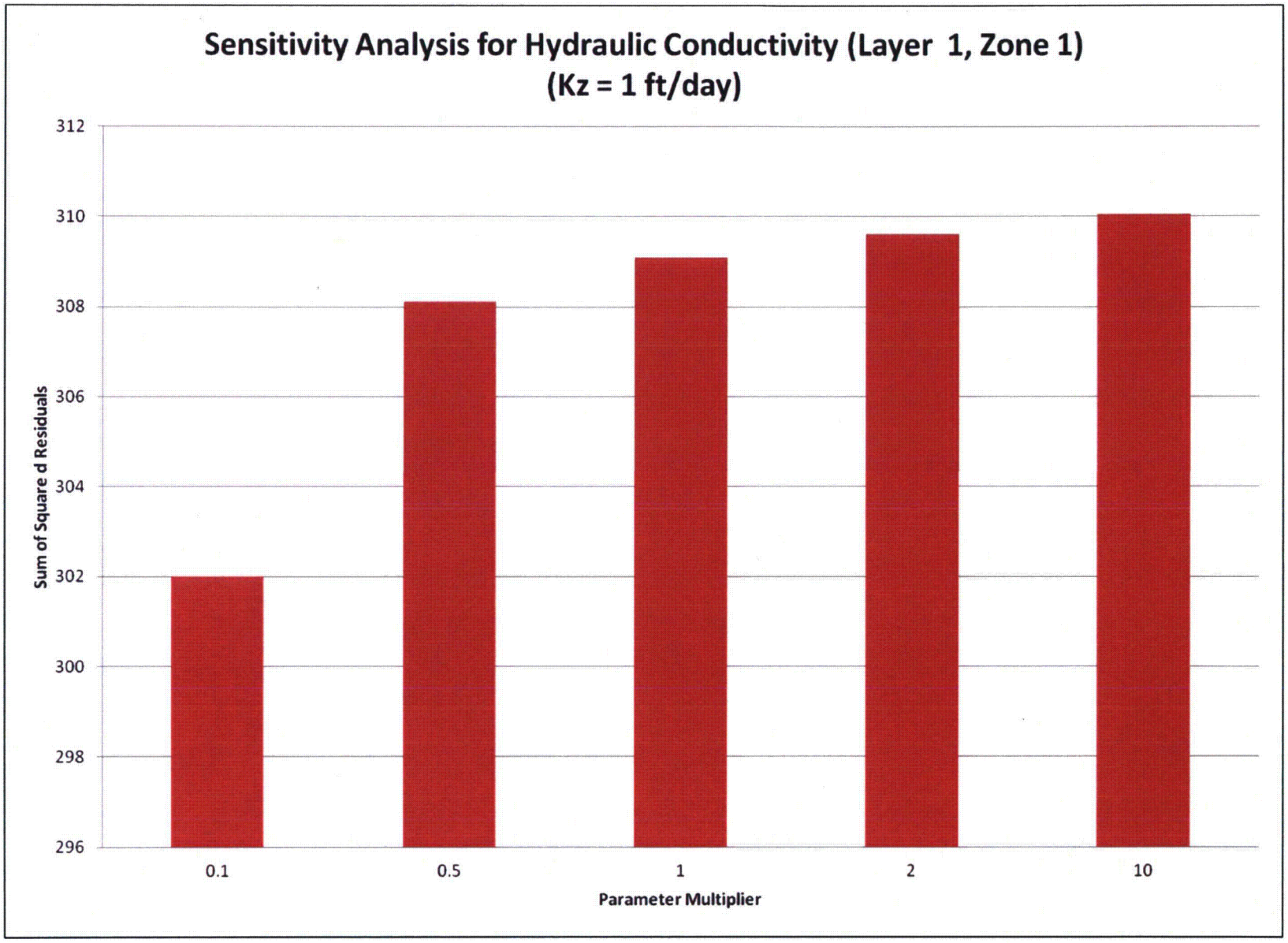
Sensitivity Analysis for Hydraulic Conductivity (Layer 1, Zone 1)
(Kz = 1 ft/day)
Sum of Square d Residuals
312
310
308
306
304
302
300
298
296
0.1
0.5
1
2
10
Parameter Multiplier

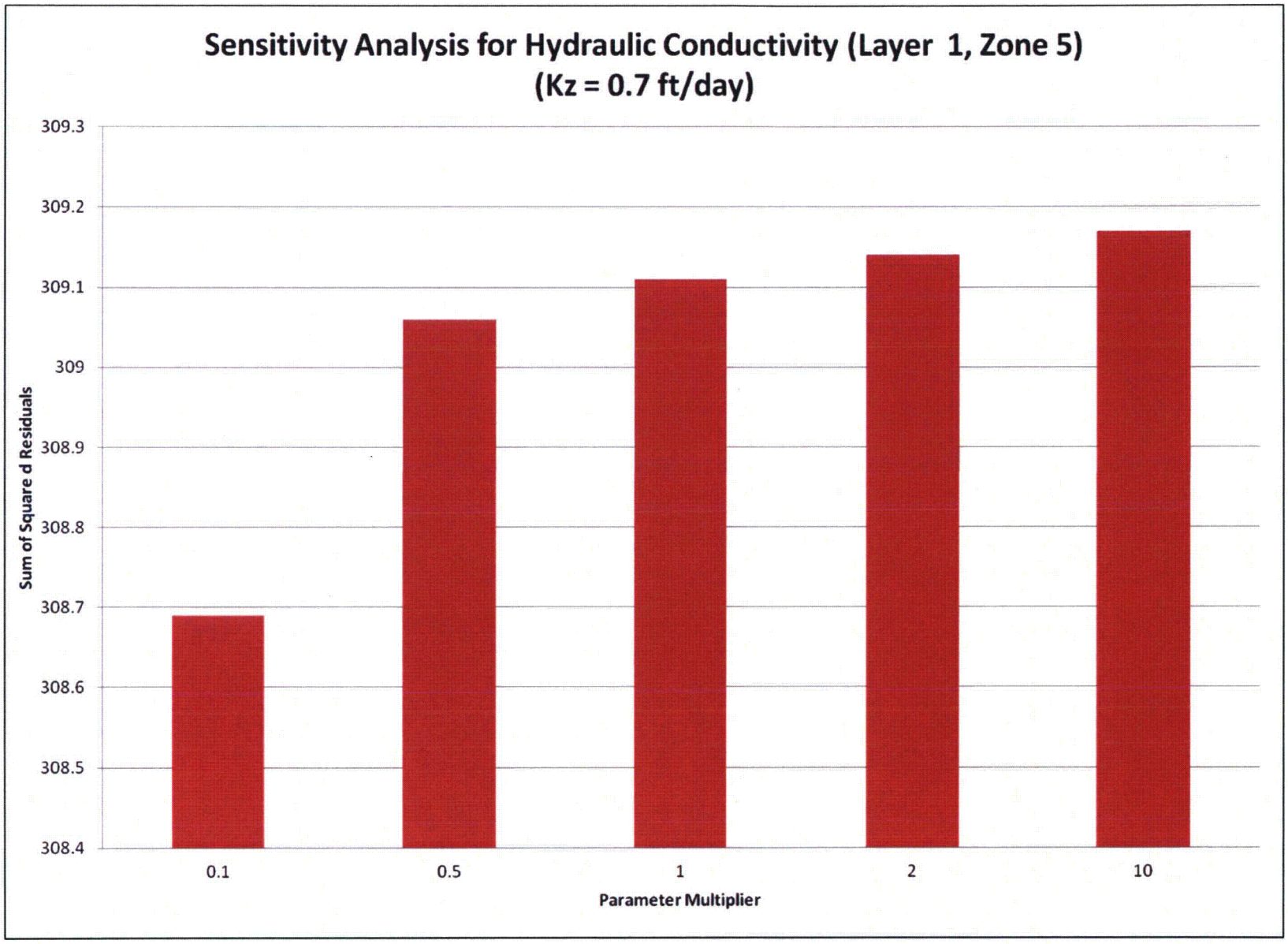
Sensitivity Analysis for Hydraulic Conductivity (Layer 1, Zone 5)
(Kz = 0.7 ft/day)
309.3
309.2
309.1
309
308.9
308.8
308.7
308.6
308.5
308.4
Sum of Square d Residuals
0.1
0.5
1
2
10
Parameter Multiplier

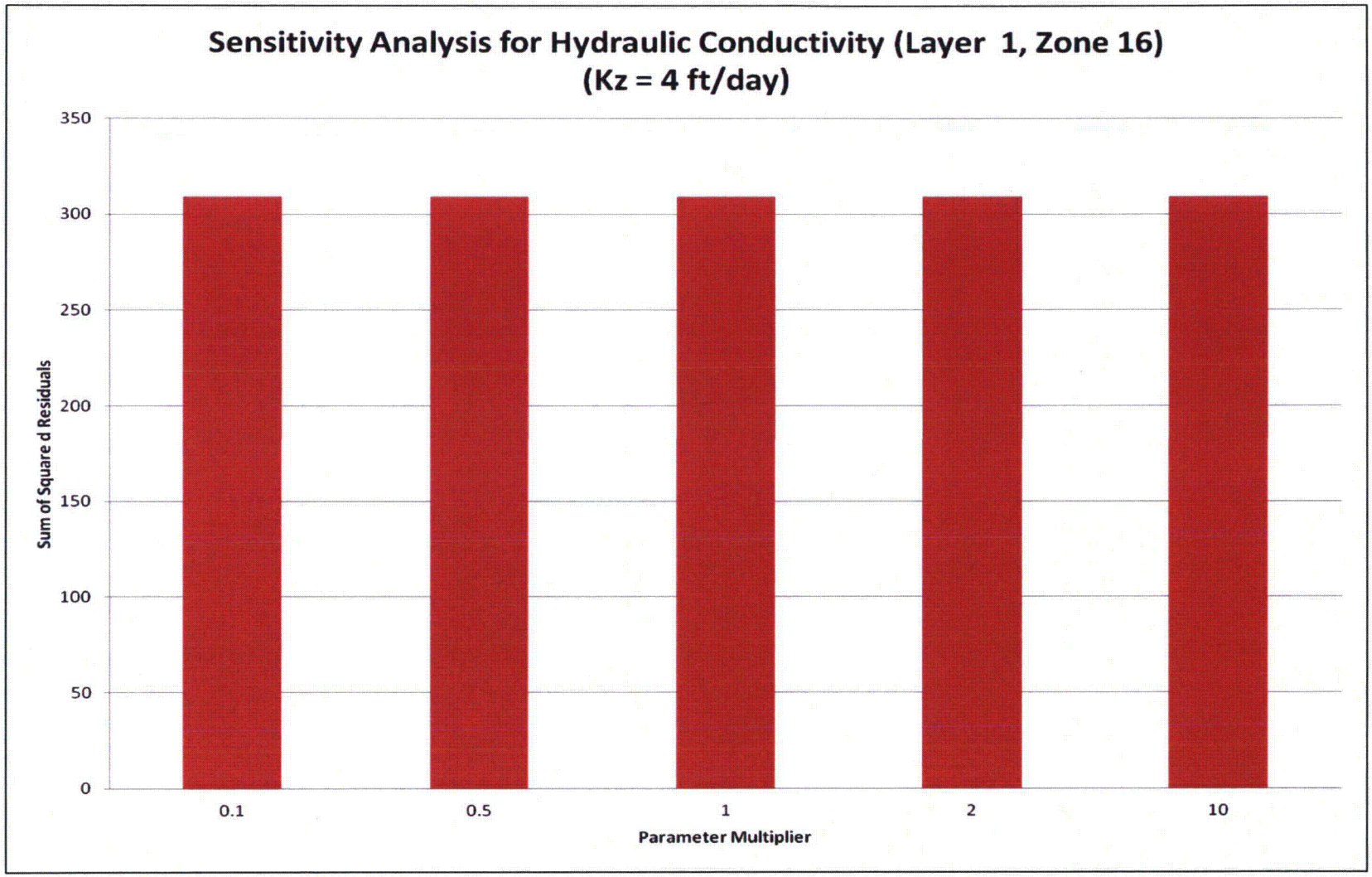
Sensitivity Analysis for Hydraulic Conductivity (Layer 1, Zone 16)
(Kz = 4 ft/day)
Sum of Squared Residuals
350
300
250
200
150
100
50
0
0.1
0.5
1
2
10
Parameter Multiplier

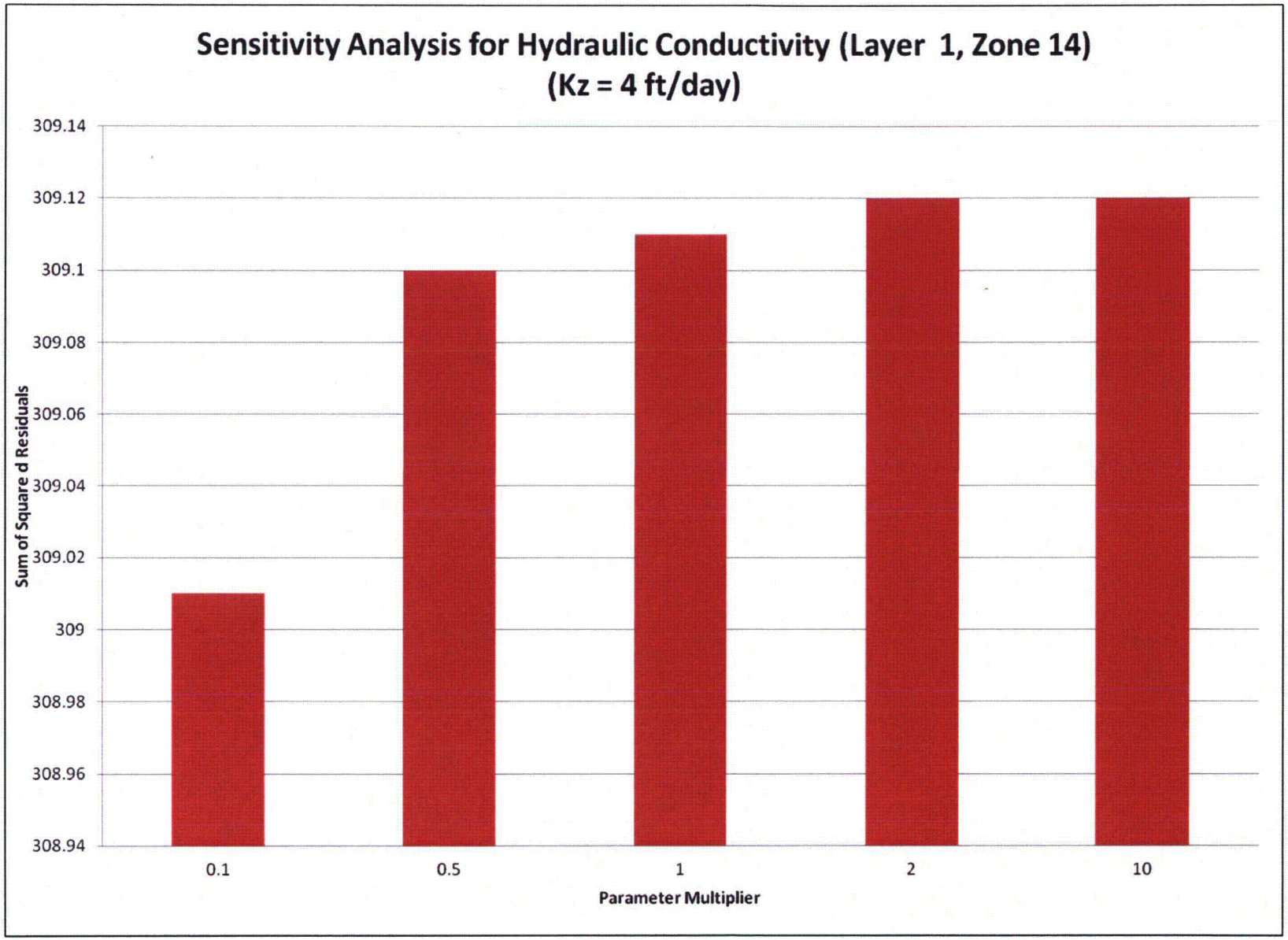
Sensitivity Analysis for Hydraulic Conductivity (Layer 1, Zone 14)
(Kz = 4 ft/day)
309.14
309.12
309.1
309.08
309.06
309.04
309.02
309
308.98
308.96
308.94
Sum of Square d Residuals
0.1
0.5
1
2
10
Parameter Multiplier

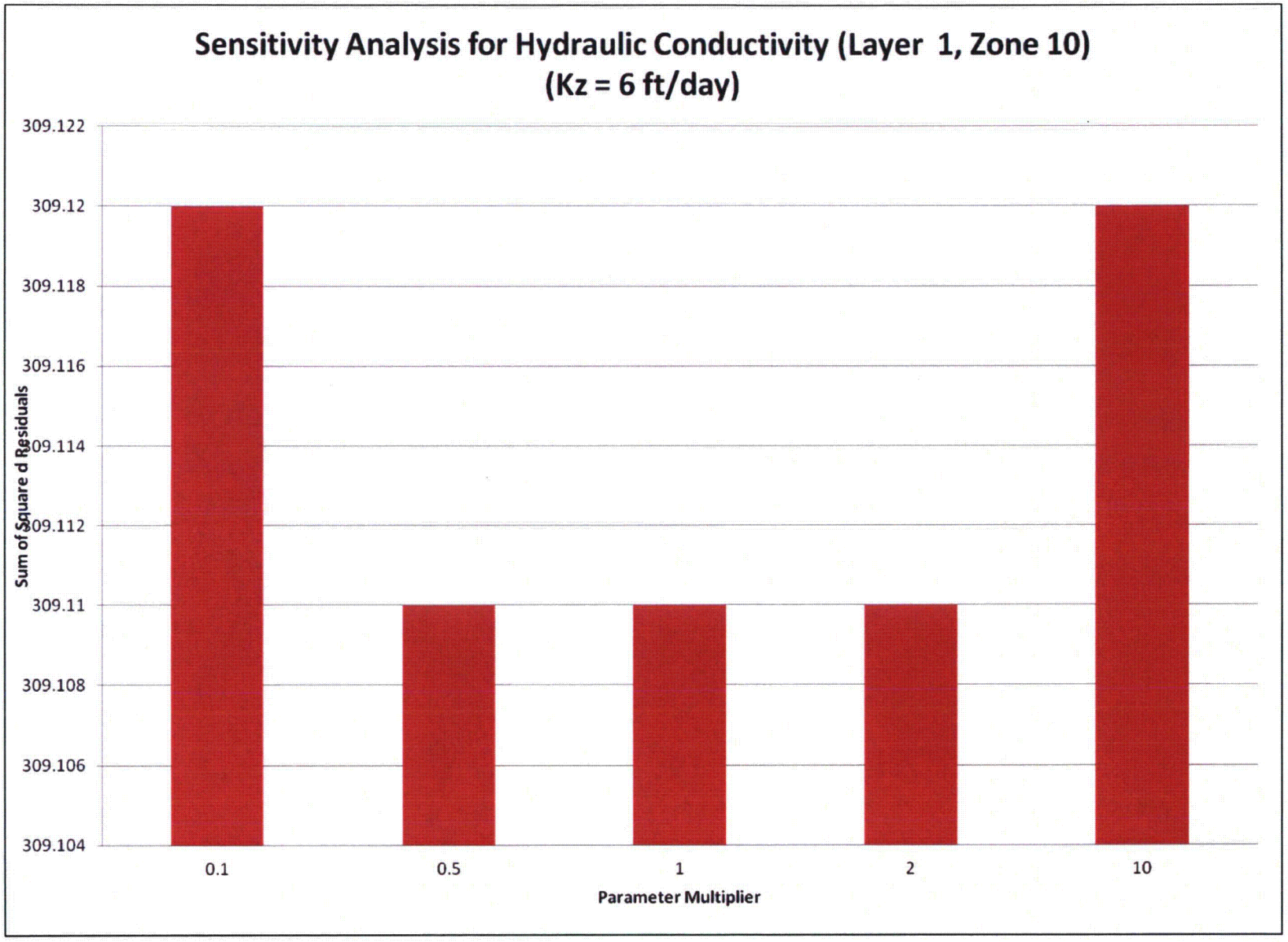
Sensitivity Analysis for Hydraulic Conductivity (Layer 1, Zone 10)
(Kz = 6 ft/day)
309.122
309.12
309.118
309.116
309.114
309.112
309.11
309.108
309.106
309.104
Sum of Squared Residuals
0.1
0.5
1
2
10
Parameter Multiplier

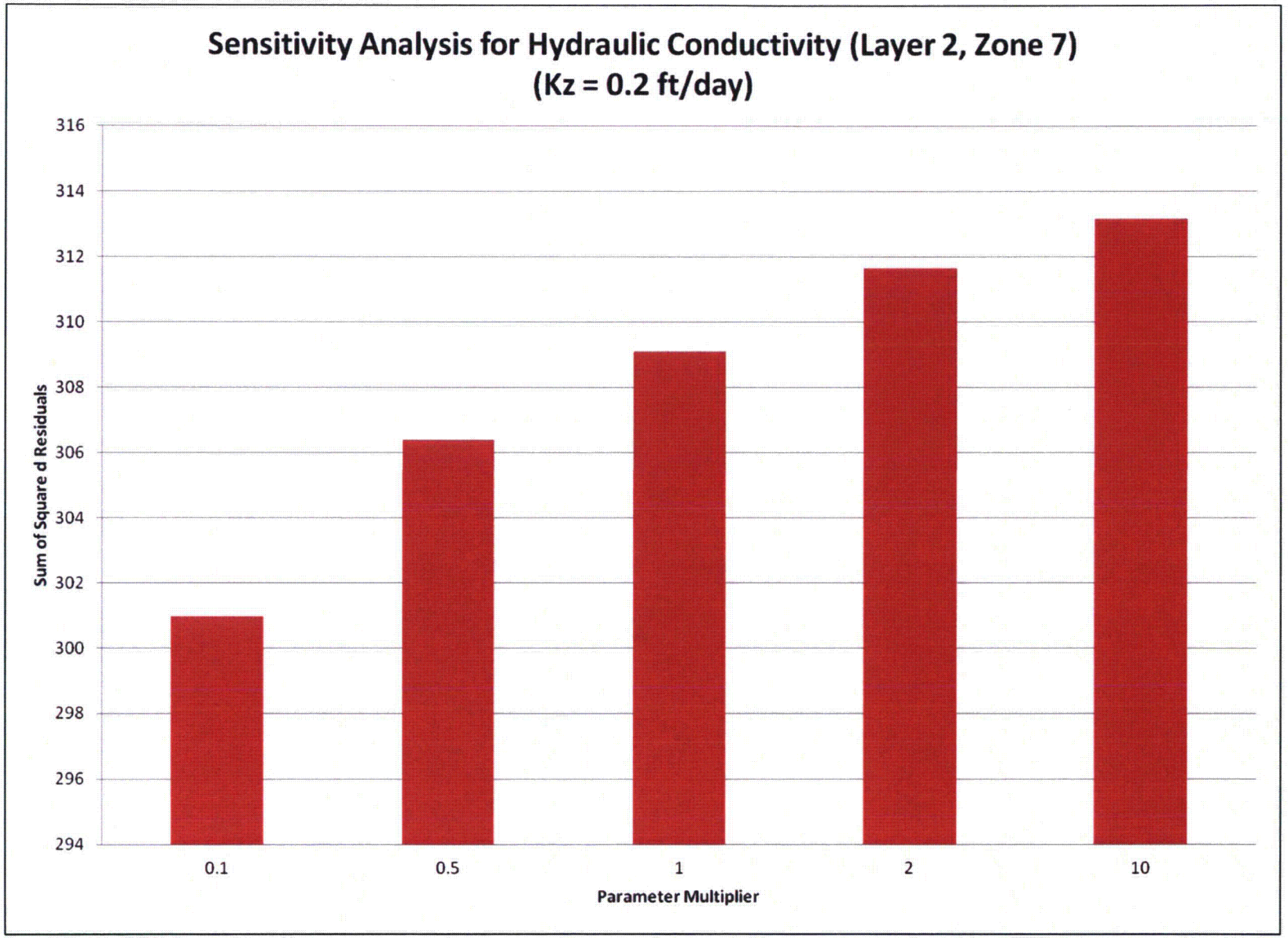
Sensitivity Analysis for Hydraulic Conductivity (Layer 2, Zone 7)
(Kz = 0.2 ft/day)
Sum of Square d Residuals
316
314
312
310
308
306
304
302
300
298
296
294
0.1
0.5
1
2
10
Parameter Multiplier

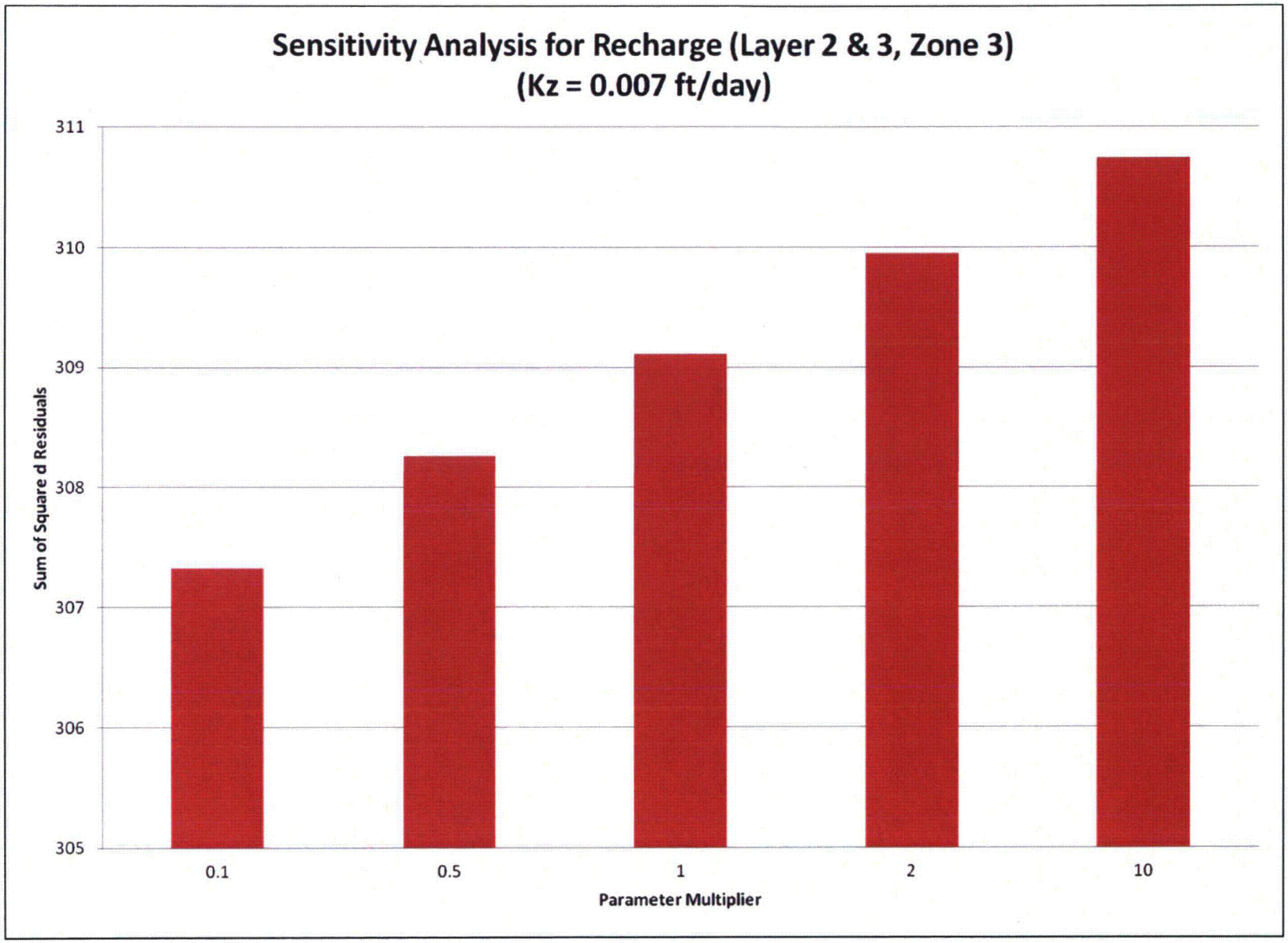
Sensitivity Analysis for Recharge (Layer 2 & 3, Zone 3)
(Kz = 0.007 ft/day)
Sum of Square d Residuals
311
310
309
308
307
306
305
0.1
0.5
1
2
10
Parameter Multiplier

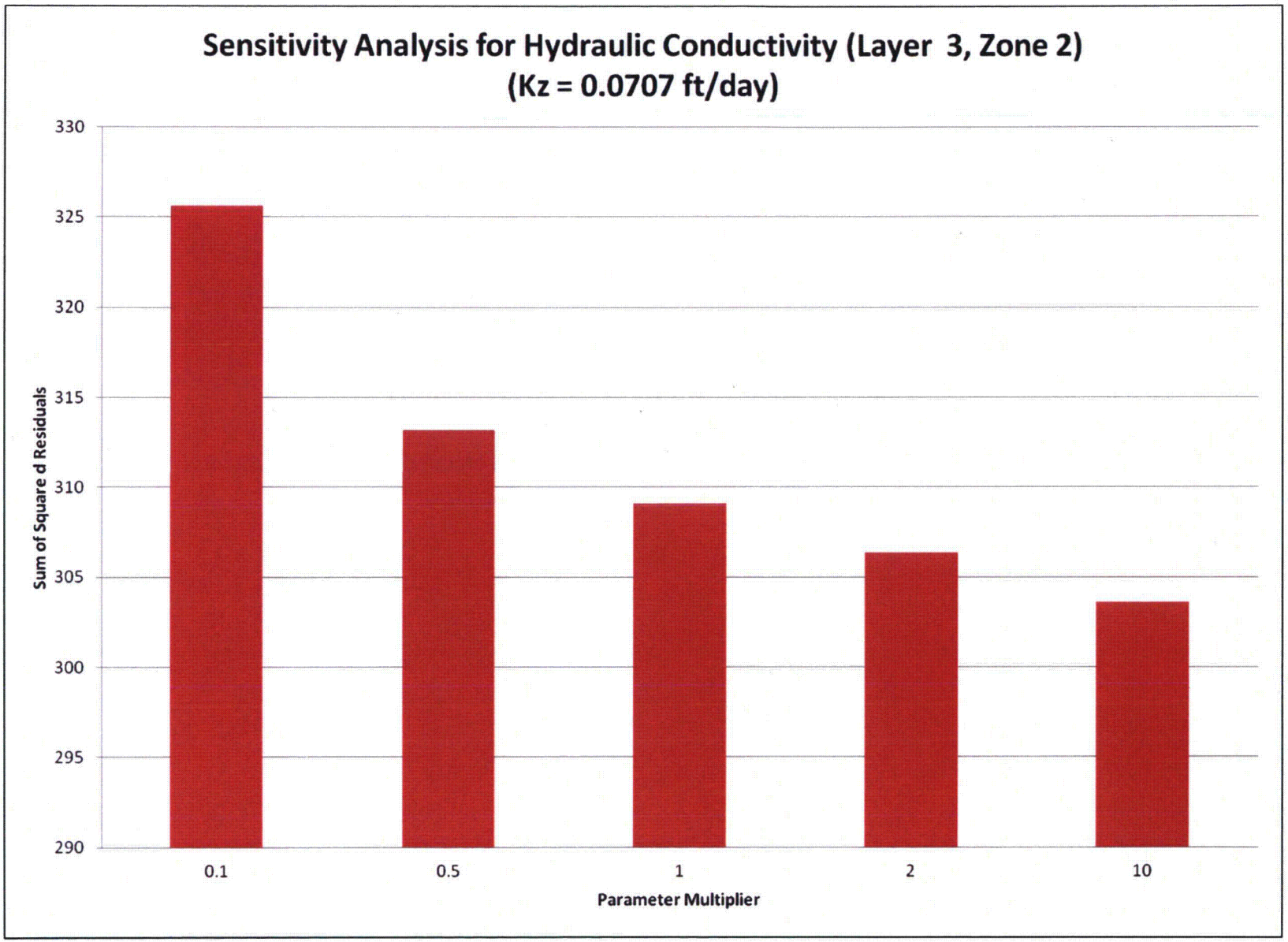
Sensitivity Analysis for Hydraulic Conductivity (Layer 3, Zone 2)
(Kz = 0.0707 ft/day)
Sum of Square d Residuals
330
325
320
315
310
305
300
295
290
0.1
0.5
1
2
10
Parameter Multiplier

Sensitivity Analysis for Recharge

Recharge (ft/day)

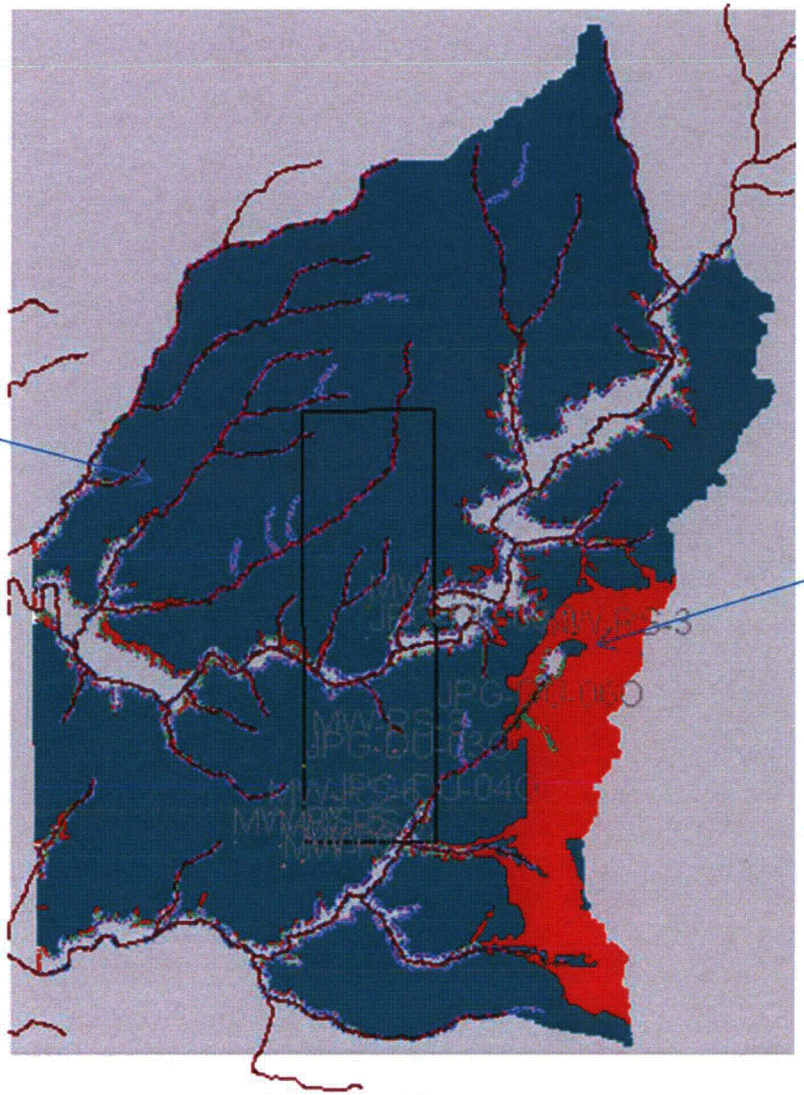

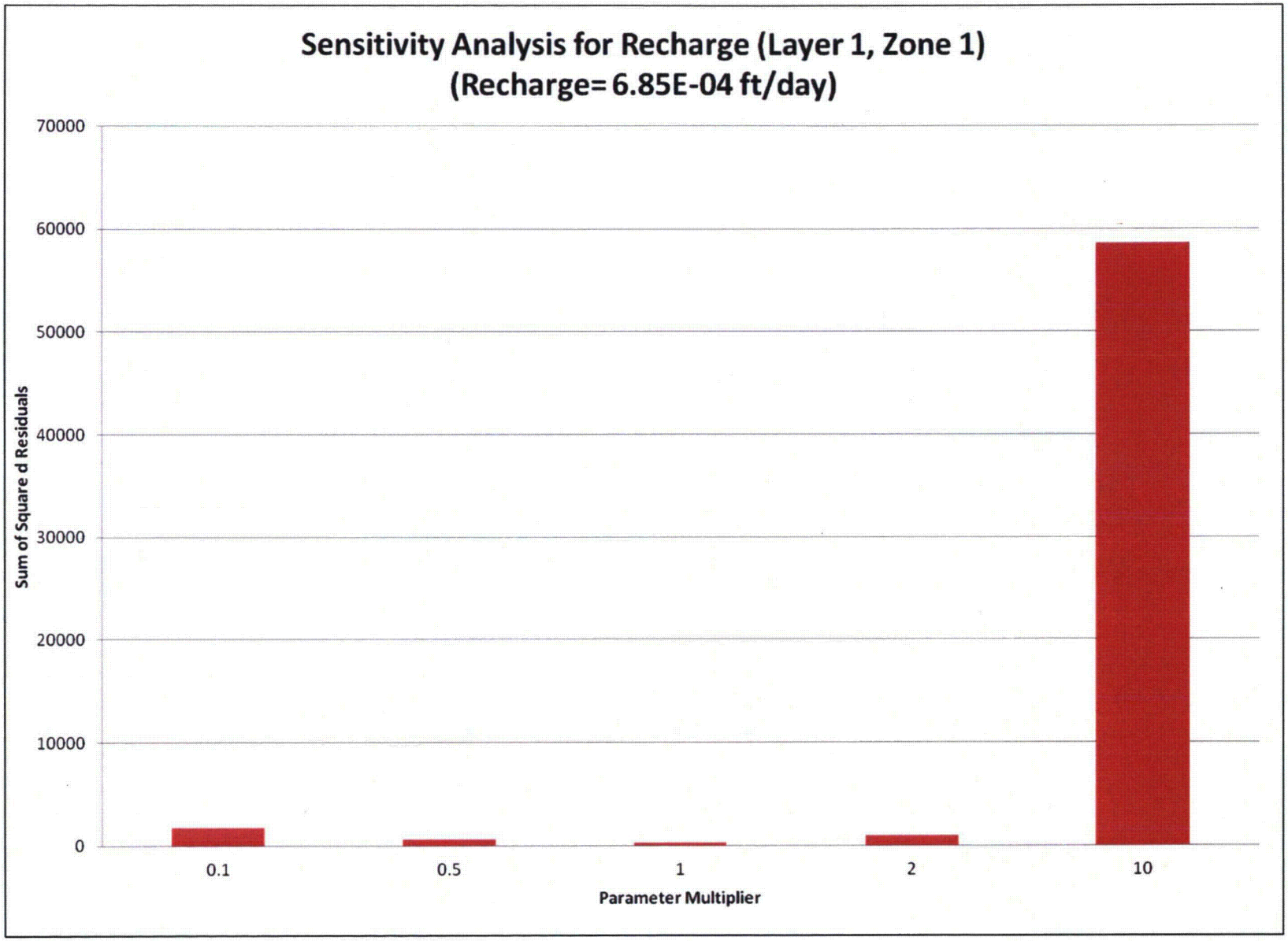
Sensitivity Analysis for Recharge (Layer 1, Zone 1)
(Recharge= 6.85E-04 ft/day)
Sum of Square d Residuals
70000
60000
50000
40000
30000
20000
10000
0
0.1
0.5
1
2
10
Parameter Multiplier

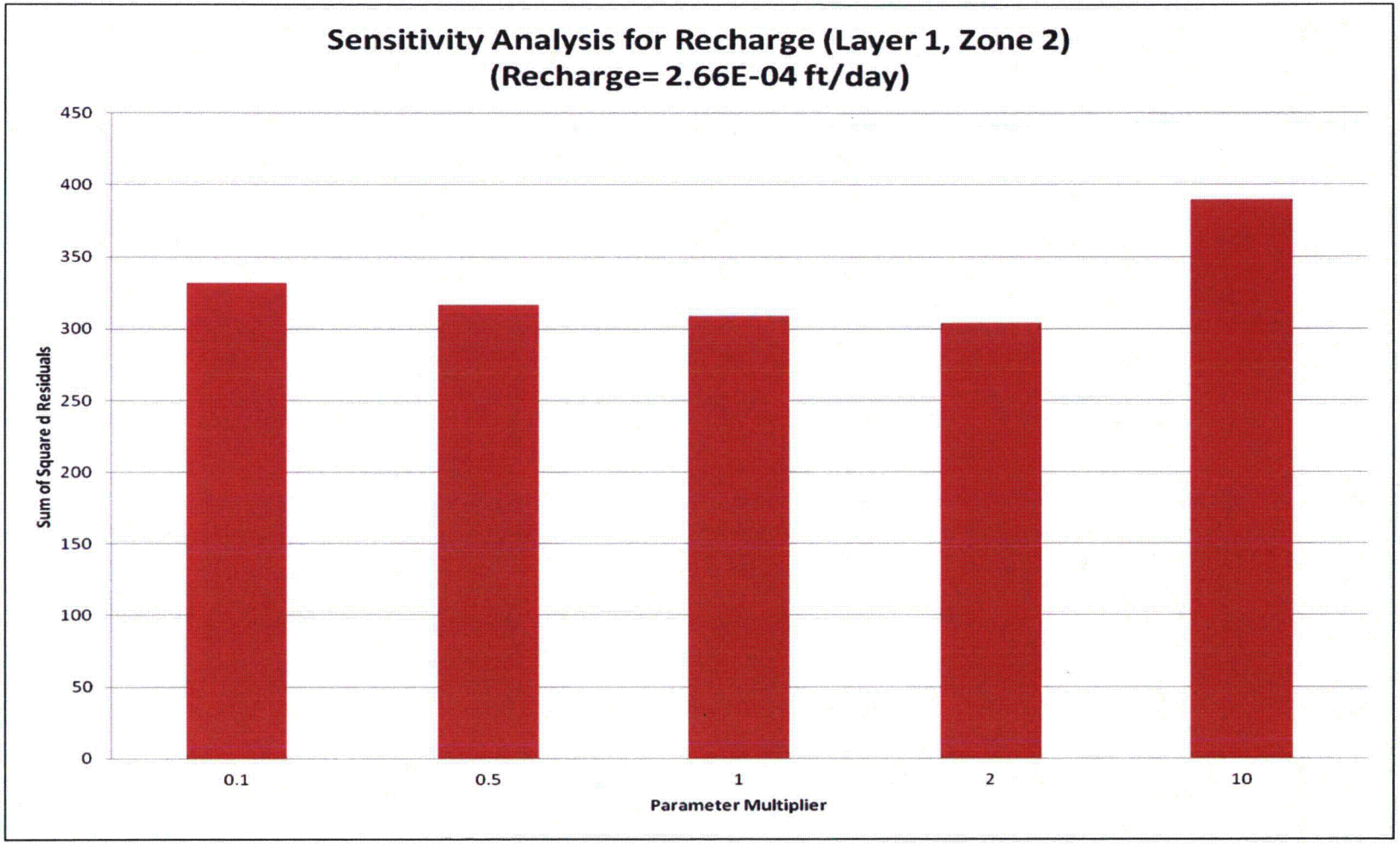
Sensitivity Analysis for Recharge (Layer 1, Zone 2)
(Recharge= 2.66E-04 ft/day)
Sum of Square d Residuals
450
400
350
300
250
200
150
100
50
0
0.1
0.5
1
2
10
Parameter Multiplier

THIS PAGE WAS INTENTIONALLY LEFT BLANK

APPENDIX C

CONCEPTUAL SITE MODEL

Depleted Uranium Impact Area
Jefferson Proving Ground, Madison, Indiana

THIS PAGE WAS INTENTIONALLY LEFT BLANK

TABLE OF CONTENTS

TABLE OF CONTENTS (Continued)

LIST OF FIGURES

LIST OF FIGURES (Continued)

LIST OF FIGURES (Continued)

LIST OF TABLES

LIST OF TABLES (Continued)

LIST OF ACRONYMS AND ABBREVIATIONS

a	Annus
A/E	Angle of Gun Elevation
ac	Acre
AEPI	Army Environmental Policy Institute
ALARA	As Low as Reasonably Achievable
APFSDS-T	Armor-Piercing, Fin-Stabilized, Discarding Sabot with Tracer
APG	Aberdeen Proving Ground
ASTM	American Society for Testing and Materials
atm	Standard Atmosphere
BGS	Below Ground Surface
Bq/g	Becquerels per Gram
BRAC	Base Realignment and Closure
CEC	Cation Exchange Capacity
CFR	Code of Federal Regulations
cfs	Cubic Feet per Second
Ci/g	Curies per Gram
cm	Centimeter
cm^2	Square Centimeter
cm^3	Cubic Centimeter
CO_2	Carbon Dioxide
cpm	Counts per Minute
CSM	Conceptual Site Model
DA PAM	Department of Army Pamphlet
DEM	Digital Elevation Model
DOD	U.S. Department of Defense
DOE	U.S. Department of Energy
DU	Depleted Uranium
Eh	Redox Potential
EOD	Explosive Ordnance Disposal
ERM	Environmental Radiation Monitoring
FAO	Food and Agriculture Organization
FEHM	Finite Element Heat and Mass Transfer Model
FeO(OH)	Goethite
FIDLER	Field Instruments for the Detection of Low Energy Radiation
FSP	Field Sampling Plan
ft	Feet
ft/d	Feet per Day
ft/m	Feet per Meter
FWS	U.S. Fish and Wildlife Service
g	Gram
$g/cm^2/y$	Grams per Square Centimeter per Year
g/cm^3	Grams per Cubic Centimeter
g/mol	Grams per Mole
$gal/day/ft^2$	Gallons per Day per Square Foot
GIS	Geographic Information System
GPS	Global Positioning System
GTL	Gun Target Line
Hcl	Hydrochloric Acid
ID	Identification

LIST OF ACRONYMS AND ABBREVIATIONS (Continued)

ICP-MS	Inductively Coupled Plasma-Mass Spectrometry
in	Inch
in^3	Cubic Inches
in/y	Inches per Year
INANG	Indiana Air National Guard
JPG	Jefferson Proving Ground
K_d	Distribution Coefficient
kg	Kilogram
km	Kilometer
km^2	Square Kilometer
L	Liter
lb	Pound
LLNL	Lawrence Livermore National Laboratory
µg	Microgram
µg/L	Micrograms per Liter
µm	Micrometer
m	Meter
m/sec	Meters per Second
m/sec^2	Meters per Square Second
MARLAP	Multi-Agency Radiation Laboratory Analytical Protocols
MARSSIM	Multi-Agency Radiation Survey and Site Investigation Manual
MDC	Minimum Detectable Concentration
Meq	Milliequivalent of Change
MeV	Mega Election Volt
mg/kg	Milligrams per Kilogram
mi	Mile
mi^2	Square Mile
mL	Milliliter
mL/g	Milliliters per Gram
mm	Millimeter
MnO_2	Pyrolusite
mrem/y	Millirems per Year
msl	Mean Sea Level
mSv/y	MilliSieverts per Year
mV	Millivolt
NaCI	Sodium Chloride
NaI	Sodium Iodide
NNDC	National Nuclear Data Center
NRC	Nuclear Regulatory Commission
NRCS	Natural Resources Conservation Service
NUREG	U.S. Nuclear Regulatory Commission Regulation
NWR	National Wildlife Refuge
ORP	Oxidation-Reduction Potential
Pa-234 m	Protactinium-234 m
pCi/g	Picocuries per Gram
pCi/L	Picocuries per Liter
PHREEQC	pH-Redox-Equilibrium
QA	Quality Assurance
QC	Quality Control

LIST OF ACRONYMS AND ABBREVIATIONS (Continued)

RDZ	Range Danger Zone
redox	Oxidation-Reduction
RESRAD	Residual Radioactivity
RI	Remedial Investigation
RSO	Radiation Safety Officer
SAIC	Science Applications International Corporation
SDZ	Surface Danger Zone
SVS	Soil Verification Study
TB	Technical Bulletin
Tc-99	Technetium-99
TECOM	(U.S. Army) Test and Evaluation Command
TEDE	Total Effective Dose Equivalent
Th-234	Thorium-234
TOC	Total Organic Carbon
TPU	Total Propagated Uncertainty
U.K.	United Kingdom
U-232	Uranium-232
U-233	Uranium-233
U-234	Uranium-234
U-235	Uranium-235
U-236	Uranium-236
U-237	Uranium-237
U-238	Uranium-238
UNEP	United Nations Environment Programme
$UO_3 \cdot 2H_2O$	Uranium (VI) Oxide
UO_2	Uranium (VI) Dioxide
$UO_4 \cdot H_2O$	Hydrated Uranium (VI) Peroxide
USDA	U.S. Department of Agriculture
USGS	U.S. Geological Survey
UXO	Unexploded Ordnance

1. INTRODUCTION

A conceptual site model (CSM) is a qualitative description of the important environmental transport and exposure pathways and their interrelationships (NRC 2006). The CSM includes a model of the site, including the source term, physical features important to modeling the transport pathways, and critical group (i.e., the group of individuals reasonably expected to receive the greatest exposure to residual radioactivity for any applicable set of circumstances). It describes the:

- Relative location and activities of the critical group
- Hydrologic and environmental transport processes important at the site
- Dimensions, location, and spatial variability of the source term used in the model
- Major assumptions made in developing the CSM (e.g., recharge of the aquifer is limited to the infiltration through the footprint of the site)
- Effects of site restrictions on transport or exposure pathways (NRC 2006).

In addition, the CSM reflects complete, potentially complete, and incomplete transport mechanisms and exposure pathways; current and reasonably foreseeable anticipated future land use; and potential receptors. The CSM serves as a planning instrument, modeling and data interpretation aid, and communication device. A central concept to understanding the site-specific conditions at the Jefferson Proving Ground (JPG) Depleted Uranium (DU) Impact Area is that doses to humans and ecosystem receptors can come from any number of exposure pathways beginning when the munitions were tested and lasting until the DU is removed from the system or until it completely corrodes into a mineralized form like that which occurs naturally (U.S. Army 2002). Thus, the residual dose to humans from DU must be assessed for a variety of pathways and for a relatively long time due to slow transport through the soils (U.S. Army 2002).

This section discusses the general CSM that was presented in the original Field Sampling Plan (FSP) (SAIC 2005a) based on historical studies. In addition, it includes significant enhancements made based on the conclusions of site characterization activities from 2005 through 2013. Updating the CSM is consistent with the following basic project goals identified in the original FSP (SAIC 2005a):

- Enhance the understanding of the nature and extent of contamination in the DU Impact Area and the fate and transport of DU in the environment
- Define and verify the CSM.

The CSM for the DU Impact Area is based on the DU penetrators that have been deposited on, or immediately below, the ground surface and/or within the surface water (streams). To better understand the information included in this appendix, Section 2 introduces the characteristics of uranium and DU. To define the source term, Section 3 describes the penetrators that were used at JPG and Section 4 discusses the expected spatial distribution of DU penetrators and fragments remaining at JPG.

DU corrosion products from the weathering of penetrators over time primarily include uranium (VI) oxide or schoepite ($UO_3 \cdot 2H_2O$), uranium (VI) dioxide (UO_2), and hydrated uranium (VI) peroxide ($UO_4 \cdot H_2O$). The corrosion of penetrators, dissolution of corrosion products, and transformation of corrosion products into secondary byproducts available for transport through the environment are presented in Section 5.

Once the DU has been deposited on the soil or into the surface water, the penetrators corrode and these corrosion products are then available for transformation and transport through the environment by several different processes. The corrosion products are transformed in the soil, which is discussed further in Section 6, and then secondary byproducts are subject primarily to transport laterally in surface runoff

and to a lesser extent vertically through the soil column to groundwater. Some migration can be expected due to the dissolution of soluble DU corrosion products and transport of dissolved species in rainfall and snowmelt, movement of dust-bound DU by wind or fire, and leaching of dissolved species through the soil column and subsequent migration in groundwater.

The physical movement of DU penetrators and/or fragments is suspected to have occurred through stream channel erosion. Some studies have been conducted to ascertain the distance that naval bottom mines move under tidal conditions (Inman and Jenkins 2002). The movement is due to the hydrodynamic and gravitational forces acting on the mines, or in this case, on DU penetrators based on Newton's second law of motion. Hydrodynamic forces are caused by water flowing against objects that include positive frontal pressure against the structure, drag along the sides, and negative pressure in the downstream side. When the hydrodynamic forces caused by stream currents in JPG creeks exceed gravitational forces, DU penetrators could move "by scour and roll or scour and slip mechanisms" (Inman and Jenkins 2002). The process involves the displacement of streambed sediments such that penetrators roll or slide along the bottom. However, very limited mechanical movement of DU penetrators or fragments is expected on land or in stream channels. While processes of stream channel erosion could cause limited migration and transport of DU penetrators or fragments (during floods and high runoff events) along streambeds in drainageways, a very small frontal surface area on which stream flow could be applied and large objects present in the channels, such as boulders, bedrock outcrops, the remnants of Wilson dam (located more than 1,600 feet [ft] [0.5 kilometer (km)] west of the western DU boundary of the DU Impact Area on Big Creek and more than 9,800 ft [3.0 km] from the western boundary of JPG along Big Creek), and at-grade river crossings, would prevent the migration of penetrators or fragments outside the boundaries of the DU Impact Area. Even transport of small corrosion products has not been observed in sediment sampling that has been conducted since 1983 presumably because DU is approximately twice as dense as lead (i.e., specific gravity of 19.1 grams per cubic centimeter [g/cm^3]). DU corrosion products and related byproducts also could be absorbed by plants and incorporated within the plant matter. This pathway is described further below.

Section 7 discusses potential pathways of exposure for human receptors within and around the DU Impact Area. The simplest and most direct exposure pathway to humans would be external radiation from direct contact with the penetrators and/or fragments, DU particulates, or DU-impacted soils. Impacted surface water and groundwater could migrate to drinking water sources. The drinking and surface water could be ingested by humans, livestock, and wildlife. Meat and/or animal products from animals ingesting DU-impacted media (i.e., vegetation, soil, water) could be ingested by humans. Humans could have contact with, and incidental ingestion of, impacted surface water during recreational activities such as fishing and hunting. Figure 1-1 summarizes the key elements of the CSM that will be discussed further in this appendix.

DU Impact Area located within Big Oaks NWR. Residual radiation dose with institutional controls for offsite resident farmer are below restricted release criteria from 10 CFR 20.1403. Residual radiation doses for subsistence farmer, industrial worker, and sportsman without institutional controls also are below restricted release criteria from 10 CFR 20.1403. Based upon dose assessment results, the critical group when controls remain in place is the Industrial Worker working on JPG (i.e., FWS worker) and the critical group with loss of controls is the subsistence farmer.

Karst features (caves, sinkholes, seeps) limited to narrow plain along Big Creek, most commonly above elevations of Big Creek and limited to depths of less than 50 feet BGS. Provides hydraulic connection between surface water and shallow groundwater.

Corrosion of DU penetrators and subsequent dissolution of the corrosion products is primary mechanism for introducing DU into soil. Most-likely time to complete corrosion and dissolution of JPG penetrator calculated to be 107 years (uncertainty ranges from 65 to 182 years).

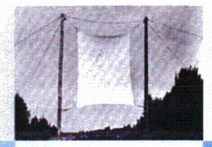

100,000 kg of **APFSDS-T DU penetrators fired from M1 and M60 tanks at soft (cloth or wood) targets (yellow triangles denote targets placed at 1,000-meter intervals). Trench formed from repeated firing along 500 Center (middle) and J (western) Firing Positions. 26,500 kg of DU penetrators/fragments recovered. Estimated 73,500 kg of DU remains.**

Former firing line with 268 gun positions (red circles denote the only 3 DU firing positions) to test munitions. Fence separates JPG into two areas:

- Army has or will transfer approximately 4,300 acres south of firing line
- Army retains ownership of 50,950 acres north of firing line
- USAF/ANANG and USFWS restrict access to areas north of firing line

Soil-weighted mean K_d values in geologic profile: loess soil sorption – 2,116 mL/g; loess soil desorption-dissolution – 354 mL/g; glacial till sorption – 6.4 mL/g.

Migration of DU to groundwater may occur where the water table is shallow (~2-4 ft BGS) in areas near streams. DU migration to groundwater does not occur through overburden at average depths to groundwater (11 ft BGS) or at greatest depths to groundwater (30-40 ft BGS).

Primary pathway of migration/transport includes dissolved DU corrosion products in surface runoff, interflow, and base flow and redepositing within JPG stream network. HSPF model calibrated, verified, and used to simulate 500-year transport predicts surface water and sediment concentrations are low (surface water <5 µg/L, sediment <5 mg/kg) where Big Creek exits DU Impact Area and lower (surface water <1 µg/L, sediment <1 mg/kg) where Middle Fork Creek exits DU Impact Area.

Legend

- DU Impact Area
- DU Impact Trench
- Installation Boundary
- Roads
- Creek
- Fence
- DU Transport
- Firing Targets
- Firing Points
- Groundwater Well
- Gate
- Surface Water Flow

CSM Summary for JPG DU Impact Area

Jefferson Proving Ground
Madison, Indiana

Figure 1-1	Date: 8/23/2013

2. CHARACTERISTICS OF URANIUM AND DU

DU, a waste product of uranium enrichment, has numerous applications, including use as armor-piercing ammunition. In addition to its use as armor-piercing ammunition, DU has been used in a variety of different applications, including tank armor, as a fluorescent additive to dental porcelain crowns (now discontinued), as X-ray shielding in hospitals, as counterweights for rudders and flaps in commercial aircraft and forklifts, and in the keels of sailing yachts.

Given the need for quality assurance (QA) testing of such ammunition, soft target testing was performed at JPG, Indiana from 18 March 1984 until 2 May 1994, shortly before the installation was closed by Base Realignment and Closure (BRAC) action (Public Law 100-526) in 1995. During this time, approximately 220,000 pounds (lb) (100,000 kilograms [kg]) of armor-piercing, fin-stabilized, discarding sabot with tracer (APFSDS-T) kinetic energy DU penetrators were fired at soft targets at JPG. These penetrators generally came to rest in the DU Impact Area downrange from the firing line (Figure 2-1). On what was generally a semi-annual basis, test support personnel recovered penetrators, which were located on or near the ground surface while being escorted by explosive ordnance disposal (EOD) technicians due to the presence of approximately 85 rounds of high-explosive unexploded ordnance (UXO) per acre in the DU Impact Area (U.S. Army 1995). These efforts recovered an estimated 25 percent of the penetrators that had been fired during the interval since the last penetrator recovery operation was performed (Personal Communication 2013a). The recovered penetrators were disposed of as radioactive waste. Given that about 58,000 lb (26,500 kg) of DU were recovered from the DU Impact Area, the residual DU source term in the DU Impact Area equates to a total of about 162,000 lb (73,500 kg). The following sections describe characteristics of uranium and DU and the detection of uranium in both laboratory and field settings.

2.1 URANIUM

Uranium, the heaviest naturally occurring element, exhibits a density of 19.1 g/cm^3 (i.e., greater than 68 percent more dense than lead). Uranium is found at an average concentration of 0.0003 percent (3 milligrams per kilogram [mg/kg]) in the Earth's crust. In seawater, the concentration is about 3 micrograms per liter (µg/L). Due to its presence in soil, rocks, surface and underground water, air, plants, and animals, it occurs also in trace amounts in many foods and in drinking water such that the daily intake of uranium is estimated to be 1 to 2 micrograms (µg) in food and 1.5 µg in consumed water (Bleise, Danesi, and Burkart 2003). A similar quantity is excreted each day in feces and urine (DOE 2009). The human body contains a total of about 56 µg of uranium, of which 32 µg (56 percent) are in the skeleton. This uranium in the human body is derived mostly from uranium naturally present in food, especially from vegetables, cereals, and table salt (Bleise, Danesi, and Burkart 2003).

The radiological and chemical properties of DU can be compared to those of natural uranium, which is ubiquitously present in the environment. Natural uranium is defined by the Nuclear Regulatory Commission (NRC) as "...uranium containing the relative concentrations of isotopes found in nature (0.7 percent uranium-235 [U-235], 99.3 percent uranium-238 [U-238], and a trace amount of U-234 [U-234] by mass). In terms of radioactivity, however, natural uranium contains approximately 2.2 percent U-235, 48.6 percent U-238, and 49.2 percent U-234..." (NRC 2012a). With respect to the isotopic content of natural uranium, it may be noted that other sources provide data that vary slightly from the percentages specified above by NRC. For example, the 2013 Toxicological Profile for Uranium (ATSDR 2013), citing the National Nuclear Data Center (NNDC) (2011) lists activity concentration percentages of 2.27, 48.7, and 49.0 percent for U-235, U-238, and U-234, respectively.

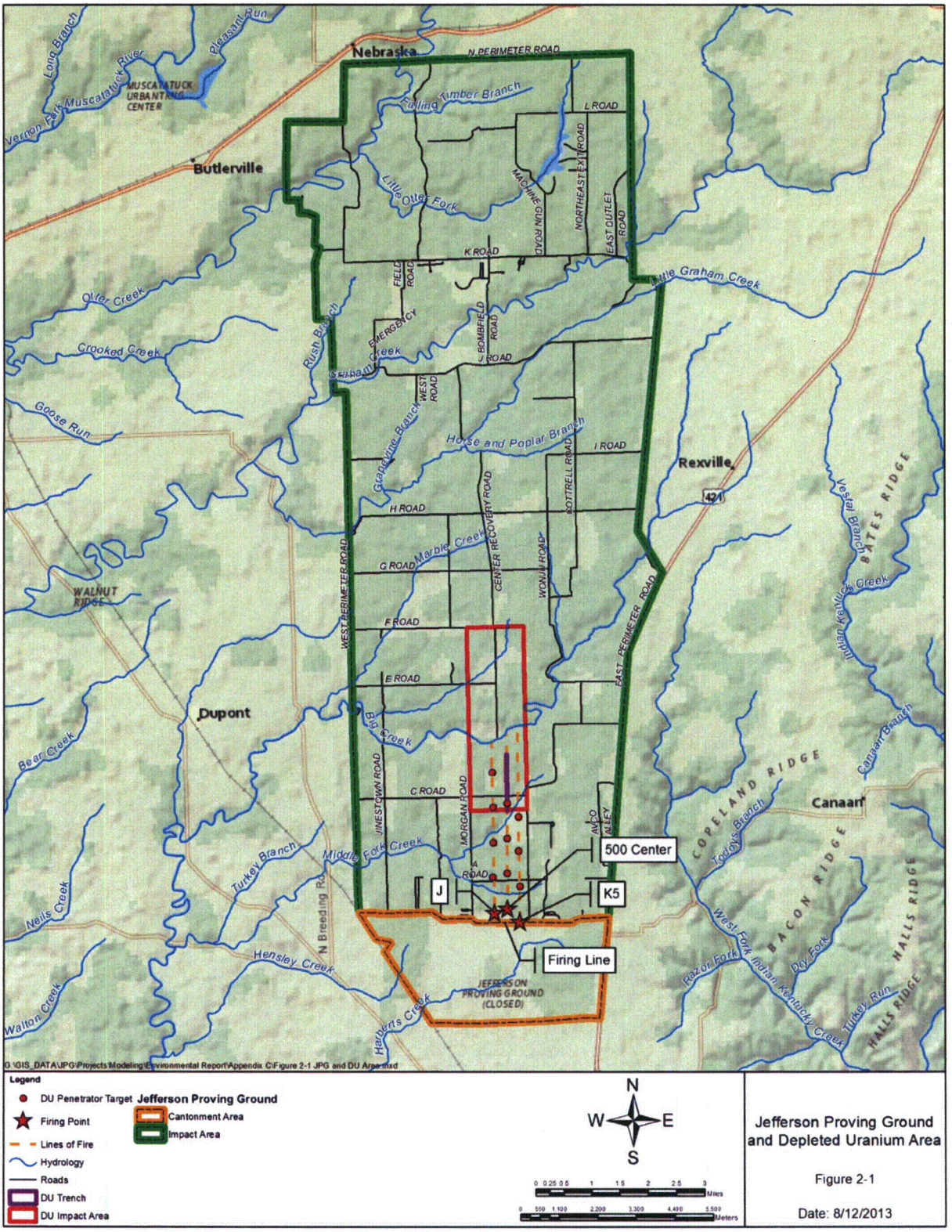
Nebraska
N PERIMETER ROAD
Falling Timber Branch
L ROAD
MACHINE GUN ROAD
NORTHEAST EXIT ROAD
EAST OUTLET ROAD
Butlerville
Little Otter Fork
K ROAD
FIELD ROAD
Little Graham Creek
Otter Creek
Crooked Creek
Rush Branch
EMERGENCY
Graham Creek
BOMBFIELD ROAD
ROAD
WEST ROAD
Goose Run
Horse and Poplar Branch
I ROAD
Rexville
421
Grassyline Branch
BOTTRELL ROAD
H ROAD
CENTER RECOVERY ROAD
Marble Creek
G ROAD
WOOLWINE ROAD
WEST PERIMETER ROAD
EAST PERIMETER ROAD
Vestal Branch
BATES RIDGE
Indian Kentucky Creek
WALNUT RIDGE
F ROAD
E ROAD
Dupont
Big Creek
Bear Creek
JINESTOWN ROAD
C ROAD
MORGAN ROAD
AVCO ALLEY
COPELAND RIDGE
Canaan Branch
Canaan
Todds Branch
500 Center
Middle Fork Creek
Turkey Branch
A ROAD
J
K5
Neils Creek
N Breeding Rd
BACON RIDGE
West Fork Indian Kentucky Creek
Dry Fork
HALLS RIDGE
Hensley Creek
Firing Line
JEFFERSON PROVING GROUND (CLOSED)
Razor Fork
Walton Creek
Halberts Creek
Turkey Run
HALLS RIDGE
G:\GIS_DATA\JPG\Projects\Modeling\Environmental Report\Appendix C\Figure 2-1 JPG and DU Area.mxd
Legend
DU Penetrator Target
Firing Point
Lines of Fire
Hydrology
Roads
DU Trench
DU Impact Area
Jefferson Proving Ground
Cantonment Area
Impact Area
N
W
E
S
0 0.25 0.5 1 1.5 2 2.5 3 Miles
0 550 1,100 2,200 3,300 4,400 5,500 Meters
Jefferson Proving Ground and Depleted Uranium Area
Figure 2-1
Date: 8/12/2013

Notably, in a closed environment, U-234 would be present in secular equilibrium with its U-238 parent such that each isotope would be present with the same activity concentration (i.e., "The ratio of U-234 to U-238 would be expected to be unity as long as the uranium stays locked inside undisturbed crustal rock in secular equilibrium with its progeny, but measurements show that the ratio is typically different than unity [USEPA 1997, 2007]. This disequilibrium occurs when the rock is disturbed by chemical or physical changes involving water. In the environment, a portion of the U-234 separates from the U-238 by what is theorized to be a physical process [alpha recoil ejection of the thorium-232 decay product from surfaces of soil particles] or a combination of physical and chemical processes [a U-238 transformation at the soil particle surface fractures the surface allowing access for water to dissolve the more soluble thorium-234 product] [NCRP 1984]. These processes can change the uranium isotope ratios in air, soil, and water" [ATSDR 2013]). The ocean, for example, contains elevated abundances of U-234. Specifically, the increased mobility of U-234 relative to other uranium isotopes reflects the production from U-238 by alpha-decay and subsequent emplacement in crystal sites damaged by alpha-recoil. Aqueous weathering of materials containing uranium results in preferential leaching of U-234 from these alpha-damaged crystal sites (Brennecka et al. 2010). As a result of these factors, U-234/U-238 ratios have been found to vary considerably due to natural causes in many water, soil, and sediment samples, and uranium ores of different geographical origins. U-234/U-238 activity ratios in water reportedly vary from 0.5 to 40 while ratios in soil typically range from 0.5 to 1.2 (Fujikawa et al. 2000). Adjusting these ranges to reflect inverse ratios (i.e., U-238/U-234 ratios) in water would vary from 0.025 to 2.0 while ratios in soil would typically range from 0.83 to 2.0. U-238/U-234 ratios also vary due to anthropogenic discharge. Fertilizer-derived uranium, for example, could be distinguished from indigenous uranium using the isotopic ratio as an indicator and could be used to trace the migration of fertilizer in the environment (Fujikawa et al. 2000).

All isotopes of uranium are radioactive with natural uranium being considered a weakly radioactive element as well as a heavy metal with chemotoxic properties. The radiotoxicity of natural uranium is about 60 percent higher than that of DU (Bleise, Danesi, and Burkart 2003). Natural uranium has three isotopes (forms): U-234, U-235, and U-238. Although U-238 and U-235 are the two most abundant isotopes by weight, U-238 and U-234 are present in natural uranium in similar activity concentrations due to secular equilibrium as described above and shown in Table 2-1. Uranium isotopes not found in nature include uranium-232 (U-232), uranium-233 (U-233), uranium-236 (U-236), and uranium-237 (U-237).

Table 2-1. Characteristics of Uranium Isotopes in Natural Uranium
Jefferson Proving Ground, Madison, Indiana

Isotope	Half-Life (Years)	Percent by Mass	Isotopic Specific Activity[a,b]	Isotopic Activity (Percent)
U-234	2.46×10^5	0.006	6.24×10^{11} (2.31×10^8)	49.2
U-235	7.04×10^8	0.72	2.16×10^6 (8.00×10^4)	2.2
U-238	4.47×10^9	99.3	3.37×10^5 (1.25×10^4)	48.6

[a] In 10 CFR 20, Appendix B, NRC defines the specific activity of natural uranium as 6.77×10^5 pCi/g (2.6×10^4 Bq/g).
[b] The units of pCi/g (Bq/g) represent activities in picocuries per gram and Becquerels per gram, respectively.

2.2 DEPLETED URANIUM

DU is defined by NRC as "...uranium with a percentage of U-235 lower than the 0.7 percent (by mass) contained in natural uranium. (The normal residual U-235 content in depleted uranium is 0.2-0.3 percent, with U-238 comprising the remaining 98.7-98.8 percent.) Depleted uranium is produced during uranium isotope separation and is typically found in spent fuel elements or byproduct tailings or residues. Depleted uranium can be blended with highly-enriched uranium, such as that from weapons, to make reactor fuel..." (NRC 2012b). Although natural uranium exhibits limited variability in its isotopic composition, the activity of DU can vary depending on the amount of U-234 and U-235 extracted during the uranium enrichment process. Table 2-2 provides the uranium isotopic composition of U.S. Department of Defense

Table 2-2. Uranium Isotopic Composition of DOD DU Munitions Jefferson Proving Ground, Madison, Indiana

Isotope	Percent by Mass	Isotopic Specific Activity[a,b,c]	Isotopic Activity (Percent)
U-234	0.0006	3.7×10^4 (1.39×10^3)	9.7
U-235	0.2	4.3×10^3 (1.60×10^2)	1.1
U-236	0.003	2.0×10^2 (7.18×10^0)	0.05
U-238	99.8	3.4×10^5 (1.24×10^4)	89.1

[a] From Battelle 2012
[b] The units of pCi/g (Bq/g) represent activities in picocuries per gram and Becquerels per gram, respectively.
[c] Total DU-specific activity: 3.8×10^5 pCi/g (1.4×10^4 Bq/g)

(DOD) DU munitions (Battelle 2012). The range of variability of activity is well-established for DU produced in and after the 1980s (i.e., U-235 concentration of 0.200 ± 0.005 percent by weight). DU produced earlier may be subject to greater variation in the isotopic activity. As such, NRC notes in a footnote in Title 10 Code of Federal Regulations (CFR) Part 20, Appendix B that the specific activity of mixtures of U-234, U-235, and U-238, if not known, shall be taken to be 1.3×10^4 Becquerels per gram (Bq/g) (3.6×10^5 picocuries per gram [pCi/g]) for DU. In addition, the variability of the isotopic activity of the three uranium isotopes making up DU is notable in that it ranges from 83.6 to 90.14 percent for U-238, 1.1 to 1.45 percent for U-235, and 8.4 to 15.2 percent for U-234. This variability is the result, in part, of the precise amount of U-234 and U-235 extracted from natural uranium during the enrichment process.

As noted in Tables 2-1 and 2-2, the U-234 activity concentration is reduced from 49.2 percent for natural uranium to 9.7 percent for DU. Concurrently, the U-235 mass concentration is reduced from 0.72 percent in natural uranium to 0.2 percent in DOD DU. The U-238 to U-234 activity ratio (Figure 2-2) and the U-235 to U-238 mass ratio are used to determine whether a given sample is indicative of natural, depleted, or enriched uranium. As discussed in greater detail in Section 2.3.1, these evaluations can use alpha spectrometry results to determine the activity concentrations and associated relationships and/or inductively coupled plasma-mass spectrometry (ICP-MS) to quantify masses.

As noted in Section 2.1, isotopic ratios of U-238/U-234 in natural uranium commonly vary from 0.025 to 2.0 in water while the ratios in soil typically range from 0.83 to 2.0. This disequilibrium occurs when a portion of the U-234 separates from the U-238 by what is theorized to be a physical process (alpha recoil ejection from surfaces of soil particles) or a combination of physical and chemical processes. Whenever large amounts of modern groundwater interact with a deposit, the deposit is expected to contain either 1) excesses of U-234, if deposition is still occurring; or 2) depletions in U-234, if deposition has stopped (Brennecka et al. 2010).

It is also notable that laboratory measurement results for samples containing long-lived uranium isotopes present in very low concentrations assume that the results follow a Poisson or Gaussian distribution. The extent to which this assumption is true depends largely on the total number of decay events occurring in the period of interest. As a consequence, the Multi-Agency Radiation Survey and Site Investigation Manual (MARSSIM) Committee promulgating the Multi-Agency Radiation Laboratory Analytical Protocols (MARLAP) Manual notes that "If the observed count is N, when the Poisson approximation is used, the standard uncertainty of N may be evaluated as $u(N) = N^{0.5}$. When N may be very small or even zero, MARLAP recommends the use of the equation $u(N) = (N+1)^{0.5}$ instead." (NRC 2004a,b,c). In addition, a potentially significant amount of variability in the U-238/U-234 ratio is introduced by the uranium enrichment process as it results in somewhat different isotopic activity concentrations being present in different DU runs.

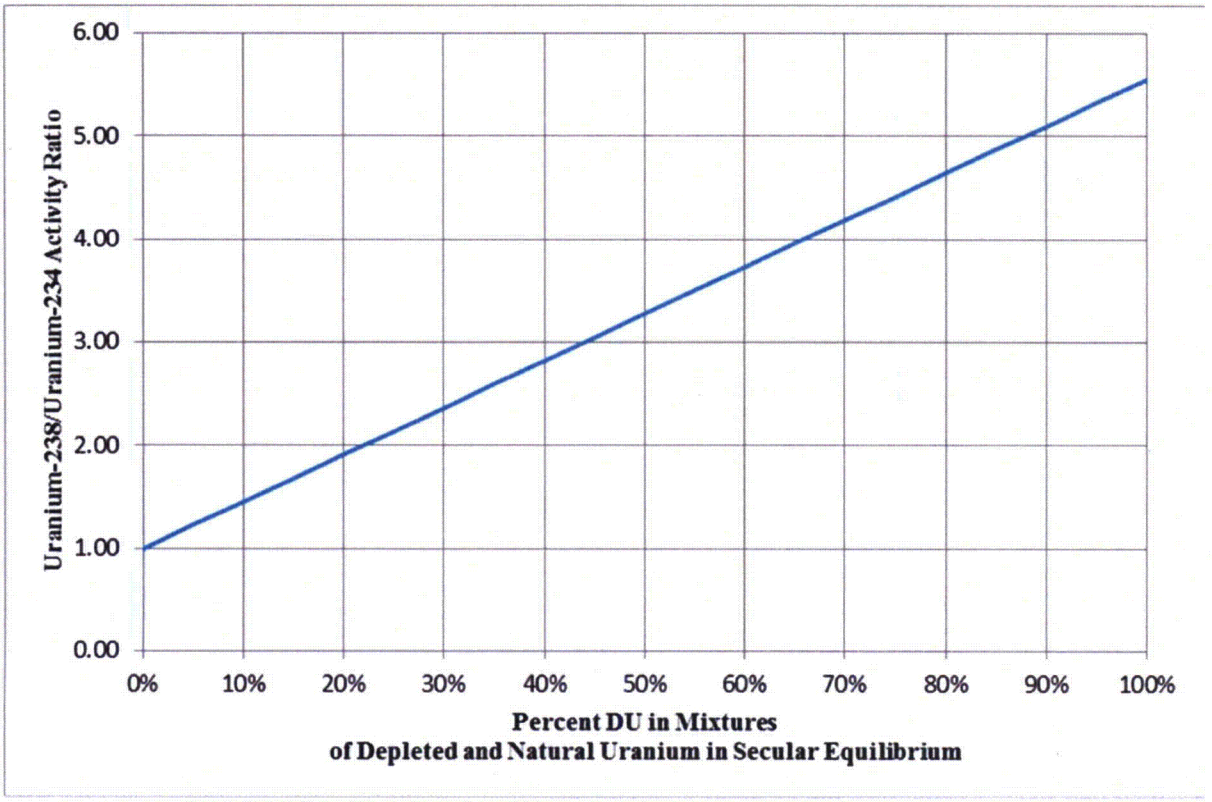

Figure 2-2. Relative U-238/U-234 Activity Ratios for Mixtures of Depleted and Natural Uranium

With respect to evaluation of results from JPG Environmental Radiation Monitoring (ERM), the net result of the cited sources of variability is such that U-238/U-234 activity ratios of two or less are representative of natural uranium whereas higher ratios are potentially indicative of DU. By contrast, U-238/U-234 ratios exceeding 3.0 determined through alpha spectrometry are potentially indicative of the presence of DU. As such, ratios exceeding 3.0 in ERM samples collected since 2011 have been investigated further to validate whether a sample result is representative of DU or natural uranium. These additional investigations of ratios exceeding 3.0 include re-analysis by ICP-MS to confirm both the total mass of uranium present in the sample and the mass relationship between U-235 and U-238. These supplemental data are used to augment U-238/U-234 activity information. Given that both natural uranium and DU are commonly present in samples and that low activity samples exhibit significant total propagated uncertainty, confirmation that a given sample exhibits DU is often problematic and confirmation by a secondary analytical method is needed often to determine if DU is present.

As a result of the extraction of U-234 and U-235, the radioactivity associated with DU is about 40 percent less than that of natural uranium (USEPA 2006). With respect to differences, it is also significant that U.S. Department of Energy (DOE) notes that "...some of the uranium feed material that was handled at DOE facilities had been reclaimed or recycled from reprocessed, spent reactor fuel. The chemical processes by which recycled uranium was purified left trace amounts of transuranic elements (e.g., neptunium, americium, and plutonium) and fission products (mainly technetium-99 [Tc-99]). The recycled uranium also contained trace amounts of uranium isotopes not found in nature, such as U-236. At the minute concentration levels in uranium from fuel reprocessing facilities, the radiological impact of these impurities was negligible in most cases. However, there were many routine chemical processes that

tended to concentrate these impurities, either in the uranium product or in reaction by-products" (DOE 2009). As such, these impurities are appropriately considered in dose assessments.

2.3 DETECTION OF URANIUM

As noted in Section 2.2, DU is less radioactive than natural uranium because some of the U-235 and most of the U-234 have been removed as a result of the processing of natural uranium into enriched uranium. U-234 and U-238 in natural uranium exhibit secular equilibrium such that they are present at approximately the same concentration. Secular equilibrium is disturbed by the extraction of most U-234 together with the U-235 such that the activity exhibited by DU is about 60 percent of that from natural uranium. As a result, radioactive emissions from DU consist primarily of U-238 and its first two daughters (thorium-234 [Th-234] and protactinium-234 m [Pa-234 m]), as shown in Table 2-3 (DOE 2009).

Table 2-3. Radiological Emissions From U-238 With Its First Two Daughters Jefferson Proving Ground, Madison, Indiana

Parent	Daughter	Half-Life*	Type of Emission	Emission Energy (MeV)	Percent Abundance
U-238	NA	4.47×10^9 y	Alpha	4.15	23
				4.20	77
	Thorium-234	24.1 d	Beta	0.095	6.2
				0.096	19
				0.188	72.5
			Gamma	0.063	3.8
				0.0924	2.7
				0.0928	2.7
	Protactinium-234 m	1.17 m	Beta	2.28	98.6
			Gamma	0.766	0.21
				1.001	0.60

Note: From (DOE 2009) DOE-STD-1136-2009, Guide to Practices for Occupational Exposure in Uranium Facilities, July.
*Half-life abbreviations reflect "y," "d," and "m" for years, days, and minutes, respectively.

DU consists primarily of U-238, which makes up 99.8 percent of the mass and 89.1 percent of the activity. Each decay of a U-238 nucleus is generally accompanied by the ejection of one alpha particle and two beta particles together with associated gamma photons. Alpha and gamma emissions are used for isotopic identification and quantification with beta particles providing an additional, generally superior, alternative to the use of alpha emissions for the quantification of surface activity on structures, materials, and equipment. All emissions are fully considered in the computation of total effective dose equivalent (TEDE) to the average member of the critical group as mandated by 10 CFR 20, Subpart E. The following sections summarize the different techniques for detecting uranium in environmental samples (Section 2.3.1) and field instruments and survey techniques that were used to measure DU at the DU Impact Area (Section 2.3.2).

2.3.1 Laboratory Analysis

Several analytical alternatives exist with which to identify and quantify uranium concentrations in environmental media samples. These include but are not limited to gamma spectrometry, alpha spectrometry, ICP-MS, and fluorometry. Gamma spectrometry and alpha spectrometry identify and quantify isotopic sample contents based on radiological emissions whereas ICP-MS provides isotope-specific uranium results based on their atomic masses. Fluorometry, by contrast, determines the concentration of total uranium "based on excitation of the uranyl ion by ultraviolet radiation (light) absorption, followed by spontaneous photon emission and decay to the ground electronic state" (ORNL 1996). Given that fluoroscopy provides total uranium rather than isotope-specific results, isotopic ratios cannot be determined using this method.

2.3.1.1 Gamma Spectrometry

Gamma spectrometry uses isotope-specific gamma photon energies to identify the isotopes present and the photon interaction rate to quantify the amount of activity present. Although U-238 emits a gamma/X-ray with an energy of 0.0496 mega electron volts (MeV) with an abundance of 0.07 percent (i.e., 7 photons are emitted for each 10,000 decays), these photons are not generally detectable. Rather, U-238's short-lived daughters are used to identify and quantify the radioactivity present. This is accomplished using Th-234 and Pa-234 m as U-238's daughters, which have half-lives of 24.1 days and 1.17 minutes, respectively, and emit gammas that are readily detectable. Given these short half-lives, the daughters readily achieve secular equilibrium such that they have the same activity concentrations as their U-238 parent. As such, gamma emissions of these daughters enable the activity of the daughter to be measured and for the activity of the U-238 parent to be inferred from the daughter activity.

U-235 emits multiple energetic gamma photons with energies (and percent abundances) of 0.1438 (10.5), 0.163 (4.7), 0.1857 (54), and 0.205 (4.7) in MeV. Although radium-226 emits gammas at 0.186 MeV, which may be misconstrued as being 0.1857 MeV gammas from U-235, other U-235 gamma emissions can be used for isotopic identification and quantification of U-235 activity present.

Gamma emissions from U-234 are limited to 0.053 MeV photons with a percent abundance of only 0.12 percent. This energy and percent abundance together with uraniuim-234's long half-life generally are such that these gamma emissions are not capable of being accurately measured. As such and given that U-234 does not have short-lived daughters, gamma spectrometry is not generally used when isotopic U-234 results are needed.

The alpha spectrometry results for a limited portion of the higher activity samples were determined to be biased high based on reported results for one alpha spectrometry sample, which exceeded the specific activity of DU as stated in 10 CFR 20, Appendix B (i.e., 3.6×10^{-7} Curies per gram [Ci/g]), and was reinforced by the reanalysis of six high-activity samples using gamma spectrometry. When the associated radioanalytical results for the two methods were subsequently compared, the alpha spectrometry results for the highest activity sample were found to be a factor of 50 times higher than the respective gamma spectrometry results. In addition, alpha spectrometry results for each of the other five samples were a factor of 3.1 to 7.2 times higher than the gamma spectrometry results for the same samples, as shown in Table 2-4.

Table 2-4. Comparison of Alpha and Gamma Spectrometry Results in High-Activity Samples Jefferson Proving Ground, Madison, Indiana

Laboratory ID	SAIC Site ID	Alpha Spectrometry Result (U-238) (pCi/g)	Result (nontracer corrected) (pCi/g)	Mass (g)	Tracer Recovery (%)	Gamma Spectrometry (U-238) (pCi/g)	Mass (g)	Dead Time (%)
8881-01	JP-PNCR-001	134,600	16,152	0.0015	12%	34,360	212.8	3.50%
8884-02	JP-PNAC-009	629,400	25,176	0.0015	4%	12,570	246.9	2%
8884-19	JP-PNAC-006	110,200	20,938	0.0015	19%	35,130	211.2	4.50%
8905-04	JP-PNCR-004	89,900	12,586	0.0015	14%	13,330	207.2	1.70%
8905-20	JP-PNAC-010	105,600	11,616	0.0015	11%	14,680	195.2	1.30%
8905-11	JP-PNAC-007	173,500	12,145	0.0015	7%	36,810	137.8	3.10%

Further quality control (QC) investigations suggested that the elevated alpha spectrometry results were associated with poor tracer recoveries and sample dilutions required to accommodate the high uranium concentrations. Based on the high bias that was encountered with alpha spectrometry, the Army subjected 136 samples to reanalysis by gamma spectrometry with the gamma spectrometry results serving as the method of record for high-activity samples (U.S. Army 2009a).

2.3.1.2 Alpha Spectrometry

Each of the naturally occurring uranium isotopes addressed herein as well as other alpha-emitting uranium isotopes such as U-233 and U-236, which are not naturally occurring, can be identified and quantified using alpha spectrometry. Alpha spectrometry quantifies isotope-specific alpha activity by a process such that the element of interest (i.e., uranium) is chemically separated and plated out on a disk, which is then counted in a vacuum to quantify the amount of alpha activity present. Similar to gamma spectrometry, the energies of the alpha particles provide a means with which to identify the isotope(s) present and the counting of alpha emissions in each region of interest provides the basis for isotope-specific quantification. For example, U-238 emits alpha particles with energies (and percent abundances) of 4.15 (23) and 4.2 (77) MeV. By contrast, U-234 emits alpha particles with energies (and percent abundances) of 4.72 (27) and 4.77 (72) MeV (Shleien 1992). Subject to overlap of the various peaks produced by the different uranium isotopes, the different energies of the alpha particles allow the isotope to be identified and for the number of counts in the region of interest to be used to quantify the isotopic activity. If total uranium results are desired in preference to isotope-specific data, samples can be processed to extract the uranium and then to determine the uranium content by counting alpha emissions in a gas flow proportional counter or in an alpha liquid scintillation counter.

Alpha spectrometry provides an excellent analytical capability with relatively low detection limits, well-established analytical and associated QA/QC protocols, and reasonable costs. As such, the Army selected alpha spectrometry (American Society for Testing and Materials [ASTM] Method D3972-90M) as the baseline method for analyzing surface water, sediment, groundwater, and soil samples collected semi-annually for the ERM program in 2004. In addition, the Army selected alpha spectrometry (ASTM D3972-90M) to measure total and isotopic uranium (U-234, U-235, and U-238) with an overall project isotopic minimum detectable concentration (MDC) goal of 0.1 picocuries per liter (pCi/L) for water samples and 0.1 pCi/g for soil and sediment samples for site characterization activities from 2008 to 2012.

2.3.1.3 ICP-MS

Unlike gamma spectrometry and alpha spectrometry, which identify and quantify isotopic uranium based on its radiological properties, ICP-MS uses the atomic mass to identify the radioisotope present and to quantify the amount of each isotope present in the sample (i.e., isotope-specific results are generated in terms of mass rather than using radiological units). ICP-MS is a multi-element technique in which samples are introduced into an argon plasma as aerosol droplets. The plasma dries the aerosol, dissociates the molecules, and then removes an electron from the components, thereby forming singly charged ions that are directed to a mass spectrometer, which rapidly scans the mass range to separate and quantify the ions present (Becker 2003). ICP-MS is noted as a "universal and extremely sensitive analytical method for the simultaneous determination of element concentrations at the trace and ultratrace levels, ICP-MS offers the possibility of isotope ratio measurements, which is invaluable for long-lived radionuclide analysis (> 10^4 a [annus or year]) and when the radioactivity is very low" (L'Annunziata 2012). Although ICP-MS provides results in terms of mass, results may be converted into radiological activity units (e.g., Bq/g or pCi/g) by the application of appropriate conversion factors.

Rather than being considered as a single technology, ICP-MS may be more appropriately considered as a group of technologies with significant variability in capabilities. Consequently, detection capabilities can vary significantly for different ICP-MS systems. For ERM samples with U-238/U-234 isotopic ratios exceeding 3.0, the Army uses ICP-MS to re-analyze the samples and determine if the weight percent U-235 falls below 0.7 percent (NRC 2012b), which is discussed in greater detail in Section 2.3.1.5.

2.3.1.4 Fluoroscopy

Fluorometric uranium analysis is based on the excitation (i.e., fluorescence) produced when the sample is fused with sodium fluoride and exposed to ultraviolet light. The resultant photon emission rate is proportional to the number of excited uranyl ions (ORNL 1996) and allows determination of the quantity of uranium present in the sample. This analytical method provides information relative to the total quantity of uranium present in the sample without regard to isotopic identification or quantification. Although the procedure was developed for urine specimens, it is usable for other materials after the uranium has been sufficiently isolated from the matrix (DOE 1997). The uranium fluorescence is quenched by many cations and some anions in the sample and enhanced by a few cations. If interfering ions are present, a direct fluorometric measurement is not suitable and an extraction method must be used to provide accurate results.

Although fluoroscopy was used for the determination of total uranium in some JPG environmental samples, given detectability considerations and the inability of fluoroscopy to provide isotope-specific data, alpha spectrometry has been used since 2004 in lieu of fluoroscopy. In addition, it is notable that the ASTM method (i.e., D2907-97, Standard Test Method for Microquantities of Uranium in Water by Fluorometry) was withdrawn in 2003 by ASTM International without replacement.

2.3.1.5 Evaluation of Laboratory Data

As noted in Section 2.1, natural uranium is defined by NRC as "...uranium containing the relative concentrations of isotopes found in nature (0.7 percent U-235, 99.3 percent U-238, and a trace amount of U-234 by mass). In terms of radioactivity, however, natural uranium contains approximately 2.2 percent U-235, 48.6 percent U-238, and 49.2 percent U-234..." (NRC 2012a). In addition as noted in Section 2.2, NRC defines DU as "...uranium with a percentage of U-235 lower than the 0.7 percent (by mass) contained in natural uranium. (The normal residual U-235 mass content in depleted uranium is 0.2-0.3 percent, with U-238 comprising the remaining 98.7-98.8 percent.)" (NRC 2012b). DU produced for the DOD contains weight/mass percentages of 0.0006, 0.2, and 99.8 for U-234, U-235, and U-238, respectively. The following bullets use these standards for natural uranium and DU activities and masses to interpret laboratory analytical data to determine if uranium is indicative of natural uranium or DU:

- ***Uranium by ICP-MS***—It is notable that U-234 is present in natural and DOD DU with approximate mass concentrations of 0.006 and 0.0006 percent, respectively. U-235, by contrast, is present in natural and DOD DU at approximately 0.7 and 0.2 percent, respectively, or factors of 100 and 300 greater than the mass concentrations of U-234. Given the large mass differences in the relative quantities of U-234 and U-235 present, U-235 mass results are generally compared directly to total mass of uranium present to determine whether individual ICP-MS sample results are indicative of natural uranium or DU. DU is present when the weight percent U-235 is less than 0.7 percent with DOD DU generally containing 0.2 percent U-235 by weight.
- ***Uranium by Activity***—Alpha spectrometry and gamma spectrometry provide results in terms of radioactivity per unit mass (pCi/g) or volume (pCi/L). As noted in Table 2-2, DOD DU contains about 9.7, 1.1, and 89.1 activity percent U-234, U-235, and U-238, respectively, whereas natural uranium contains 49.2, 2.2, and 48.6 activity percent U-234, U-235, and U-238, respectively. As such, the activity concentration of U-234 decreases from 49.2 percent in natural uranium to 9.7 percent in DOD DU or by a factor of about 5. The U-235 activity, by contrast, decreases from 2.2 percent in natural uranium to 1.1 percent in DOD DU or by a factor of two. The U-234/U-235 ratio for natural uranium is about a factor of 22. Although this ratio decreases to a factor of approximately 9 in DOD DU, it is notable that in each case, the U-234 activity concentration is significantly higher than that of U-235. As a result of the associated increase in detection sensitivity when using alpha spectroscopy, the U-238/U-234

activity concentration is generally used in preference to the U-238/U-235 activity concentrations to draw conclusions. Individual alpha spectrometry sample results yielding U-238/U-234 activity ratios of three or less are indicative of natural uranium whereas higher ratios are potentially indicative of DU.

2.3.1.6 Total Propagated Uncertainty

All measurements have some finite level of associated uncertainty. Consistent with the MARLAP Manual (NRC 2004a,b,c), the following sources of total propagated uncertainty (TPU) should be considered when evaluating isotopic uranium data based on radioactivity:

- Radiation counting
- Instrument calibration (e.g., counting efficiency)
- Tracers, carriers, or other methods of yield measurement
- Variable instrument backgrounds
- Variable counting efficiency (e.g., due to the instrument or to source geometry and placement)
- Contamination of reagents and tracers
- Interferences, such as crosstalk and spillover
- Baseline determination (gamma-ray spectrometry)
- Laboratory subsampling
- Volume and mass measurements
- Determination of counting time and correction for dead time
- Time measurements used in decay and ingrowth calculations
- Approximation errors in simplified mathematical models
- Published values for half-lives and radiation emission probabilities.

The counting uncertainty of a radiation measurement (historically called "counting error") is the component of TPU caused by the random nature of radioactive decay and radiation counting. Radioactive decay is inherently random in the sense that two atoms of a radionuclide will generally decay at different times, even if they are identical in every discernible way. Radiation counting is also inherently random unless the efficiency of the counting instrument is 100 percent. Although the counting uncertainty for a single gross radiation counting measurement can be estimated using the Poisson approximation as the square root of the observed counts, when the number of counts is small or even zero, MARLAP recommends that uncertainty be estimated as the square root of the number of counts plus one instead (i.e., that the uncertainty {uN} be estimated as $u(N) = (\{N + 1\}^{0.5})$ [NRC 2004a,b,c]). As such, the counting uncertainty and TPU associated with background and near background results for isotopic uranium by alpha spectrometry (or gamma spectrometry) are commonly a significant percentage of the individual sample results. As such, counting uncertainty must be fully considered when evaluating radiological activity data.

2.3.2 Gamma Walkover Surveys

Gamma walkover surveys serve as screening tools to identify areas that exhibit gamma radioactivity that is elevated with respect to background count rates to facilitate further investigation of such areas. These surveys are performed using a sodium iodide (NaI) gamma scintillation radiation detector, which is interconnected to a data collection (logging) device and a global positioning system (GPS). The detector is maintained about 4 inches (in) (10 centimeters [cm]) above the ground surface and collects data each second consisting of the gamma count rate and location. The system provides both an audible response that is proportional to the count rate and a meter reading of the applicable count rate. To perform a gamma walkover survey, the surveyor proceeds forward at a speed of about 1.6 ft (0.5 meters [m]) per second while moving the detector in a serpentine manner. During the course of the survey, the surveyor investigates any elevated count rates that are identified. Data subsequently are downloaded and

printed, typically at the end of each day. Data then are depicted on maps with color-coding that is indicative of the count rate at each location; thus, areas with elevated count rates are easily identified.

Various sizes and geometries of NaI gamma scintillation detectors are used depending on the characteristics of the gamma and X-ray fields to be evaluated and the desired detection sensitivity. More common general detection hardware includes detectors with cylindrical crystals 2 in (5.1 cm) in diameter and 2 in (5.1 cm) in length (i.e., 2 by 2 in) or 3 by 3 in (7.6 by 7.6 cm) as well as field instruments for the detection of low energy radiation (FIDLERs) with crystals 5 in (13 cm) in diameter and 0.063 in (1.6 millimeters [mm]) thick; and systems with single or multiple large volume crystals each of which is commonly 4 in (10 cm) wide, 4 in (10 cm) high, and 16 in (41 cm) long. The average background count rate exhibited by a given detector is dependent in part on the detector size with count rates of 6,000 to 10,000 counts per minute (cpm) being common for 2- by 2-in (5.1- by 5.1-cm) detector. Further, although the surveyor constantly searches for elevated count rates, a count rate of 1,500 to 2,000 cpm above background is typically required for this detector to provide evidence of elevated count rates. The scan MDC for DU in soil is reported in U.S. Nuclear Regulatory Commission Regulation (NUREG)-1507, Minimum Detectable Concentrations with Typical Radiation Survey Instruments for Various Contaminants and Field Conditions (NRC 1995), as 56 pCi/g when using a 2- × 2-in NaI detector. DU penetrator fragments as small as 0.37 cubic inches (in^3) (6 cubic centimeters [cm^3]) are easily locatable on the soil surface during a typical scan using an investigation threshold of 2,000 cpm above background. Similarly, technical evaluation indicates that a DU penetrator fragment as small as 0.61 in^3 (10 cm^3) can be located easily below 2 in (5 cm) of soil during a typical scan (again assuming an investigation threshold of 2,000 cpm above background). The following table extracted from Appendix A of JPG FSP Addendum 7 (SAIC 2008a) provides information regarding the "Modeled Count Rate Versus DU Fragment Size" for DU fragments located on the ground surface and under 2 in (5 cm) of soil.

Table 2-5. Modeled Count Rate Versus DU Fragment Size at a Distance of 25 Centimeters Jefferson Proving Ground, Madison, Indiana

DU Fragment Size (cm^3)[a,b]	Net Count Rate for DU Fragment on Ground Surface (cpm)[a,b]	Net Count Rate with DU Fragment Beneath 5 cm of Soil (cpm)[a,b]
0.31 in^3 (5.0 cm^3)	1,700	1,100
0.37 in^3 (6.0 cm^3)	2,000	1,300
0.43 in^3 (7.0 cm^3)	2,400	1,500
0.49 in^3 (8.0 cm^3)	2,700	1,700
0.55 in^3 (9.0 cm^3)	3,000	1,900
0.61 in^3 (10.0 cm^3)	3,300	2,100
[a] All data rounded to two significant digits [b] CPM = counts per minute		

In summary, although a 0.061-in^3 (1-cm^3) piece of DU located on the surface of the survey area can be detected, the smallest piece that can be detected with confidence during a normal scan survey using conservative assumptions is a 0.37-in^3 (6-cm^3) fragment. The smallest piece of DU covered with 2 in (5 cm) of soil that can be detected with confidence during a normal scan survey using conservative assumptions is a 0.61-in^3 (10-cm^3) fragment. Given that DU penetrators are much larger than these minimum sizes, a surveyor can reliably detect penetrators or portions thereof during routine surveys irrespective of whether the DU is located on the surface or under 2 in (5 cm) (or more) of soil.

In addition to the modeling reflected above, the Army performed radiological surveys of a full-size, large-caliber, DU anti-armor penetrator with a nominal length of 24 in (61 cm) on the ground surface and at various depths below ground surface (BGS). Table 2-6 reflects the count rates encountered.

Table 2-6. Variation of Penetrator Count Rate With Distance Below Ground Surface Jefferson Proving Ground, Madison, Indiana

Depth	Count Rate (cpm)[a,b]
On ground surface	1.0×10^6
3.6 in (9.1 cm)	3.6×10^5
7.2 in (18 cm)	2.5×10^5
11 in (27 cm)	1.3×10^5
14 in (37 cm)	4.0×10^4
18 in (45 cm)	1.7×10^4

[a] All data rounded to two significant digits
[b] CPM = counts per minute

Based on the above empirical data and given use of the typical scan investigation threshold of 2,000 cpm above background, subsurface DU penetrators should be able to be located to depths of at least 18 in (45 cm) BGS. In addition, detector response of radiation survey instruments is proportional to the uranium concentration of DU penetrator corrosion products. As such, detectability of corrosion products is a function of the uranium concentration together with the depth of the corrosion layer BGS. Empirical data for this scenario have not been collected to date at JPG because the depths and concentrations of DU vary widely.

3. DU PENETRATORS USED AT JPG

Large caliber (i.e., 105- and 120-mm) anti-armor DU penetrators were proof tested at JPG in accordance with NRC Materials License SUB-1435. DU ammunition rounds are nonexplosive projectiles composed of a DU body with aluminum nose cone and tail fins to stabilize the round in flight. DU is used because it has an exceptionally high specific gravity (approximately 19.1 g/cm^3), which allows it to penetrate steel armor.

Specific 105-mm DU penetrators tested at JPG included the models M774 and M833 (USACE 1995). In addition, M829-series (i.e., M829 and M829A2) 120-mm penetrators were tested at JPG (USACE 1995). This section summarizes information regarding the developments and advancements in anti-armor penetrators, masses and dimensions of DU penetrators used at JPG, duration of testing, and masses of DU fired at and recovered from the DU Impact Area.

3.1 DU PENETRATOR BACKGROUND

In the mid-1970s, given the technical difficulties, which were encountered with tungsten carbide penetrators, Army engineers and scientists in coordination with DOE's Battelle Pacific Northwest Laboratories developed the M774 DU kinetic energy penetrator for use in the M60A3 tank. This 105-mm uranium/titanium alloy penetrator served as the basis for the M833 105-mm kinetic energy cartridge that incorporated a longer monolithic DU penetrator, which both enabled it to travel at a higher velocity and reduced the weight of the sabot. As threats became more sophisticated, the M833 was replaced by the M900 DU projectile, which currently meets Army and Marine Corps 105-mm tank ammunition needs and is in its fourth generation (U.S. Army 2013a).

Given the need for 120-mm anti-armor ammunition, the M829 was developed as the first in a series of 120-mm armor piercing cartridges. The M829 was subsequently superseded by the M829A1, M829A2, and M829A3 (or M829E3) in sequence. The M829E4 is the latest version of the 120-mm tank ammunition (Deagel 2011), although it was developed after JPG closed and, as such, was never tested at JPG.

Isotopic uranium composition of DOD munitions is reflected in Table 2-2. The uranium in the DU penetrators is in the form of DU metal, which has been hardened by reducing the carbon content and alloyed with 0.75 weight percent titanium to reduce the overall corrosion rate and improve mechanical properties of the penetrators (Battelle 1990; Bleise, Danesi, and Burkart 2003). As discussed in Section 2.2, DU produced pursuant to reprocessing may contain low concentrations of transuranic elements (e.g., neptunium, americium, and plutonium) and fission products (mainly Tc-99) (U.S. Army 2000, Pollanen et al. 2003).

With respect to the mass of DU contained in penetrators, "the Army Environmental Policy Institute (AEPI 1995) puts the approximate masses of the 105- and 120-mm penetrators as used in the 1991 Gulf War at 3.9 and 4.9 kg, respectively" (Battelle 2012). In addition, Department of the Army Technical Bulletin (TB) 9-1300-278 (U.S. Army 1996) cites DU masses of 7.41 lb (3.4 kg), 8.08 lb (3.7 kg), 6.9 lb (3.1 kg), and 8.69 lb (4 kg) for the M774, M833, M827, and M829, respectively. TB 9-1300-278 also notes that the masses of the XM919, XM900E1, and M829A1 were classified at the time of publication.

Figure 3-1 shows the dimensions and weights/masses for the APFSDS-T DU ammunition fired from 105- and 120-mm guns into the DU Impact Area. Based on the masses shown in Figure 3-1 and the estimated 162,040 lb (73,500 kg) mass of residual DU present at the DU Impact Area, a total of approximately 15,000 to 19,000 penetrators could remain in the DU Impact Area.

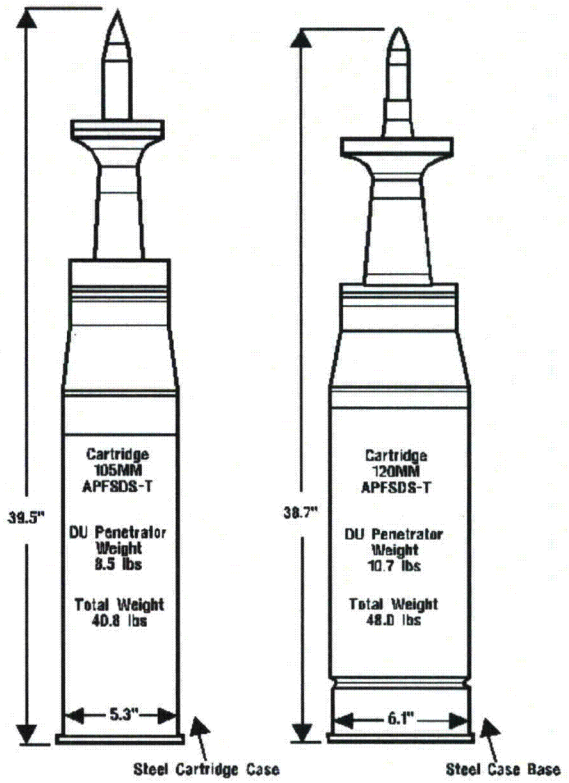

Figure 3-1. Dimensions and Weights of DU Ammunition

Figure 3-2 shows the aluminum sabot, which keeps the penetrator centered in the barrel of the gun, as the sabot petals are being shed shortly after the round exits the gun tube (USATHAMA 1990a). Figure 3-2 also shows the DU penetrator that travels to the target, which is the black, long, pointed, dart-like object that is situated in the center of the photograph.

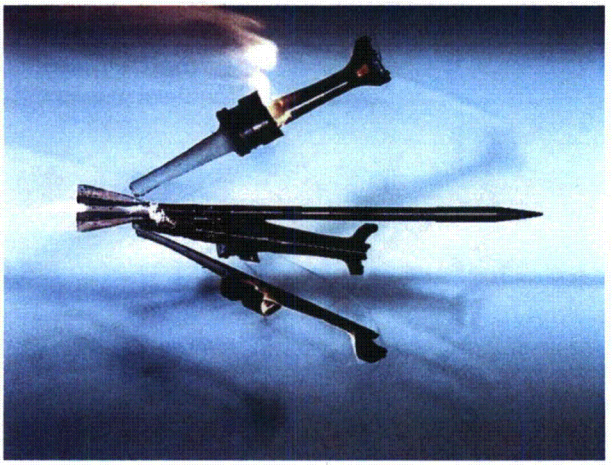

Figure 3-2. Discarding Aluminum Sabot Petals From DU Ammunition

3.2 DU PENETRATOR TESTING AT JPG

Figure 3-1 summarizes the duration of testing and mass of DU fired at and recovered from JPG. The figure is a scanned copy of a slide based on information available in June 1995 after the last DU round had been fired and after the last DU recovery action was conducted by the JPG Radiation Safety Officer (RSO) at that time (Personal Communication 2013b). The slide was part of the JPG Commander's briefing that covered all aspects of JPG operations and history. The briefing was presented to the JPG Jefferson County Reuse Board and other potentially interested parties in their efforts to request the transfer of property south of JPG's firing line from the Army during the property screening process under the BRAC closure law (Personal Communication 2013b).

As shown in Figure 3-3, approximately 220,462 lb (100,000 kg) of DU projectiles were fired into the DU Impact Area. Although not specifically required by NRC Materials License SUB-1435, the Army took actions to recover and dispose of spent DU rounds in order to extend the useful life of the DU Impact Area. Semiannual cleanup activities resulted in the recovery of approximately 58,423 lb (26,500 kg) of DU projectiles and projectile fragments from the DU Impact Area. Approximately 162,040 lb (73,500 kg) of DU is estimated to remain in the DU Impact Area.

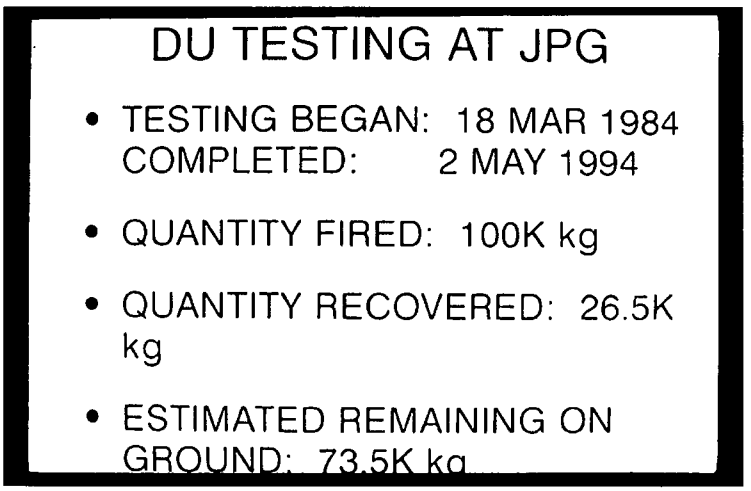

Figure 3-3. DU Ammunition Proof Testing Summary

DU penetrator proof testing performed at JPG was limited to soft target testing to verify the accuracy of the penetrators. All DU rounds were fired by experienced experts from fixed firing positions with steel plate-covered concrete pads and blast shields at cloth (Figure 3-4) or plywood targets placed at 1,000-m intervals starting 1,000 m from gun positions extending up to 4,000 m. The purpose of the proof testing was to check, investigate, and evaluate munitions to determine whether test items conformed to specifications, that they were capable of doing what they were designed to do, and that they met combat requirements. When projectiles travel at supersonic speeds, technicians ascertained accuracy by measuring shockwaves in X-Y coordinates by 70 mini-computers scoring hits on 20- by 20-ft cloth targets with an Accubar System, where shockwaves were accurate within 0.1 in.

Although hard target testing was not conducted, information relative to anti-armor (i.e., hard target) impact of DU penetrators is incorporated herein for completeness because the inhalation or ingestion of DU as an aerosol in sufficient quantity may lead to detrimental effects (Battelle 2012). With regard to their use as anti-armor munitions, NRC notes that "DU is preferred to other metals, because of its high density, its pyrophoric nature (DU self-ignites when exposed to temperatures of 600° to 700°C and high pressures), and its property of becoming sharper, through adiabatic shearing, as it penetrates armor

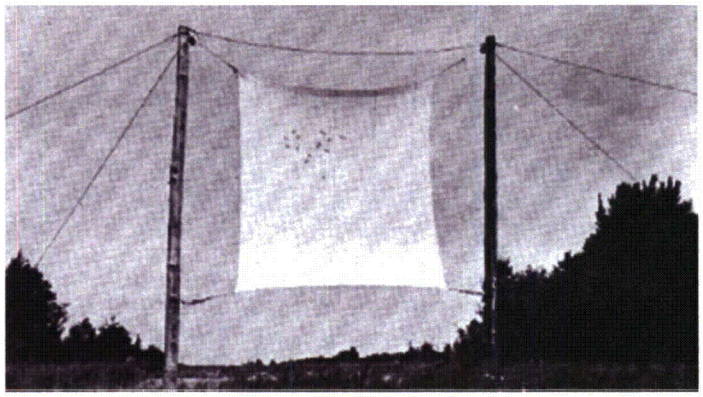

Figure 3-4. 20- by 20-Foot Cloth Targets Located at 1,000 to 3,000 Meters From Firing Points

plating. On impact with targets, DU penetrators ignite, breaking up in fragments, and forming an aerosol of particles (DU dust) whose size depends on the angle of the impact, the velocity of the penetrator, and the temperature. These fine dust particles, can catch fire spontaneously in air. Small pieces may ignite in a fire and burn, but tests have shown that large pieces, like the penetrators used in anti-tank weapons, or in aircraft balance weights, will not normally ignite in a fire" (NRC 2012c). Aerosolization is directly proportional to the hardness of the armor being impacted but is normally expected to be in the range of 10 to 35 percent and may be as high as 70 percent on impact or when DU catches fire. The aerosol generated is reported to be smaller than 5 micrometers [µm] such that they are within the respirable particle range and may remain windborne for an extended time (Henden, Brugge, and Panikkar 2005). Since hard target testing did not occur at JPG, the rounds did not burn or aerosolize as they may have if they had been fired against hardened targets or armor plating.

The majority of DU rounds remained intact after having been fired, though some broke into pieces upon impact with the ground. The penetrators tended to skip and ricochet when they impacted the ground because of the considerable momentum, which allowed them to travel a considerable distance downrange even after impact (USATHAMA 1990b).

4. RESIDUAL DISTRIBUTION OF PENETRATORS

Approximately 220,462 lb (100,000 kg) of DU projectiles were fired at soft targets in the DU Impact Area of which approximately 58,423 lb (26,500 kg) of DU projectiles and projectile fragments were recovered, which leaves approximately 162,040 lb (73,500 kg) of DU suspected to remain in the DU Impact Area. As shown in Figure 2-1, the DU penetrators were test fired from three fixed-gun positions on the east-west oriented firing line. Penetrators were fired from fixed firing positions with steel plate-covered concrete pads with blast shields (Monsanto 1984). Penetrators were fired at soft (cloth or wood) targets placed at intervals of 3,280 ft (1,000 m), starting at 3,280 ft (1,000 m) from each gun position. Since they were not fired at hard targets (e.g., dismantled tanks, armored personnel carriers), the penetrators traveled through the soft targets, hit the earth/buried itself, or ricocheted/continued travelling until each penetrator lost all kinetic energy and fell to the ground. Approximately 7 percent (11,343 lb; 5,145 kg) were fired from the J Firing Position, 89 percent (144,215 lb; 65,415 kg) were fired from the 500 Center Firing Position, and 4 percent (6,482 lb; 2,940 kg) were fired from the K5 Firing Position.

The locations where DU penetrators remain after being fired from three fixed locations at nine different targets are not known. An understanding of the quantities and locations of DU that remains within the DU Impact Area is needed to define the source term for fate and transport modeling, residual radiation dose modeling, and other purposes such as estimating waste volumes for the calculation of remediation costs. Soil sampling, penetrator sampling, and gamma walkover surveys were conducted to characterize the source term. Soil and penetrator samples were collected in the 1990s (SEG 1995, 1996) and more samples were collected in 2008/2012 for the site characterization (SAIC 2008a) associated with decommissioning the DU Impact Area. Each of these sampling efforts also included gamma walkover surveys to identify areas with higher levels of radioactivity, presumably related to DU penetrators and/or corrosion products.

While hundreds of samples were collected and several miles of gamma walkover survey data were collected over large areas, uncertainty remains in the actual locations of the thousands of DU penetrators that remain in the DU Impact Area. Since JPG-specific surface danger zones (SDZs) for predicting the distribution of DU penetrators are not available or are classified, a geographic information system (GIS) modeling approach was used to develop a composite site-specific SDZ for all penetrator models, fired from each firing position, and fired at all nine targets. The composite SDZ is used to determine the spatial distribution of residual DU within the DU Impact Area. The following sections include an evaluation of the following characteristics to develop the SDZ and spatial distribution of residual DU: characteristics of penetrators used, estimates of distances penetrators traveled, predictions of dispersion and ricochet patterns, and estimates of spatial masses from penetrator impacts in the DU Impact Area.

4.1 DESCRIPTION OF SURFACE DANGER ZONES

An SDZ is defined as "The ground and airspace designated within the training complex (to include associated safety areas) for vertical and lateral containment of projectiles, fragments, debris, and components resulting from the firing, launching, or detonation of weapon systems to include explosives and demolitions" (U.S. Army 2009b). The SDZ must contain projectiles, fragments, debris, and components such that the "...Probability of hazardous fragment escapement must not present a greater hazard than 1:1,000,000 (10^{-6}) (unlikely) to the public..." (U.S. Army 2009b). Therefore, any SDZ developed for DU penetrators fired at JPG should contain nearly all penetrators and fragments thereof.

As shown in Figure 4-1, SDZs for artillery testing and training are commonly shaped like fans, so they are often called "range fans." They are weapon-specific depictions that are overlaid on maps or figures to delineate site-specific danger areas using actual locations of firing points, targets, and topographic features. Figure 4-1 (U.S. Army 2009b) shows the components that make up SDZs for tank fired cartridges such as the M774, M833, M829, and M829A2 fired from M1 Abrams Main Battle

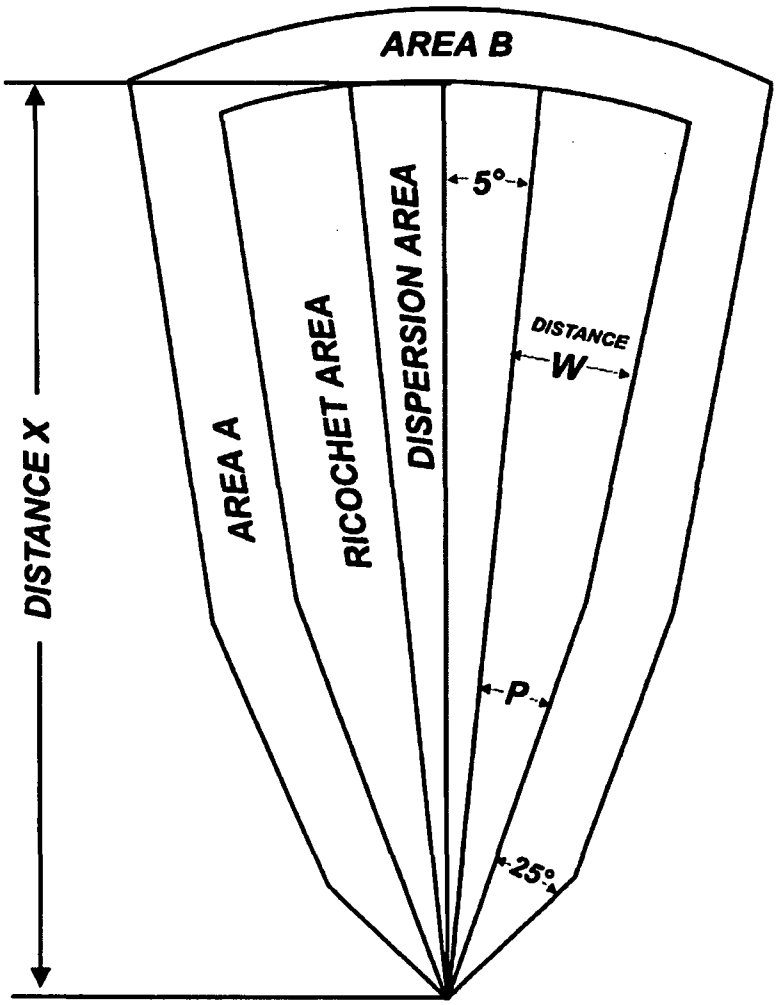

Figure 4-1. SDZ for Firing Tank Cannon Cartridges

Tanks or M60 Main Battle Tanks. These four cartridges are the penetrator models used at JPG that are listed in Department of Army Pamphlet (DA PAM) 385-63 (U.S. Army 2009b).

The SDZ depicted in Figure 4-1 is a symmetrical, fan-shaped polygon that is bisected by an imaginary line running from the bottom of the figure to a point near the top. The bottom of the figure where all lines intersect is the firing point. For the discussion in the following sections, all penetrators were fired from this location. The center line running straight up from the firing point is called the "Gun Target Line" (GTL) or "line of fire." Figure 2-1 uses orange dashed lines to depict the lines of fire for the three firing positions (red stars in Figure 2-1) that run in a northerly direction at targets (small red circles in Figure 2-1).

The line of fire as shown in Figure 4-1 is straight, but in reality, dispersion to the left and right of this line is expected and planned for. Even if multiple rounds of the same model and ammunition lot were fired from the same weapon at the same firing position using the exact same elevation and direction settings, penetrators will be scattered laterally (bearing) and in depth (range) in a dispersed pattern around the aim point following the laws of probability and normal distributions. Although human errors occur when firing artillery, the Dispersion Areas in SDZs (left and right of line of fire in Figure 4-1) account for

the inherent errors beyond the control of personnel. Dispersion Areas extend 5° to the right/left (east/west) of the line of fire to the boundary with the Ricochet Areas to account for uncontrollable causes of dispersion, such as the following (DND 2002):

- Variations of conditions in the bore such as the condition of propellant, arrangement of powder grains, ignition temperature of charge, weight of projectile, form of rotating bands, seating of projectile/ramming, and round to round temperature
- Inaccuracies in bearing and elevation settings on gun carriages, physical limitations on precision in scale settings, and nonuniform reactions to firing stresses
- Changes in air resistance during flight due to differences in penetrator weights, velocities, and shapes that may vary from round to round as well as changes in meteorological conditions such as wind, humidity, and temperature that may change from shot to shot.

Ricochet Areas are situated to the right/left (east/west) of the Dispersion Areas to contain penetrators after making initial impacts with the ground. Ricochet Areas are characterized by Angle P, which begins at the firing points, and Distance W, which establishes the maximum lateral distance a projectile will ricochet after impacting within the Dispersion Area. Additional details about the Angle P, Distance W, and other information needed to define the dimensions of the Ricochet Areas are discussed in Section 4.3.

Areas A and B shown in Figure 4-1 represent secondary danger areas or buffer zones that contain fragments, debris, and components of frangible or explosive projectiles and warheads after they function (e.g., detonate, deflagrate) around the impact area. Since DU penetrators are not frangible or explosive, neither Area A nor Area B has been incorporated into the SDZs for JPG DU penetrators.

4.2 ESTIMATE OF DISTANCES TRAVELED

One of the key characteristics of SDZs for DU penetrators based on Army guidance (U.S. Army 2009b, Table 12-2) is the maximum range (distance) that the DU penetrators could travel if penetrators were fired at an angle of gun elevation (A/E) of 10°. The maximum ranges based on A/E of 10° from DA PAM 385-63 (U.S. Army 2009b) for all DU penetrators included in the pamphlet are listed in Table 4-1.

Table 4-1. Maximum Ranges of DU Penetrator Travel Distance Jefferson Proving Ground, Madison, Indiana

DU Penetrator Model	Maximum Range at 10° (ft/m)
M774 (105-mm)	77,247/23,545
M833 (105-mm)	86,093/26,241
M829 (120-mm)	96,430/29,392
M829A2 (120-mm)	99,282/30,261

However, the maximum ranges based on Army guidance (U.S. Army 2009b) do not appear to apply to penetrators fired at JPG for the following reasons:

- Unclassified reports indicate that the maximum effective range for the M1A1 tank is approximately 3,500 m and that engagement ranges approaching 4,000 m were successfully demonstrated during Operation Desert Storm.
- Footnote 2, from Table 12-2 in DA PAM 385-63 (U.S. Army 2009b) specifically states, "The elevation of fire from the firing position to the target will not exceed 5°." The distances based on an elevation of 10° are presumably meant to err on the side of safety by extending the length of the SDZ to ensure that all munitions fall within the defined boundaries.

- If fired at an angle of 10°, penetrators would have traveled well above (likely by hundreds of feet) the targets used for testing, which were located a maximum distance of 4,000 m from the firing positions, as shown in Figure 2-1. Therefore, if the penetrators had actually been fired at an angle of 10°, technicians would not have been able to accomplish the fundamental purpose of the tests in ascertaining the accuracy of the penetrators, since they would not have impacted the targets.
- If fired at an angle of 10°, some penetrators would have traveled well beyond the northern boundary of the DU Impact Area and, in some cases, could have traveled beyond the northern boundary of JPG. Again, technicians would not have accomplished the fundamental purpose of the testing, since penetrators would not have impacted the targets to ascertain their accuracy.

Lacking data for distances traveled by penetrators after firing, a two part, physics-based approach was used to replace the maximum ranges for penetrators listed in DA PAM 385-63 (U.S. Army 2009b). The first phase was conducted to determine the A/E needed for penetrators to pass through the targets, which were assumed to be placed 9 m above the ground based on the distances between and heights of poles and sizes of targets (Figure 3-4). The second phase uses A/E from the first phase to extend the line of fire until it impacts the ground beyond the target. There are several creeks between the firing points and the points of impact that causes 15 to 20 m of change in topographic relief. Therefore, both phases were completed in conjunction with GIS and a digital elevation model (DEM) to account for elevation changes.

An Excel spreadsheet was set up to calculate the elevation of the penetrator at different distances from the firing point. The distance penetrators traveled from the gun (x) was calculated using the following equation:

$$x = V_i \Delta t \cos(A/E)$$

Where:

V_i = Initial velocity of penetrator (meters per second [m/sec])
Δt = Timestep (0.05 seconds)
A/E = Angle of gun elevation (degrees).

The height of the penetrator (z) relative to the topographic elevation of the gun was calculated using the following equation:

$$z = V_i \Delta t \sin A/E - \frac{1}{2} g \Delta t^2$$

Where:

V_i = Initial velocity of penetrator (m/sec)
Δt = Timestep (0.05 seconds)
A/E = Angle of gun elevation (degrees)
g = Gravity (9.8 meters per square second [m/sec^2]).

Travel times ranged from approximately 0.37 seconds (i.e., travel time from the firing point to the 1,000-m target) to approximately 2.2 seconds (i.e., travel time from the firing point to the 3,000-m target). A timestep of 0.05 seconds was arbitrarily used to provide a series of data points for evaluation. This timestep provided sufficient detail to optimize x and z in combination to ascertain the correct A/E needed for penetrators to hit the targets. Since x is known for each target (1,000, 2,000, 3,000, and 4,000 m), A/E was adjusted iteratively until the value for z corresponded with the elevation of the target height (9 m above ground) minus the height of the gun (2.8 m above the ground) for each known distance. The results of these calculations are shown in the cross-sections in Figures 4-2 through 4-13 as the 1,000-,

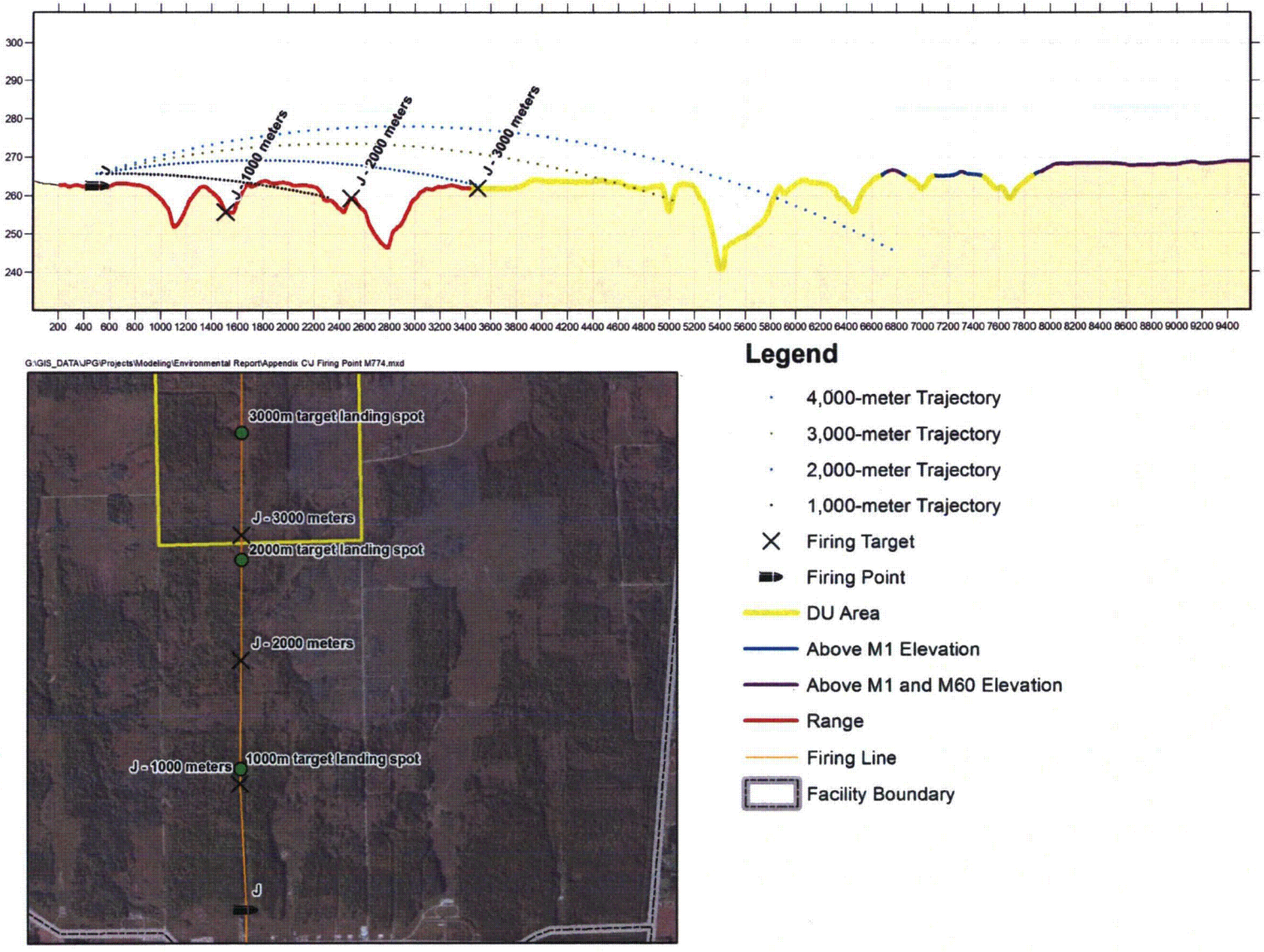

Figure 4-2. Cross-Section/Plan View for Estimation of Distance M774 Penetrators Traveled After Firing From J Firing Position

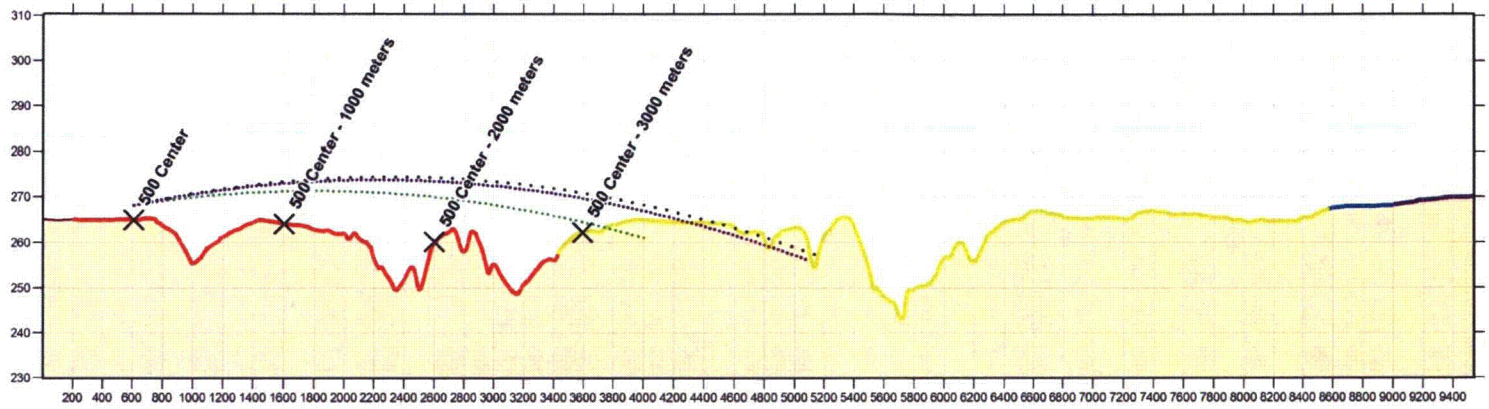

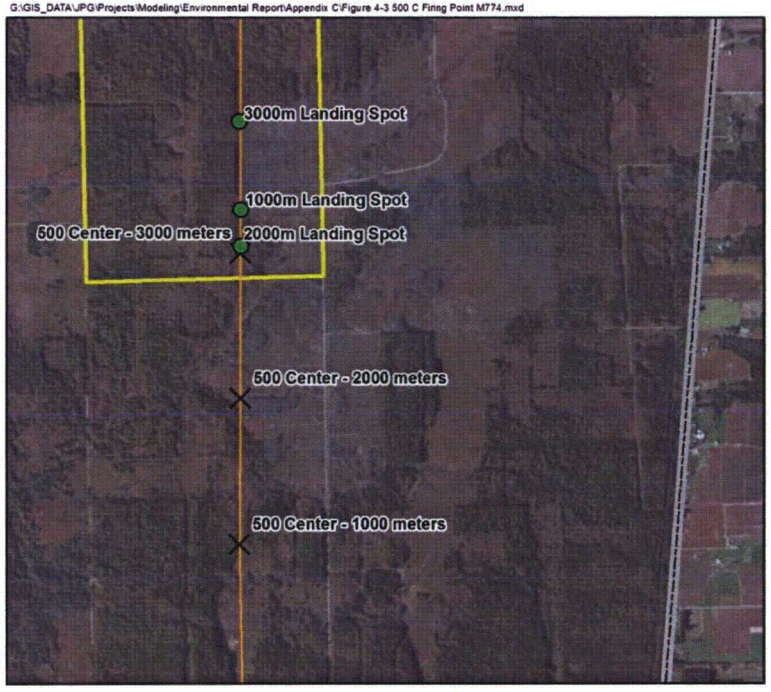

Figure 4-3. Cross-Section/Plan View for Estimation of Distance M774 Penetrators Traveled After Firing From 500 Center Firing Position

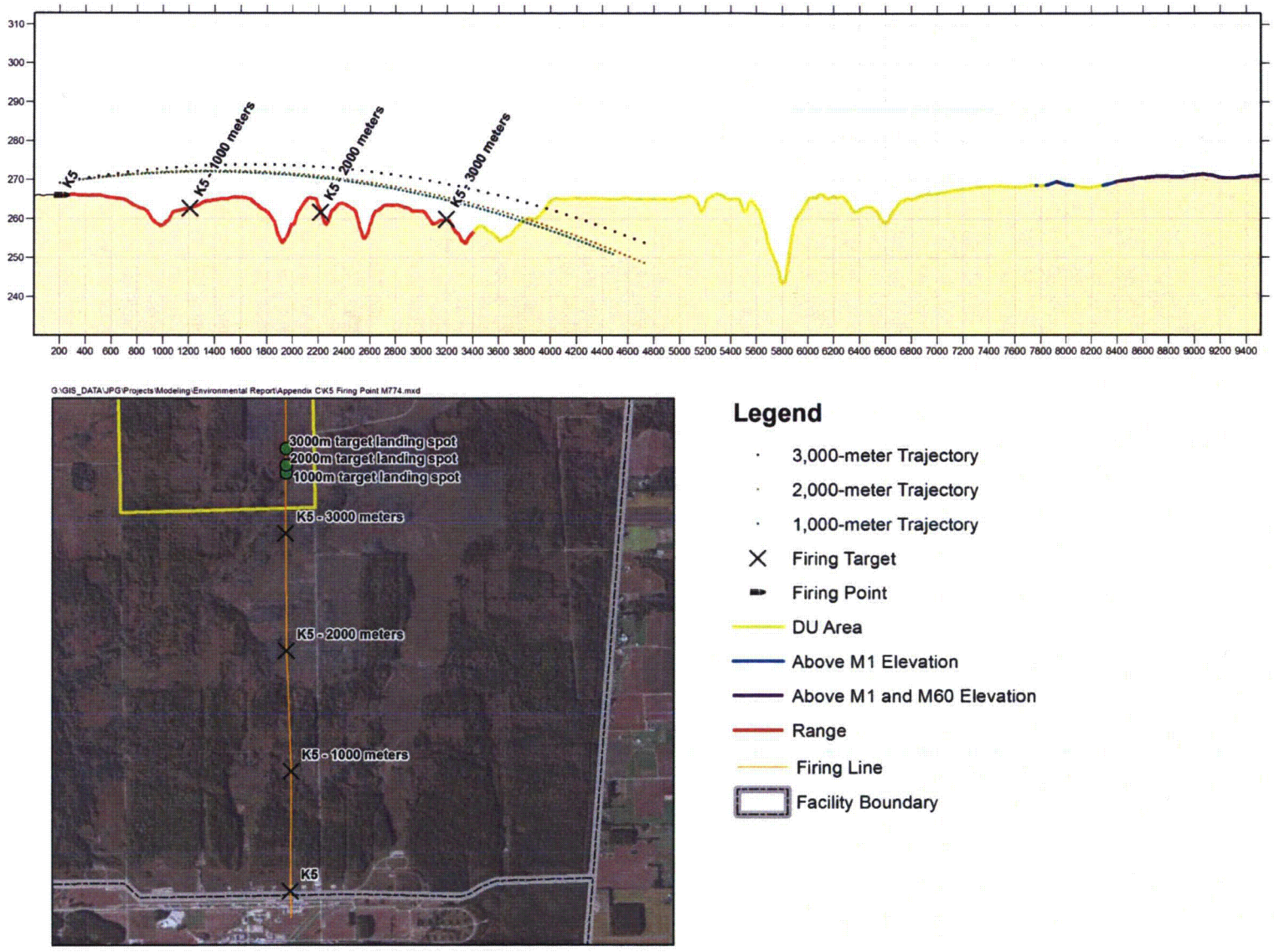

Figure 4-4. Cross-Section/Plan View for Estimation of Distance M774 Penetrators Traveled After Firing From K5 Firing Position

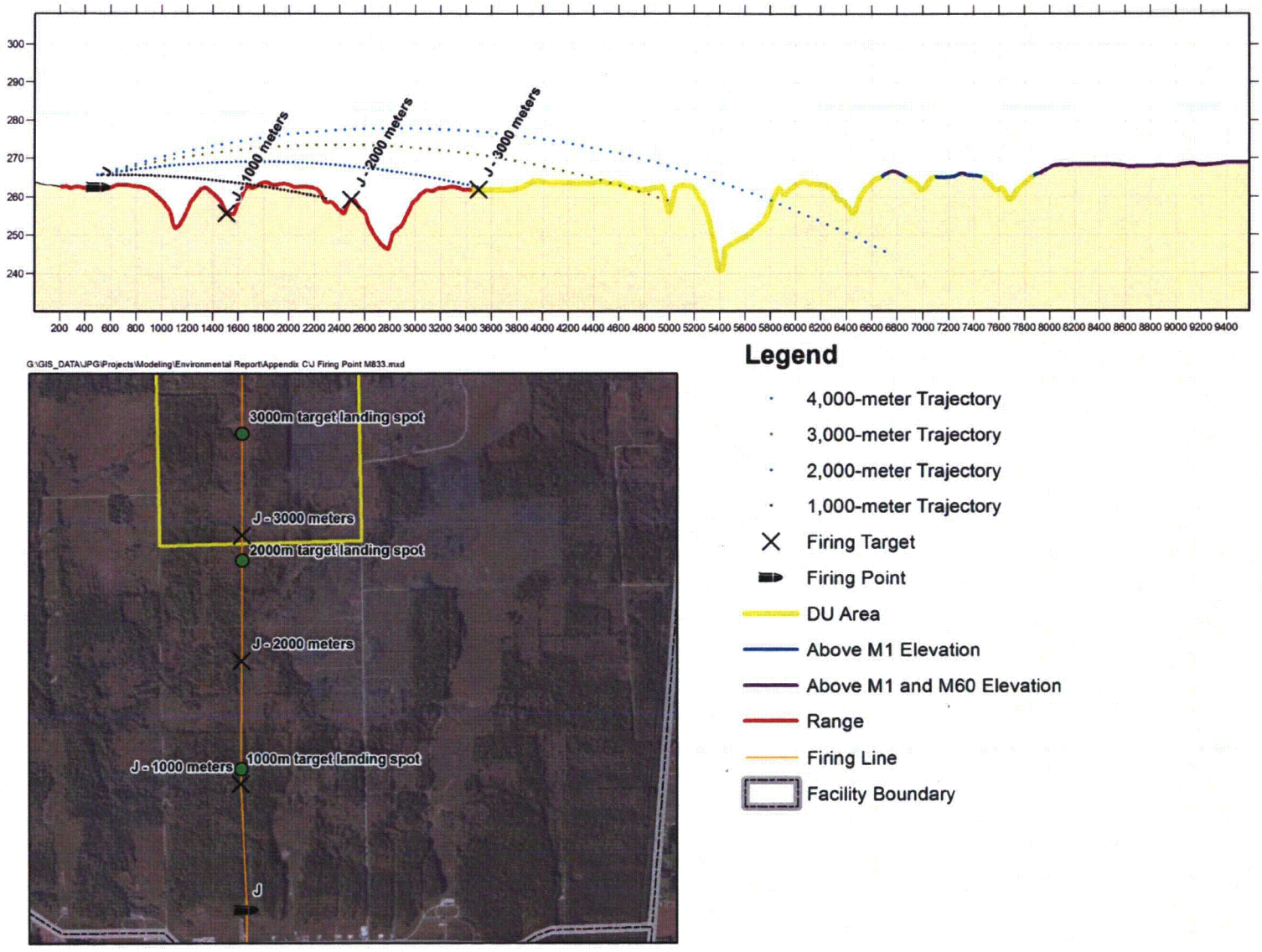

Figure 4-5. Cross-Section/Plan View for Estimation of Distance M833 Penetrators Traveled After Firing from J Firing Position

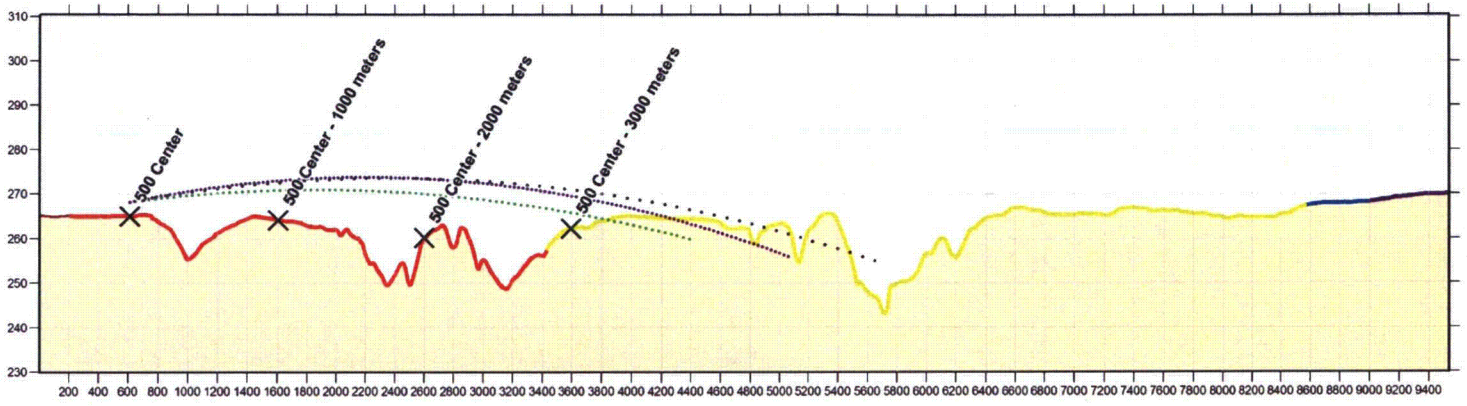

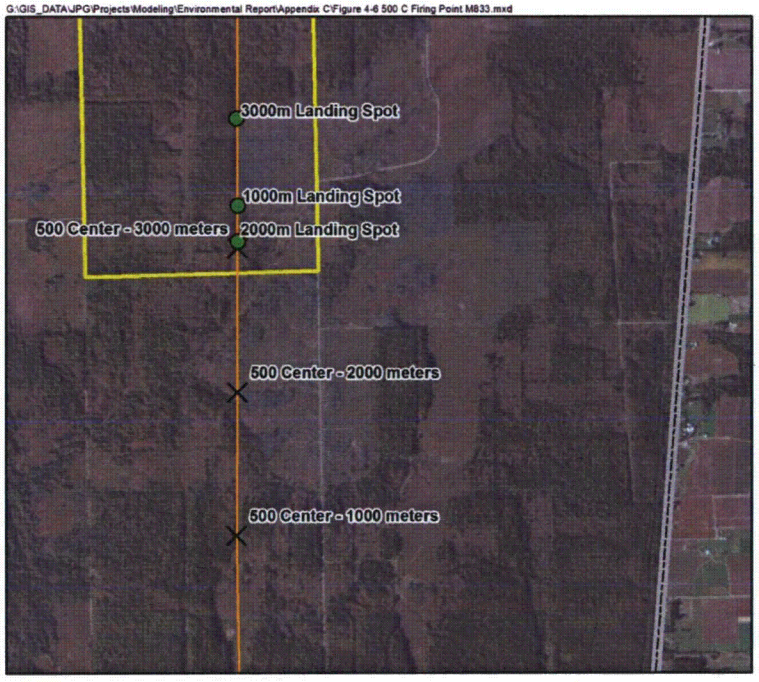

Legend

- 1,000-meter Trajectory
- 2,000-meter Trajectory
- 3,000-meter Trajectory
- Firing Target
- Firing Point
- Above M1 Elevation
- Above M60 Elevation
- DU Area
- Range
- Firing Line
- Facility Boundary

Figure 4-6. Cross-Section/Plan View for Estimation of Distance M833 Penetrators Traveled After Firing from 500 Center Firing Position

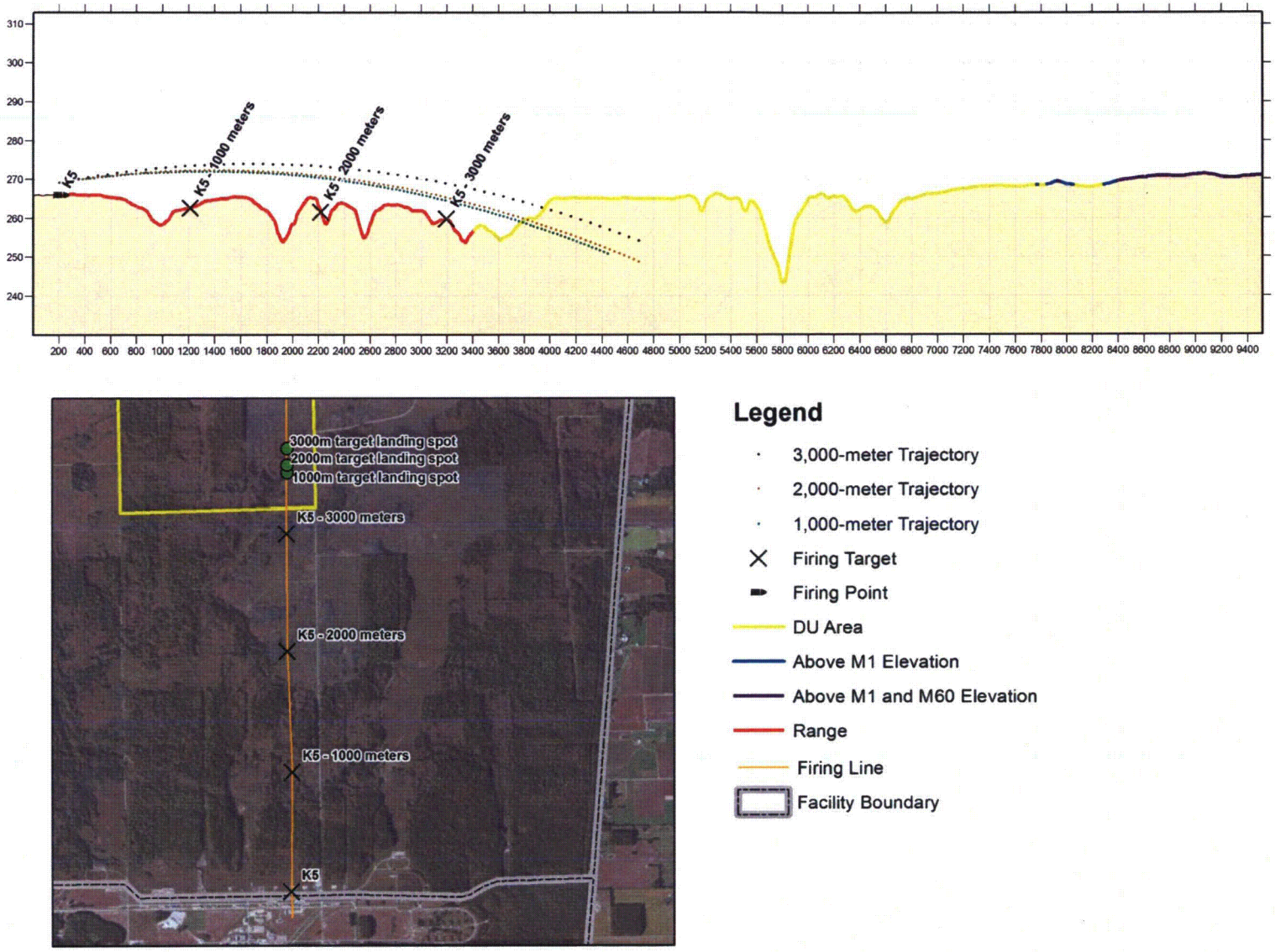

Figure 4-7. Cross-Section/Plan View for Estimation of Distance M833 Penetrators Traveled After Firing from K5 Firing Position

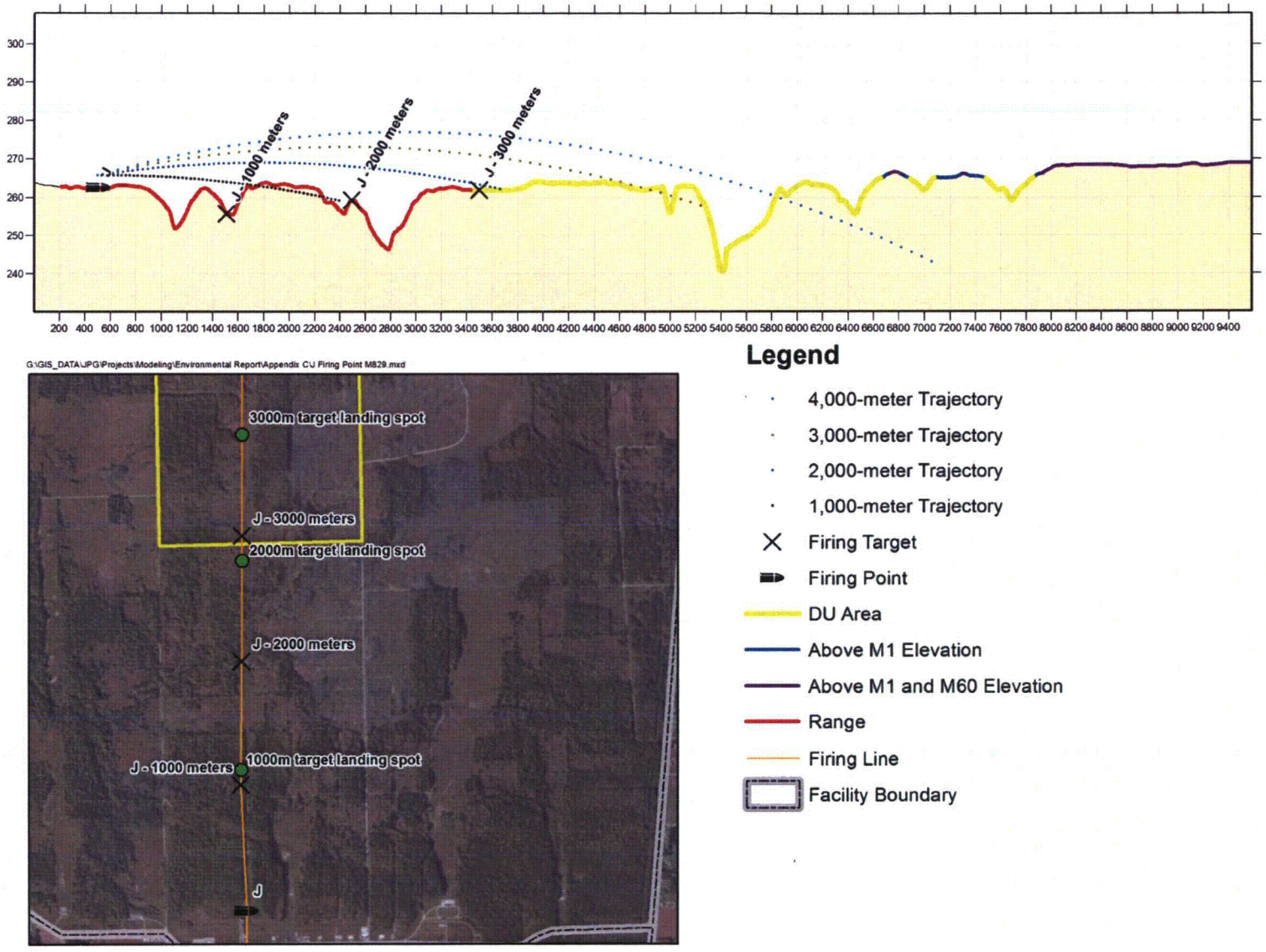

Figure 4-8. Cross-Section/Plan View for Estimation of Distance M829 Penetrators Traveled After Firing from J Firing Position

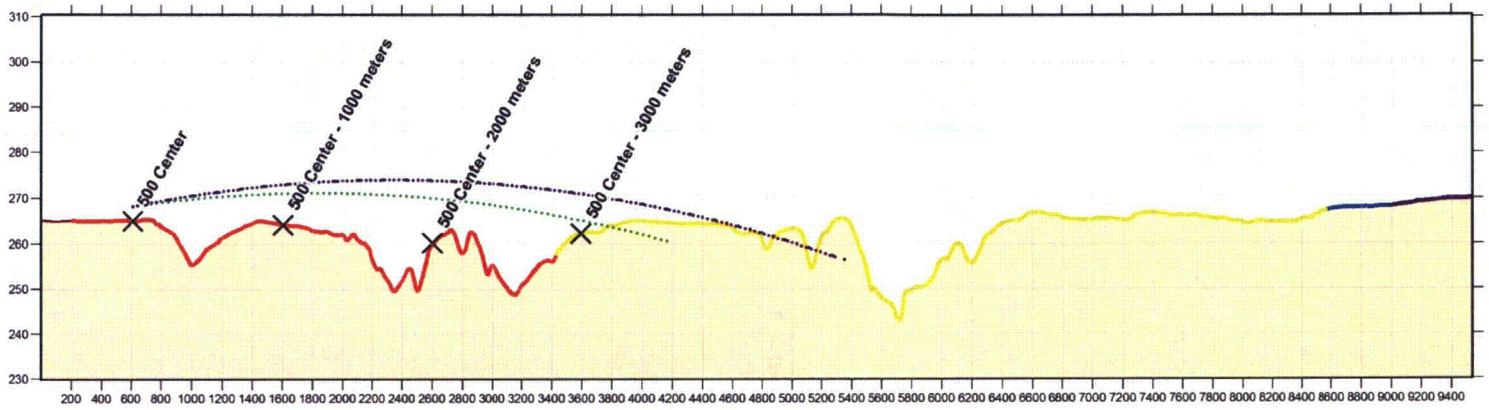

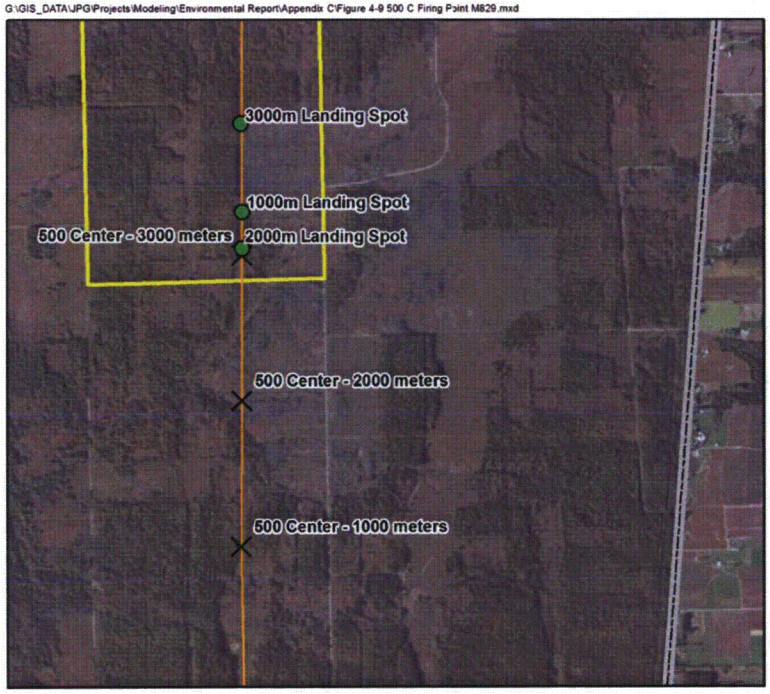

Figure 4-9. Cross-Section/Plan View for Estimation of Distance M829 Penetrators Traveled After Firing from 500 Center Firing Position

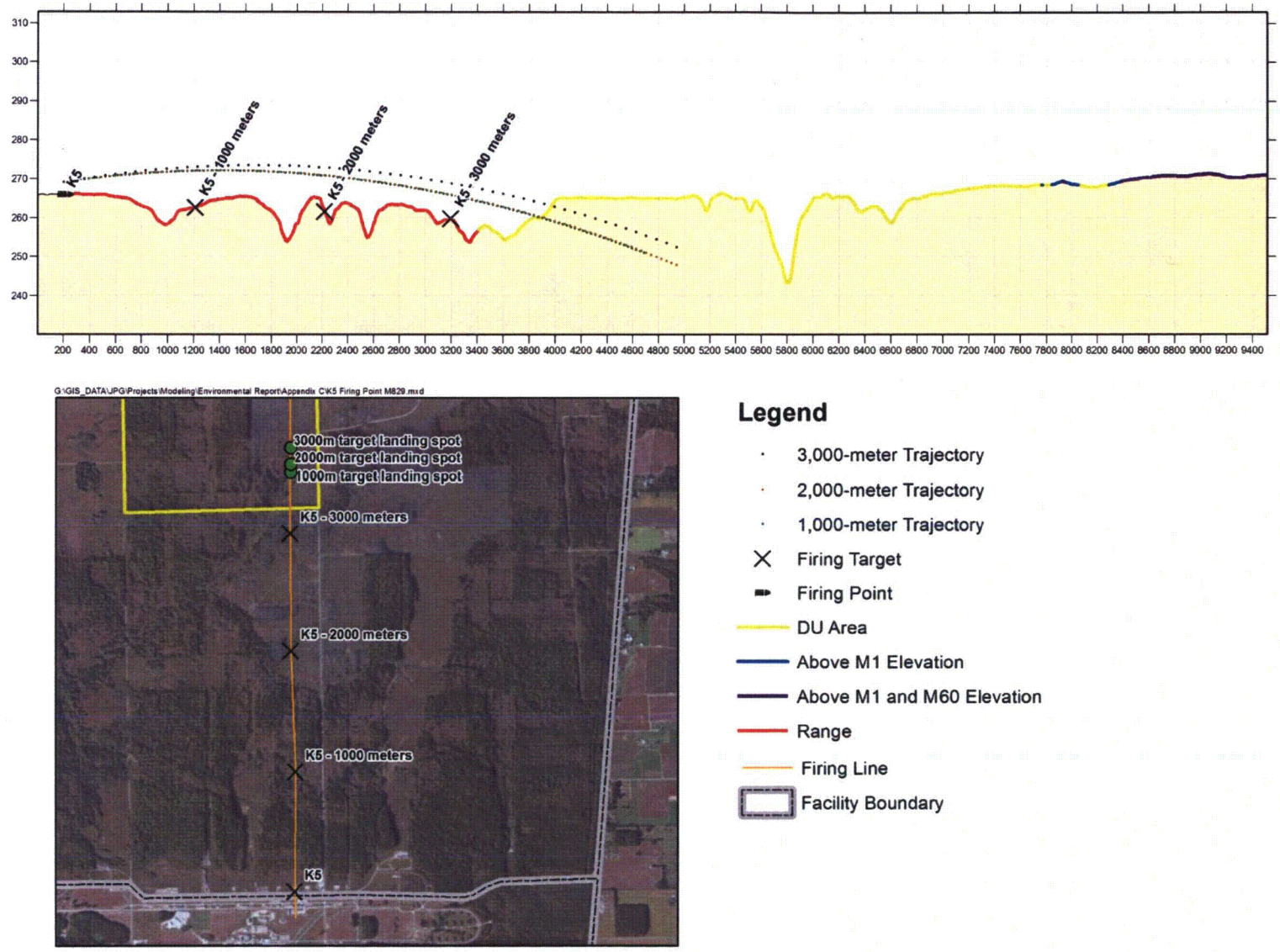

Figure 4-10. Cross-Section/Plan View for Estimation of Distance M829 Penetrators Traveled After Firing from K5 Firing Position

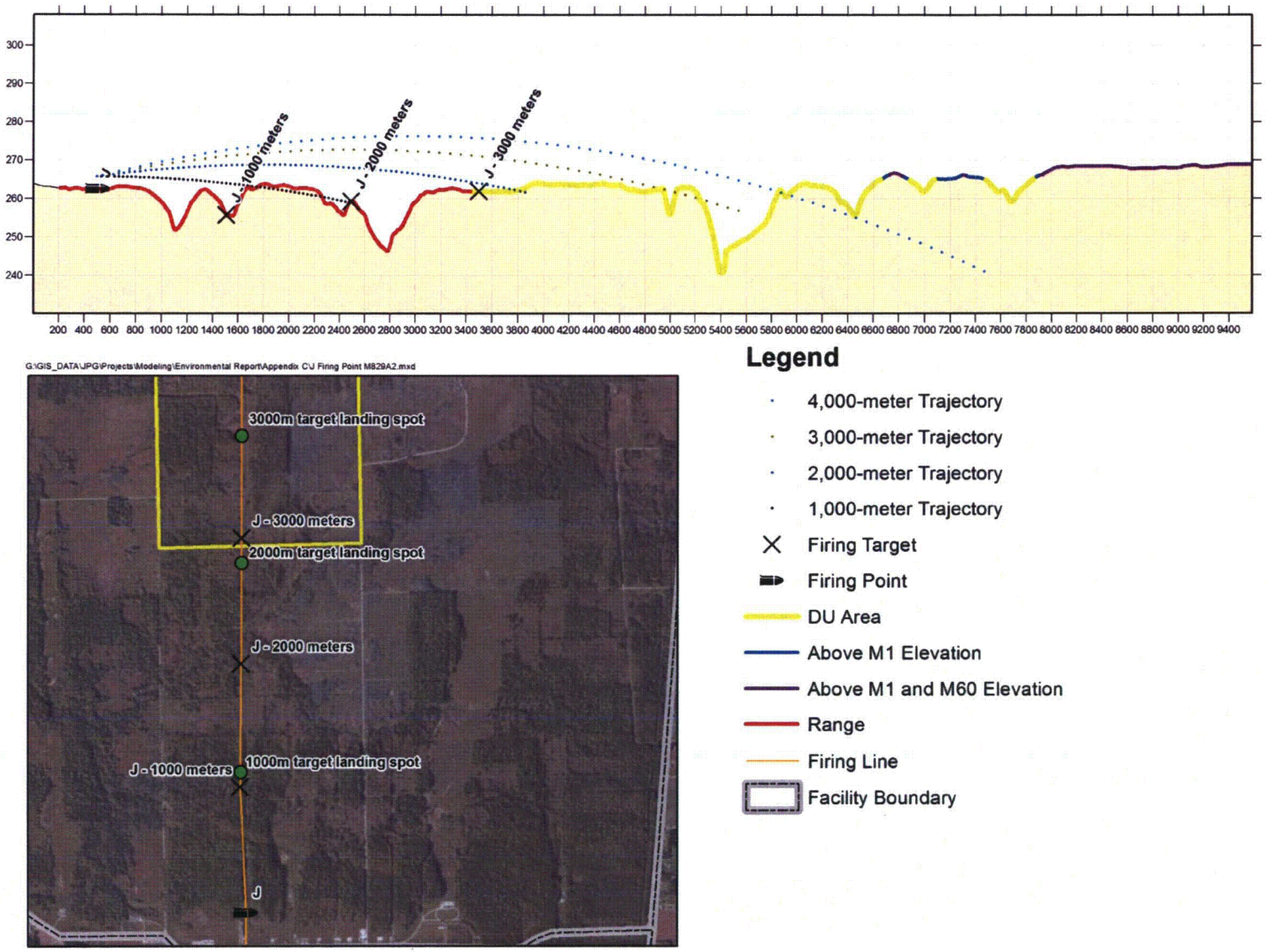

Figure 4-11. Cross-Section/Plan View for Estimation of Distance M829A2 Penetrators Traveled After Firing from J Firing Position

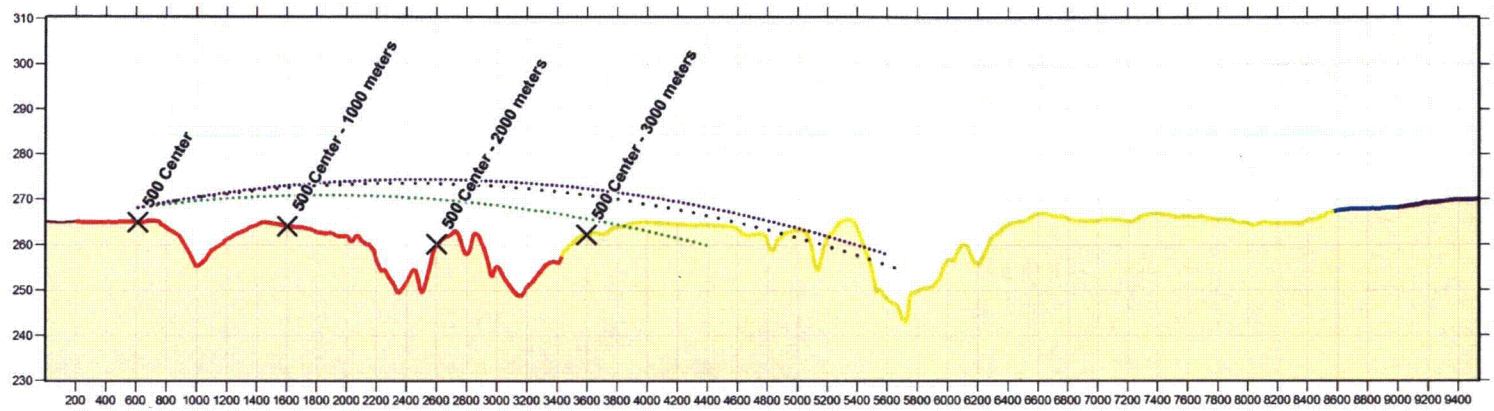

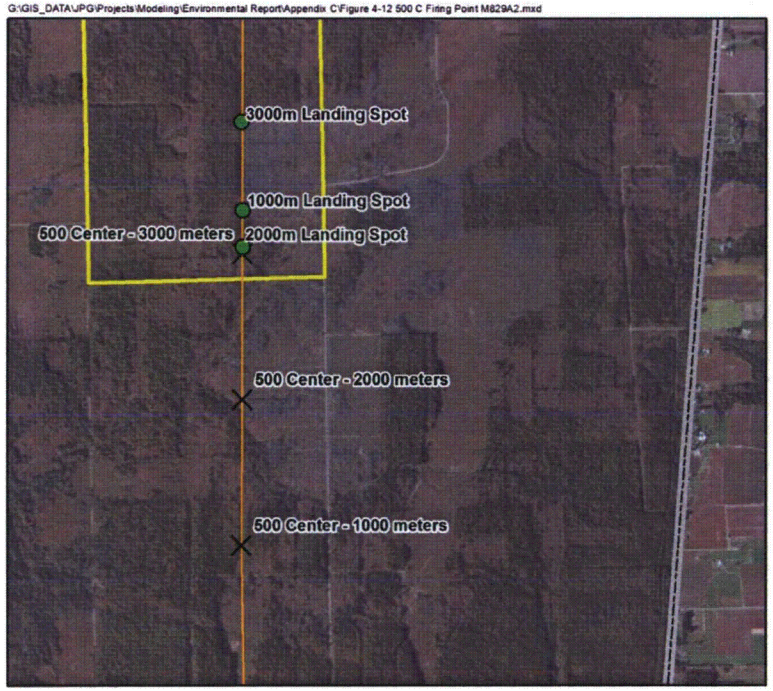

Figure 4-12. Cross-Section/Plan View for Estimation of Distance M829A2 Penetrators Traveled After Firing from 500 Center Firing Position

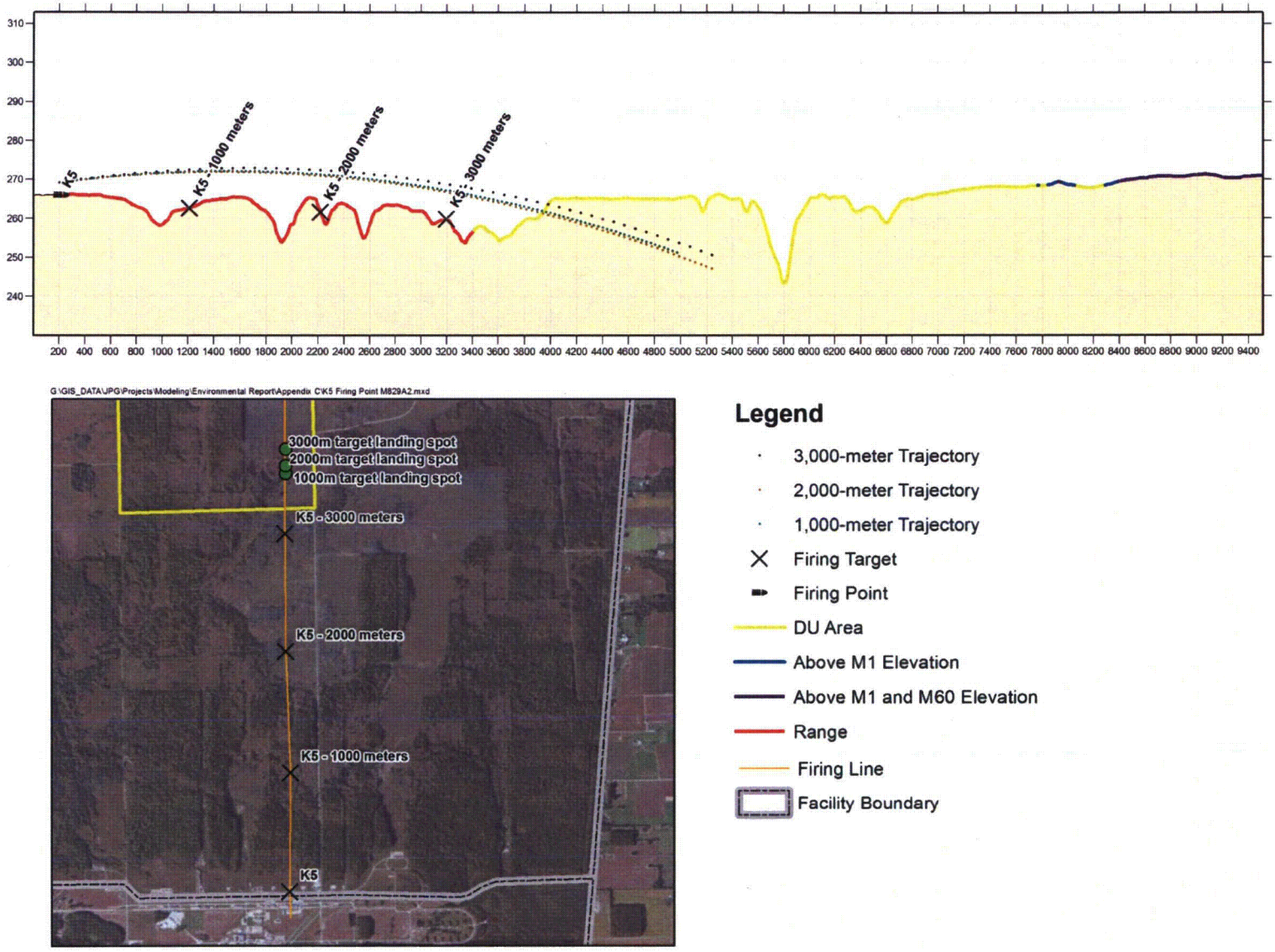

Figure 4-13. Cross-Section/Plan View for Estimation of Distance M829A2 Penetrators Traveled After Firing from K5 Firing Position

2,000-, and 3,000-m trajectories (dotted lines) and the 4,000 m trajectory for the J firing point, which is the only firing point with a target at that distance.

After determining A/E, the same equations then were used to determine the point of initial penetrator impact with the ground. These points of impact are subsequently used in Section 4.3 to estimate dispersion and ricochet patterns for final resting points of penetrators and estimates of mass over area. The input factors for and results of these calculations are shown in Table 4-2 and depicted in Figures 4-2 through 4-13 for the three firing positions for all four penetrator models (M774, M833, M829, and M829A2).

Accounting for the topographic relief is essential. Note that the topographic relief shown in Figures 4-2 through 4-13 has been exaggerated by 30 times. Based on the cross-section and plan views of penetrators fired from the J Firing Position at the 1,000-m target (Figure 4-2), it appears that penetrators fall short of the DU Impact Area. Since this is the only firing position with a 4,000-m target that appears on some maps of the DU Impact Area, it is likely that the Army did not use the 1,000-m target and, instead, used the 4,000-m target to collect data for three different points from the J Firing Position. In addition, Figure 4-3 shows that the initial point of impact for penetrators fired from the 500 Center Firing Position at the 1,000-m target actually travel farther than penetrators aimed at the 2,000-m target. This is because the 2,000-m target is 3 m in elevation below the 1,000-m target. This also explains why the A/E in Table 4-2 for the 2,000-m target of 0.355° is less than the A/E of 0.427° for the 1,000-m target.

4.3 ESTIMATES OF DISPERSION AND RICOCHET PATTERNS

The previous section discussed the minimum ranges/distances of initial penetrator impacts. This section uses that information to predict random side-to-side dispersion along with directions and distances traveled after ricochets occurred when penetrators impacted the ground. This information will subsequently be used in Section 4.4 to determine where penetrators likely remain in the DU Impact Area.

Penetrator firing took place from specifically identified, fixed positions and penetrators were fired at stationary targets. Cloth or wood (20 by 20 ft in size) was strung with cables from poles that were spread approximately 25 m apart several meters above the ground, as shown in Figure 3-4. Since the firing took place in these narrow corridors, the DU projectiles impacted in nearly the same areas in their respective lines of fire. With thousands of repeated impacts in relatively small areas along the line of fire originating from the 500 Center Firing Line (Figure 4-14), this firing protocol resulted in the formation of a trench that was reportedly 3.4 ft (1 m) deep, 16.4 to 26.3 ft (5 to 8 m) wide, and approximately 3,937 ft (1,200 m) long (SEG 1996). A detailed analysis of the terrain and gamma walkover survey data indicates that the penetrators and corrosion products cover an area approximately 6,270 ft (1,911 m) long and 82 ft (25 m) wide. In addition, a second trench was identified for the J Firing Position (Figure 4-15) that covers an area approximately 1,929 ft (588 m) long and 82 ft (25 m) wide. For these reasons, we have assumed that dispersion could extend up to 25 m in a side-to-side corridor perpendicular to the line of fire, as shown in Figure 4-16.

As stated above and shown in Figure 4-16, Ricochet Areas, which contain penetrators after making initial impacts with the ground, are defined by Angle P and Distance W. Angle P bounds the area of lateral deflections as shown conceptually on the left side of Figure 4-16. Maximum deflection (Distance W) is the maximum horizontal ricochet distance. Values for Angle P and Distance W used to establish dispersion and ricochet patterns are provided in DA PAM 385-63 (U.S. Army 2009b) and listed in Table 4-3.

In 2010, the Army declassified the Results of Ricochet Tests of Projectile, 120-mm, APFSDS-T, XM829 (U.S. Army 1984). The U.S. Army Test and Evaluation Command (TECOM) of Aberdeen, Maryland conducted a test to collect ricochet data based on 10 rounds fired at several angles of impact on earthen (turf) targets. The purpose of the test was to determine the range danger zone (RDZ) envelope for

Table 4-2. Input Factors and Results for Calculation of Firing Angles/Elevations
Jefferson Proving Ground, Madison, Indiana

Factor	M774			M833			M829			M829A2		
	J	500 Center	K5	J	500 Center	K5	J	500 Center	K5	J	500 Center	K5
Input Factors												
Initial (Muzzle) Velocity (m/s)	1,508			1,494			1,580			1,680		
Gravity (m/s²)	9.8											
Ground Elevation of Firing Point (m)	262	265	266	262	265	266	262	265	266	262	265	266
Height of Gun (m)	3.2											
Elevation of Gun (m)	266	268	269	266	268	269	266	268	269	266	268	269
Distance to 1,000-m Target (m)	1,005	996	996	1,005	996	996	1,005	996	996	1,005	996	996
Distance to 2,000-m Target (m)	1,988	1,992	2,000	1,988	1,992	2,000	1,988	1,992	2,000	1,988	1,992	2,000
Distance to 3,000-m Target (m)	2,994	2,986	2,982	2,994	2,986	2,982	2,994	2,986	2,982	2,994	2,986	2,982
Distance to 4,000-m Target (m)	3,990	--	--	3,900	--	--	3,900	--	--	3,900	--	--
Ground Elevation of 1,000-m Target (m)	255	264	263	255	264	263	255	264	263	255	264	263
Ground Elevation of 2,000-m Target (m)	259	261	262	259	261	262	259	261	262	259	261	262
Ground Elevation of 3,000-m Target (m)	262	262	260	264	262	260	262	262	260	262	262	260
Ground Elevation of 4,000-m Target (m)	264	--	--	264	--	--	264	--	--	262	--	--
Height of Target (m)	9											
Elevation of 1,000-m Target (m)	264	273	272	264	273	272	264	273	272	264	273	272
Elevation of 1,000 m Target Relative to Firing Point (m)	-1.7	4.8	2.8	-1.7	4.8	2.8	-1.7	4.8	2.8	-1.7	4.8	2.8
Elevation of 2,000-m Target (m)	268	270	271	268	270	271	268	270	271	268	270	271
Elevation of 2,000 m Target Relative to Firing Point (m)	2.3	1.8	1.8	2.3	1.8	1.8	2.3	1.8	1.8	2.3	1.8	1.8
Elevation of 3,000-m Target (m)	271	271	269	271	271	269	271	271	269	271	271	269
Elevation of 3,000 m Target Relative to Firing Point (m)	5.3	2.8	-0.2	5.3	2.8	-0.2	5.3	2.8	-0.2	5.3	2.8	-0.2
Elevation of 4,000-m Target (m)	273	--	--	273	--	--	273	--	--	273	--	--
Elevation of 4,000 m Target Relative to Firing Point (m)	6.9	--	--	6.9	--	--	6.9	--	--	6.9	--	--
Mass of Penetrator (kg)	3.36			3.67			3.94			3.94		
Outputs												
Angle of Gun Elevation (A/E) for 1,000-m Target (m)	0.027	0.398	0.285	0.030	0.402	0.287	0.015	0.389	0.273	0.002	0.378	0.260
Angle of Gun Elevation (A/E) for 2,000-m Target (m)	0.313	0.298	0.299	0.316	0.302	0.303	0.291	0.276	0.277	0.265	0.250	0.251
Angle of Gun Elevation (A/E) for 3,000-m Target (m)	0.470	0.421	0.365	0.478	0.429	0.372	0.438	0.391	0.332	0.400	0.350	0.291
Angle of Gun Elevation (A/E) for 4,000-m Target (m)	0.591	--	--	0.594	--	--	0.540	--	--	0.490	--	--
Distance to Initial Point of Impact (m)	3,025	3,155	3,575	3,000	3,210	3,575	3,150	3,165	3,700	3,250	3,200	3,760

Figure 4-14. Aerial View of 500-Center DU Trench (Early 1990s)

Figure 4-15. DU Trench from J Firing Position (October 2008)

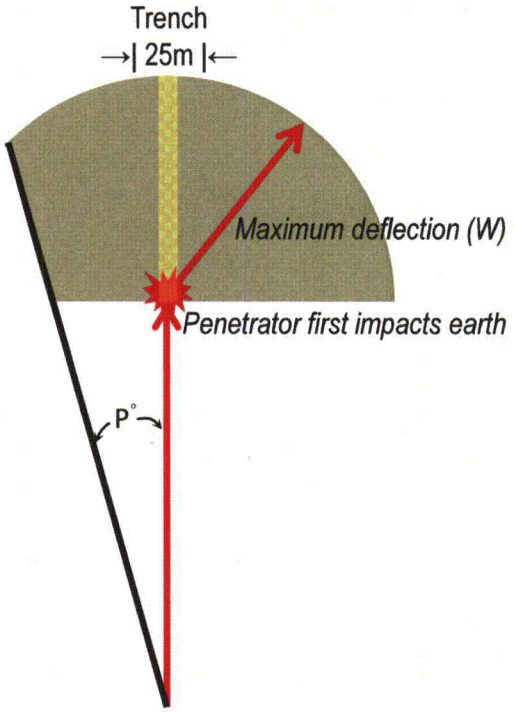

Figure 4-16. Conceptual Approach for Estimating Dispersion/Ricochet Patterns

Table 4-3. Maximum Ranges of DU Penetrator Travel Distance Jefferson Proving Ground, Madison, Indiana

DU Penetrator Model	Maximum Deflection (W) (ft/m)	Ricochet Angle (P) (degrees)
M 774 (105-mm)	3,346/1,020	12°
M833 (105-mm)	5,909/1,801	16°
M 829 (120-mm)	3,510/1,070	11°
M 829A2 (120-mm)	4,593/1,400	26°

the XM829 projectile, which is defined by the maximum range, deflection, and height that will contain all possible ricocheting projectiles or projectile parts. The portion of the results pertaining to DU penetrator testing at JPG is summarized in Table 4-4. The highest deflection value shown in Table 4-4 (1,046 m for end-on ricochets fired at 1,000 m) is similar to the value of maximum deflection (Distance W) for the M829 projectile of 1,070 m shown in Table 4-3.

In addition to summarizing the test results, the Ricochet Tests report (U.S. Army 1984) also provided the following details regarding the condition of penetrators after they impacted the ground: "After the projectile impacted, it was severely damaged and its ballistics greatly changed. All test rounds observed on film broke into many pieces. The largest piece was estimated to be 401-mm (15.8") long by 21-mm (.83") in diameter. It is expected that this would be the largest piece that will remain intact after any earth impact…"

Table 4-4. Ricochet Test Data for 120-mm APFSDS-T XM829 Conducted on Earthen Targets Jefferson Proving Ground, Madison, Indiana

Orientation [a]	Target Range (ft/m)	Range to Impact (ft/m)	Range [b] (ft/m)	Deflection (ft/m)
End-on	1,000	1,867	9,939	1,046
	2,000	2,575	10,381	1,014
	3,000	3,425	10,936	974
Tumbling	1,000	1,867	3,903	318
	2,000	2,575	4,567	312
	3,000	3,425	5,362	305
Broadside	1,000	1,867	3,367	244
	2,000	2,575	4,046	239
	3,000	3,425	4,859	234

[a] Projectile orientation after impact
[b] Range from weapon to projectile stop (range to impact plus ricochet) measured on the line of fire

Truncated, semi-circularly shaped polygons representing the dispersion and ricochet patterns were developed using Angle P and Distance W for each penetrator model from DA PAM 385-63 (U.S. Army 2009b). The points of initial impact in each polygon, which is located at the bottom in the center of each polygon, were situated over the initial points of penetrator impact based on predictions described in the previous section. Figure 4-17 illustrates the different dispersion/ricochet patterns for the four penetrator models (M774, M833, M829, and M829A2) fired from each firing point (J, 500 Center, and K5).

A grouping of dispersion/ricochet patterns for each of the four penetrator models (M774, M833, M829, and M829A2) was extended to the next point of impact along the 500 Center line of fire. Personal communication (2013a) confirms that the trench along the 500 Center line of fire was formed during the first few months of firing such that subsequent penetrators could travel downrange beyond Big Creek.

The pie-shaped SDZ for firing tank cannon cartridges shown in Figure 4-1 and the truncated semi-circularly shaped polygons representing dispersion/ricochet patterns depicted in Figure 4-17 are distinctly different in appearance. The lower end of the SDZ between the firing position and the initial point of impact has been eliminated from the dispersion/ricochet patterns. This is because SDZs for operational ranges (Figure 4-1) are meant to limit personnel access and construction of structures within the SDZ, whereas SDZs for the DU Impact Area are used to predict where DU penetrators may remain. Since few, if any, penetrators would have been aimed at points short of targets because of potential safety hazards presented to personnel, this area has been excluded from the SDZs for predicting DU distribution. This approach is conservative because assuming a higher density of penetrators within a smaller area (i.e., by excluding the lower portion of the SDZ) leads to higher concentrations for the source term and subsequently higher residual radiation doses and higher predicted concentrations in surface water and groundwater in fate and transport modeling.

4.4 ESTIMATES OF MASSES FROM PENETRATOR IMPACTS

The process of estimating the masses from penetrator impacts by location within the DU Impact Area begins with predicting where penetrators are more and less likely to land within the dispersion/ricochet areas discussed in the previous section. While the sizes of the dispersion/ricochet patterns developed for each penetrator model will differ, the potential for DU penetrators to impact certain areas within the dispersion/ricochet pattern is essentially the same regardless of penetrator model. The potential for impact is based on observations made during gamma walkover surveys and after evaluating gamma walkover results shown in Figure 4-18. During walkover surveys conducted along the three lines of fire (south/north oriented paths), most penetrators appeared to have been distributed in fairly narrow corridors from 20 to 30 m in width. Penetrators were most apparent where trajectories likely

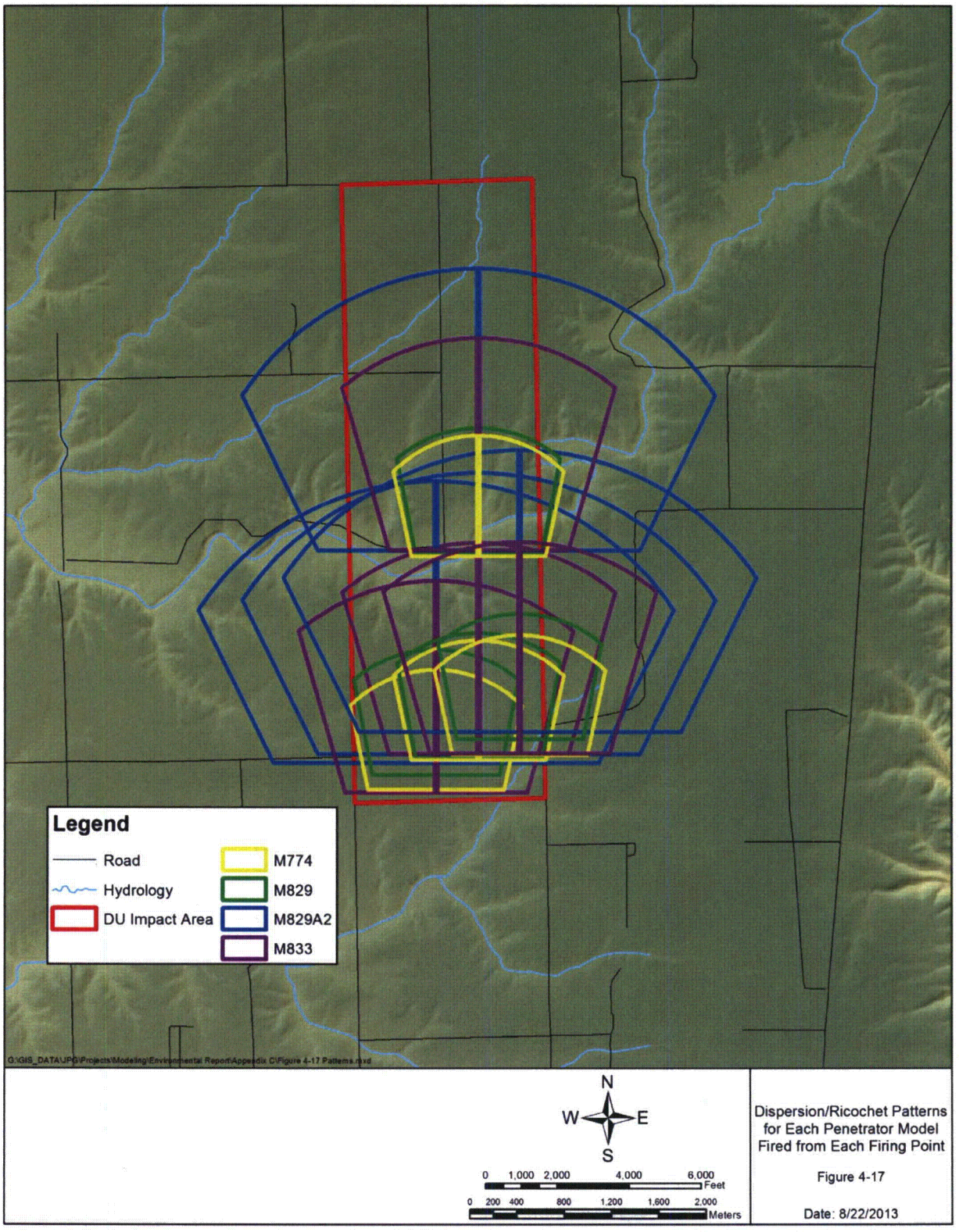
Legend
Road
Hydrology
DU Impact Area
M774
M829
M829A2
M833
G:\GIS_DATA\JPG\Projects\Modeling\Environmental Report\Appendix C\Figure 4-17 Patterns.mxd
N
W
E
S
0 1,000 2,000 4,000 6,000 Feet
0 200 400 800 1,200 1,600 2,000 Meters
Dispersion/Ricochet Patterns for Each Penetrator Model Fired from Each Firing Point
Figure 4-17
Date: 8/22/2013

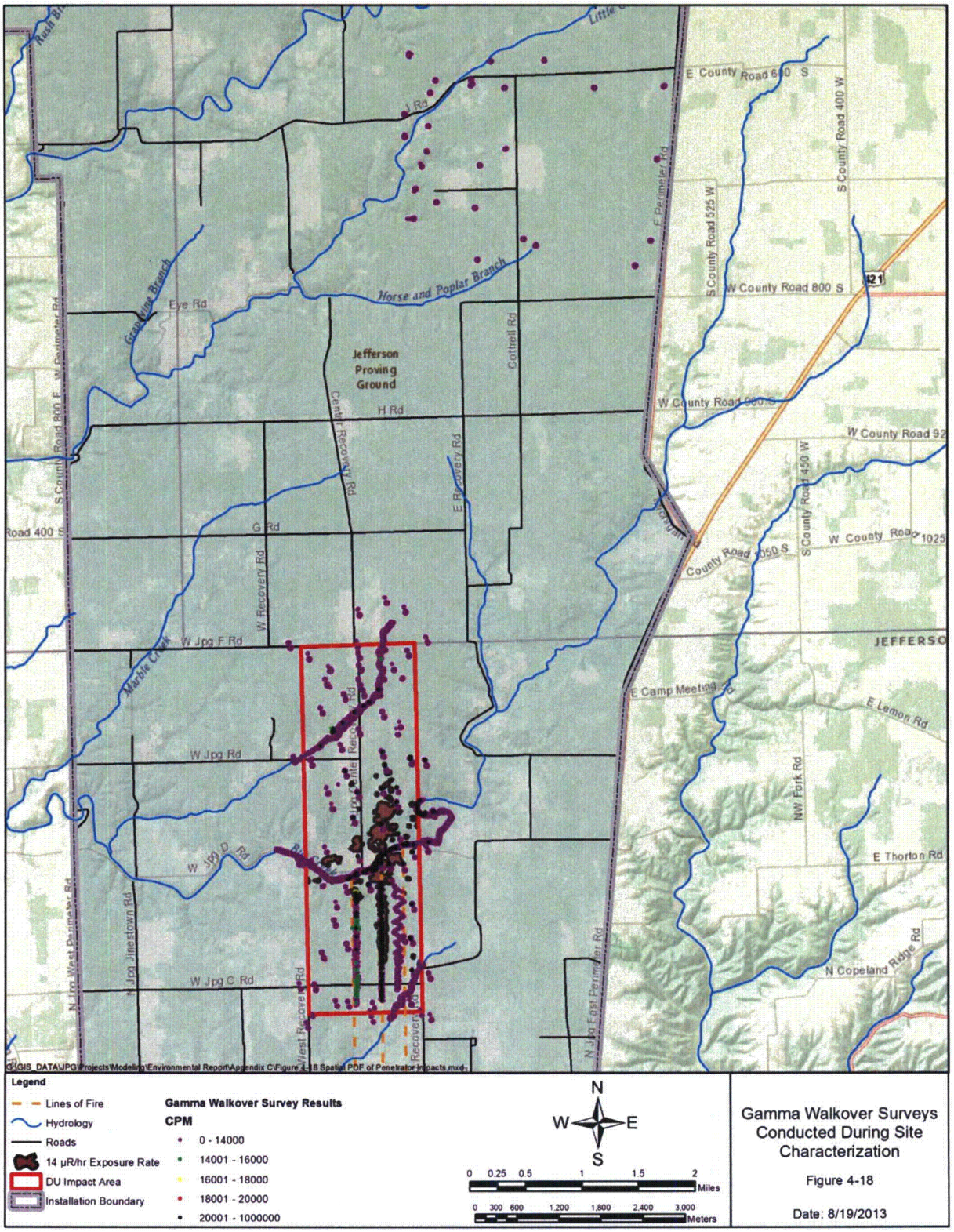
Jefferson Proving Ground
Horse and Poplar Branch
Eve Rd
H Rd
G Rd
W Jpg F Rd
W Jpg Rd
W Jpg D Rd
W Jpg C Rd
E Recovery Rd
W Recovery Rd
Cottrell Rd
E County Road 600 S
W County Road 800 S
S County Road 400 W
S County Road 525 W
S County Road 450 W
E Camp Meeting Rd
E Lemon Rd
NW Fork Rd
E Thorton Rd
N Copeland Ridge Rd
N Jpg East Perimeter Rd
Legend
Lines of Fire
Hydrology
Roads
14 µR/hr Exposure Rate
DU Impact Area
Installation Boundary
Gamma Walkover Survey Results
CPM
0 - 14000
14001 - 16000
16001 - 18000
18001 - 20000
20001 - 1000000
N
W
E
S
0 0.25 0.5 1 1.5 2 Miles
0 300 600 1,200 1,800 2,400 3,000 Meters
Gamma Walkover Surveys Conducted During Site Characterization
Figure 4-18
Date: 8/19/2013

intersected with elevated terrain. During gamma walkover surveys completed along the creeks (east/west or northeast/southwest oriented paths), however, penetrators were detected along Big Creek and the northern tributary of Big Creek in areas between and outside corridors generally associated with the lines of fire. In particular, as shown in Figure 4-18, some DU penetrators were identified approximately 250 m east of the eastern boundary of the DU Impact Area, which is approximately 450 m east of the closest line of fire (i.e., associated with K5 Firing Position). While some lateral movement of penetrators could have occurred after penetrators landed (e.g., movement in stream channels during storm events), this movement likely would have been from east to west because of the direction of surface water flow. Thus, it seems unlikely that any penetrators were moved to these locations from stream flow and more likely that they landed there after being fired.

Based on observations and conclusions made during and after gamma walkover surveys, the spatial distribution for penetrator impacts is built on the assumption that the majority (i.e., 50 percent) of the DU penetrators impacted in a 25-m central strip where laterally scattered penetrators dispersed after being fired. The remaining DU mass (i.e., 50 percent) is divided equally on each side of that central corridor to account for ricochets. The conceptual depiction of this spatial distribution is shown in Figure 4-19.

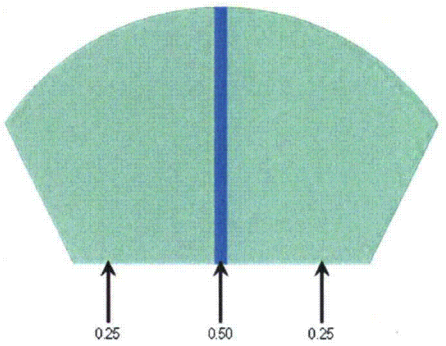

Figure 4-19. Spatial Distribution of Penetrator Impacts for a Single Dispersion/Ricochet Area

After building shapefiles of spatial distributions in ArcGIS® using the dimensions applicable to each of the four penetrator models (M774, M833, M829, and M829A2), the mass of DU was distributed proportionally to the respective firing position as follows: 89 percent (65,415 kg; 144,215 lb) fired from 500 Center Firing Position, 7 percent (5,145 kg; 11,343 lb) fired from J Firing Position, and 4 percent (2,940 kg; 6,482 lb) fired from K5 Firing Position. The mass for each firing position was further apportioned equally by firing model, except for the M829A2 model, which received a lower proportion because it was not produced until 1994. A mass equivalent to 24.5 percent was assigned to each of the following models: M774, M833, and M829. A mass of 2 percent was assigned to model M829A2 based on the 4-month period over the entire 123 months of penetrator testing that occurred between 18 March 1984 and 2 May 1994. Then, the shapefiles were placed at the point of initial impact and layered one on top of another, as shown in Figure 4-17. Sixteen total layers were combined in this way ([four spatial PDFs for each penetrator model × three firing positions where each model was fired] + spatial PDFs for each of four penetrator models placed at the point of initial impact north of Big Creek). The resulting masses from penetrator impacts were calculated within each area and masses for overlapping area resulting from the numerous overlays were the result of weighted averages based on the respective area sizes and mass of DU per acre (ac). A conceptualized example calculation using arbitrary values for two penetrator distributions with overlap in one small area is illustrated in Figure 4-20.

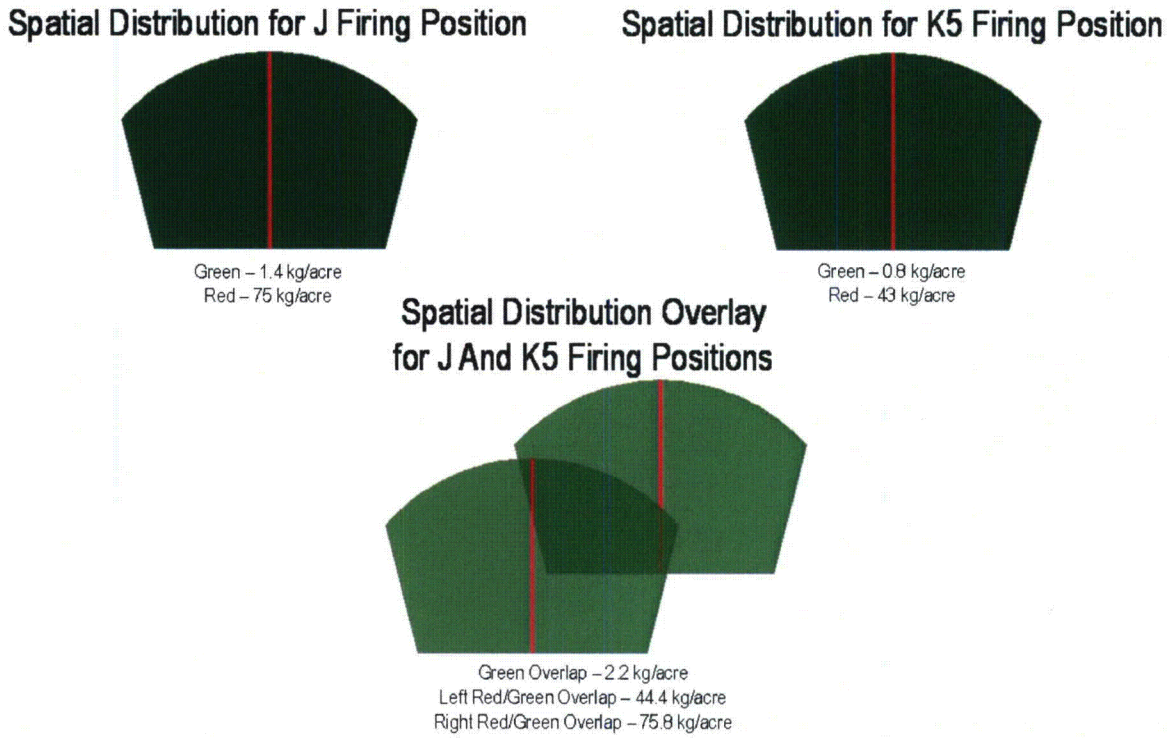

Figure 4-20. Conceptualized Example Calculations for Spatial Distribution of DU Penetrator Mass for Two Overlapping Distributions

The masses of DU were calculated at each point in space over the entire area from the overlays of numerous shapefiles to estimate the DU masses within the combined area of all the shapefiles to create the final composite SDZ. Figure 4-21 shows the resulting distribution of DU penetrator mass.

As shown in Figure 4-21, the primary impact locations were in the trench associated with the 500 Center Firing Position, which covers an area of approximately 11.3 ac (0.046 km^2) with an estimated penetrator density greater than 515 penetrators per ac. Secondary impact locations developed when the projectiles skipped or ricocheted, either whole or in fragments, covering an area approximately 3,844 ac (15.6 km^2) with an estimated penetrator density ranging from 3 to 515 penetrators per ac. Figure 4-12 shows the spatial distribution for the DU penetrators suspected of remaining at and around the JPG DU Impact Area and Table 4-5 summarizes the masses based on the spatial distribution. The total area covers approximately 3,844 ac (15.6 km^2).

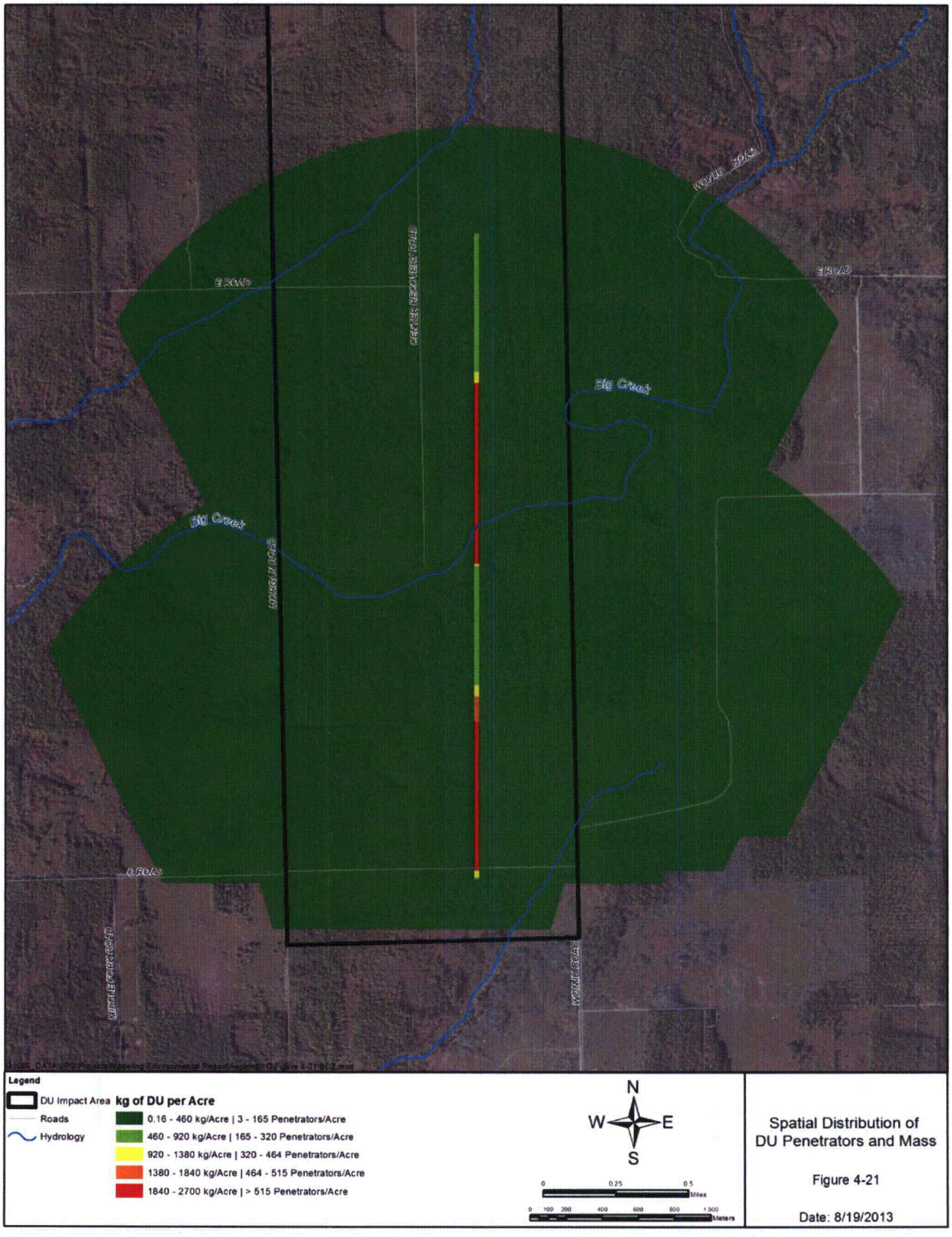
E ROAD
CENTER RIDGE ROAD
Big Creek
Big Creek
E ROAD
C ROAD
Legend
DU Impact Area
Roads
Hydrology
kg of DU per Acre
0.16 - 460 kg/Acre | 3 - 165 Penetrators/Acre
460 - 920 kg/Acre | 165 - 320 Penetrators/Acre
920 - 1380 kg/Acre | 320 - 464 Penetrators/Acre
1380 - 1840 kg/Acre | 464 - 515 Penetrators/Acre
1840 - 2700 kg/Acre | > 515 Penetrators/Acre
N
W
E
S
0 0.25 0.5 Miles
0 100 200 400 600 800 1,000 Meters
Spatial Distribution of DU Penetrators and Mass
Figure 4-21
Date: 8/19/2013

Table 4-5. Estimates of DU Mass and Numbers of Penetrators Jefferson Proving Ground, Madison, Indiana

Penetrator Density	DU Density (kg/ac)	Size Area (ac)	Size Area (%)	Mass (kg)	Mass (%)	Penetrators
3 to 165 penetrators/ac	≤ 460	3,822	99	41,778	57	10,604
165 to 320 penetrators/ac	460 to 920	8.9	0.23	5,748	8	1,460
320 to 464 penetrators/ac	920 to 1,380	1.1	0.027	1,320	2	336
464 to 515 penetrators/ac	1,320 to 1,840	0.89	0.023	1,630	2	414
Greater than 515 penetrators/ac[a,b]	≥ 1,840	11.3	0.30	23,023	31	5,844
Total	**NA**	**3,844**	**100**	**73,500**	**100**	**18,658**

[a] Trench in 500 Center line of fire north of Big Creek: 1,008 m (3,307 ft) x 25 m (82 ft) (6.2 ac) and includes 13,599 kg (29,980 lb) of DU.
[b] Trench in 500 Center line of fire south of Big Creek: 824m (2,705 ft) x 25 m (82 ft) (5.1 ac) and includes 9,424 kg (20,777 lb) of DU.

THIS PAGE WAS INTENTIONALLY LEFT BLANK

5. CORROSION OF PENETRATORS AND DISSOLUTION OF CORROSION PRODUCTS

As noted above, DU is in metallic form originally but oxidizes readily in the environment – a process similar to the formation of rust on iron objects. It is the resulting breakup and dissolution of these corrosion products that is largely responsible for environmental contamination.

The focus of this section is the corrosion of DU penetrators and the subsequent dissolution of the corroded penetrators in the soil at the JPG DU Impact Area. The objective of this study is to determine the rate at which DU corrodes and the rate at which the resulting corrosion products enter the soil. This source term of DU then will be used in computer models that simulate movement of the DU in the environment.

5.1 CHEMISTRY OF DU CORROSION

Uranium metal is unstable when in contact with oxygen and water. Uranium oxides form on the penetrator or fragment surfaces according to the following reaction, in which uranium is in its tetravalent (U[IV] or U^{+4}) form:

$$U + O_2 \rightarrow UO_2 \text{ (uraninite)}$$

In contact with the atmosphere, uraninite is unstable and oxidizes further to its hexavalent form (U[VI] or U^{+6}):

$$UO_2 + \tfrac{1}{2} O_2 \rightarrow UO_3$$

In the presence of water, these oxides are hydrated to form minerals such as schoepite ($UO_3 \bullet nH_2O$) (UNEP 2003, Stevenson 2010). This corrosion process is clearly evident in the appearance of penetrators recovered from wartime areas or military proving grounds.

Penetrators retrieved from the soil have generally shown signs of two different corrosion products, one black and one yellow. For example, Figure 5-1 (UNEP 2003) shows a penetrator recovered from the soil in Bosnia. This penetrator had been in the soil for approximately 7 to 8 years and had approximately doubled in size through the formation of corrosion products on its surface. Analysis of the penetrators from Bosnia as well as those found in soils elsewhere has shown that uranium in these oxides is in both a tetravalent and hexavalent state, with the black and yellow phases subsequently identified as $UO_2(OH)_2$ and $UO_3 \bullet 2H_2O$ (schoepite[1]), respectively.

Figure 5-1. Penetrator Removed From the Soil in Bosnia

[1] The UNEP report refers to this compound as schoepite, but other documents refer to it as meta-schoepite to distinguish it from the mineral schoepite, which has a chemical formula of $(UO_2)_8O_2(OH)_{12} \bullet 12(H_2O)$.

Figure 5-2 illustrates some of the important chemical phenomena related to corrosion and dissolution of the DU penetrators. In field-moist oxic conditions, which are optimum for corrosion, DU oxidizes and hydrolyzes to form a mixture of yellow and black corrosion products identified as $UO_3 \cdot 2H_2O$ and $UO_2(OH)_2$, respectively. Both of these corrosion products dissolve over time with continued exposure to water, releasing uranyl (UO_2^{2+}) ions into the surrounding soil and pore water (see Section 6 for further discussion of the geochemistry of the dissolved DU).

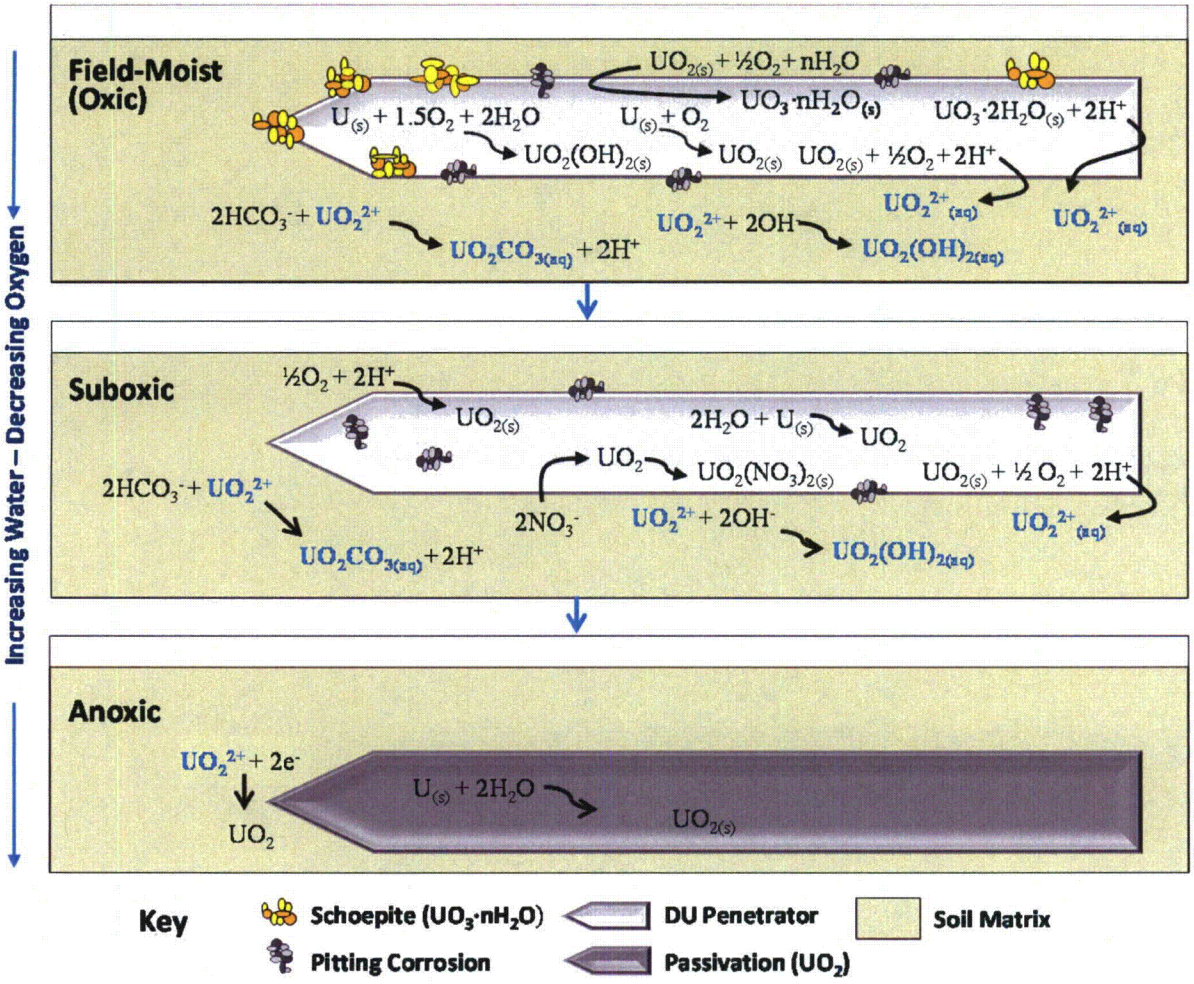

Figure 5-2. Corrosion, Dissolution, and Geochemical Processes in the Soil and Pore Water (Adapted from Handley-Sidhu et al. 2010)

Under waterlogged conditions, the soil and pore water surrounding the penetrator become progressively starved for oxygen, resulting in suboxic or anoxic (reducing) conditions. Under suboxic conditions, Handley-Sidhu et al. (2009b) have noted that the penetrator surface corrodes primarily by localized pitting and the formation of black-gray UO_2. Corrosion and dissolution rates are much slower under suboxic conditions than under oxic conditions. Under anoxic conditions, Handley-Sidhu et al. (2009b) noted that the penetrator surface can become passivated (i.e., made unreactive through alteration of the surface layer or coating of the surface with a thin inert layer) by the formation of a UO_2 surface layer and oxidation essentially ceases.

5.2 CORROSION RATE

As illustrated in Table 5-1, the ambient environment surrounding the DU has a significant effect on the corrosion rate. Testing has shown that the corrosion rate in moist air is approximately 0.0065 grams per square cubic meters per year ($g/cm^2/y$) (Weirick and Douglass 1976). In distilled water, the corrosion rate is an order of magnitude higher at 0.072 $g/cm^2/y$ (Trzaskoma 1982). In water with 3.5 to 5 percent sodium chloride (NaCl) (approximating a marine environment), the corrosion rate is roughly an order of magnitude higher than that in distilled water at a rate from 0.40 to 1.47 $g/cm^2/y$ (Trzaskoma 1982; McIntyre, Lefeave, and Musselman 1988). The DU corrosion rate in soil is also variable and is known to depend on soil pH, water content, and burial depth among other factors. The following discussion outlines some key findings with respect to DU corrosion in soil.

Table 5-1. Measured Corrosion Rates for Depleted Uranium Jefferson Proving Ground, Madison, Indiana

Ambient Conditions	Corrosion Rate ($g/cm^2/y$)	Source
Moist Air (110% Humidity)	0.0065	Weirick and Douglass (1976)
Distilled Water	0.072	Trzaskoma (1982)
Water with 3.5 to 5% NaCl	0.4 to 1.47	Trzaskoma (1982); McIntyre, Lefeave, and Musselman (1988)
Field Moist Soil	0.1 to 0.49	Schimmack et al. (2005), Schimmack et al. (2007), Handley-Sidhu et al. (2009a), Handley-Sidhu et al. (2009b)
Waterlogged Soil	0.01 to 0.02	Handley-Sidhu et al. (2009_)
Soil in the Balkans	0.1 to 0.36*	UNEP (2002), UNEP (2003)
*Estimated based on UNEP measurements of the mass of corrosion products on recovered penetrators (see text).		

Schimmack et al. (2005 and 2007) performed experiments with bare penetrator fragments weighing 145 to 264 grams (g) in cylindrical (19 cm in diameter) columns containing approximately 3.3 kg of dry soil mass. Two different soils were used: a sandy-loamy soil referred to as a cambisol[2] and a silty-loamy soil referred to as luvisol. The pH values for the two soils were 5.6 and 5.8, respectively. The average organic content of the two soils was 2.1 percent. A weekly rainfall of 16 mm was simulated (approximately 33 inches per year [in/y]), which likely resulted in field-moist conditions. The penetrator fragments were placed 1 to 2 cm below the surface of the soil and 1 to 2 cm from the bottom of the 10-cm deep soil column.

The tests were continued for 3 years. After the first year of testing, the corrosion rate was found to vary from 0.056 to 0.19 $g/cm^2/y$ with a mean value of 0.11 $g/cm^2/y$. After 3 years of testing, the average corrosion rate over the 3 years was found to have increased to a range from 0.14 to 0.24 $g/cm^2/y$, with a mean of 0.19 $g/cm^2/y$. Considering only the last 2 years, the average corrosion rate over that period was 0.23 $g/cm^2/y$.

The environmental conditions experienced by DU penetrators at JPG are very close to those simulated in the column tests by Schimmack et al. (2005 and 2007). The Food and Agriculture Organization (FAO) of the United Nations provides maps showing soil types at locations around the globe. According to FAO, the dominant soil types in and around JPG are cambisol and luvisol (FAO 2012), the two soil types used in the column tests. The pH range of the soils in the tests (5.6 to 5.8) is comparable to the pH values range measured for the JPG soils (mean for the three soils sampled ranged from 5.1 to 6.5) (reference JPG soil analysis in this report). The organic content of the soils in the tests (mean of 2.1 percent) is comparable to the organic content of the soils at JPG (mean of 1.2 to 1.5 percent) (reference JPG soil analysis in this report). The 33 in of annual rainfall simulated in the tests is comparable to the average rainfall at JPG of 47 in/y.

[2] These are FAO of the United Nations classifications. Soil maps indicate that luvisol is a predominant soil type in and around JPG with cambisol also being present nearby (FAO 2012).

Handley-Sidhu et al. (2009a) reported results from column testing with penetrator coupons in dune sand collected adjacent to the Eskmeals firing range in the United Kingdom (U.K.). The corrosion rate under "field-moist"[3] conditions was 0.1 g/cm^2/y. The pH for the field moist sand was 7.4. High purity water was added each month to compensate for water loss due to evaporation. The amount of water added to the soil was not reported.

Handley-Sidhu et al. (2009b) also reported results from column testing with penetrator coupons in silty-loam soil collected from the North Wyke Research Station in the U.K. The pH of this soil was between 5 and 6. As in the Eskmeals dune sand testing, an unspecified quantity of high purity water was added each month to compensate for water loss due to evaporation. The corrosion rate for "field-moist" conditions was determined to be 0.49 g/cm^2/y. For waterlogged soil, the corrosion rate was considerably smaller at 0.02 g/cm^2/y or lower. The authors noted that these estimates ignored the lag-time during the initial corrosion period. Thus, the results may be representative of a steady corrosion behavior.

Corrosion rate information can also be determined based on DU recovered as part of a United Nations Environment Programme (UNEP) study of environmental impacts resulting from wartime usage in the former Yugoslavia (UNEP 2002, 2003). Penetrators recovered from varying soil depths were subjected to chemical and mechanical cleaning to remove the layer of corrosion products. The penetrators then were weighed and the weight compared to their initial mass.

These studies found that penetrators recovered from the Bosnia/Herzegovina region had lost from 66 to 93 g of DU over the approximately 7-year and 1-month period that they had been in the ground (UNEP 2003). Penetrators recovered from soils in Serbia and Montenegro had lost 11 to 38 g over approximately 2 years and 5 months of soil exposure (UNEP 2002). The UNEP report indicates that the soil in regions of Bosnia and Herzegovina in which the penetrators were recovered has a pH of 7.4 to 7.8. No soil pH was reported for the Serbia/Montenegro site in the UNEP report. The annual rainfall reported for the Bosnia/Herzegovina region is approximately 40.5 in/y (The World Bank 2013).

The mass losses for the recovered penetrators can be converted to corrosion rates by dividing by the years of exposure and the approximate surface area of the 30-mm penetrators used in the A-10 ammunition (estimated at approximately 44 square centimeters (cm^2) based on dimensions provided in the UNEP report [UNEP 2002]). The resulting corrosion rates are 0.21 to 0.30 g/cm^2/y for the Bosnia/Herzegovina penetrators and 0.1 to 0.36 g/cm^2/y for the Serbia/Montenegro penetrators. These results are consistent with the corrosion rates measured in the column experiments.

Because of the similarity between the environmental conditions at JPG and those simulated in the column tests and experienced by penetrators recovered from the Balkans, it is likely that the corrosion rate experienced by buried JPG penetrators will be between 0.1 and 0.4 g/cm^2/y, with a most likely value of approximately 0.25 g/cm^2/y. In the DU source term analysis presented in Section 5.4, the corrosion rate will be treated as an uncertainty.

As mentioned earlier in this section, penetrators on the surface of the soil or buried in waterlogged soil will likely experience considerably lower corrosion rates than those measured in the column tests or in the Balkans. It is also possible that penetrators buried deep in the ground (several feet) also will experience much slower corrosion due to the lower ambient oxygen concentration at these depths. Thus, the assumed corrosion rate of 0.25 g/cm^2/y may represent an upper bound to the corrosion experienced by the JPG penetrators.

[3] The term "field-moist conditions" simply indicates the general condition of soils sampled from the field. The specific water content of such soils is not specified but is intermediate between air-dried and waterlogged soils. Testing has shown that field-moist conditions generally produce the highest corrosion rates.

5.3 DISSOLUTION OF CORROSION PRODUCTS

Schoepite, which is the dominant DU corrosion product, is known to slowly dissolve when exposed to water. Schoepite dissolution releases uranyl ions $(UO_2)^{2+}$ into the soil. The released uranyl ions then form a variety of chemical compounds with the constituents of the soil and water. The specific compounds that are formed and their mobility in the soil and water depend on the composition and pH of the soil and water. See Section 6 for further discussion of uranium speciation in soil and water.

Tests and field observations indicated that a significant layer of corrosion products is attached to the penetrator at any time. A dissolution rate can be inferred based on observations of the overall rate of corrosion and the mass of corrosion products remaining on the surface of the penetrator.

As part of the column experiments discussed in Section 5.2, Schimmack et al. (2005, 2007) measured the mass of uranium in soil, in leachate, and still adhered to the penetrators. The resulting mass balance accounted for approximately 100 percent of the mass lost by the penetrator. After 1 year of testing, the percentage of corroded DU still adhered to the penetrators ranged from 32 to 51 percent, with a mean of 40 percent (Schimimack et al. 2005). The percentage in the soil ranged from 46 to 72 percent, with a mean of 58 percent. The amount of corroded DU in the leachate was a small fraction of a percent.

After 3 years of testing, the percentage of corroded DU in the soil ranged from 51 to 67 percent, with a mean of 60 percent, and the percentage in the leachate ranged from 0.003 to 0.65 percent, with a mean of 0.13 percent (Schimimack et al. 2007). The remaining mass (approximately 40 percent) was still adhered to the penetrators.

Two penetrator fragments recovered from the soil in Bosnia and Herzegovina were examined to determine the amount of corrosion products still adhered to the penetrator after about 7 years (UNEP 2003). One penetrator had 33.7 of 79.3 g (42.5 percent) of total corrosion products adhered to the penetrator. The other had 17.3 of 66.3 g (26 percent) still adhered. The average of these two measurements is 34.3 percent, which is comparable to the 40 percent value measured in the column experiments.

Based on the observation that approximately 40 percent of the corrosion products are still adhered to the penetrator, it can be concluded that the dissolution rate of the corrosion products was approximately 60 percent of the corrosion rate in both the column tests and under field conditions in Bosnia and Herzegovina. Because of the similarity between the environmental conditions at JPG and those simulated in the column tests and experienced by recovered penetrators, it is likely that the dissolution rate at JPG will be similar to this. Based on the best-estimate corrosion rate of 0.25 $g/cm^2/y$, this would infer a dissolution rate of approximately 0.15 $g/cm^2/y$. (Note that the dissolution rate is calculated per unit surface area of the corroded penetrator.) In the DU source term analysis presented in Section 5.4, the dissolution rate will be treated as an uncertainty.

As noted above, the dissolution rate depends on the corrosion rate and the availability of water. Penetrators on the surface of the soil will have lower corrosion rate and less continuous exposure to water; thus, these penetrators would likely exhibit much lower dissolution rates. Penetrators in waterlogged soil will have a slower corrosion rate but greater exposure to water. Given the measured corrosion rate in waterlogged soil of 0.02 $g/cm^2/y$ and conservatively assuming continuous immersion in water instantly dissolves the corrosion products, the dissolution rate would be 0.02 $g/cm^2/y$, which is still well below the 0.15 $g/cm^2/y$ assumed in the source term analysis in Section 5.4. In addition, in waterlogged soil, the combined effects of lower oxygen availability and biological activity are known to produce reducing conditions in the soil (see discussion in Section 6.4). Under these conditions, uranium is reduced to tetravalent form, U(IV), which significantly reduces the corrosion and dissolution rates. Thus, it is likely that using a dissolution rate of 0.15 g/cm^2-y in the source term analysis provides an upper bound to the actual source term for the JPG penetrators.

5.4 ESTIMATING THE SOURCE OF DU INTO THE SOIL

Based on the preceding discussion, the rate at which DU corrosion products enter the soil can be estimated. The experiments by Schimmack, et al. (2005, 2007) show that steady corrosion occurs after a lag time of 1 to 2 years. The steady corrosion rate is given in terms of a mass flux (i.e., in grams of DU corroded per unit surface area of the bare penetrator per unit time). The experiments also show that the rate of dissolution of the corrosion products also reaches a steady state condition after this period. The dissolution rate also can be specified as a mass flux, which, in this case, is the mass of DU per unit surface area of the corroded penetrator per unit time. As noted in Section 5.2, laboratory testing and field observations have indicated that after 1 to 7 years of exposure to soil conditions, approximately 40 percent of the corroded DU is still adhered to the penetrator. This implies that the steady dissolution rate is approximately 60 percent of the corrosion rate.

An Excel spreadsheet was set up to calculate the time-dependent source of DU into the soil due to dissolution. The spreadsheet calculation includes the following steps:

1. Calculate the reduction in the penetrator diameter during a timestep using the following equation:

$$\Delta D = 2\frac{\dot{m}''_{cor}\Delta t}{\rho_{DU}}$$

Where:

$\dot{m}''_{cor}$ = The corrosion rate per unit area of uncorroded penetrator (g/cm^2/y)
Δt = Timestep (yr)
ρ_{DU} = Density of DU (g/cm^3).

2. Calculate the reduction in the mass of the uncorroded penetrator during the timestep using the following equation (assumes the penetrator is a right circular cylinder and neglects corrosion of the ends of the cylinder):

$$\Delta m = \pi\left(\frac{D_i{}^2 - D_{i+1}{}^2}{2}\right)L\rho_{DU}$$

Where:

D_{i+1} = Diameter of the uncorroded penetrator at the end of the timestep
D_i = Diameter of the uncorroded penetrator at the beginning of the timestep
L = Length of the penetrator.

3. Calculate the mass of DU entering the soil during the timestep using the following equation:

$$\Delta m_{soil} = \dot{m}''_{diss}\pi D_{c,i}L\Delta t$$

Where:

$\dot{m}''_{diss}$ = The dissolution rate per unit area of corroded penetrator (g/cm^2/y)
$D_{c,i}$ = Puter diameter of corroded penetrator at the start of the timestep (cm).

4. Calculate the mass of DU in corrosion products still adhered to the penetrator using the following equation:

$$m_{cor} = \sum \Delta m - \sum \Delta m_{soil}$$

Where:

The summations are over all timesteps up to and including the current timestep.

5. Calculate the mass of DU corrosion products adhered to the penetrator using the following equation:

$$m_{cp} = m_{cor} \frac{MW_{cp}}{MW_{DU} N_{DU}}$$

Where:

MW_{cp} = Molecular weight of the corrosion products (gram per mole [g/mol])
MW_{DU} = Molecular weight of DU (g/mol)
N_{DU} = Number of moles of DU per mole of corrosion products.

In the calculations presented below, it is assumed that the corrosion products are schoepite $[(UO_2)_8O_2(OH)_{12}\cdot 12(H_2O)]$, which has 8 moles of uranium per mole, a molecular weight of 2,612 g/mol, and a density of 4.8 g/cm^3. In reality, the corrosion products are likely to be a mixture of different compounds. However, because the molecular weight of the corrosion product, MW_{cp}, is controlled largely by the contribution from uranium, the ratio MW_{cp}/N_{DU} is not very sensitive to the particular corrosion product that is assumed.

6. Calculate the thickness of the layer of corrosion products using the following equation:

$$t_{cp} = \sqrt{\frac{m_{cp}/\rho_{cp}}{\pi L} + \left(\frac{D_{i+1}}{2}\right)^2} - \frac{D_{i+1}}{2}$$

Where:

ρ_{cp} = Density of the corrosion products (g/cm^3).

7. Calculate the outer diameter of the corroded penetrator using the following equation:

$$D_{c,i+1} = D_{i+1} + t_{cp}$$

To calculate the time-dependent source of corrosion products into the soil, the following parameters must be specified: the corrosion and dissolution rates in units of g/cm^2/y, the dimensions and initial mass of the penetrator, the molecular weight and density of the assumed corrosion product, and the number of moles of uranium per mole of the assumed corrosion product. Table 5-2 shows the most likely values for each of these parameters. Figure 5-3 shows the calculated time-dependent source of uranium into the soil based on these values. The figure displays the mass of DU entering the soil per year per penetrator.

Table 5-2. Best-Estimate Values Used in the DU Source Term Model Jefferson Proving Ground, Madison, Indiana

Parameter	Most Likely Estimate Value	Notes
DU Corrosion Rate	0.25 g/cm²/y	Calculated per unit surface area of remaining DU metal
Dissolution Rate	0.15 g/cm²/y*	Calculated per unit surface area of corroded penetrator (outer surface)
Moles of U per Mole of Corrosion Products	8	Assumes schoepite
Density of Corrosion Products	4.8 g/cm³	Assumes schoepite
Density of DU	18.9 g/cm³	
Dimensions of the Penetrator: Outside Diameter Length	 1.012 in (2.570 cm) 16.04 in (40.74 cm)	Assumes an M833 penetrator
Penetrator Initial Mass	4.00 kg (8.8 lb)	Calculated based on penetrator dimensions and DU density
*Calculated by multiplying the DU corrosion rate by 1 minus the fraction adhered to the penetrator.		

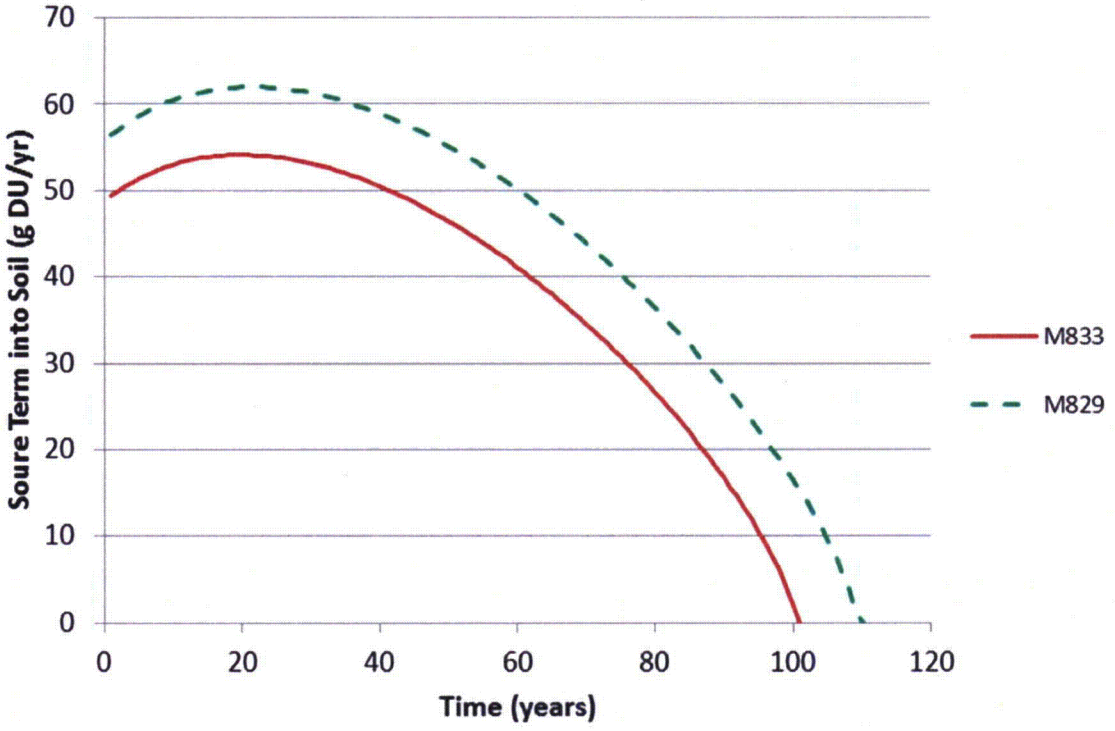

Figure 5-3. Calculated DU Source Term into the Soil (per Penetrator) Based on Most Likely Estimate Parameters

Table 5-2 displays dimensions for an M833 penetrator used on 105-mm cartridges. In addition, 120-mm cartridges also were fired at JPG. These projectiles have a slightly larger M829A2 penetrator with the following dimensions: 1.10 in (2.79 cm) in diameter, and 16.88 in (42.89 cm) in length. These penetrators have a mass of approximately 10.7 lb (4.9 kg). The time-dependent source term for these larger penetrators also is shown in Figure 5-3.

As discussed above, there is uncertainty in the corrosion and dissolution rates. This uncertainty is of two types: uncertainty in the actual corrosion rate for a given set of environmental conditions and uncertainty in the corrosion rate related to variability in the environment in which the penetrator resides. The current uncertainty analysis addresses only the first type of uncertainty and assumes a nominal set of environmental conditions; specifically, penetrators buried at shallow depths in field-moist soil. These are the conditions about which we have the most reliable information from both laboratory tests and field observations. As previously discussed, these conditions are likely to produce the highest net DU source term.

In order to capture this uncertainty in the estimated DU source term into the soil, a series of Monte Carlo simulations was run using the Crystal Ball® software. Crystal Ball is a Microsoft® Excel add-in that allows the user to specify uncertainty distributions for values used in the spreadsheet model. It then repeatedly samples from these distributions and reruns the spreadsheet model to calculate the resulting uncertainty distribution for the model outputs. The uncertainty distributions used in the Monte Carlo DU source term simulations are shown in Table 5-3 and Figures 5-4 and 5-5.

Table 5-3. Uncertainty Distribution Used in the Monte Carlo Simulations Jefferson Proving Ground, Madison, Indiana

Parameter	Distribution and Parameters	Distribution Parameters
DU Corrosion Rate	Normal	5th percentile = 0.10 g/cm²/y 95th percentile = 0.40 g/cm²/y
Fraction of Corrosion Products Adhered to the Penetrator*	Uniform	Minimum = 0.35 Maximum = 0.45
*Used to calculate the dissolution rate [= DU corrosion rate × (1 – Fraction adhered to the penetrator)].		

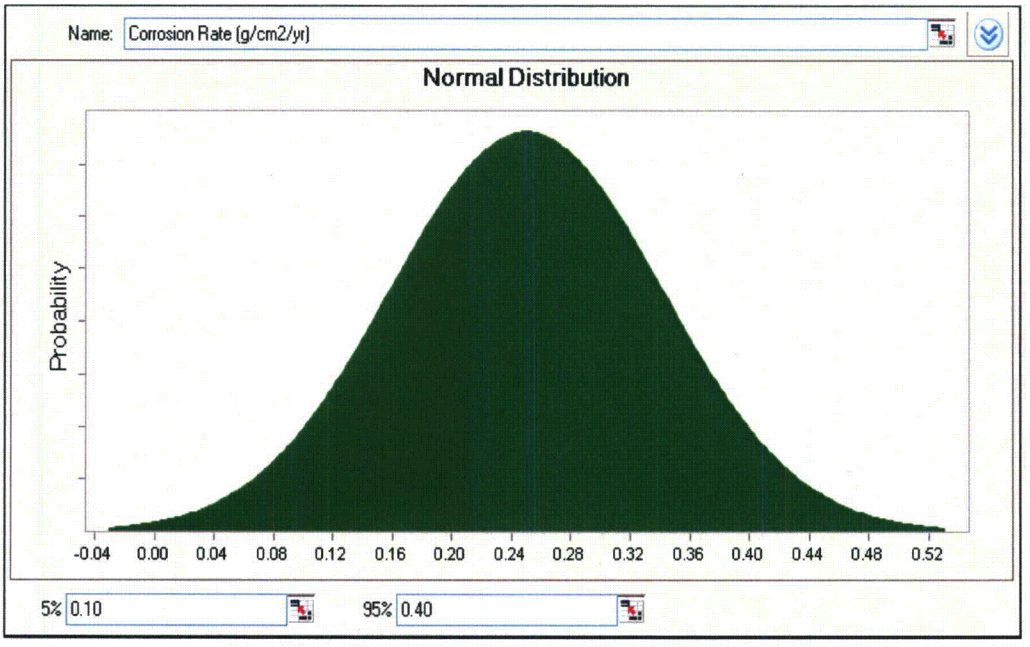

Figure 5-4. Probability Distribution for the Corrosion Rate

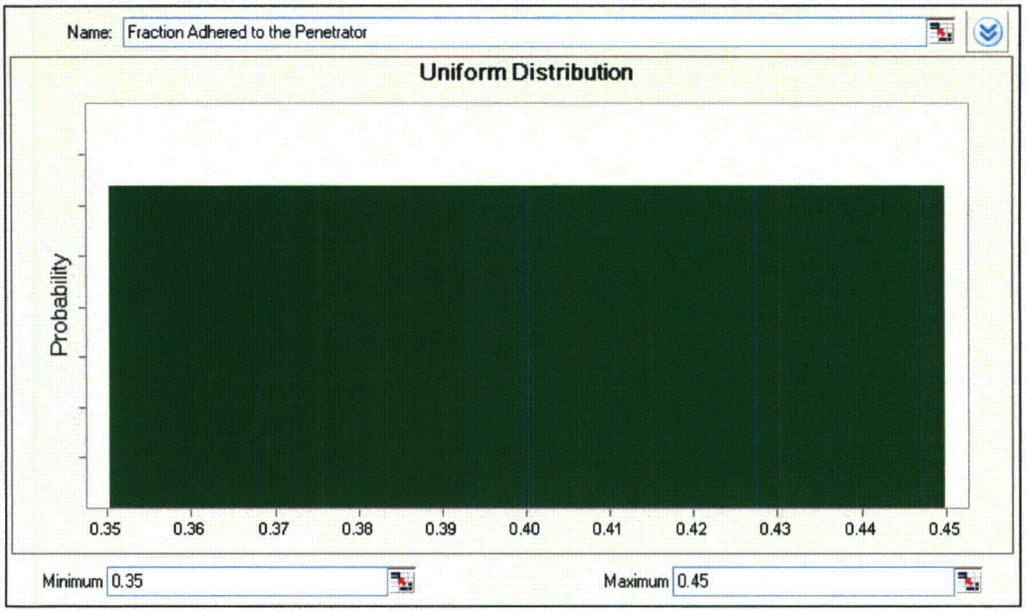

Figure 5-5. Probability Distribution for the Fraction Adhered to the Penetrator

In addition to the uncertainties captured in Table 5-3, there is also some uncertainty in the number of specific models of DU penetrators or relative fractions actually remaining in the DU Impact Area. In the uncertainty analysis discussed below, it is assumed that half of the fired penetrators are M833 and half are M829.

The Crystal Ball® software was run in a series of 10,000 Monte Carlo simulations to generate 10,000 curves similar to the one shown in Figure 5-4. In addition, the average source term for each 10-year period was determined for each of the simulations. The 5th and 95th percentiles of each 10-year average source term then were determined and these values were used to determine a time-dependent source term that best represents the 5th and 95th percentile curves. The resulting 5th and 95th percentile curves are shown in Figure 5-6 along with the best-estimate curve from Figure 5-3. The calculated times to complete corrosion and dissolution of the penetrator are as follows: most likely estimate – 107 years; 5th percentile – 182 years (slowest corrosion and dissolution); 95th percentile 65 – years (fastest corrosion and dissolution).

As noted previously, the figure shows the mass of DU entering the soil per year per penetrator. The source terms shown in the figure can be converted to a per kg basis by dividing the calculated values in the figure by the mass of a penetrator. Assuming a 50/50 mix of M833 and M829 penetrators were fired, the average penetrator mass is approximately 9.6 lb (4.4 kg).

5.5 USE IN THE FATE AND TRANSPORT MODELS

To use these values in the model, it is necessary to multiply the source term by the number of penetrators (or mass of DU) in a given location. Since the calculation is for a point source of DU, the distribution of penetrators or penetrator mass per unit volume of soil needed for fate and transport modeling was discussed in Section 4.

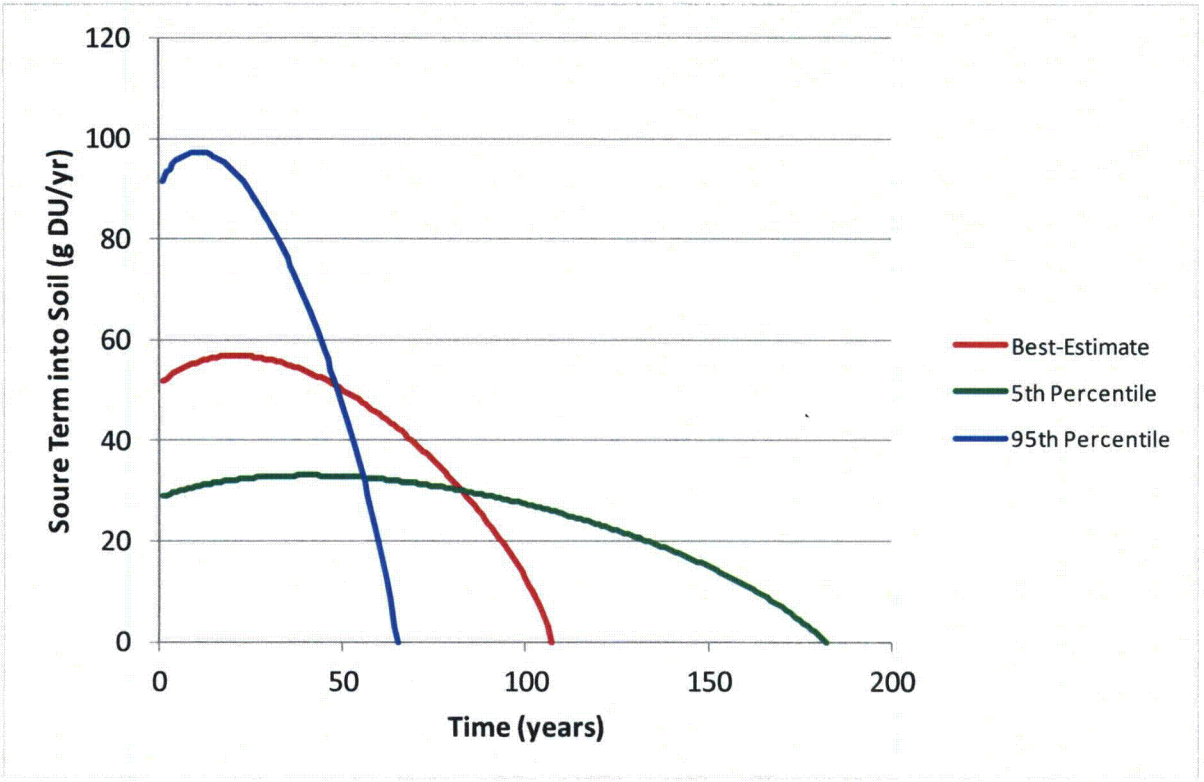

Figure 5-6. Most Likely Estimate and Bounding Curves for the DU Source Term into Soil (per Penetrator)

THIS PAGE WAS INTENTIONALLY LEFT BLANK

6. GEOCHEMICAL ANALYSIS

Geochemical modeling can be used to describe chemical interactions in the soil, including interactions among dissolved chemical species, dissolution of immobile solid phases, or formation and precipitation of new immobile solid phases. These analyses are generally performed using computer codes such as PHREEQC (pH-REdox-EQuilibrium) (Parkhurst and Appelo 2013) or MINTEQA2 (AGC 2003) using site-specific data to the extent possible.

Geochemical modeling using the PHREEQC software was performed to support the JPG CSM. The PHREEQC software was used to provide insights into the speciation of uranium in both the distribution coefficient (K_d) tests and under field conditions at JPG. All calculations were run assuming chemical equilibrium between the various constituents. Equilibrium between soil and water was calculated to result in a net dissolution of some soil constituents. The dissolved soil constituents then reacted to equilibrium with the water. Reaction kinetics were not modeled so that all equilibrium reactions were assumed to occur instantaneously.

6.1 PHREEQC INPUT PREPARATION

PHREEQC requires input on the chemical composition of soil and pore water. Modeling of uranium speciation in near surface soil assumed equilibration with rainwater. Modeling of deeper glacial till soil assumed equilibration with groundwater. Inputs to the PHREEQC model included specification of the water and soil chemical composition.

6.1.1 Composition and Mass of Water

Detailed chemical analyses are available for both rainwater and groundwater. Rainwater was obtained from a rainwater collection station established south and west of the DU Impact Area. The following pH and oxidation reduction potential (ORP) of the rainwater were measured at an ambient temperature of 17.4°C: pH 6.0 and ORP 376 millivolts (mV). The groundwater sample was collected in March 2012 from one of the monitoring wells drilled at the site (JPG-DU-060). The following pH and ORP of the groundwater were measured at an ambient temperature of 11.8°C: pH 7.28 and ORP 13 mV. The chemical compositions of the rainwater and groundwater samples are provided in Tables 6-1 and 6-2. See Section 6 of Appendix D for further discussion of the rainwater and groundwater analysis.

Table 6-1. Composition of the Rainwater Sample Jefferson Proving Ground, Madison, Indiana

Constituent	Concentration (µg/L)
Aluminum	30
Calcium	2,930
Iron	491
Magnesium	228
Manganese	12
Potassium	423
Sodium	323
Chloride	280
Nitrate	16
Sulfate	1,000
Alkalinity	3,500
Total Organic Carbon	3,500
Total Inorganic Carbon	550
Silicon	128

Table 6-2. Composition of the Groundwater Sample Jefferson Proving Ground, Madison, Indiana

Constituent	Concentration (µg/L)
Aluminum	2,380
Calcium	86,800
Iron	2,360
Magnesium	27,500
Manganese	167
Potassium	1,070
Sodium	25,800
Chloride	8,300
Nitrate	16
Sulfate	51,600
Alkalinity	329,000
Total Organic Carbon	1,100
Total Inorganic Carbon	79,500
Silicon	16,400

For convenience, the mass of water in the K_d simulations was assumed to be 1 kg (mass of 1 liter [L]) rather than 100 g (100 milliliter [mL]) and all masses and volumes were scaled-up by a factor of 10 relative to the masses and volumes in the tests.

The mass of water in the soil speciation calculations was assumed to be the mass of water corresponding to the field capacity in 1,000 cm^3 of soil. For the silt-loam soils at JPG, the field capacity was estimated to be 0.32 cm^3 of water per cm^3 of soil (Saxton and Rawls 2006). Thus, the mass of water used in the PHREEQC was 0.32 kg. The same water mass was used in both the loess-rainwater and glacial till-groundwater simulations.

6.1.2 Composition and Mass of Soil

The soils at JPG have been characterized in terms on their relative clay, silt, and sand compositions, their soil pH, and their cation exchange capacity (CEC). The average soil characteristics for the three predominant soil types at JPG are summarized in Tables 6-3 and 6-4.

Table 6-3. Soil Texture Summary Jefferson Proving Ground, Madison, Indiana

Soil Type	Depth (ft)	Clay (%)	Silt (%)	Sand (%)	Gravel (%)
Avonburg/Cobbsfork	0 to 4	32.6	49.5	17.2	0.7
Cincinnati/Rossmoyne	0 to 4	31.1	45.0	22.2	1.1
Grayford/Ryker	0 to 4	29.5	52.0	17.5	1.0
Loess Average*	0 to 4	31.5	47.8	19.5	0.9
Glacial Till	6 to 16	36.2	39.5	23.6	0.7
*Represents the numerical average of all samples of all three loess soil types					

Table 6-4. Measured Soil Parameters
Jefferson Proving Ground, Madison, Indiana

Soil Type	Depth (ft)	Iron (mg/kg)	Manganese (mg/kg)	ph	Total Carbon (mg/kg)	Total Organic Carbon (mg/kg)	Cation Exchange Capacity (meq/100g)
Avonburg/Cobbsfork	0 to 4	10,249	83	5.7	3,135	2,955	9.7
Cincinnati/Rossmoyne	0 to 4	27,797	720	5.3	4,066	4,012	9.5
Grayford/Ryker	0 to 4	13,473	436	5.2	5,033	4,957	11.5
Loess Average*	0 to 4	18,299	409	5.5	3,787	3,676	9.8
Glacial Till	6 to 16	21,445	643	8.6	14,259	2,783	11.8
*Represents the numerical average of all samples of all three loess soil types							

The iron, manganese, total carbon, and total organic carbon (TOC) content of the soils were determined analytically, but limited chemical composition information is available for the other constituents of the soils at JPG. As a result, some assumptions on the soil composition had to be made[4].

Although the iron and manganese content of the soils were determined, the mineral form of the iron and manganese is not known. The iron content of the soils at JPG was determined to generally range from 10,000 to 30,000 mg/kg of soil. Based on soil color information, it is likely that the predominant iron mineral was goethite (FeO[OH]), which gives the soil a characteristic yellow to brown color. At JPG, the manganese content of the soils typically ranged from 100 to 700 mg/kg of soil. It is believed to be in the form of pyrolusite (MnO_2), which is known to be one of the predominant manganese-bearing minerals in soil.

Clay minerals are hydrous aluminum phyllosilicates, sometimes with variable amounts of iron, magnesium, alkali metals, alkaline earths, and other cations. Typical clay minerals include the following groups:

- Kaolin group, which includes the minerals such as kaolinite
- Smectite group, which includes di-octahedral smectites such as montmorillonite and nontronite and tri-octahedral smectites such as saponite
- Illite group, which includes the clay-micas
- Chlorite group, includes a wide variety of similar minerals with considerable chemical variation.

The composition of the clays at JPG was assumed based on studies of Illinoian and pre-Illinoian loess (Beavers et al. 1954), which is believed to be the primary parent material for the soils at JPG (USDA 1985). Based on this information, the following average mineral composition was assumed for the clays at JPG: 65 percent montmorillonite, 20 percent illite, and 15 percent chlorite.

Silt is a fine granular material with a characteristic size between that of sand and clay. It is created by a variety of physical processes capable of splitting or eroding primary rock crystals. It is composed primarily of quartz and feldspar, but may contain other minerals eroded from the local bedrock. In the PHREEQC analysis, the silt component is assumed to be a mixture of quartz, feldspar, and a carbonate mineral, which in the PHREEQC simulations was chosen to be dolomite because of its prevalence in the bedrock at the JPG site. The amount of carbonate mineral is determined based on the inorganic carbon

[4] Since the time the geochemical modeling was completed, analyses have been completed to determine the composition of the JPG soils. This analysis generally confirms the assumed soil composition with the exception that the JPG soils have a slightly lower calcium oxide and magnesium oxide concentration than assumed in the PHREEQC analysis. These were relatively minor constituents of the assumed soil composition, so it is likely that the PHREEQC results would not change significantly with the inclusion of this updated information into the PHREEQC model.

fraction measured for the JPG soils. The remaining silt fraction is assumed to be equally split between quartz and feldspar. The sand component of the soil is assumed to be entirely composed of quartz.

Because the water mass used in the PHREEQC K_d simulations is scaled up by a factor of 10 from the 100 g used in the tests, the soil mass used in the PHREEQC simulations is scaled up from 4 to 40 g. The soil mass in the soil speciation simulations is 1,200 g, which is based on an assumed soil volume of 1,000 cm^3 and an assumed soil density of 1.2 g/cm^3. Constituents of the soil participate in the aqueous speciation of uranium only to the extent that they are calculated to dissolve. Dissolution is calculated in PHREEQC based on equilibrium between the soil and aqueous phases.

6.1.3 Composition and Mass of Uranium

Since the objective of the current geochemical analysis is to determine speciation of uranium in solution, the amount and chemical form of uranium must be provided as input to PHREEQC.

For the PHREEQC simulations of the K_d tests, uranium was input as an initial component of the rainwater or groundwater solution. The uranium spike concentration in the K_d tests ranged from 3 to 20 µg/L with 10 µg/L being the most commonly used. Only the 10 µg/L concentration was modeled in the PHREEQC simulations. The uranium was modeled as 10 µg/L of uranyl nitrate hexahydrate in the initial rainwater or groundwater solution.

For the PHREEQC soil speciation simulations, the uranium was assumed to be a component of the soil mixture and was assumed to be present initially as schoepite, which has been observed as the primary corrosion product of uranium on penetrators recovered from soil. The mass of schoepite assumed to be present in the soil was based on the uranium concentration measured in the soil below the penetrators at JPG (see Table 6-2 of Appendix D). The uranium mass in the soil was converted to moles of schoepite by dividing first by the molecular weight of uranium (approximately 238 g/mol) and then by the number of moles of uranium per mole of schoepite. Schoepite is modeled as $UO_2{:}2H_2O$ in the various PHREEQC databases, so one mole of uranium was assumed per mole of schoepite.

6.1.4 Other Inputs

PHREEQC calculates equilibrium between solid, liquid, and gas phases. Because carbonate formation is known to be an important factor in uranium speciation in soils, it was important to simulate equilibration between carbon dioxide (CO_2) in the gas phase and carbonates in the soil and water. Two partial pressures of CO_2 were simulated in the PHREEQC calculations: one corresponding to the partial pressure of CO_2 in the atmosphere and another that reflects higher CO_2 levels measured in soil and water due to plant respiration. In PHREEQC, the partial pressure of a gas is input as the base 10 logarithm of the partial pressure (in atmospheres). The atmospheric CO_2 partial pressure was input as -3.5, corresponding to a partial pressure of approximately $10^{-3.5}$ or 0.032 standard atmospheres (atm). Calculations run with an enhanced CO_2 level were run with a CO_2 partial pressure input as -2.0, corresponding to a CO_2 partial pressure of $10^{-2.0}$ or 0.01 atm. This is comparable to the measured CO_2 partial pressures in unsaturated soils at depths greater than 0.5 m below grassland or woodland vegetation (Appelo and Postma 2005). At shallower depths, the CO_2 partial pressure is lower, reaching atmospheric levels at the surface. As might be expected, the CO_2 level in the soil also exhibits seasonal variations, with maximum levels measured during the peak growing season (Reardon, Allison, and Fritz 1979).

PHREEQC models cation exchange with clays based on default equilibrium constants for the list of cations provided in the databases included with the code[5]. The user supplies the moles of available exchange capacity, which is calculated by dividing the measured CEC by the equivalent charges per mole. For the soils at JPG, the CEC was measured in terms of milliequivalents (meq) of charge capacity

[5] The databases used in the PHREEQC simulations include the following cations in the exchange calculation relevant to the current simulations: Ca^{2+}, Mg^{2+}, K^{+}, Mn^{2+}, Na^{+}, $AlOH^{2+}$, Al^{3+}, and Fe^{2+}. The uranyl oxycation, UO_2^{2+} is not included with the PHREEQC databases and so was not included in the exchange calculation.

per 100 g of soil. The exchange capacity is multiplied by the mass of soil in the PHREEQC simulation to give the moles of charge equivalents to be input.

In addition to cation exchange, PHREEQC has the capability to model sorption of uranium and other heavy metals due to surface complexation if appropriate complexation modeling parameters are input by the user (e.g., density of surface sites and surface area per gram of sorbing mineral). Surface complexation depends on the specific chemical composition of the soil. This type of detailed modeling was considered beyond the scope of the current study given the information demands for completing the analysis.

There are several chemical databases available to the user in PHREEQC. Only some of the databases include chemical species and minerals containing uranium. The Lawrence Livermore National Laboratory (LLNL) database (LLNL.DAT in PHREEQC), which is one of the user-selectable databases, was used for the majority of the simulations reported below. As discussed in the results section, a few simulations were repeated with alternative databases to determine the impact of database selection on the calculated results.

6.2 MODELING APPROACH

Uranium speciation was modeled in PHREEQC as a series of reaction steps, each of which was assumed to proceed to equilibrium. Simulations were performed to model uranium speciation in the K_d adsorption tests and under field conditions at JPG. The modeling approaches used for these simulations are described below.

6.2.1 Modeling Approach in the K_d Simulations

The following reaction steps were modeled in the K_d simulations:

1. Equilibrate water (rainwater or groundwater) with uranyl nitrate hexahydrate.
2. Equilibrate the solution from Step 1 with soil, while maintaining the pH at the desired level (5.6 in the soil-rainwater simulations and 7.7 in the till-groundwater simulations).
3. Using the solution from Step 2, perform cation exchange calculations to simulate cation exchange with clay in the soil.

As the headspace in the K_d batch tests was only 20 to 25 mL and the vials were sealed, there was little opportunity for CO_2 in the headspace to react with the soil-water mixture. Therefore, CO_2 equilibration was not modeled in the PHREEQC K_d simulations.

K_d tests were performed for all three loess soil types at JPG and for glacial till. The tests with loess used rainwater, whereas the tests with glacial till used groundwater. The majority of the K_d tests evaluated adsorption of dissolved uranium by soil, but a few desorption-dissolution tests also were performed with uranium adsorbed to loess soils. Only uranium speciation in the adsorption tests was modeled.

Although the K_d tests were performed for all three loess soil types, the soil compositions and characteristics soil parameters were sufficiently similar that only a single characteristic loess soil was modeled in the PHREEQC simulations. The soil composition used in the simulations is similar to the average Avonburg/Cobbsfork soil shown in Tables 6-3 and 6-4.

In the PHREEQC simulations, pH adjustments are made by adding hydrochloric acid (HCl) to simulate the undetermined acidifying reactions in the soil. Potential acidifying reactions could include reactions with organic material or other chemical constituents not accounted for in the assumed soil composition.

6.2.2 *Modeling Approach in the Field Simulations*

The following reaction steps were modeled reaction in the field simulations:

1. Equilibrate water (rainwater or groundwater) with soil containing schoepite and with CO_2 at the assumed ambient partial pressure.
2. Using the solution from Step 1, perform cation exchange calculations to simulate cation exchange with clay in the soil and adjust the pH of the resulting solution to the desired level (5.6 in the soil-rainwater simulations and 7.7 in the till-groundwater simulations).
3. Based on the mineral saturation indices in the solution from Step 2, allow precipitation of any uranium-containing minerals that are supersaturated.

As in the PHREEQC K_d simulations, a single characteristic loess soil, similar to the average Avonburg/Cobbsfork soil shown in Tables 6-3 and 6-4, was used in the field simulations. In the simulations, pH adjustments were made if needed by adding HCl to simulate undetermined acidifying reactions in the soil.

6.3 RESULTS

PHREEQC outputs the composition and chemical properties of the aqueous solution after each reaction step, including a listing by valence state. It also reports saturation indices for minerals dissolved in solution. Saturation indices greater than 0.0 indicate minerals that are supersaturated in the solution and would be expected to precipitate. Uranium speciation results for the K_d simulations are outlined below.

6.3.1 *Uranium Speciation in K_d Simulations*

This section presents the results from PHREEQC simulations for the K_d adsorption tests. Calculated results for uranium speciation in the aqueous phase are presented.

6.3.1.1 Speciation in the Soil-Rainwater Adsorption Tests

PHREEQC calculations were performed to simulate uranium speciation in the adsorption K_d tests with soil and rainwater. Table 6-5 presents the calculated uranium speciation results both before and after addition of the soil. In both cases, oxidizing conditions are calculated and nearly all of the uranium is present in hexavalent form. Before soil addition, approximately two-thirds of the uranium is present as aqueous uranyl or uranyl hydroxide species, with the remaining one-third as uranyl carbonate species. When soil is added, PHREEQC calculates dissolution of a small fraction of the quartz, illite, and chlorite and complete dissolution of the small quantity of dolomite assumed to be present. The resulting change to the chemistry of the solution causes a shift in the uranium speciation to a much higher percentage of uranyl carbonate species. After soil addition, 59 percent of the uranium is present as uranyl carbonate species with the remaining 41 percent as uranyl hydroxide species.

Table 6-5. PHREEQC Results for Uranium Speciation in the Soil-Rainwater Adsorption Tests Jefferson Proving Ground, Madison, Indiana

Before Soil Addition			After Soil Addition*		
Species	Molality	U Mole Fraction	Species	Molality	U Mole Fraction
U(VI) Total	1.99E-08		U(VI) Total	1.99E-08	
$UO_2(OH)_2$	8.75E-09	43.9%	UO_2CO_3	1.09E-08	54.7%
UO_2CO_3	6.87E-09	34.5%	$UO_2(OH)_2$	5.50E-09	27.6%
UO_2OH^+	2.86E-09	14.3%	UO_2OH^+	1.85E-09	9.3%
UO_2^{2+}	1.23E-09	6.1%	UO_2^{2+}	8.64E-10	4.3%
$UO_2(CO_3)_2^{2-}$	1.71E-10	0.9%	$UO_2(CO_3)_2^{2-}$	7.69E-10	3.9%
*Results reflect equilibration with soil and cation exchange					

6.3.1.2 Speciation in the Till-Groundwater Adsorption Tests

PHREEQC calculations were performed to simulate uranium speciation in the adsorption K_d tests with glacial till and groundwater. Table 6-6 presents the calculated uranium speciation results both before and after addition of the till. In both cases, oxidizing conditions are calculated and nearly all of the uranium is present in hexavalent form. Both before and after addition of the till to the rainwater, more than 99 percent of the uranium is in the form of aqueous uranyl carbonate species, with less than 1 percent as uranyl hydroxide species. As in the K_d simulations for the soil-rainwater mixture, addition of the till is calculated to result in dissolution of a small fraction of the quartz, illite, and chlorite.

Table 6-6. PHREEQC Results for Uranium Speciation in the Till-Groundwater Adsorption Tests Jefferson Proving Ground, Madison, Indiana

Before Soil Addition			After Soil Addition*		
Species	Molality	U Mole Fraction	Species	Molality	U Mole Fraction
U(VI) Total	1.99E-08		U(VI) Total	1.99E-08	
$UO_2(CO_3)_2^{2-}$	1.10E-08	55.32%	$UO_2(CO_3)_3^{4-}$	1.14E-08	57.3%
$UO_2(CO_3)_3^{4-}$	8.75E-09	43.95%	$UO_2(CO_3)_2^{2-}$	8.33E-09	41.8%
UO_2CO_3	7.71E-11	0.39%	$UO_2(OH)_2$	1.33E-10	0.7%
$UO_2(OH)_2$	6.13E-11	0.31%	UO_2CO_3	2.92E-11	0.1%
$UO_2(OH)_3^-$	1.68E-12	0.01%	$UO_2(OH)_3^-$	1.26E-11	0.1%
*Results reflect equilibration with soil and cation exchange					

6.3.2 Uranium Speciation in Soil

This section presents the results from PHREEQC simulations of uranium speciation in soil and water of glacial till at JPG. Two sets of calculations are presented: simulations of a loess soil-rainwater mixture and simulations of a glacial till-groundwater mixture. As discussed in Section 6.2, the primary differences between these simulations and the K_d simulations are in the relative amounts of soil, water, and uranium being modeled. In these simulations, the mass ratio of soil to water is 1,200 to 320 (3.75 to 1), whereas in the K_d the mass ratio in simulations of soil to water was 1 to 25. In addition, the chemical form of uranium is assumed to be different. In the K_d simulations, uranium was added in the form of uranyl nitrate hexahydrate and in these simulations, uranium is added as schoepite. In all of the PHREEQC calculations, the schoepite dissolves completely and, as in the K_d tests, all of the uranium goes into solution.

Results are presented for two different ambient CO_2 levels: one that corresponds to atmospheric CO_2 and another that reflects higher ambient CO_2 levels that could result from biological process, such as plant respiration.

6.3.2.1 Speciation in Loess

Uranium speciation was modeled in loess soil containing rainwater at its field capacity, estimated to be approximately 0.32 cm^3 of water per cm^3 of dry soil for the silt-loam soil characteristic of the JPG site. As noted previously, the soil composition modeled in these simulations is similar to the average Avonburg/Cobbsfork soil.

Table 6-7 shows the calculated uranium speciation for an assumed ambient CO_2 level corresponding to atmospheric conditions. The results shown in the table are calculated by PHREEQC after rainwater is equilibrated with the schoepite-contaminated soil, cation exchange occurs between the solution and clay, and the calculated pH is adjusted to the desired value (5.7 in these simulations). In the resulting solution, approximately two-thirds of the uranium is calculated to exist in the form of aqueous uranyl carbonate species with the remaining one-third in the form of uranyl or uranyl hydroxide species.

Table 6-7. Loess-Rainwater Uranium Speciation Before Soddyite Precipitation – Atmospheric CO_2 Level Jefferson Proving Ground, Madison, Indiana

Species	Molality	U Mole Fraction
U(VI)	9.94E-06	
UO_2CO_3	2.76E-06	27.3%
$UO_2(OH)_2$	2.31E-06	23.2%
$(UO2)_2CO_3(OH)_3^-$	1.83E-06	36.7%
UO_2OH^+	6.06E-07	6.1%
UO_2^{+2}	2.14E-07	2.1%
$UO_2(CO_3)_2^{2-}$	1.73E-07	1.7%
$(UO2)_3(OH)_5^+$	5.67E-08	1.7%

The relative amounts of carbonate and hydroxide species is similar to that calculated in the K_d loess-rainwater simulations. As in the K_d simulations, mixing of soil and water is calculated to result in dissolution of several constituents of the soil, such as quartz, illite, chlorite, and dolomite. In this case, the larger mass of soil in the simulation results in a higher concentration of dissolved mineral constituents. This results in a solution that PHREEQC calculates to be supersaturated in a uranium mineral soddyite [$(UO_2)_2SiO_4$:$2H_2O$], as well as in a number of other minerals.

Another PHREEQC calculation step was performed in which precipitation of soddyite was simulated. This resulted in almost a 99.8 percent reduction in the amount of uranium in solution and altered the uranium speciation slightly, with approximately half of the uranium as uranyl carbonate species and half as uranyl hydroxide species (see Table 6-8).

Table 6-8. Loess-Rainwater Uranium Speciation After Soddyite Precipitation – Atmospheric CO_2 Level Jefferson Proving Ground, Madison, Indiana

Species	Molality	U Mole Fraction
U(VI) Total	2.11E-08	
UO_2CO_3	9.62E-09	45.5%
$UO_2(OH)_2$	8.00E-09	37.9%
UO_2OH^+	2.10E-09	9.9%
UO_2^{+2}	7.40E-10	3.5%
$UO_2(CO_3)_2^{2-}$	6.08E-10	2.9%

Although soddyite has frequently been found in uranium-contaminated soils (Wang et al. 2005; Buck, Dietz, and Bates 1995), the results from this calculation should not be considered as a realistic representation of what might be expected in JPG soils. Other competing phenomena that were not modeled, such as surface complexation, may occur and affect the soddyite saturation level in solution. For example, in a series of controlled experiments to assess the kinetics of surface complexation and soddyite dissolution/precipitation, Giammar noted that uranium sorption due to surface complexation was much more rapid than dissolution/precipitation (Giammar 2001). Uranium sorbed by surface complexes would not be available to be precipitated as soddyite. Therefore, although soddyite precipitation may occur, it would likely not occur to the extent modeled in these PHREEQC simulations.

Tables 6-9 and 6-10 show the calculated uranium speciation before and after soddyite precipitation when enhanced ambient CO_2 levels are assumed. For these cases, the higher ambient CO_2 levels result in more uranyl carbonate formation. Before soddyite precipitation, greater than 97 percent of the uranium is present in solution as uranyl carbonate species. After soddyite precipitation, the percentage as uranyl

Table 6-9. Loess-Rainwater Uranium Speciation Before Soddyite Precipitation – Enhanced CO_2 Level Jefferson Proving Ground, Madison, Indiana

Species	Molality	U Mole Fraction
U(VI)	9.94E-06	
$UO_2(CO_3)_2^{2-}$	4.41E-06	44.5%
UO_2CO_3	4.28E-06	43.1%
$(UO_2)_2CO_3(OH)_3^-$	3.91E-07	7.9%
$UO_2(OH)_2$	2.96E-07	3.0%
UO_2OH^+	8.39E-08	0.8%
UO_2^{2+}	3.70E-08	0.4%
$UO_2(CO_3)_3^{4-}$	2.51E-08	0.3%

Table 6-10. Loess-Rainwater Uranium Speciation After Soddyite Precipitation – Enhanced CO_2 Level Jefferson Proving Ground, Madison, Indiana

Species	Molality	U Mole Fraction
U(VI) Total	2.49E-07	
$UO_2(CO_3)_2^{2-}$	1.20E-07	48.2%
UO_2CO_3	1.17E-07	46.8%
$UO_2(OH)_2$	8.04E-09	3.2%
UO_2OH^+	2.28E-09	0.9%
UO_2^{+2}	1.01E-09	0.4%

carbonates is approximately 95 percent. The calculations indicate that 97.5 percent of the uranium precipitates from solution as soddyite.

6.3.2.2 Speciation in Till

Tables 6-11 through 6-13 show the uranium speciation calculated by PHREEQC for the glacial till-groundwater mixture assuming ambient CO_2 at atmospheric levels. For this condition, the higher alkalinity and pH of the till-groundwater solution strongly favors uranyl carbonate formation with 88 percent uranyl carbonates before soddyite precipitation and 77 percent uranyl carbonate formation after soddyite precipitation. The calculations show a 99.6 percent reduction in the aqueous uranium concentration due to soddyite precipitation. As indicated in Section 6.3.2.1, the calculated soddyite precipitation may or may not be realistic, since surface complexation, which was not modeled in the PHREEQC simulations, may be kinetically faster.

Table 6-11. Till-Groundwater Uranium Speciation Before Soddyite Precipitation – Atmospheric CO_2 Level Jefferson Proving Ground, Madison, Indiana

Species	Molality	U Mole Fraction
U(VI)	9.95E-06	
$UO_2(CO_3)_2^{2-}$	3.10E-06	31.2%
$(UO_2)_2CO_3(OH)_3^-$	2.48E-06	49.8%
$UO_2(OH)_2$	1.11E-06	11.1%
$UO_2(CO_3)_3^{4-}$	6.26E-07	6.3%
$UO_2(OH)_3^-$	9.21E-08	0.9%
UO_2CO_3	6.00E-08	0.6%

Table 6-12. Till-Groundwater Uranium Speciation After Soddyite Precipitation – Atmospheric CO_2 Level Jefferson Proving Ground, Madison, Indiana

Species	Molality	U Mole Fraction
U(VI) Total	3.72E-08	
$UO_2(CO_3)_2^{2-}$	2.31E-08	62.0%
$UO_2(OH)_2$	8.02E-09	21.6%
$UO_2(CO_3)_3^{4-}$	4.71E-09	12.7%
$UO_2(OH)_3^-$	6.68E-10	1.8%
UO_2CO_3	4.40E-10	1.2%
$(UO2)_2CO_3(OH)_3^-$	1.32E-10	0.7%

Table 6-13. Till-Groundwater Uranium Speciation – Enhanced CO_2 Level Jefferson Proving Ground, Madison, Indiana

Species	Molality	U Mole Fraction
U(VI)	9.91E-06	
$UO_2(CO_3)_3^{4-}$	7.94E-06	80.13%
$UO_2(CO_3)_2^{2-}$	1.96E-06	19.77%
$UO_2(OH)_2$	5.44E-09	0.05%
UO_2CO_3	2.98E-09	0.03%

Table 6-12 shows the calculated uranium speciation for the till-groundwater mixture assuming enhanced ambient CO_2 levels related to biological processes. For this condition, the greater ambient CO_2 concentration increases uranyl carbonate formation such that more than 99.9 percent of the uranium in solution is in the form of uranyl carbonate species. In this calculation, soddyite was at concentrations in the aqueous solution below saturation so no precipitation of soddyite was calculated.

In both sets of calculations, the calculated uranium speciation is similar to that calculated for the till-groundwater K_d simulations.

6.4 ADDITIONAL PHREEQC MODELING

Additional PHREEQC modeling was performed to evaluate the impact of biological activity such as plant respiration. Plants use photosynthesis to store energy by the following reactions:

Reduction of C	$CO_2 + 4\ e^- + 4\ H^+ \rightarrow CH_2O + H_2O$
Balancing Reaction	$2\ H_2O \rightarrow 2O_2 + 4e^- + 4\ H^+$
Overall	$CO2 + H2O \rightarrow CH2O + O2$

The stored energy is subsequently acquired (plant respiration) by the following reactions:

Oxidation of C	$CH_2O + H_2O \rightarrow CO_2 + 4\ e^- + 4\ H^+$
Reduction of O_2	$2O_2 + 4e^- + 4H^+ \rightarrow 2\ H_2O$
Overall	$CH_2O + O_2 \rightarrow CO_2 + H_2O$

There are similar chemical processes related to bacterial interactions in the soil.

If oxygen becomes depleted in the ambient soil environment, such as during flooded conditions, alternate electron acceptors are used. In order of preference based on their oxidation-reduction (redox) potential:

$NO_3^- \rightarrow N_2$ (or other reduced N forms)
$Mn^{4+} \rightarrow Mn^{2+}$
$Fe^{3+} \rightarrow Fe^{2+}$
$SO_4^{2-} \rightarrow S_2^-$ (or H_2S)

In other words, oxygen (O_2) has the highest redox potential and is oxidized first, followed by nitrate (NO_3^-), then tetravalent manganese (Mn^{4+}) then ferric or trivalent iron (Fe^{3+}) and then sulfate (SO_4^{2-}). This means that as a soil becomes reducing, the redox potential generally moves in accordance with the sequence shown above.

Reducing conditions due to biological activity can be simulated in PHREEQC by including formaldehyde (CH_2O) as a reactant. By adjusting the number of moles of CH_2O that react, the redox potential can be reduced such that U(IV) is favored over U(VI). In the loess-rainwater speciation calculation with enhanced CO_2 only 9×10^{-5} moles of CH_2O was sufficient to change the redox potential so that uranium was found almost entirely as U(IV). Under these conditions, the aqueous solution is calculated to be supersaturated in uraninite (largely crystalline UO_2). PHREEQC calculates that more than 99.99 percent of the uranium would precipitate as uraninite under these conditions. Uraninite is known to be very stable in soil, since it dissolves very slowly and is therefore relatively immobile. Moreover, as discussed in Section 5.3, reducing conditions greatly reduce the initial corrosion and dissolution rates of the DU penetrator.

Once oxidizing conditions were restored, the precipitated uraninite would reform schoepite, which would subsequently dissolve as in the original loess-rainwater simulations, and the uranium speciation shown in Table 6-9 would eventually be restored.

Soil series descriptions for the JPG soils indicate that areas with somewhat poorly drained soils exhibit redoximorphic features or soil mottling (USDA 1985). This soil appearance is suggestive of reducing conditions, which likely occurs during the growing season when the ground is saturated or flooded. Under these conditions, there is significant biological activity but an inadequate supply of available oxygen. As simulated by PHREEQC, these conditions would promote reduction of U(VI) to U(IV) and precipitation of uranite.

6.5 SUMMARY

A series of geochemical modeling simulations has been completed using the PHREEQC software in order to determine uranium speciation in the pore water at JPG. Simulations were performed for soil-rainwater mixtures and for glacial till-groundwater mixtures. Two partial pressures of CO_2 were simulated: one corresponding to atmospheric levels and one corresponding to higher levels in the soil resulting from plant respiration. PHREEQC calculations were also performed to simulate uranium speciation in solution in the K_d adsorption tests described in Appendix D. Oxidizing conditions were calculated in all of these simulations.

The PHREEQC simulations show that uranium speciation is sensitive to the soil-water mixture, with the more alkaline glacial till-groundwater mixture having a much higher percentage of uranyl carbonate species than the loess-rainwater mixture. This difference is significant because uranyl carbonate species are known to be more mobile in soil and less likely to be adsorbed by soil constituents.

The simulations also showed that uranium speciation is sensitive to the CO_2 partial pressure in the soil, with higher CO_2 pressures associated with a higher percentage of uranyl carbonate species. The CO_2 partial pressure is known to vary with depth and level of plant growth. At shallow soil depths and during

the times of the year that plants are not actively growing, the CO_2 partial pressure will be close to atmospheric levels.

The PHREEQC simulations also showed the uranium speciation in the K_d tests is similar to that calculated for the corresponding soil-water mixture when an atmospheric CO_2 partial pressure is assumed. Thus, the K_d tests are believed to provide a good simulation of the conditions experienced by penetrators buried at or near the surface when soil conditions are oxidizing.

Additional PHREEQC calculations were performed to simulate reducing conditions, such as might occur during the growing season when the soil is periodically flooded. Under these conditions, the PHREEQC simulations showed that U(VI) is reduced to U(IV) and uraninite (UO_2) precipitates from solution. Uraninite is insoluble in the soil and is not easily transported. Once oxidizing conditions are restored, the uraninite oxidizes and hydrates to form schoepite. The schoepite then can be dissolved by water and uranium would speciate, as described above.

7. TRANSPORT MECHANISMS

Figure 7-1 is an alternative representation of the CSM that focuses on DU release mechanisms, exposure media, potential exposure pathways, and potential receptors for the DU Impact Area and surrounding region. The transport mechanisms are described in further detail below.

The type of release affects the type and amount of DU released into the environment and the potential for exposure of humans and wildlife. In general, during the testing of DU penetrators, DU either can be released as particles in aerosols and residual metallic fragments created upon impacts with targets or nearly intact penetrators that missed their targets. While DU testing had occurred at JPG (between 1984 and 1994), humans and wildlife could have been exposed to DU from inhaling and inadvertently ingesting particles in aerosols released from the DU munitions. However, as testing operations have not been conducted at JPG since 1994, and any aerosols created by the impact of the DU penetrators with the ground surface were limited because the tests were nondestructive testing on soft cloth or wood (nonarmored) targets for trajectory purposes, this pathway is negligible. However, the inhalation of any resuspended particles from contaminated soil or dust is included.

DU that had been distributed on or immediately below the ground surface and/or within the surface water (streams) of the DU Impact Area as a result of the testing may be transported throughout the environment by several different processes. DU in the soil or surface water can be subject to physical movement by erosion (during floods and high runoff events), and these processes may cause migration and transport of DU penetrators along the ground surface and along the surface water drainageways. Corrosion of the DU in the surface water or soil could enable soluble forms of DU to be absorbed by plants and incorporated within the plant matter for uptake by wildlife. Although vegetation may be burned as part of a management effort or unintended fires (e.g., from lightning), the levels of DU carried in smoke associated with natural vegetation (such as the controlled burns at JPG) is not likely significant (Williams et al. 1998, U.S. Army 2001). Leached DU from the penetrators and/or fragments in the surface water potentially could be transported to groundwater and surface water, which in turn could migrate to drinking water sources and be ingested by humans, livestock, and wildlife.

7.1 GROUNDWATER PATHWAY

Hydrostratigraphic units at the DU Impact Area include overburden and bedrock. Overburden is defined as unconsolidated sediments occurring above the bedrock and consists mainly of soils, loess, and glacial till with minor amounts of alluvium deposited along streams. The underlying bedrock consists of interbedded limestone, dolomite, and shale. The upper portion of the bedrock referred to here as shallow bedrock (upper 40 to 60 ft of bedrock) is more permeable than deep (bedrock below 40 to 60 ft) bedrock.

Monitoring well boring logs exist for the wells within the DU Impact Area as well as for additional wells south of the firing line. Observations and sampling during borehole advancement serves as the primary data source on subsurface conditions at JPG. Depth to bedrock data are summarized in Table 7-1 for the characterization wells installed in 2007, ERM wells installed in 1983 and 1988, and Range Study Program wells installed in 2002 (Figure 7-2).

The characterization wells installed within and near the DU Impact Area were complete in the overburden (designated with "O" as part of the well identification, e.g., JPG-DU-06O), shallow bedrock (designated with "I" as part of the well identification, e.g., JPG-DU-6I), and deep bedrock (designated with "D" as part of the well identification, e.g., JPG-DU-6D). Some wells were installed as clusters of well pairs or triplets. Complete details on well installation are provided in the Well Construction and Surface Water Data Report (SAIC 2008b).

Figure 7-1. CSM of DU Transport Through the Environment for the DU Impact Area

Table 7-1. Depth to Bedrock at DU Impact Area and Vicinity
Jefferson Proving Ground, Madison, Indiana

Well ID	Date Installed	Ground Surface Elevation	Top of PVC Elevation	Total Depth of Boring	Top of Bedrock		Lithology in Exposed Open Interval
		FAMSL	FAMSL		FTBGS	FAMSL	
DU Impact Area Characterization Wells							
JPG-DU-01D	6/14/2007	838.26	841.15	113.1	19.5	818.76	Limestone
JPG-DU-01I	6/15/2007	838.06	841.23	41.7	20	818.06	Limestone
JPG-DU-02D	5/20/2007	800.92	803.83	119.3	0.65	800.27	Limestone
JPG-DU-02I	5/21/2007	800.93	803.94	49.0	16	784.93	Limestone, shale
JPG-DU-03I	12/12/2007	862.14	865.6	120.6	40.6	821.54	Limestone
JPG-DU-03O	12/12/2007	862.1	865.54	25.0	>25	NA	Clay, sand, and gravel
JPG-DU-04D	11/29/2007	864.18	867.13	120.8	46.2	817.98	Limestone
JPG-DU-04I	12/3/2007	864.32	867.38	65.5	47	817.32	Limestone
JPG-DU-04O	12/4/2007	864.11	867.28	47.0	>47	NA	Gravel and clay
JPG-DU-05D	11/19/2007	843.67	847.26	130.7	5.7	837.97	Fossiliferous Limestone
JPG-DU-05I	11/27/2007	843.71	847.21	34.9	5.8	837.91	Limestone
JPG-DU-06D	6/17/2007	872.79	875.76	118.7	35.7	837.09	Limestone
JPG-DU-06I	6/18/2007	872.91	875.65	48.4	35.4	837.51	Limestone
JPG-DU-06O	11/13/2007	872.56	876.02	25.0	>25	NA	Clayey sand, sandy/gravelly clay
JPG-DU-07D	11/15/2007	842.58	846.53	120.4	5.7	836.88	Fossiliferous Limestone
JPG-DU-07I	11/18/2007	842.39	846.33	60.4	5.6	836.79	Limestone
JPG-DU-08D	5/23/2007	815.36	818.58	139.3	6	809.36	Limestone
JPG-DU-08I	5/24/2007	815.44	818.59	39.3	6	809.44	Limestone, dolomite, shale
JPG-DU-09D	6/2/2007	846.1	849.07	119.5	34	812.1	Limestone
JPG-DU-09I	6/2/2007	846.45	849.38	74.0	34	812.45	Limestone
JPG-DU-09O	6/3/2007	846.63	849.63	34.0	>34	NA	Clay with sand and gravel
JPG-DU-10D	6/6/2007	870.71	873.64	118.75	72.5	798.21	Limestone, shaley limestone
JPG-DU-10O	6/7/2007	870.39	873.51	71.8	71.8	798.59	Sand, silt, clay
ERM Program Wells							
MW-1	12/6/1983	851.75	853.58	33.2	4.5	847.25	Limestone
MW-2	12/13/1983	848.25	850.49	23.7	7	841.25	Limestone
MW-3	12/13/1983	870.96	873.64	42.8	18.5	852.46	Limestone
MW-4	12/14/1983	898.92	902.19	28	10	888.92	Siltstone/ Limestone
MW-5	12/7/1983	801.91	804.36	33.4	5.6	796.31	Limestone
MW-6	12/17/1983	858.44	861.22	40	>40	NA	Silty Clay
MW-7	12/8/1983	850.99	853.7	53.7	26.5	824.49	Limestone
MW-8	12/9/1983	838.97	841.28	28.2	14.5	824.47	Limestone
MW-9	9/9/1988	819.85	819.96	38.2	3.7	816.15	Limestone & Shale
MW-10	9/18/1988	865.91	866.14	41.3	>41.3	NA	Sandy to Clayey Silt
MW-11	9/19/1988	809.49	809.89	41.9	2.1	807.39	Limestone & Shale
Range Study Program Wells							
MW-RS1	8/20/2002	865.39	867.78	13.5	8	857.39	Limestone & Clayey Silt
MW-RS2	8/16/2002	873.28	875.83	25.7	9	864.28	Limestone
MW-RS3	8/17/2002	879.19	881.57	12.5	>12.5	NA	Silty Clay
MW-RS4	8/19/2002	858.21	860.85	13	>13	NA	Silty Clay & Fine Sand
MW-RS5	8/18/2002	851.42	853.98	12.9	>12.9	NA	Silty Clay & Fine Sand
MW-RS6	8/18/2002	858.24	860.68	14.8	>14.8	NA	Silty Clay & Sand
MW-RS7	8/19/2002	859.42	862.02	12.5	>12.5	NA	Silty Clay & Sand
MW-RS8	8/21/2002	865.03	867.14	15.7	>15.7	NA	Silty Clay & Sand

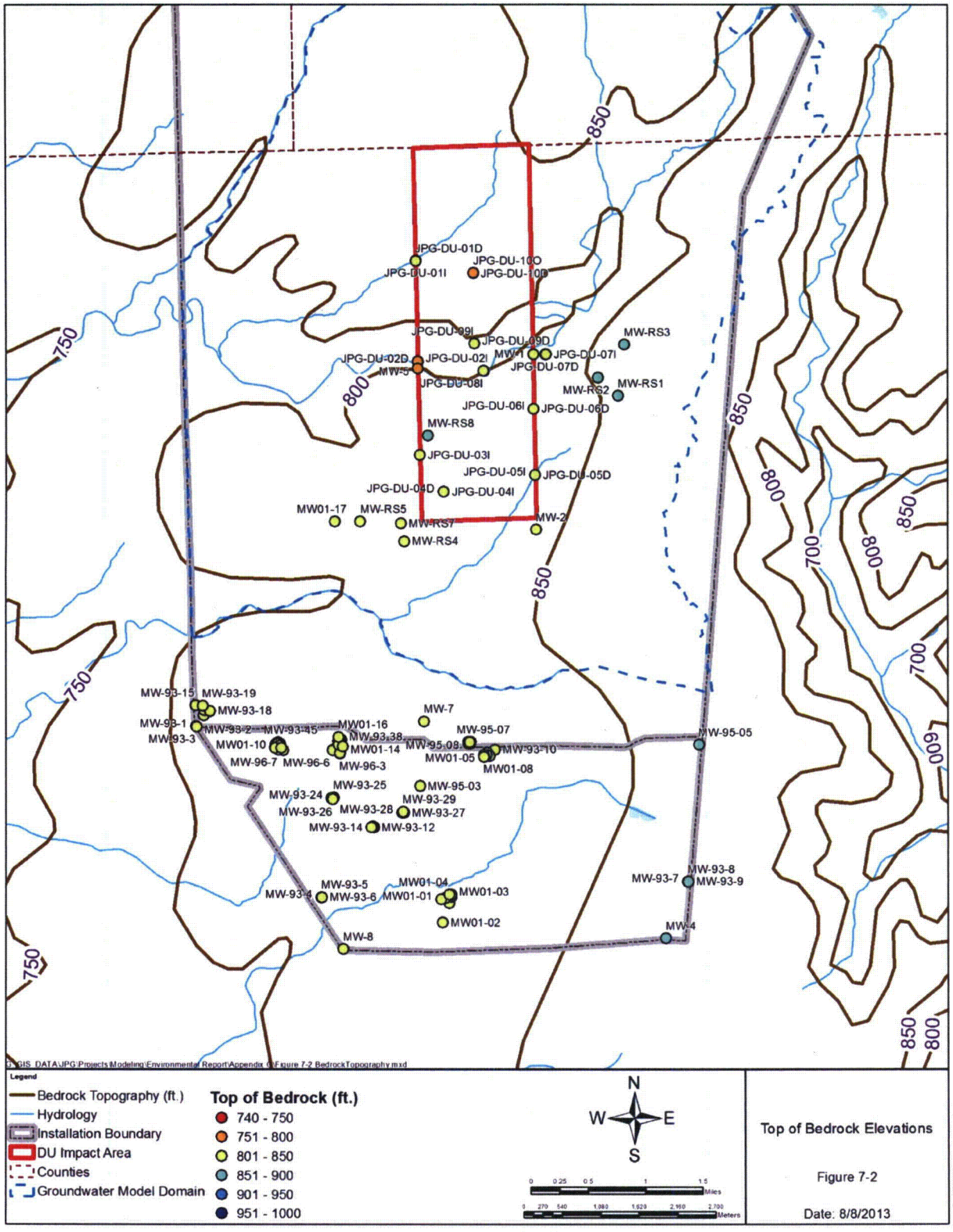
JPG-DU-01D
JPG-DU-01I
JPG-DU-10O
JPG-DU-10D
JPG-DU-09I
JPG-DU-09D
MW-RS3
JPG-DU-02D
JPG-DU-02I
MW-1
JPG-DU-07I
JPG-DU-07D
MW-5
JPG-DU-08I
MW-RS2
MW-RS1
JPG-DU-06I
JPG-DU-06D
MW-RS8
JPG-DU-03I
JPG-DU-05I
JPG-DU-05D
JPG-DU-04D
JPG-DU-04I
MW01-17
MW-RS5
MW-RS7
MW-2
MW-RS4
MW-93-15
MW-93-19
MW-93-18
MW-7
MW-93-1
MW-93-2
MW-93-45
MW01-16
MW-95-07
MW-93-3
MW01-10
MW-93-38
MW01-14
MW-95-08
MW-95-05
MW-93-10
MW01-05
MW-96-7
MW-96-6
MW-96-3
MW01-08
MW-93-25
MW-95-03
MW-93-24
MW-93-29
MW-93-26
MW-93-28
MW-93-27
MW-93-14
MW-93-12
MW-93-5
MW01-04
MW-93-4
MW-93-6
MW01-01
MW01-03
MW-93-7
MW-93-8
MW-93-9
MW01-02
MW-4
MW-8
750
800
850
700
600
D:\GIS_DATA\JPG\Projects\Modeling\Environmental Report\Appendix D\Figure 7-2 BedrockTopography.mxd
Legend
Bedrock Topography (ft.)
Hydrology
Installation Boundary
DU Impact Area
Counties
Groundwater Model Domain
Top of Bedrock (ft.)
740 - 750
751 - 800
801 - 850
851 - 900
901 - 950
951 - 1000
N
W
E
S
0 0.25 0.5 1 1.5 Miles
0 270 540 1,080 1,620 2,160 2,700 Meters
Top of Bedrock Elevations
Figure 7-2
Date: 8/8/2013

7.1.1 Overburden

The overburden consists of the unconsolidated materials or overburden present above the bedrock. As determined from the well installation and well logs, the depth of the overburden materials range from 0.65 to 72.5 ft, with an average depth to bedrock of 20.8 ft. The overburden materials consist of glacial tills and loess. A soil verification study (SVS) was completed and the results of the study are provided in Section 2 of the Well Location Selection Report (SAIC 2007) in which the soils present within the DU Impact Area are described in detail.

The soil in the study area is composed of mostly fine-grained materials, which appear to have a low permeability. At five well locations, sufficiently permeable materials were observed that would provide sufficient well yield to provide a suitable groundwater monitoring and sampling point. The majority of the existing monitoring wells that were completed in the overburden have been observed or documented in previous reports to have low well yields.

Overburden ranges from less than 1 to 72.5 ft based upon wells drilled in and around the DU Impact Area. The majority of soils within the DU Impact Area are somewhat poorly or poorly drained silty loam derived from the underlying loess or tills.

Seven soil series are mapped in the DU Impact Area (USDA NRCS 2005): Avonburg, Cincinnati, Cobbsfork, Grayford, Holton, Rossmoyne, and Ryker. An SVS (SAIC 2007) was conducted to confirm the soil series as mapped by the U.S. Department of Agriculture (USDA). All seven soil series have similar texture, consisting of silt loam derived from different parent materials and having different slopes. Table 7-2 summarizes the soil series. Six soil series are derived from parent material consisting of loess, underlying till-derived paleosols, and limestone residuum, and one soil series is derived from alluvium on floodplains:

- ***Cincinnati Series***—Deep, well-drained soils formed on mantle of loess
- ***Cobbsfork Series***—Poorly drained soils on broad summits of till plains; formed in loess and underlying till-derived paleosols
- ***Holton Series***—Deep, poorly drained soils formed in loaming alluvium on floodplains
- ***Grayford Series***—Deep, well-drained soils formed in loess, till of Illinoian age, and residuum from limestone on dissected till plains and sinkholes
- ***Avonburg Series***—Very deep, somewhat poorly drained soils formed in loess and underlying paleosol in till
- ***Rossmoyne Series***—Very deep, moderately well-drained soils formed on mantle of loess and underlying till of Illinoian age
- ***Ryker Series***—Very deep, well-drained soils formed in loess, underlying drift, and residuum from limestone on till plains.

Results from the field observations indicate the soil mapping units delineated on the Natural Resources Conservation Service (NRCS) map are reasonably accurate. From the soil borings observed, the site soil conditions may be wetter than indicated by the NRCS soil survey map. The field data indicate that the somewhat poorly drained Avonburg series may be grouped together with the poorly drained Cobbsfork series for the purpose of interpretation. Combined, these two soil series would comprise approximately 55 percent of the DU Impact Area. The well-drained Cincinnati and Rossmoyne series also may be grouped together, since both have a fragipan subsurface diagnostic horizon, which tends to perch water during parts of the year, and this combination would account for another 32 percent of the DU Impact Area. The well-drained Grayford, Ryker, and somewhat poorly drained Holton series all have somewhat unique soil conditions.

Table 7-2. Soil Series at the DU Impact Area Jefferson Proving Ground, Madison, Indiana

Soil Series[a]	Map Symbol[a]	Slope[a]	Depth[a]	Drainage Class	Taxonomic Classification[a]	Total Acreage as Mapped[a]	Percent of Total Acres[a]	Saturated Hydraulic Conductivity (m/s)[b]
Avonburg	Av	0-6%	Very Deep	Somewhat Poorly Drained	Fine-silty, mixed, active, mesic Aeric Fragic Glossaqualf	311.97	14.8	Upper solum moderately high to high 4.23×10^{-2} to 1.41×10^{-1}
Cincinnati	Cn	1-18%	Very Deep	Well Drained	Fine-silty, mixed, active, mesic Oxyaquic Fragiudalf	409.12	19.4	Moderate permeability
Cobbsfork	Co	0-1%	Very Deep	Poorly Drained	Fine-silty, mixed, active, mesic Fragic Glossaqualf	861.47	40.7	Upper solum 1.41×10^{-2} to 1.41×10^{-1}
Grayford	Gr	2-35%	Deep	Well Drained	Fine-silty, mixed, active, mesic Ultic Hapludalf	144.81	6.8	Moderately high to high 4.23×10^{-2} to 1.41×10^{-1}
Holton	Ho	0-2%	Very Deep	Somewhat Poorly Drained	Coarse-loamy, mixed, active, nonacidic, mesic, Aeric Endoaquept	36.22	1.7	Moderately high to high
Rossmoyne	Ro	0-25%	Very Deep	Moderately Well Drained	Fine-silty, mixed, superactive, mesic Aquic Fragiudalf	259.85	12.3	Moderate above fragipan, moderately slow below fragipan
Ryker	Ry	0-18%	Very Deep	Well Drained	Fine-silty, mixed, active, mesic Typic Paleudalf	90.8	4.3	NA

[a] From Tables 2-1 through 2-3 of the Final Well Location Selection Report (SAIC 2007)
[b] From Appendix A of the Final Well Location Selection Report – official soil series descriptions (SAIC 2007)

The portion of the DU Impact Area (>55 percent) with somewhat poorly and poorly drained soil exhibits redoximorphic features (soil mottling) that indicate a reducing environment exists in the shallow (<3 ft) subsurface for some period of time during the growing season. Redoximorphic features or soil drainage mottling are color patterns in the soil formed by the oxidation and reduction of iron and/or manganese caused by saturated or near saturated conditions within the soil. This reducing environment is sufficient to reduce the ferric iron to ferrous iron. The presence of ferrous or ferric iron is an indicator of the oxidative state. No direct measurements of redox potential (Eh) for soil were obtained during this investigation. Corrosion of metals and, therefore, DU penetrators can be greatly affected by the environment in which they are located. DU penetrator corrosion rates and processes are much lower under reducing conditions than those present under oxidizing conditions.

Loess occurs above the glacial till. The boundary between the loess and glacial till is transitional and not sharply defined due to similar lithology; most loess is derived from the underlying glacial till. The presence of gravel and split spoon blow counts (a substantial increase in blow counts was used to indicate presence of till) is used in this effort to differentiate loess from the underlying glacial till. Review of the site characterization well logs shows loess thickness ranges from 0 to 11 ft with an average of 6.3 ft. ERM and Range Study well logs show slightly greater depth to the glacial till but with less precision as split spoons (and therefore lithology descriptions) were collected at 5-ft intervals in the overburden.

Site-specific K_d was measured at JPG to characterize how DU may adsorb to or desorb from site soils during fate and transport. Two basic tests (sorption and desorption-dissolution) were used to estimate the site-specific K_d and desorption-dissolution potential, respectively, for DU. Sorption tests were performed for site soils and glacial till. Rainwater collected at the site was spiked with uranium at known concentrations and mixed with representative soils collected from background locations to determine what fraction of uranium would adsorb to the soils. Similarly, groundwater spiked with uranium at known concentrations was mixed with glacial till samples to determine uranium sorption to glacial till in the saturated zone. Desorption tests consisted of passing rainwater collected at the site through impacted soil samples (collected beneath penetrators) to determine the fraction of uranium that could desorb from impacted soils as rain water comes in contact with the soils. Results from the tests are summarized in Table 7-3. In summary, sorption tests showed lowest K_d (lowest fraction of uranium portioning onto the till) for groundwater in glacial tills. Sorption tests for soils at the surface showed high K_d (uranium strongly sorbed to soils). Desorption-dissolution tests indicated a higher fraction of uranium

Table 7-3. Summary of DU Batch Testing Results
Jefferson Proving Ground, Madison, Indiana

Soil Type	Number of Tests	Minimum Value	Maximum Value	Average Value
K_d (mL/g): Rainwater Sorption for Loess Soil Types				
Avonburg/Cobbsfork	10	1,058	3,831	2,290
Cincinnati/Rossmoyne	9	57	4,470	2,132
Grayford/Ryker	4	1,073	1,421	1,208
K_d (mL/g): Groundwater Sorption for Glacial Till				
Avonburg/Cobbsfork	3	0.93	1.03	0.98
Cincinnati/Rossmoyne	1	11.7	11.7	11.7
Grayford/Ryker	2	16	20	18
R_d (mL/g): Desorption by Loess Soil Type				
Avonburg/Cobbsfork	1	189	189	189
Cincinnati/Rossmoyne	1	591	591	591
Grayford/Ryker	1	507	507	507

will partition to rainwater in contact with highly impacted soils beneath or near the penetrators. Figure 7-3 illustrates the determination of the loess-glacial till interface and the approximate zones where the different K_ds are applicable.

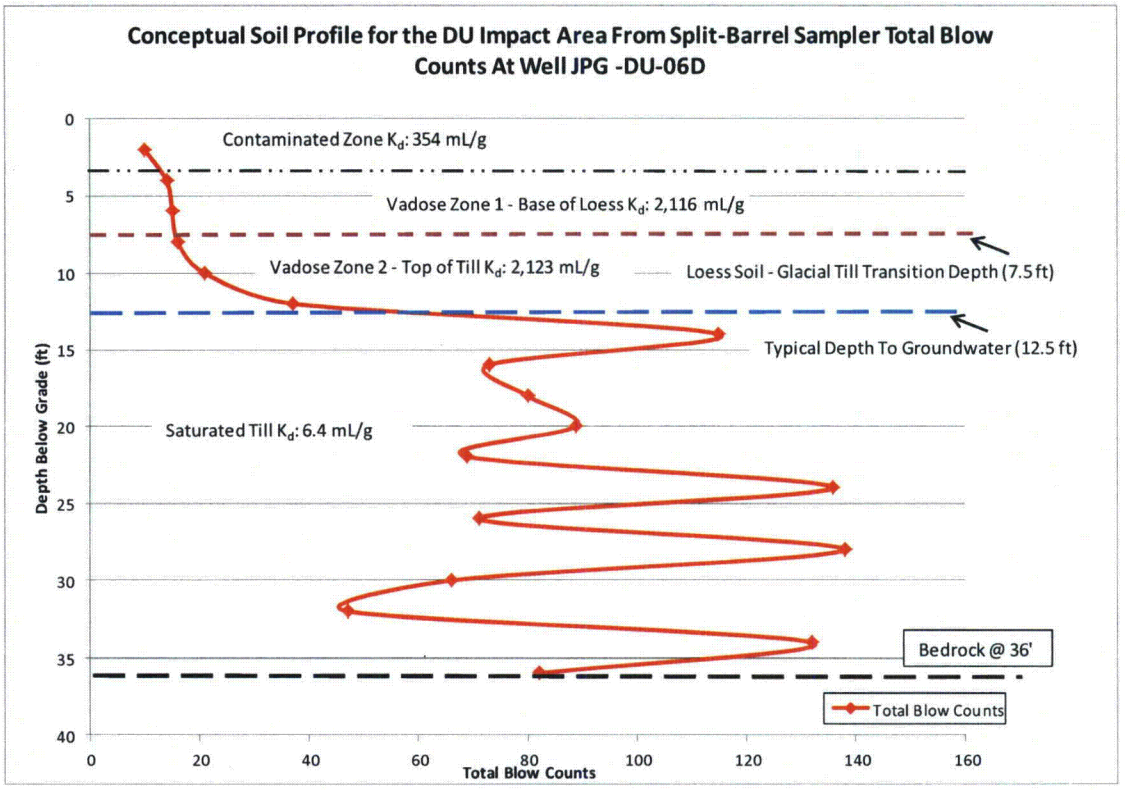

Figure 7-3. Example Soil Density Profile Through Loess Soil and Glacial Till at Well Location JP-DU-06

7.1.2 Bedrock Zone

The depth to carbonate bedrock ranges from less than 1 to 72.5 ft BGS. Relief on the top of bedrock is nearly 100 ft with the top of bedrock ranging in elevation from 784.93 to 888.92 ft above mean sea level (msl). In addition to the bedrock picks developed in the boring logs, additional information was obtained from a bedrock topographic map from the state of Indiana's GIS Atlas (http://inmap.indiana.edu/dload_page/geology.html). Bedrock topography in this file was converted from the original published map, Indiana Geological Survey Miscellaneous Map 36 (Indiana Geological Survey 2002). The contours define the elevation/topography of the bedrock surface in Indiana. As the date of the bedrock map predates the monitoring well boring logs, the map was adjusted in the vicinity of a groundwater model developed for the site to take into account the additional information gained from the site-specific data (Figure 7-2).

Karst features have been observed at JPG and specifically within the DU Impact Area consisting of surface expressions of small sinkholes, caves along Big Creek, and weathered jointing (fracturing) of bedrock observed at outcrops along Big Creek. Caves and solution features appear to be most commonly above the groundwater table and above the elevation of Big Creek. Wells were located on fracture traces and using geophysical techniques to selectively test areas where karst development would be greatest. However, results of the well drilling, field observations and an analysis of published reports and previous studies demonstrate that karst activity within and immediately surrounding the DU Impact Area is limited

in depth and lateral extent, confined to the shallow bedrock (generally less than 50 ft BGS), and more prevalent in and adjacent to stream valleys:

- Of all of the new wells installed, only a single very minor solution feature was observed in each of the borings at the JPG-DU-02 well pair location (along Big Creek) during the well installation. The solution feature was located at a depth of 23 to 23.5 ft BGS. The absence of karst/weathered conditions in 19 borings cored in 10 locations that were expected to be preferentially developed demonstrates that karst weathering is not a predominant feature in the DU Impact Area.
- Karst development and the presence of a karst controlled groundwater flow network appears to be limited to within the narrow erosional plain along Big Creek and offsite along lower sections of Middle Fork Creek. Observations by Science Applications International Corporation (SAIC) soil scientists and geologists indicate no sinkholes or closed depressions in the elevated areas above this plain. Sheldon (1997) reported on extensive field reconnaissance work completed from January 1994 to April 1997 in and surrounding the DU Impact Area, in which caves, sinkholes, and karst features were recorded and catalogued. Sheldon's only reported, observed, and documented cave locations within the DU Impact Area were along Big Creek (Sheldon 1997).
- The observations of karst features and weathering onsite concur with the following statements by Herring (2004), "...the majority of sinkholes or depressions occur along the larger stream valleys (especially Big Creek)...," "...water well records...indicate a few feet of crevices, broken limestone, or mud seams within the limestone bedrock, generally at depths less than 50 feet below land surface...," and "...The Silurian carbonates...show limited karst development in Jefferson County. These rocks contain thinner limestones and more layers of shale, conditions that significantly limit karst development."

7.1.3 Water Levels

Water level data were collected periodically from wells installed at JPG. Results from these point measurements indicate the water level depths in overburden (Table 7-4) range in depth from less than 2 ft to nearly 40 ft BGS and average 11 ft BGS. Water levels in the shallow bedrock from wells that are paired with overburden wells are generally a few feet lower but follow the same general patterns, indicating a downward gradient and hydraulic connection between the overburden and shallow bedrock. Water levels in deep bedrock wells are generally much lower than those in the shallow/intermediate bedrock; show very slow recovery following sampling or attempted slug testing, indicating limited communication between the shallow/intermediate and deep bedrock; and have limited flow within the deep bedrock (at least at the locations of the installed monitoring wells).

Continuous recorders were installed in 15 monitoring wells within and adjacent to the DU Impact Area (Figure 7-4). Note that not all wells were equipped with continuous recorders. Three general types of responses are noted:

- Overburden wells and intermediate wells located in upland areas away from creeks generally show seasonal fluctuations that range from a few feet to as much as 9 ft. A gradual decline in water levels occurred within these wells from the late spring of 2008 through the summer of 2008 during a period of below normal precipitation, followed by recovery to similar or in some cases higher water levels that preceded the decline. Monitoring wells showing this type of response include JPG-DU-01I, JPG-DU-03I, JPG-DU-06O, JPG-DU-06I, JPG-DU-09O, JPG-DU-09I, and MW-2.

Table 7-4. Depths to Groundwater in Overburden Wells
Jefferson Proving Ground, Madison, Indiana

Station ID	Event/Date(s)				
	Quarterly Aug 07	Quarterly Nov 07	Site Wide Jan 08	Quarterly Feb 08	Quarterly Feb 09
	8/16/2007	11/15/07-11/16/07	1/23/2008	2/12/2008	2/2/2009
	DTW	DTW	DTW	DTW	DTW
JPG-DU-03O	---	---	6.26	5.21	7.88
JPG-DU-04O	---	---	11.03	9.95	12.91
JPG-DU-06O	---	---	5.69	4.72	8.26
JPG-DU-09O	12.55	12.13	11.29	11.59	13.57
JPG-DU-10O	38.74	39.75	38.14	37.66	39.02
MW-6	21.54	9.91	6.34	7.02	5.84
MW-10	9.51	8.73	2.62	1.79	2.98
MW-RS1	---	---	2.23	2.34	2.73
MW-RS3	10.89	11.14	6.92	6.59	7.57
MW-RS4	---	4.84	5.7	3.61	3.21
MW-RS5	---	9.38	5.61	4.95	3.34
MW-RS6	10.61	10.21	6.93	6.11	8.79
MW-RS7	---	10.14	7	6.05	8.55
MW-RS8	12.25	13.19	4.36	3.46	5.24

Min	**9.51**	**4.84**	**2.23**	**1.79**	**2.73**
Average	**16.58**	**12.94**	**8.58**	**7.93**	**9.28**
Max	**38.74**	**39.75**	**38.14**	**37.66**	**39.02**

Min	**1.79**
Average	**11.06**
Max	**39.75**

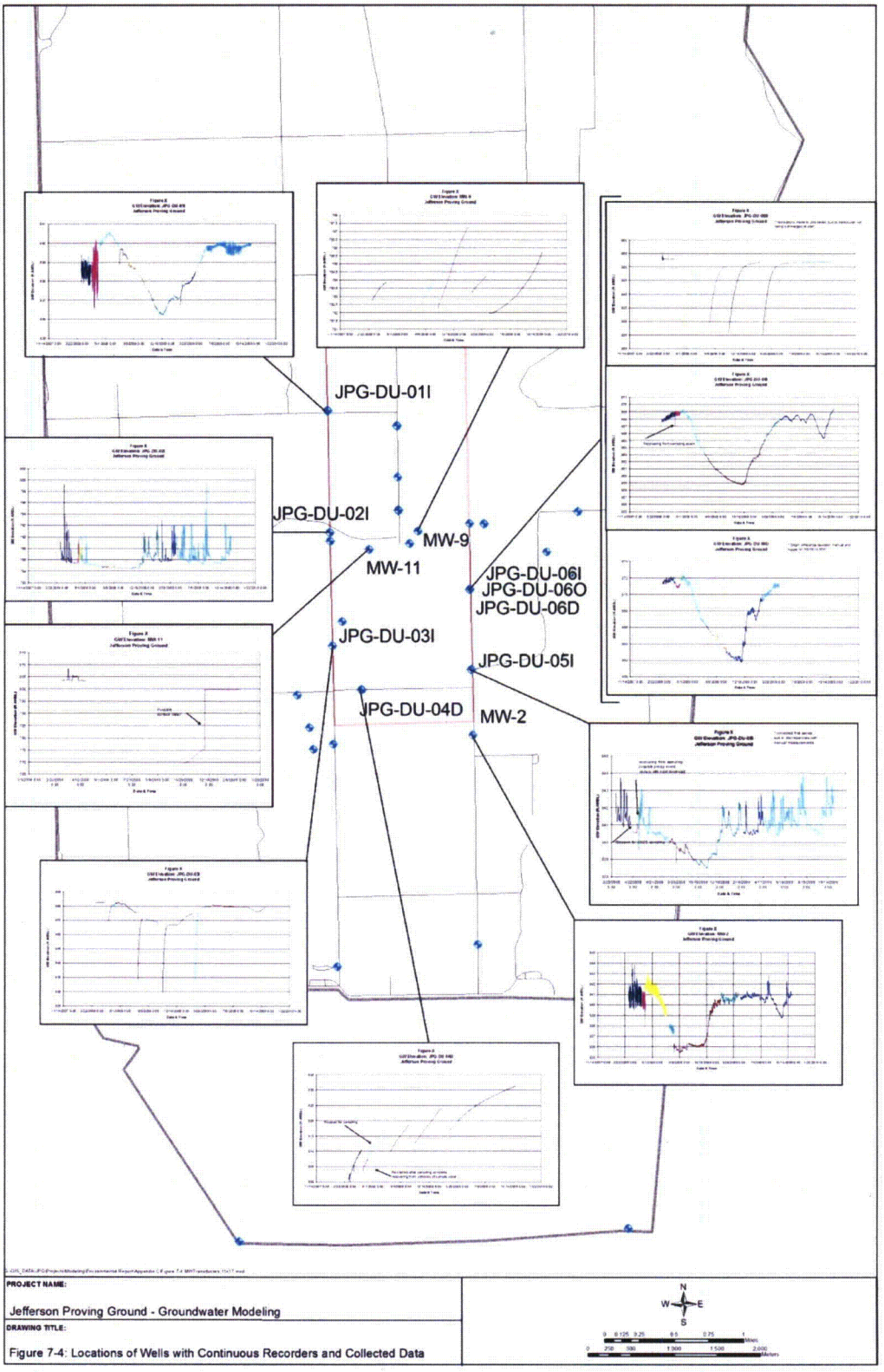
JPG-DU-01I
JPG-DU-02I
MW-9
MW-11
JPG-DU-06I
JPG-DU-06O
JPG-DU-06D
JPG-DU-03I
JPG-DU-05I
JPG-DU-04D
MW-2
PROJECT NAME:
Jefferson Proving Ground - Groundwater Modeling
DRAWING TITLE:
Figure 7-4: Locations of Wells with Continuous Recorders and Collected Data
N
W
E
S

- Shallow/intermediate bedrock wells near creeks exhibit similar response to changes in stream stage, indicating hydraulic connection between the shallow bedrock and adjacent creeks. Monitoring wells showing this type response include JPG-DU-02I adjacent to Big Creek at the western boundary of the DU Impact Area and JPG-DU-05I adjacent to Middle Fork Creek at the eastern boundary of the DU Impact Area. One other monitoring well with a continuous recorder, JPG-DU-03I, was located adjacent to a tributary to Big Creek but did not show the same hydraulic connection to creek stage.
- Deep bedrock wells and some shallow/intermediate bedrock wells exhibit very slow recovery to sampling events or attempts to slug test the wells. These wells indicate the very low permeability within the bedrock at their respective locations. Monitoring wells showing this type of response include JPG-DU-04D, JPG-DU-06D, JPG-DU-08I, JPG-DU-09D, MW-9, and MW-11.

Plots illustrating water level data collected from wells containing continuous recorders are included as Attachment 1 to this appendix. A brief description of each also is included.

Water level data from overburden and shallow/intermediate bedrock wells indicate flow directions roughly follow surface topography. Given the number of wells and spacing between wells, contour maps based upon observed water level data were not created. However, observations pertaining to flow directions and gradients can be made from the measured data. The direction of groundwater flow is roughly the same as the surface water drainage, which is to the west-southwest over most of the installation. The variability in the depth to groundwater in bedrock wells may reflect the occurrence of fractures in bedrock. SEC Donahue, Inc. (1992) noted that in the vicinity of incised surface drainages, the potentiometric surface slopes toward the streams at roughly the same gradient as the surface topography. Therefore, on a local scale, the bedrock groundwater tends to discharge to surface streams. Data from the site characterization wells, range study wells, and ERM wells support this observation.

7.1.4 Hydraulic Conductivity

Data analysis of slug tests performed on the wells in the vicinity of the DU Impact Area and hydraulic conductivity results for each of the wells tested are summarized in Tables 7-5 (overburden) and 7-6 (shallow bedrock) (SAIC 2010).

The hydraulic conductivity in the overburden and shallow bedrock is highly variable. Both zones included several wells where slug testing was not performed due to very slow water level recovery. The respective hydraulic conductivity in these cases is estimated to be at the low end of published literature values. Calculated hydraulic conductivities summarized below for both the overburden and shallow bedrock can be thought of as at the higher range of representative values at JPG but representative of the transmissible portions of each hydrostratigraphic zone.

Table 7-5. Overburden Slug Test Results
Jefferson Proving Ground, Madison, Indiana

Well	Hydraulic Conductivity		Notes
	(gpd/ft^2)	(ft/d)	
JPG-DU-03O	2.4	0.32	
JPG-DU-04O	4.1	0.55	
JPG-DU-06O	5.3	0.71	
JPG-DU-09O	0.01	1.30E-03	
JPG-DU-10O	NA	NA	Very slow recovery
MW-10	NA	NA	Very slow recovery

Table 7-6. Shallow Bedrock Slug Test Results
Jefferson Proving Ground, Madison, Indiana

Well	Hydraulic Conductivity		Notes
	(gpd/ft^2)	(ft/d)	
JPG-DU-01I	0.15	0.02	
JPG-DU-02I	18.55	2.48	Solution void
JPG-DU-03I	NA	NA	Very slow recovery
JPG-DU-04I	10.40	1.39	
JPG-DU-05I	0.08	0.01	
JPG-DU-06I	4.27	0.57	
JPG-DU-07I	NA	NA	No recovery
JPG-DU-08I	NA	NA	No recovery
JPG-DU-09I	NA	NA	Very slow recovery
MW-2	0.56	0.08	
MW-3	0.40	0.05	
MW-5	0.26	0.04	
MW-7	3.00	0.40	
MW-RS-2	10.20	1.36	

The range in hydraulic conductivity values in overburden wells is from 0.0013 to 0.71 feet per day (ft/d) (0.01 to 5.3 gallons per day per square foot [gal/day/ft^2]) with a geometric mean for all overburden wells of 0.11 ft/d (0.85 gal/day/ft^2). The geometric mean for the overburden wells with JPG-DU-09O removed is 0.5 ft/d (3.74 gal/day/ft^2). The published range for till is approximately 1.3 to 1.3×10^{-6} ft/d (10 to 0.00001 gal/day/ft^2) (Freeze and Cherry 1979), putting the JPG average overburden hydraulic conductivity estimate in the upper range.

Hydraulic conductivity measured in overburden materials during the Final Phase II Remedial Investigation (RI) included the following results:

- Slug tests results ranging from 0.031 to 0.24 ft/d
- Matrix hydraulic conductivity ranging from 9.6×10^{-5} to 2.8×10^{-4} ft/d
- Small-scale fractures: 1.6×10^{-3} ft/d
- Large-scale fractures: 0.06 ft/d.

The geometric mean hydraulic conductivity value for shallow bedrock wells, including JPG-DU-02I where a 6-in solution void is present, is 0.18 ft/d (1.33 gal/day/ft^2). Without JPG-DU-02I, the geometric mean is slightly lower at 0.13 ft/d (0.99 gal/day/ft^2). The published range for limestone and dolomite is approximately 1.3 to 0.003 ft/d (10 to 0.02 gal/day/ft^2) (Freeze and Cherry 1979), putting the JPG hydraulic conductivity value on the upper end of the published range for limestone and dolomite and at the low end of solution enhanced, or karst limestone. Factoring in the several wells that could not be tested would reduce the shallow bedrock hydraulic conductivity.

Deeper bedrock permeability is clearly lower than overburden or shallow bedrock, although remains unquantified due to the incomplete recovery of wells following development or incomplete recovery following installation of the data logger transducer/slug the night before testing. The above traits have led to a qualitative estimate of permeability for the deep bedrock on the order of 0.003 ft/d (0.02 gal/day/ft^2), which is at the low end of published values for limestone (Freeze and Cherry 1979).

In terms of the CSM, slug testing has quantified the permeability of overburden and shallow bedrock with values relatively similar for both hydrostratigraphic zones. Results suggest on a local scale that the overburden can transmit groundwater horizontally, possibly in discrete coarser-grained zones in the till, and that the till is likely in hydraulic communication with shallow bedrock. Slug test results confirm portions of each medium will essentially not transmit groundwater or transmit it very slowly. Water will reside for long periods of time in these low-permeability areas. The response of shallow bedrock well JPG-DU-02I to slug testing and the resultant hydraulic conductivity value estimate indicates that the shallow limestone may be more permeable on an average, large-scale basis than the overlying till, especially where the till is thin and rock is most susceptible to dissolution over time and subsequent enhanced fracture permeability.

Based on observed very slow recovery in deeper bedrock wells (following development, sampling, etc.) and the inability to conclusively slug test these wells relative to the hydraulic conductivity values for overburden and shallow bedrock, there is a pronounced reduction in average rock permeability below an average depth of 29 to 33 ft into the bedrock. The deeper limestone bedrock may be three or more orders of magnitude lower in hydraulic conductivity than either the overburden or the shallow, solution enhanced bedrock. The lack of secondary porosity features at depth is the likely explanation for the pronounced decrease in permeability with depth in the DU Impact Area. There is little to no transmission of groundwater within this deeper rock.

In addition, data were taken based on wells south of the firing line from the RI performed at the site. The hydraulic conductivity of the till ranges from 0.079 to 0.24 ft/d in the area south of the firing line, based on slug tests in wells (Rust E&I 1998, MWH 2002). Small-scale fractures and sand lenses within the till contributed to the higher hydraulic conductivity measured by the slug tests.

Slug and pump tests were completed on 51 wells located south of the firing line screened in the bedrock aquifer. The hydraulic conductivity of the bedrock aquifer computed from slug tests ranges from 0.048 to 1.66 ft/d (MWH 2002). The pumping test results indicate hydraulic conductivities range from 0.40 to 17.3 ft/d in the bedrock (MWH 2002).

7.1.5 Geotechnical Properties

The published range of porosity in glacial till is 12 to 41 percent with an average value of 26 percent (Kresic 2007). The published range of porosity in loess is 44 to 57 percent with an average value of 49 percent (Kresic 2007). Published bulk density of overburden materials is 1.92 g/cm^3 (Telford, Sheriff, and Geldart 1990).

The published range of porosity in dolomite is 1 to 32 percent with an average value of 7 percent (Kresic 2007). For limestone, the published range in porosity is 0 to 65 percent with an average value of 8 percent. Specific yield in carbonate bedrock is reported at 1 to 5 percent (USATHAMA 1988). Bulk density of limestone ranges from 1.92 to 2.90 g/cm^3; dolomite bulk density ranges from 2.28 to 2.90 g/cm^3 (Telford, Sheriff, and Geldart 1990).

Grain size analysis of 26 loess soil samples indicates the three shallow loess soil types have very similar grain size distributions consistent with the field-determined silty clay and sandy loam soil descriptions made at the time of sampling. The three loess soil types are very similar, containing approximately 29 to 33 percent clay, 45 to 52 percent silt, 18 to 23 percent sand, and 1 percent or less gravel. Figure 7-5 shows the relative differences in grain sizes for the three soils. This textural composition is consistent with a silty clay to clayey silt loam.

7.1.6 Groundwater Use

The groundwater under JPG generally is of poor quality and is not used for drinking purposes or for other purposes in any significant capacity. The drinking water at JPG is obtained from the city of

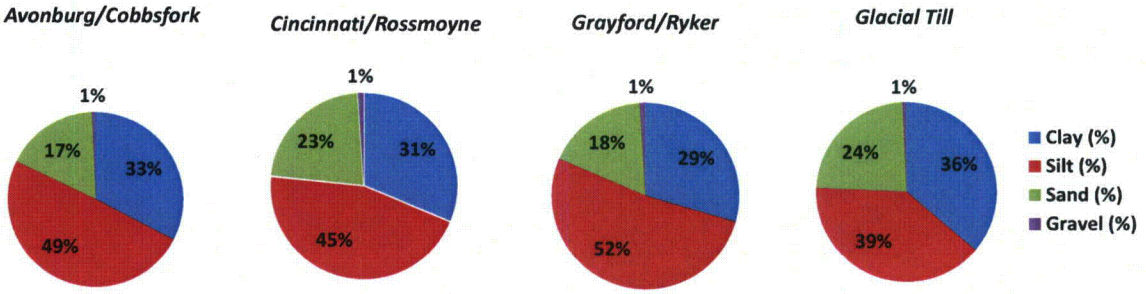

Figure 7-5. Particle Size Comparison of JPG Soil Types

Madison Municipal Supply Systems and the Canaan Deposits in the Ohio River Valley, approximately 5 miles (mi) (8 km) from JPG (MWH 2002). Seven test holes drilled into the carbonate bedrock during initial development of the installation were unable to locate groundwater in sufficient quantities to support facility operations.

7.1.7 Water Budget

The water budget analysis (SAIC 2007) determined for an average precipitation year of 47 in, 56 percent (26.3 in) is lost to evapotranspiration, 8 percent (3.8 in) becomes groundwater recharge, and the remaining 36 percent (16.9 in) is runoff. Weather data collected at Madison, Indiana (1976 to 2007) and from the U.S. Fish and Wildlife Service (FWS) on JPG were used to determine evapotranspiration rates. During this period, annual precipitation ranged from 33.24 to 60.93 in and actual evapotranspiration ranged from 17.2 to 29.7 in/y (SAIC 2007). Groundwater recharge rates were determined from base flow studies conducted for the neighboring Brush Creek and the larger Muscatatuck River (to which Big Creek and all JPG streams are tributaries). For comparison, published estimates indicate groundwater recharge at 4 to 8 in/y for southern Indiana (Bechert and Heckard 1966). Brush Creek in particular demonstrates the extremely flashy nature that is observed within the JPG streams; Brush Creek is similar in size and hydrology to the JPG streams. Large runoff volumes are observed quickly following a precipitation event followed by a rapid fall off to base flow conditions. The SAIC (2007) water budget assumes most groundwater re-emerges as base-flow into streams. Therefore, percolation losses to deep groundwater (deep bedrock) are insignificant.

7.2 GROUNDWATER MODELING SUMMARY AND CONCLUSIONS

The groundwater pathway was evaluated through modeling using the Finite Element Heat and Mass Transfer Model (FEHM) to simulate groundwater flow and potential for DU transport through the soil column to groundwater. The groundwater flow system beneath JPG was modeled using MODFLOW-SURFACT™ (HydroGeoLogic, Inc. 1996). Modeling results indicate limited potential for DU migration via the groundwater pathway. Observed uranium sampling results in the environmental media at JPG show limited migration of DU in shallow soils and essentially no evidence of DU migration to groundwater away from surface water bodies. Low uranium concentrations observed near creeks may be the result of creek-groundwater interactions or shallow migration in soils near the creeks and are not necessarily indicative of migration via the groundwater pathway. Sections 7.2.1 and 7.2.2 summarize the results of the FEHM and MODFLOW-SURFACT modeling conducted for the JPG DU Impact Area. Additional details are provided in Appendix M.

7.2.1 Soil to Groundwater Results

Model predictions using the FEHM soil column model indicate very limited migration to groundwater within 1,000 years based on observed site conditions and conservative input parameters like

source DU concentration and (lowest) distribution coefficients (desorption-dissolution K_d) determined from site-specific testing:

- Migration to groundwater may occur where the water table is shallow (~2 to 4 ft BGS). Shallow groundwater typically occurs in areas near streams.
- Migration to groundwater does not occur through the overburden at average depths to groundwater (11 ft BGS), nor at the depths typical of overburden near the bulk of remaining penetrators (30 to 40 ft BGS).

7.2.2 Groundwater Results

The groundwater flow model was developed and calibrated to February 2009 measured water levels. The groundwater contribution to streams within the model domain is 5.5 cubic feet per second (cfs) distributed across all of the streams in the model domain:

- The volume of groundwater discharge to Big Creek from the area beneath the DU Impact Area trench is 0.09 cfs
- The volume of groundwater discharge to Middle Fork Creek from the area beneath the DU Impact Area trench is 0.05 cfs.

Nearly all (99.5 percent) groundwater exiting the model domain does so by discharge to streams; 0.5 percent of groundwater exiting the model domain does so at the western model boundary. Prediction of DU fate and transport in the groundwater system was not performed because DU is not expected to transport through the vadose zone to groundwater at a detectable mass.

7.3 SURFACE WATER PATHWAY

Based on the limited recharge to the aquifer, limited observed permeability with depth, and expected low hydraulic conductivity with depth, the surface water pathway may be the most significant potential migration pathway from the DU Impact Area. The hydrographs from nearby U.S. Geological Survey (USGS) stream gauges and preliminary results from stream gauges onsite indicate that surface runoff after a precipitation event spikes rapidly and dissipates quickly. This may be an indication that the majority of sediment moved from the DU Impact Area could occur during short durations during peak runoff conditions. These would be times when considerable flows in the streams would potentially carry particulates, either sediments with DU attached or DU particles, and deposit them downstream when flow velocities dissipate. Combined with the highly erodible soils within the DU Impact Area, this pathway appears to be potentially significant.

The DU Impact Area is within the Muscatatuck Plateau physiographic region and is characterized by broad uplands covered by glacial till with entrenched valleys (Gray 2001). The glacial deposits overlie Paleozoic bedrock consisting of interbedded limestone, dolomite, and shale, and overburden thicknesses based on previously installed monitoring wells range from 10 to greater than 65 ft thick (U.S. Army 2002). According to Franzmeier, Steinhardt, and Schulze (2004), the glacial till is Pre-Wisconsinan age and thought to be Illinoian age or older and is covered with a thick (>6 ft thick) mantle of Wisconsinan age loess (wind deposited silt). The soil region that encompasses the DU Impact Area is described as "moderately thick loess over weathered loamy glacial till" (USDA NRCS 1999).

The DU Impact Area is incised by two streams (i.e., Middle Fork Creek and Big Creek and associated tributaries). The surface relief generally is a result of erosion and down cutting associated with the streams and surface water flow to the streams. The surface water drainage is characterized as exhibiting a dendritic pattern that discharges to the streams. The vegetative cover consists of wooded areas containing deciduous trees and open spaces populated with grasses, sedges, and other herbaceous plants. FWS uses controlled burns (management of vegetation by prescribed fires) to manage some of the grassland areas. A wide variety of wildlife inhabits the area, including terrestrial crayfish and other

burrowing animals that may cause localized bio-turbation (i.e., reworking of soils and sediments by animals or plants) of the soil.

The entire DU Impact Area has undergone anthropogenic disturbance of various types and magnitude. Prior to the establishment of JPG, the majority of the land was agricultural and the soils were disturbed in the act of tilling the lands. Following the establishment of JPG, disturbances ranged from installation and maintenance of the infrastructure (e.g., utility trenching, construction of buildings/structures, and road building) to testing operations in impact fields (i.e., disturbance by detonation) for a great number and variety of munitions between 1941 and 1994.

7.3.1 Modeling Domain and Description

Transport of DU via surface water runoff represents a significant potential pathway for the migration of DU from the DU Impact Area and adjacent areas. Development of the numerical model for JPG began with a model describing the area and key components of the surface water pathway, identification of data sources, and code selection. The modeled area (including the DU Impact Area) falls within the USGS hydrologic unit (0512020701) of the Muscatatuck River and is drained by Big Creek and Middle Fork Creek. Big Creek includes two smaller tributaries: Marble Creek and Camp Creek. The total area included for the surface water model extends to the confluence of Middle Fork Creek with Big Creek, covering a total area of roughly 44,949 ac (Figure 7-6). The majority of this area consists of Big Creek with 34,060 ac; Marble Creek (3,053 ac) and Camp Creek (5,843 ac) occur downstream from the DU Impact Area. The Middle Fork Creek drainage area consists of 10,889 ac.

The area is characterized by limited aquifer recharge and exhibits relatively low and decreasing permeability with depth. An analysis of hydrologic components suggests that surface water may be the most significant potential migration pathway from the DU Impact Area. The hydrographs from nearby USGS stream gauges and results from onsite stream gauges indicate that surface runoff after a precipitation event spikes rapidly and dissipates quickly, resulting in sharp rising and falling limbs. When stream flow rates are high, DU migration may include either sediment with DU attached and/or the disintegrated DU particles moving with the flow and followed by deposition downstream when flow velocities dissipate.

The land use patterns in the JPG watershed are fairly diverse. Erosion processes that can mobilize and transport soil from the DU Impact Area to streams such as Big Creek or Middle Fork Creek are illustrated in Figure 7-7. Rain falling on the land surface can detach soil particles, making them available to wash off in overland flow. Scouring of soils also can occur during precipitation runoff events. Land cover influences the amount of soil (or sediment) eroded. Farm land typically has greater erosion rates than forested or grass lands. Precipitation falling in upland areas of the watershed that were either uncultivated/bare or under active agriculture are expected to generate a large amount of sediment relative to the forested and grassy areas comprising the DU Impact Area.

This sediment and runoff will be transported by Big Creek and Middle Fork Creek through the DU Impact Area, where nonimpacted sediment and runoff from upstream will mix with the impacted sediment generated by erosion within the DU Impact Area. As this flow moves downstream from the DU Impact Area, additional mixing with nonimpacted sediment and runoff occurs. The cumulative output of sediment from the DU Impact Area is assessed in the modeling at points downstream from the area to the confluence of Middle Fork Creek with Big Creek (approximately 2 mi from the site boundary).

7.3.2 Runoff Generation

Surface runoff (or simply runoff) is the portion of total precipitation that flows over the ground surface to a receiving surface water stream and is the primary transport mechanism for eroded soils. Interflow represents the portion of precipitation that migrates above the water table and can be a component of runoff if the interflow reaches a surface water discharge point before reaching the water

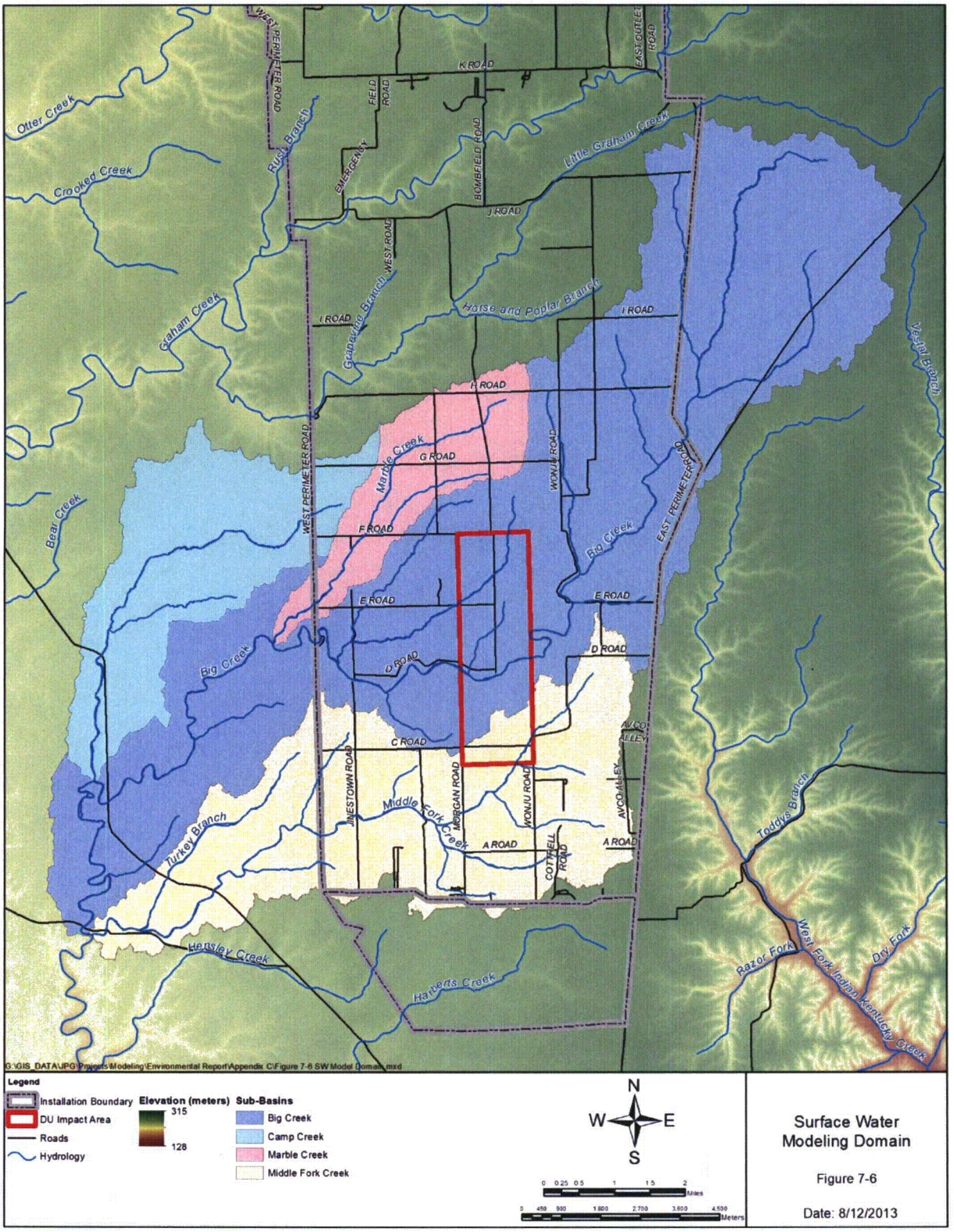
K ROAD
J ROAD
I ROAD
H ROAD
G ROAD
F ROAD
E ROAD
D ROAD
C ROAD
A ROAD
WEST PERIMETER ROAD
EAST PERIMETER ROAD
EAST OUTLET ROAD
FIELD ROAD
EMERGENCY
BOMBFIELD ROAD
WEST ROAD
WONJU ROAD
MORGAN ROAD
JAMESTOWN ROAD
AVCO ALLEY
COTTRELL ROAD
Otter Creek
Crooked Creek
Rush Branch
Little Graham Creek
Graham Creek
Grapevine Branch
Horse and Poplar Branch
Marble Creek
Beal Creek
Big Creek
Middle Fork Creek
Turkey Branch
Hensley Creek
Harbens Creek
Toddys Branch
Razor Fork
West Fork Indian Kentucky Creek
Dry Fork
G:\GIS_DATA\JPG Projects\Modeling\Environmental Report\Appendix C\Figure 7-6 SW Model Domain.mxd
Legend
Installation Boundary
DU Impact Area
Roads
Hydrology
Elevation (meters)
315
128
Sub-Basins
Big Creek
Camp Creek
Marble Creek
Middle Fork Creek
N
W
E
S
0 0.25 0.5 1 1.5 2 Miles
0 450 900 1,800 2,700 3,600 4,500 Meters
Surface Water Modeling Domain
Figure 7-6
Date: 8/12/2013

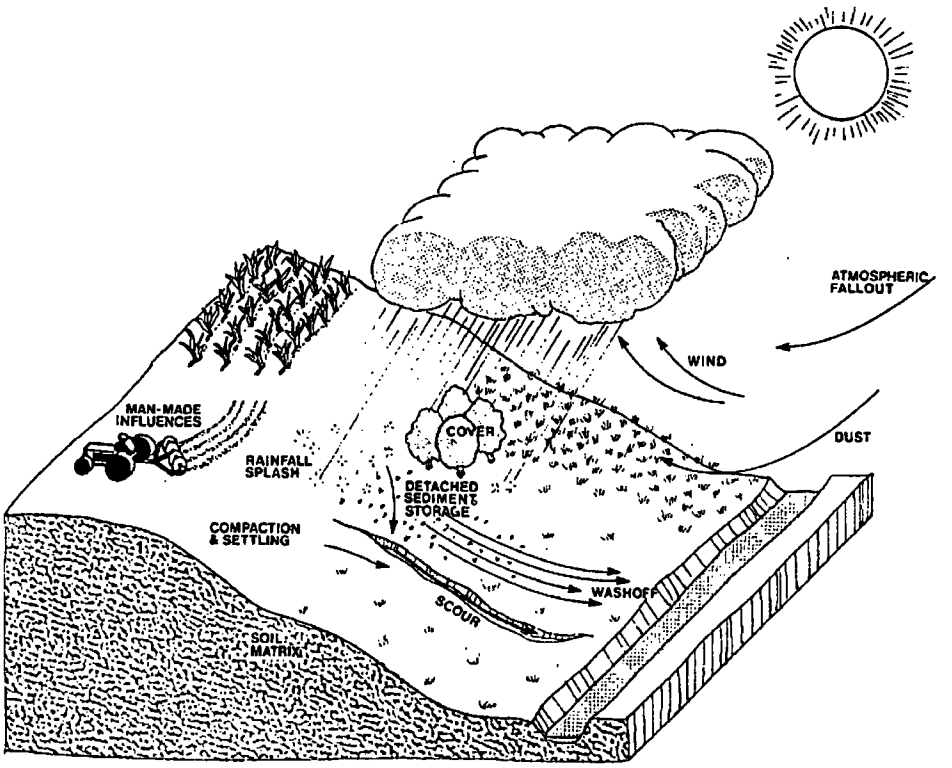

Figure 7-7. Erosion Processes and Overland Sediment Transport (USEPA 2001)

table. Runoff at JPG is highly correlated to precipitation (rainfall or snowmelt). Peak flows are flashy and generally occur immediately following a precipitation or melting event. Conceptually, the site can be divided into several sub-watersheds (sub-basins), with each sub-basin described by its land use, vegetative cover, topography, and other physical characteristics to assess the timing and percentage of precipitation that will return into stream segments as runoff.

In addition to runoff, the soil type, nature and spatial extent of vegetation, and topographic characteristics of sub-basins will determine the amount and type of sediment (size fractions) that will be carried (by the runoff) into the stream network.

7.3.3 Surface Water Routing

Most precipitation events generate surface and/or subsurface runoff from sub-basins into associated streams (also referred to as channels or reaches). At JPG, a significant part of the subsurface runoff (interflow and base flow) and the direct surface runoff eventually enters a network of streams. The total runoff and the dissolved and entrained DU are routed through this stream network. Spatial and temporal variations in stream flow, stage and concentration of sediments, and associated DU concentrations in surface water can be estimated.

The connectivity of the various stream channels was determined by the surface topography and reflects the overland flow system under prevailing site conditions. The National Hydrography Dataset in conjunction with the digital elevation model for the area was used to establish the stream drainage network. The width, depth, side slopes (curvature), bed slope, and surface roughness of the streams determine their transport capacity, stage versus specific flow rate relationship (rating curve), and the characteristics of the runoff hydrograph (the timings of low and peak flows in the watershed).

7.3.4 Sediment Transport

Precipitation intensity, duration and spatial distribution, land slopes, soil characteristics, and land use patterns determine the erosion potential and the composition of sediment (size fractions) entering the stream network. Once within the stream network, surface water flow velocity (channel velocity) is one of the most critical flow characteristics governing the fate and transport of sediments and the associated DU. Flow rates are determined by the bed slope, surface roughness, stream stage, and cross section configuration (slopes and floodplain extents) of the flow channels.

In sections with rapid flow, sediments in suspension are likely to stay in suspension and part of the bed load may scour and re-suspend into the overlying column of water and be transported downstream. In stream segments associated with low and mild flow velocities such as in areas associated with larger cross-sections and/or low flows (due to seepage and evaporation losses and diversions upstream), sediments in suspension have the tendency to settle out and become part of the bed load. This process normally starts with heavier particles (sand) followed by lighter (silt, clay) fractions. In general, lighter particles are more likely to remain in suspension and transport downstream.

7.3.5 DU Transport

One of the primary mechanisms for DU transport in the surface water is likely to be the DU fraction adsorbed to the sediments. The laboratory estimated K_d for DU suggests a potential for preferential transport of DU adsorbed to the sediments, particularly to the clay and silt size fractions. Other pathways include DU dissolved in the overland flow, interflow, and base-flow. A small fraction may include the larger DU particles disintegrating from the penetrators and transporting under high-flow conditions away from the DU penetrators and depositing downstream either within the sub-basin or the stream. Transport of DU fragments is believed unlikely except in extraordinary circumstances (such as flash flood like conditions), due to the high density and size of the fragments. However, as explained in Section 1, large objects present in the stream channels, such as boulders, bedrock outcrops, and at-grade river crossings, would prevent the migration of penetrators or fragments outside the boundaries of the DU Impact Area. In addition, the remnants of the former Wilson Dam more than 1,600 ft (0.5 km) west of the western boundary of the DU Impact Area on Big Creek and almost 10,000 ft (3 km) from the western boundary of JPG along Big Creek) would act as an additional physical impediment for the transport of DU penetrators beyond the boundaries of JPG. Lastly, since DU is approximately 1.65 times as dense as lead, the distance any DU may be transported during any such flood or high runoff event is minimal at best. Therefore, this phenomenon is not discussed further.

The most critical physical characteristics controlling DU transport are the K_ds; penetrator corrosion and dissolution rates of corrosion products; and the diameter, length, and density of the penetrators. DU will partition between solid phase, dissolved phases, and adsorbed fractions. The kinetics (rate) is largely governed by the mass transfer rates between these phases. The dissolved fraction will mix into the stream flow and transport downstream with some sorption or partitioning to sand, silt, and clay sediments in the channel. DU adsorbed to sand, silts, and clay in suspension or as bed sediment may undergo desorption (this is likely to be a very small fraction as reverse reactions are generally slow).

7.4 BIOTRANSFER PATHWAYS

Historical sampling of biota has occurred at JPG and the data suggest that DU levels in biota are not a concern (U.S. Army 2002). However, most samples were collected during and before the mid-1990s. Thus, a major component of the site characterization was to obtain more recent data to account for potential degradation of DU projectiles and subsequent migration of DU throughout a portion of the JPG environment over the more recent past.

Deer hunts are held annually on the former JPG reservation at Big Oaks National Wildlife Refuge (NWR), providing a mechanism of human exposure to contamination from earlier munitions tests.

Approximately 400 to 800 deer are harvested per year. Local residents from surrounding communities who hunt deer at or near JPG are concerned about potential adverse health effects from exposure to DU. Although NRC has acknowledged that DU concentrations in the most recently collected deer samples were low from a human health perspective, there were modest DU increases in kidney and bone compared to background. As a result, NRC expressed concern that concentrations may continue to increase to levels that could affect human health (NRC 2004d). Therefore, deer sampling was conducted as part of the site characterization associated with decommissioning the DU Impact Area.

There also is potential for DU uptake by wildlife other than deer. Although most wildlife other than deer would not be consumed by humans, uptake and subsequent movement through the nondeer part of the food web could cause adverse effects in these organisms. As a result, sampling of biota other than deer was considered but determined to be unnecessary, as explained below.

7.4.1 DU Transfer to Flora

Plants are generally poor accumulators of uranium and concentrations of uranium in plants are several orders of magnitude lower than those in the soil in which they grow (Royal Society 2002). However, despite the generally low transfer of uranium from soil to plants, certain plant species (i.e., microbial species such as fungi, yeasts, algae, and other unicellular bacteria [Hu, Norman, and Faison 1996, reported in Royal Society 2002], black spruce and some forest plants [Thomas 2000, reported in Royal Society 2002], sugar beets and sunflowers [Erikkson and Evans 1983 and Dushenkov et al. 1997, reported in Royal Society 2002], and Indian mustard [*Brassica juncea*] [Edenspace 2004]) have been shown to exhibit high uptake of uranium. Nonvascular plants (mosses and lichens) generally accumulate higher concentrations than vascular plants (Cramp et al. 1990, reported in Royal Society 2002).

7.4.2 DU Transfer to Fauna

Ingestion of microbial and plant species with accumulation of DU presents a route by which higher trophic levels of wildlife can be exposed. Some accumulation of uranium has been observed in animals. Measurements of uranium in tissues of animals grazing in uranium-contaminated areas have been reported to be higher than those in control areas. Few measurements of uranium in wild animals have been made but those compiled do not report significant accumulation in tissues (e.g., Clulow et al. 1998), although they are measurable and often elevated in whole animal samples at contaminated sites (Royal Society 2001). Ingestion of animal species with accumulation of DU presents a route by which higher trophic levels of wildlife can be exposed.

Ingestion of contaminated soil could be an important exposure pathway for animals as animals typically eat more soil than humans (e.g., incidentally when licking fur or pelts or as part of their diet). Wildlife may be exposed indirectly to DU by ingestion of plants that have taken up DU or where DU has been deposited on the leaves by wind dispersion.

Areas to the west, north, and east of the DU Impact Area are hunted for turkey and deer under the control of FWS. Of these, humans would likely consume more deer meat. The size of the home range of a deer is approximately 1 square mile (mi^2) (Smith 1991). Based on the size of the DU Impact Area, a number of deer could forage exclusively there, although hunting is prohibited within the DU Impact Area. There is potential for deer to forage in the DU Impact Area (1 mi [1.6 km] in width by 3.25 mi [5,230 m] long) and then be harvested by hunters in nearby hunting zones. Portions of the nearby hunting zones are less than 0.5 mi (0.8 km) from the western boundary of the DU Impact Area, while portions of the nearby hunting zones are approximately 1 mi (1.6 km) from the eastern boundary of the DU Impact Area. However, due to the size of Big Oaks NWR, the relatively limited home range of deer, and the limited number of hunting zones near the DU Impact Area, the potential is remote for hunters in most of the

hunting zones at Big Oaks NWR to harvest deer that have encountered DU in or near the DU Impact Area.

A total of 50 deer liver, kidney, or bone samples were collected and analyzed for U-234 and U-238 isotopes in 1984, 1987, 1992, and 1993 (Table 7-7) (SEG 1996). The deer were collected from within the DU Impact Area. No deer were collected from a background or uncontaminated location as part of this investigation. Although measurements of total uranium did not include the U-235 isotope, U-235 is a very small portion of the total uranium concentration. Concentrations of total uranium isotopes analyzed in the samples were low (less than 0.4 pCi/g) and did not indicate an impact from DU (U.S. Army 2002).

Table 7-7. Historical Deer Sampling by Year at JPG
Jefferson Proving Ground, Madison, Indiana

Year	Number of Deer	Number of Samples	Tissue Type	Associated Report
1984	9	19	Liver, kidney, and bone	Ebinger and Hansen (1996)
1984	4	4	Unspecified location or body part	Ebinger and Hansen (1996)
1987	16	16	Bone, kidney, or liver	Ebinger and Hansen (1996)
1992	3	6	Kidney, liver	Ebinger and Hansen (1996)
1993	5	5	Kidney*	Ebinger and Hansen (1996)
1996	1	3	Liver, kidney, and bone	SEG (1996)
Total	38	53		
* Organ is assumed to be kidney in Ebinger and Hansen (1996).				

Three deer tissue samples (one liver, one kidney, and one bone sample) were collected during the site characterization survey (Table 7-7) (Ebinger and Hansen 1996). These tissue samples were collected from a 4- to 5-year-old female deer within the DU Impact Area. No deer were collected from a background or uncontaminated area as part of this investigation. Concentrations of total uranium in the samples were 0.09, 0.15, and 0.42 pCi/g for liver, kidney, and bone tissue samples, respectively. The U-238 to U-234 activity ratios of 0.63, 0.43, and 0.64 for the liver, kidney, and bone tissues, respectively, did not indicate the presence of DU contamination in the deer tissue.

NRC was concerned that modest increases of total uranium concentrations in kidney (from 0.05 to 0.151 pCi/g) and bone (0.0003 to 0.416 pCi/g) compared to background were indicative of a potential trend of increasing concentrations of uranium in deer tissue that could affect human health (NRC 2004d). However, based on the data collected from 1984 to 2006, total uranium concentrations in deer tissue are not increasing over time. For all of the samples where isotopes of both U-238 and U-234 were detected and an isotopic ratio could be calculated, the U-238/U-234 ratio was less than 2 in all of the sampling events, indicating the absence of DU in all deer tissues collected to date.

A more robust deer sampling program was conducted in 2005 and 2006. Specific deer tissue samples were collected from each deer. Kidney, bone (3 to 4 in from foreleg), liver, and muscle were collected. Each sample was approximately 100 g, except for the bone, which was approximately 30 g. Teeth samples also were collected to determine the age of the deer in the event that it would be beneficial in interpreting the data (e.g., to determine if there was a correlation between the age of the deer and the presence of DU in the tissue). Samples were analyzed for isotopes of U-234, U-235, and U-238 from a total of 30 deer harvested from three areas (i.e., DU Impact Area, nearby hunting zones, and background hunting zones). A total of 120 tissue samples and the associated duplicates from the bone, liver, kidney, or muscle of the deer were analyzed. Muscle tissue had not been collected previously at JPG because uranium (either natural or DU) is more likely to accumulate in bone, kidney, or liver. It was included for this project because muscle most often is consumed by people in larger quantities.

Table 7-8 presents the ranges of total uranium concentrations and average total uranium concentrations per tissue type per sample area. In general, average total uranium concentrations were

Table 7-8. Summary of Total Uranium in Deer Tissue
Jefferson Proving Ground, Madison, Indiana

Exposure Unit	Tissue Type	Number of Samples[a]	Range of Total Uranium Concentration[b] (pCi/g)	Average Total Uranium Concentration[b] (pCi/g)
Background Hunting Zone [c]	Bone	11	0.007-0.033	0.016
DU Impact Area	Bone	11	0.008-0.069	0.02
Nearby Hunting Zone	Bone	11	0.0004-0.032	0.013
Background Hunting Zone [c]	Kidney	11	0.003-0.074	0.019
DU Impact Area	Kidney	11	0.004-0.014	0.009
Nearby Hunting Zone	Kidney	11	0.007-0.022	0.012
Background Hunting Zone [c]	Liver	11	0.007-0.020	0.012
DU Impact Area	Liver	11	0.004-0.016	0.01
Nearby Hunting Zone	Liver	11	0.005-0.022	0.012
Background Hunting Zone [c]	Muscle	11	0.005-0.020	0.012
DU Impact Area	Muscle	11	0.001-0.019	0.008
Nearby Hunting Zone	Muscle	11	0.008-0.021	0.013

[a] Eleven samples were collected from 10 deer. One duplicate sample was collected from each tissue type in each exposure unit.
[b] In instances where an isotope of uranium was not detected, the isotope was assumed to be present at the reporting limit.
[c] These hunting zones are more than 5 mi north of the DU Impact Area within the Big Oak NWR.

slightly higher in tissues less likely to be consumed by hunters (bone and kidney tissues) compared to tissues more likely to be consumed by hunters (liver and muscle), as expected for uranium. The highest total uranium concentration (0.074 pCi/g) from any tissue type was detected in a kidney sample from the background hunting zone, whereas the lowest total uranium concentration (0.014 pCi/g) from any tissue type was detected in a kidney sample from the DU Impact Area. The highest average total uranium concentration (0.019 pCi/g) was detected in kidney from the background hunting zone. Each sampling area had the highest average total uranium concentrations for at least one tissue type. There is overlap between total average uranium concentrations in the different tissues between the different sample groups. These results suggest that tissue concentrations of total uranium are similar throughout JPG, regardless of how close the deer were collected to the DU Impact Area.

Table 7-9 identifies the specific deer samples with the maximum total uranium concentrations per tissue type per area. For each tissue type in each sample area, a different deer had the maximum total uranium concentration. These data again support that tissue concentrations of total uranium are similar throughout JPG as no one deer or no few deer consistently had the maximum total uranium concentrations for each tissue type.

In Table 7-10, the number of deer with at least one of the uranium isotopes (U-234, U-235, and U-238) detected is presented. In some deer, there were no detections of any isotopes. Uranium isotopes were detected less frequently in kidney and liver than in bone and muscle samples, but just barely. Based on the total uranium data presented in Tables 7-8 through 7-10, there is no indication that one group of deer had been exposed to greater levels of uranium.

Similar to the previous deer sampling results from 1984 to 1993 discussed in Ebinger and Hansen (1996), concentrations of total uranium in the deer tissue samples were low and uranium isotopes often were below method detection limits (0.0017 to 0.107 pCi/g). Concentrations of total uranium in the 2005/2006 sampled deer tissue ranged from 0.0004 to 0.074 pCi/g. The maximum concentrations of total uranium in the 2005/2006 deer were less than the maximum concentrations associated with the deer sampling results presented in both the Ebinger and Hansen report (Ebinger and Hansen 1996) and the site characterization survey (SEG 1996).

Table 7-9. Tissue-Specific Summary Data from Deer Sampling Jefferson Proving Ground, Madison, Indiana

Tissue/Location	Tissue Sample with Maximum Total Uranium Concentration*	Maximum Total Uranium Concentration (pC/g)
Bone		
DU Impact Area	DR-DUIA-01	0.0689
Nearby Hunting Zone	DR-NHZ-02D	0.0323
Background Hunting Zone	DR-BHZ-10	0.0334
Kidney		
DU Impact Area	DR-DUIA-09	0.0142
Nearby Hunting Zone	DR-NHZ-01	0.0222
Background Hunting Zone	DR-BHZ-07	0.0743
Liver		
DU Impact Area	DR-DUIA-04D	0.0163
Nearby Hunting Zone	DR-NHZ-07	0.0221
Background Hunting Zone	DR-BHZ-06	0.0196
Muscle		
DU Impact Area	DR-DUIA-07	0.0187
Nearby Hunting Zone	DR-NHZ-01	0.0205
Background Hunting Zone	DR-BHZ-09	0.0202
* In instances where an isotope of uranium was not detected, the isotope was assumed to be present at the reporting limit and included in the total uranium concentration.		

Table 7-10. Summary of Deer Tissue with Uranium Isotopes Detected Jefferson Proving Ground, Madison, Indiana

Exposure Unit	Tissue Type	Number of Deer with U-234, U-235, or U-238 Detected	Any Indication of DU?*
Background Hunting Zone	Bone	7 of 10	No
DU Impact Area	Bone	7 of 10	No
Nearby Hunting Zone	Bone	7 of 10	No
Background Hunting Zone	Kidney	6 of 10	No
DU Impact Area	Kidney	4 of 10	No
Nearby Hunting Zone	Kidney	4 of 10	No
Background Hunting Zone	Liver	6 of 10	No
DU Impact Area	Liver	5 of 10	No
Nearby Hunting Zone	Liver	5 of 10	No
Background Hunting Zone	Muscle	9 of 10	No
DU Impact Area	Muscle	4 of 10	No
Nearby Hunting Zone	Muscle	8 of 10	No
* Samples exhibiting U-238/U-234 ratios less than 2 are likely of natural origin.			

Based on the sampling data (SAIC 2006), consumption of deer tissue does not appear to be a potentially significant exposure pathway for DU at JPG. Of the 132 samples analyzed, DU was not detected in any tissue samples. Based on qualitative observation of the data, deer collected within the DU Impact Area did not have total uranium levels or uranium isotopic ratios that differed from either the nearby hunting zones or background hunting zones. If DU uptake were occurring in deer, higher total uranium levels and isotopic ratios greater than 2 would be expected in the deer from the DU Impact Area, where the greatest potential for exposures occur, but the total uranium levels were not elevated and all ratios were lower than 2.

The concentrations of uranium in deer are below those detected historically at JPG. There does not appear to be any increasing trends in the 2005/2006 deer samples compared to the 1996 deer sample. At Aberdeen Proving Ground (APG), where DU also has been tested, the presence or absence of DU in deer tissue could not be confirmed. However, as DU testing commenced in the 1970s at APG, there has been

another decade for degradation and subsequent uptake into deer compared to JPG. The use of hard targets at APG also would have created more finely dispersed uranium available for uptake. Although the ecosystems at APG and JPG are not exactly the same, it is reasonable to conclude that factors at APG are more conducive for bioaccumulation of DU. One attribute of increased uptake would be higher total uranium concentrations. As this does not appear to be the case (APG deer had lower total uranium concentrations than JPG deer), the APG data, while not conclusive, support that uptake of DU by deer is not a potentially significant exposure pathway to humans.

As specified in the FSP (SAIC 2005a) and Addendum (SAIC 2005b), the trigger to collect tissue data from other biota was based on a weight-of-evidence approach using the results of the abiotic sampling as well as the deer tissue sampling. Using the abiotic data, none of the existing JPG ERM reports provided conclusive evidence of elevated levels of DU migrating outside the DU Impact Area. In addition, no increasing or decreasing trends were identified in the ERM reports. DU was not detected in any deer samples collected during the most recent sampling, including those from the DU Impact Area, the area most likely for exposure and subsequent uptake. In fact, the concentrations of total uranium in deer are below those detected historically at JPG. As a result, there were no triggers to support further testing of deer, and no testing of other biota was conducted. However, it should be noted that potential residual radiation doses associated with human uptake of DU through ingestion of produce, beef, and dairy tissue is included in the dose analysis as a potential exposure pathway (Section 8).

THIS PAGE WAS INTENTIONALLY LEFT BLANK